GONÇALO MARIA REIMÃO PINTO DE FRANÇA DORIA

DNA NANOPROBES FOR MOLECULAR DETECTION (NANOSSONDAS DE DNA PARA DETECÇÃO MOLECULAR)

Dissertação apresentada para obtenção do Grau de Doutor em Engenharia Biológica – especialidade Engenharia Genética, pela Universidade Nova de Lisboa, Faculdade de Ciências e Tecnologia.

LISBOA
2010

Nº de arquivo

“copyright”

ACKNOWLEDGEMENTS

None of the results achieved during this thesis would be possible without the support of many people and institutions. Although the following words will never be enough to express all my gratitude to them, I would like here to present my appreciation for all their support given during the ups and downs of this journey. So, I would like to thank:

- My PhD advisors, Professors Pedro Baptista and Ricardo Franco, for supporting and putting up with me during these past four years, and for the very helpful comments, suggestions, improvements and corrections made to this dissertation. In particular, I would like to thank Pedro for the constant support and insightful discussions about the research that were instrumental in helping me crank out this thesis. I have learned a great deal from him since the early times where I had the privilege to have him as a teacher. I will be forever grateful for his friendship, comprehension, guidance and inspiration to enter the nanobiotechnology world. I would also like to thank Ricardo for the many insightful discussions and suggestions made to this thesis, and for always supporting my ideas and making available the means to achieve them. Without him, I would never have had the opportunity to meet STAB VIDA and work on this thesis, and for that I am also forever grateful.

- STAB VIDA, Lda., especially the CEO, Orfeu Flores, for all the financial support and for giving me the opportunity to achieve this PhD dissertation. In particularly, I would like to thank Orfeu for his friendship and entrepreneurship guidance, which allowed me to broaden my knowledge outside the scope of science. Thanks to him, I have also learned a great deal regarding the preparation and writing of European projects, which will certainly be a great tool for my future. I would also like to thank all STAB VIDA's members, especially Daniela, Carla, Rui and Nanci, for all the support given throughout these years.

- Fundação para a Ciência e Tecnologia, for the financial support (SFRH/BDE/15544/2005) provided to conduct this thesis and to attend national and international scientific meetings.

- Fundação Luso-Americana para o Desenvolvimento, for the financial support granted to attend scientific meetings in USA and share ideas overseas.

- The Department of Life Sciences (former Secção Autónoma de Biotecnologia) and the Departament of Chemistry, and all their members, for all the support given throughout these years and for providing the conditions to achieve my research goals.

- Profª Leonor Osório for having so kindly received me at her lab, and to everyone that has worked there with me during these years, especially Pedro, Wafaa, Elisabete, David, Sandra,

Filipa, Maria, Ana, André, Filipe, Solange, João, Larguinho, Jorge, Goku, Veigas, Conde, Carina, Rita, Ana, Margarida, Inês, among others, for all the help provided and for making this a pleasant and amusing journey. A special thank you goes to my wingman, colleague and friend, André Vidal Pinheiro, for the many insightful discussions and suggestions made to my work, and for all the support given throughout.

- The REQUIMTE members, especially Profª. Eulália Pereira, Peter Eaton, João Carlos Lima, José Luis Capelo, Pedro Quaresma, Inês Gomes, João Cortez and Inês Osório for all the unconditional help provided. A special thank you goes to Eulália for all the enlightening discussions regarding colloids, to João Carlos for all the clarifications on spectroscopy, and to Peter for all the AFM work and insightful discussions that provided a great help in understanding the details at the nanoscale.

- The CREM members, especially César, Ana Paula, Sofia, João, Christophe, Marco, Maggy, Maria José, Joana and Jorge, for all the support and help provided.

- The CENIMAT members, Profª. Elvira Fortunato, Prof. Rodrigo Martins, Leandro, Leonardo, Iwona and Javier, for the devotion and enthusiasm given into developing the low-cost colorimetric sensor that is certainly a great add-in to the work of this thesis.

- Prof. Nuno Santos, from Instituto de Medicina Molecular, for having so kindly received me at his lab and provided access to DLS equipment, and also for the insightful discussions regarding the zeta potential.

- Prof. Bernhard Baumgartner, from the University of Göttingen, for providing the samples related to DOR and for all the valuable information on this target.

- Prof. Jean-Jacques Cassiman and Prof. Ronny DeCorte, from the Katholieke Universiteit Leuven, for providing the samples related to CYP2D6 and for all the insightful discussions regarding this target.

- My family and friends, especially to my parents, brothers, nieces, grand-parents, uncles, cousins and girlfriend, Joana, for helping me become what I am today and for being at my side throughout my life, and especially throughout this chapter. A big thank you to all of you!

- Anyone that I have missed in the list above.

All of you have gained my respect and a place in my heart! Thank you!

Gonçalo

SUMÁRIO

O principal objectivo desta tese foi desenvolver um método simples e barato para a detecção de ácidos nucleicos em amostras biológicas, baseado nas propriedades colorimétricas de nanopartículas de ouro. As nanopartículas de ouro foram sintetizadas e funcionalizadas com oligonucleotídeos de DNA modificados com um grupo tiol (nanossondas de ouro), permitindo assim reconhecer uma sequência alvo de interesse. As nanossondas de ouro foram caracterizadas e utilizadas num método colorimétrico para a detecção de DNA, com uma resolução ao nível de uma base, seguindo uma abordagem *non-cross-linking* – após um aumento da força iónica, as nanossondas de ouro agregam e a solução muda de vermelho para azul devido à deslocação para comprimentos de onda maiores da banda de ressonância de plasmónica superficial (SPR), típica das nanopartículas de ouro; a presença de um alvo complementar à sequência da nanossonda, previne a agregação das nanossondas de ouro e a solução mantêm a sua cor vermelha original. Foi também avaliada a utilização de nanopartículas de liga ouro:prata funcionalizadas com oligonucleotídeos modificados com um grupo tiol (nanossondas de liga ouro:prata) para o desenvolvimento de um método *non-cross-linking* em multiplex.

Considerando a disponibilidade de amostras clínicas e os interesses comerciais da STAB VIDA, Lda., foram seleccionados três alvos biológicos para levar a cabo a prova do conceito da detecção de mutações pontuais/polimorfismos de base única (SNP) e desenvolver o método de *non-cross-linking* - mutações pontuais associadas a β-talassémia; um SNP (i.e. DOR1C/G) associado ao gene *Diabetes and Obesity Regulated* (DOR), associado a diabetes e obesidade; um *tag* SNP (i.e. CYP1846G/A) localizado no gene do citocromo P450 2D6 (CYP2D6), associado a uma forma não funcional do CYP2D6 que é responsável pelo metabolismo de xenobióticos.

De forma a optimizar o método, foram efectuados estudos para melhor compreender o mecanismo envolvido na detecção *non-cross-linking*. O uso de Microscopia de Força Atómica (AFM), espectroscopia de fluorescência e medidas de mobilidade electroforética (análise de Ferguson) permitiram clarificar a natureza das forças envolvidas na agregação diferencial colorimétrica do método *non-cross-linking* e optimizar as nanossondas de ouro para a descriminação de SNP/mutações pontuais à temperatura ambiente.

Demonstrou-se que o método *non-cross-linking* pode ser utilizado na detecção de SNP/mutações pontuais à temperatura ambiente, com uma sensibilidade de 73 e 75 nM para amplicões ssDNA/dsDNA e oligonucleotídeos ssDNA, respectivamente.

ABSTRACT

The main objective of this thesis was to develop a simple and inexpensive method for nucleic acid detection in biological samples based on the colorimetric properties of gold nanoparticles. Gold nanoparticles were synthesized and functionalized with thiol-modified DNA oligonucleotides (Au-nanoprobes) able to recognize a target sequence of interest. These Au-nanoprobes were characterized and then used in a colorimetric method for DNA detection with a single base resolution based on a non-cross-linking approach - upon increasing ionic strength, Au-nanoprobes aggregate and the solution changes color from the original red to blue, due to the red-shift of the typical Surface Plasmon Resonance (SPR) band of gold nanoparticles; the presence of a complementary target to the probe sequence, prevents aggregation of the Au-nanoprobes and the solution remains red. The use of gold-silver alloy nanoparticles functionalized with thiol-modified DNA oligonucleotides (AuAg-nanoprobes) to further develop a multiplex non-cross-linking method was also assessed.

To carry out the proof-of-concept for single base mutation/Single nucleotide polymorphism (SNP) detection and further develop this non-cross-linking method, three different targets were selected considering clinical samples availability and the commercial interests of STAB VIDA, Lda. Single point mutations associated to β-thalassemia were chosen for the proof-of-concept. Later, to further evaluate the versatility of the method, two other targets were chosen: an SNP within the Diabetes and Obesity Regulated (DOR) gene (i.e. DOR1C/G), associated with diabetes and obesity; and a tag SNP within the Cytochrome P450 2D6 (CYP2D6) gene (i.e. CYP1846G/A), associated to a non-functional CYP2D6, which is responsible for the metabolism of xenobiotics.

Studies were also conducted to better understand the underlying mechanisms involved in the non-cross-linking detection, towards the optimization of the method. The use of Atomic Force Microscopy (AFM), fluorescent spectroscopy and electrophoretic mobility measurements (Ferguson analysis) allowed clarifying the nature of the forces involved in the differential colorimetric non-cross-linking aggregation and further optimize the Au-nanoprobe design to SNP/single point mutation discrimination at room temperature.

It has been demonstrated that the non-cross-linking method can be used for detection of SNP/single point mutations at room temperature. The detection sensitivity of the non-cross-linking method using Au-nanoprobes was determined to be 73 and 75 nM for ssDNA/dsDNA amplicons and ssDNA oligonucleotide targets, respectively.

SYMBOLS AND NOTATIONS

3SR - self-sustained sequence replication

A - Hamaker constant

AFM - Atomic Force Microscopy

Ag - Silver

ARMS - Amplification Refractory Mutation System

Au - Gold

AuAgNPs - Alloy Gold-Silver Nanoparticles

AuNPs - Gold Nanoparticles

CCC - Critical Coagulation Concentration

CCD - Charge-Coupled Device

d - Distance between the Centers of Two Particles

ddNTPs - Dideoxynucleosides Triphosphate

DHPLC - Denaturing High Performance Liquid Chromatography

DLS - Dynamic Light Scattering

DLVO - Derjaguin–Landau–Verwey–Overbeek Theory

DMSO - Methyl Sulfoxide

DNA - Deoxyribonucleic Acid

dNTPs - Deoxyribonucleotide Triphosphate

dsDNA - Double strand Deoxyribonucleic Acid

DTT - DL-Dithiothreitol

ε_0 - Permitivity of Free Space

ε - Dielectric Constant

e - Elementary Charge

EM - Extensive Metabolizer

FAM - Fluorescein Amidite

FDA - U.S. Food and Drug Administration

FISH - Fluorescent *in situ* Hybridization

FRET - Fluorescence Resonance Energy Transfer

HDA - Helicase-dependent Amplification

HRM - High Resolution Melting

I - ionic strength of the electrolyte

ICP - Inductively Coupled Plasma

IM - Intermediate Metabolizers

k_B - Boltzmann Constant

LAMP - Loop-mediated Isothermal Amplification

LC-MS - Liquid Chromatography-Mass Spectrometry

LNA - Locked Nucleic Acids

Mrd. - Milliard

mRNA - Messenger Ribonucleic Acid

n_∞ - Total Ion Concentration in the Bulk Solution

N_A - Avogadro number

NPs - Nanoparticles

nt - Nucleotide

PCR - Polymerase Chain Reaction

PEG - Poly(ethylene glycol)

PM - Poor Metabolizer

PNA - Protein Nucleic Acids

POC - Point-Of-Care

QDs - Quantum Dots

RCA - Rolling Circle Amplification

RFLP - Restriction Fragment Length Polymorphism

RNA - Ribonucleic Acid

R_S - Nanoparticle radius

SDA - Strand Displacement Amplification

SDS - Sodium Dodecyl Sulfate

SERS - Surface-enhanced Raman Spectroscopy

SNP - Single Nucleotide Polymorphism

SPR - Surface Plasmon Resonance

ssDNA - Single strand Deoxyribonucleic Acid

T - Absolute Temperature

TEM - Transmission Electron Microscopy

UM - Ultrarapid Metabolizer

κ - Function of the Ionic Composition

Υ - Reduced Surface Potential

ΦA - Attraction Potential Energy

ΦR - Repulsion Potential Energy

ΦT - Total Potential Energy

TABLE OF CONTENTS

FIGURE INDEX

TABLE INDEX

Pg

CHAPTER 1. General Introduction

The unraveling of the human genome has revolutionized the understanding of many aspects of human disease at the molecular level, and provided a host of opportunities to identify new disease markers.[1] Since then, other large-scale biological projects have emerged, such as the Encyclopedia of DNA Elements (ENCODE), which aims to identify all of the functional elements in the human genome,[2] or the International HapMap Project, which aims to determine the haplotype structure of human chromosomes in various ethnic groups.[3]

Several types of DNA variations can be found in the human genome (e.g. insertions and/or deletions of one or more bases, duplications, polymorphisms, etc.), but the most common are single nucleotide polymorphisms (SNPs), accounting for around 68% of all detected changes.[4] There are millions of different SNPs that can be located in very different genomic regions – in coding regions where they may modify the activity of a protein (non-synonymous SNP/missense SNP); in the boundary exon/intron where they may modify the splicing process; other intronic SNPs and synonymous SNPs (base changes in the coding region that do not lead to an amino acid change) can also change mRNA stability with potential implications for gene expression. This can also occur as a consequence of SNPs located in the promoter region or intragenic regions, in the latter case as a consequence of enhancing mechanisms.[5-7] All this individual genetic variability has been associated with individual susceptibility to several multifactorial diseases, such as cancer, diabetes, and to the individual response to therapeutics.[8,9] For this reason, the use of molecular tools for genotyping is becoming increasingly more important as the understanding of disease susceptibility and progression markers improves. However, the number of SNPs estimated to commonly occur in the human genome is approximately 10 million, which, with present technology, hampers the complete genotyping of an individual at an affordable cost. This is where the HapMap Project comes in handy, by identifying the common haplotypes in four populations from different parts of the world and also identifying "tag" SNPs which uniquely identify these haplotypes. Haplotypes are a combination of alleles at multiple *loci* that are located nearby each other within a chromosome. Hence, they undergo recombination only very rarely and are, usually, inherited in blocks across generations. Alleles are alternative DNA sequence variations at the same physical gene *locus*, which may result in different phenotypic traits. The conjugation of alleles in a person’s chromosomes is what is known as a genotype. Since the number of tag SNPs that contain most of the information about the patterns of genetic variation is estimated to be between 300,000 to 600,000, one can virtually genotype a whole-genome just by characterizing a far fewer fraction of the 10 million estimated SNPs.

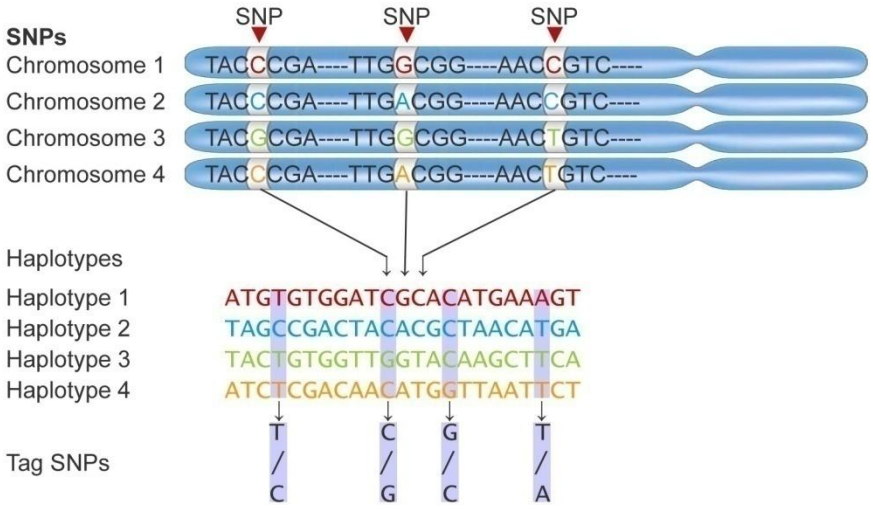

Figure 1.1 – Relation between SNPs, haplotypes and tag SNPs. Adjacent SNPs identified in the genome of multiple individuals are compiled into haplotypes, then tag SNPs allow to uniquely identify each haplotype.

Different disease and metabolic susceptibilities can be a consequence of genetic variants present in a single gene (i.e. single-gene or Mendelian disorders), or in a combination of multiple genes (i.e. polygenic disorders), or of a combination of genetic variants and environmental factors (i.e. multifactorial disorders). In the case of Mendelian disorders, more than 4000 disorders have been described and many more are being discovered each year (for a list of Mendelian disorders go to Online Mendelian Inheritance in Man (OMIM) database - http://www.nslij-genetics.org/search-omim.html).[10] These include autosomal dominant, autosomal recessive, X-linked, Y-linked and mitochondrial-related disorders. Autosomal dominant disorders occur when only one mutated autosomal allele is necessary to express a disease's phenotype, while autosomal recessive disorders require that both autosomal alleles are mutated for the disease's phenotype to be expressed. Hence, characterization of both alleles is compulsory in genetic testing, to identify homozygous and heterozygous patterns. X-linked, Y-linked and mitochondrial-related disorders occur when the mutations that lead to the disorder are located in genes on the X-chromosome, Y-chromosome or mitochondrial DNA, respectively.

While true single-gene disorders are relatively rare, most inherited disorders are actually multifactorial, meaning that other factors (e.g. environment) can influence the probability of an individual that carries a specific disorder-associated mutation(s) being affected with a specific genetic disease.[11,12] It is worth emphasizing that genetic testing should always be associated with other sources of information (e.g. family health and ethnic background, lifestyle, etc.), in order to conduct a more precise risk assessment and better seize the benefits of the post-genomic era information.[13] Moreover, genetic testing should always be considered as a predisposition assessment tool rather than predictive diagnostics.

Now, one of the great challenges of modern molecular detection is to integrate all this new genetic information into procedures suitable for implementation in rapid, cost-effective and reliable assays. While some of which are already used in the contemporary clinical laboratory in a regular basis, others are still in development.

1.1 Molecular Diagnostics – state of art

Current molecular diagnostic methods rely in several types of technological platforms: i) enzymatic amplification; ii) restriction enzyme analysis; iii) hybridization analysis; iv) chromatographic analysis; v) melting analysis or vi) DNA sequencing.

Several enzymatic-based amplification methods are available, including PCR, self-sustained sequence replication (3SR) and strand displacement amplification (SDA).[14] Among these amplification methods, PCR is considered the *gold standard* in nucleic acid detection and has become the most predominant technology in molecular diagnostics. PCR is a very specific technique based on the use of a thermo stable DNA polymerase that, after a thermal cycling process, is able to exponentially amplify a short fragment of DNA (amplicon) from just a few copies of a DNA template, using a set of primer oligonucleotides and deoxynucleoside triphosphates (dNTPs).[15,16] PCR has been used to discriminate templates that differ by only a single nucleotide residue, through a strategy known as amplification refractory mutation system (ARMS) or allele-specific PCR, which relies on designing the primer 3'-end nucleotide to overlap the polymorphic residue.[17] The amplification efficiency is greatly reduced when a mismatch between the 3'-end of the primer and the template occurs, due to a lack of 3' to 5' exonuclease activity in *Taq* polymerase (the DNA polymerase commonly used in PCR). The confirmation of a successful amplification by PCR is, usually, carried out by electrophoresis in a gel matrix and using a DNA intercalating fluorescent dye to help visualize the amplicon fragments. However, the presence of an amplicon of the expected length cannot confirm the specificity of the reaction, i.e. the genetic makeup of the product. At most, is an indication that the PCR has targeted the specific template for which the primers where designed. This is particularly important because PCR is very sensitive to contaminations that may lead to the amplification of spurious amplicons with the expected size.

More recently, the development of a Real-time PCR method, which uses DNA oligonucleotide probes that fluoresce when hybridized with a complementary DNA, has partially circumvented this issue due to the inherent increased specificity of using a probe.[18] Real-time PCR also allows target DNA template quantification in real-time through the quantification of fluorescence emitted by the probes. Apart from the probes, a fluorescent dsDNA intercalating dye can also be used for real-time quantification of amplification, but with the inconvenience of reduced specificity.[19]

Besides the Real-time PCR, several other variants of the PCR method have been developed to achieve a specific goal (e.g. multiplex PCR, asymmetric PCR, nested PCR, reverse transcription PCR, etc.). In the case of asymmetric PCR, one of the strands of the DNA template is preferentially amplified by using a great excess of the primer that hybridizes with the chosen strand.[20] This procedure yields a mix of dsDNA and ssDNA amplicons, which can be ideal to probe hybridization due to circumventing double strand competition, i.e. hybridization kinetics competition between probe/dsDNA, and dsDNA reannealing. However, this PCR method is inefficient and requires extra cycles of PCR due to the slow linear amplification later in the reaction, after the limiting primer has been used up. Nevertheless, the reaction inefficiency can be reduced if the primers melting temperature (Tm) is calculated using the nearest-neighbor formula which takes into account the primer differential concentration.[21] This is what is considered in the Linear-after-the-exponential (LATE)-PCR method.[22]

Isothermal amplification methods have also been developed to overcome the need for expensive thermal cycling machinery required by the PCR (e.g. strand displacement amplification, rolling circle amplification (RCA), loop-mediated isothermal amplification (LAMP)).[23] Among these, LAMP gathers the best properties for molecular diagnosis in clinical laboratory and at point-of-care (POC). The method relies on autocycling strand displacement DNA synthesis by a *Bst* DNA polymerase in presence of a template DNA, dNTPs and a set of four primers (two inner and two outer), that together recognize six distinct sequences on the template DNA.[24] Through this approach, the specificity of the method is greatly enhanced when compared to other amplification-based methods and 10^9 to 10^{10} fold amplification is usually achieved after 1 hour at a constant temperature (e.g. 60ºC). LAMP's final amplification product presents a stem-loop DNA structure, encompassing alternate inverted repeats of the target sequence with multiple loops that appear with a ladder-like pattern in agarose gel electrophoresis, which hampers size analysis or its direct use in other techniques, such as sequencing. Nevertheless, product amplification can also be followed in real-time by photometry due to the turbidity caused by increasing quantity of magnesium pyrophosphate in solution, as result of a successful amplification.[25] LAMP has also shown to be efficient in the presence of known PCR inhibitors such as blood, serum, plasma or heparin[26, 27] and to work without an initial heat denaturation of the template DNA.[28]

Restriction enzymes can also be used to characterize DNA due to their ability to cut DNA at a specific nucleotide sequence known as restriction sites. A restriction fragment length polymorphism (RFLP) analysis can be performed to characterize genotypes by digesting DNA with one or more restriction enzymes and later analyze the resulting DNA fragments patterns by gel electrophoresis.[29] In the presence of a polymorphism within the restriction site, the resulting fragments' lengths will differ. However, restriction enzyme-based analyses can only be used to characterize the DNA sequences that are recognized by the available

restriction enzymes and do not allow to determine the exact position of the polymorphism within their restriction sites.

Hybridization assays are a fundamental tool in molecular genetics, taking advantage of the ability for individual single-stranded nucleic acid molecules to form double-stranded molecules, i.e. to hybridize. Hybridization takes place when the interacting single-stranded molecules have a sufficiently high degree of base complementarity, accordingly to Watson-Crick base pairing (Guanine-Cytosine and Thymine-Adenine).[30] Standard hybridization assays use a labeled (e.g. fluorescent, radioactive) nucleic acid probe to identify a related DNA or RNA molecules, i.e. with a significantly high degree of sequence similarity, within a sample of unlabeled nucleic acid molecules. Well known hybridization assays that rely on such probes include Southern and Northern blot,[31,32] fluorescent *in situ* hybridization (FISH) assays,[33] and, more recently, DNA-microarrays/chips technologies.[34] In the latter, a high-throughput DNA analysis can be performed due to highly density arrays of DNA oligonucleotides that are functionalized in chips made of glass, silicon, or plastic. The target hybridization is usually spotted by using fluorophore- or chemiluminescence-labeled targets or probes - in this case hybridization occurs in a sandwich conformation between the immobilized DNA oligonucleotide, the target and the probe. Applications for this technology include gene expression analysis and genotyping for point mutations, SNPs and short tandem repeats (STRs). In general, hybridization assays are very specific and sensitive (depending on the labeling). However, despite the specificity of Watson-Crick base pairing, mismatches between the target nucleic acid and the probe can only be detected in highly stringent conditions and normally require controlled temperatures. Also, background noise can be a problem in hybridization assays due to non-specific probe hybridization.

Melting analysis has been historically used to characterize physical states of DNA, determine base contents and detect sequence differences between two ssDNA sequences of different sources (i.e. by forming heteroduplexes).[35] This was usually done by characterizing the dissociation profiles of DNA following the hyperchromic effect of DNA in the UV spectrum along a temperature ramp. Since then, this technique has evolved along the years, mainly due to the development of the Real-time PCR technique which gave rise to DNA intercalating dyes and fluorescent probes that can also be used to characterize dsDNA melting profiles.[36] More recently, a high resolution melting (HRM) analysis has urged with the development of new high-resolution instruments and novel saturation dyes which do not inhibit PCR when used at concentrations that yield maximum fluorescence (saturation).[37] So now, melting curves can be used for mutation scanning, sequence matching and multiplex genotyping, in a fast and accurate way.[38]

Chromatography can be used to separate, purify and characterize nucleic acids. For example, denaturing high performance liquid chromatography (DHPLC) allows to analyze genetic variations, such as mutations and chromosomal breakpoints.[39] The method exploits

the differential retention of homo- and heteroduplex DNA species on a reversed-phase chromatographic column under conditions of partial thermal denaturation. Liquid chromatography-mass spectrometry (LC-MS) is another technique that can be used to analyze DNA samples, along with other mass spectrometry methods (e.g. MALDI-MS, ESI-MS).[40]

Despite all these technologies and methods developed for DNA genotyping, DNA sequencing is the ultimate reference technique for DNA characterization, allowing determination of the precise sequence of a DNA strand. Nevertheless, this technique is usually still the last resource method due to the associated high cost, laborious and time consuming procedures. The most popular DNA sequencing techniques are based on the Sanger method which relies on a chain-termination approach.[41] Basically, this method uses normal dNTPs as well as dideoxynucleosides triphosphate (ddNTPs) to halt chain elongation by a DNA polymerase. This yields DNA fragments of different lengths that can be later separated and analyzed by electrophoresis. Through this chain-termination approach it is only possible to sequence fairly short strands (100 to 1000 bp). Longer sequences must be subdivided into smaller fragments and subsequently re-assembled to give the overall sequence. More recently, the high demand for low-cost sequencing has driven to the development of high-throughput second generation sequencing technologies. These include microelectrophoretic methods, sequencing by hybridization, real-time observation of single molecules, and cyclic-array sequencing (e.g. pyrosequencing).[42]

To summarize, current molecular diagnostic methods have come a long way towards better, faster, cost-effective and reliable assays. Nevertheless, most are still time consuming and require expensive equipment (e.g. Real-time PCR, DNA sequencing), expensive reagents (e.g. fluorescent dyes, DNA polymerases) and highly specialized laboratories and personnel. In the end, all this restricts their use at the POC or in a larger number of laboratories, especially in countries with fewer resources available to healthcare. Working at the nanoscale may allow decreasing the costs associated with genetic tests without jeopardizing sensibility and reliability, thus making them available to a broader population worldwide.

1.2 Nanotechnology

Nanotechnology involves the study and control of matter on a nanometer (one billionth of a meter) scale – for reference, the DNA double-helix has a diameter of 2 nm. Its birth has been associated with Richard Feynman and his famous talk "There's plenty of room at the bottom" at an American Physical Society meeting at Caltech on December 29th, 1959.[43] Since then, nanotechnology has led to the development of new materials and devices with a wide-range of applications, such as in electronics, mechanics, medicine, etc.

Two main approaches can been used to create structures at the nanoscale: the “bottom-up” approach, where nanostructures are built from molecular components; and the “top-down” approach, where nanostructures are eroded from larger structures. Top-down techniques suffer from the need to remove large amounts of material, while bottom-up techniques usually suffer from poor monodispersity due to the need to arrest growth at the same point for all the nanostructures. Some tools and techniques have been developed to help with the delicate task of working at the nanoscale, such as scanning probe-based microscopes (e.g. Atomic Force Microscopy – AFM), lithography techniques (e.g. electron beam lithography; dip pen lithography), self-assembly techniques (e.g. DNA mediated assembly) and chemical synthesis (e.g. colloidal chemistry, supramolecular chemistry).[44-48] While lithography techniques are commonly used for top-down approaches, the others are mostly bottom-up techniques.

In particular, AFM can be used to manipulate nanostructures, but it is more commonly used to characterize the three-dimensional profiles of structures at the nanoscale and measure interacting forces. The AFM device consists of a cantilever with a sharp tip that is used to scan a sample in a flat surface or manipulate the nanostructures. In the scanning mode, when the tip is brought into proximity of the sample surface, forces between the tip and the sample lead to a deflection of the cantilever according to Hooke's law.[49] These forces can be of different natures: mechanical contact forces, van der Waals forces, electrostatic forces, magnetic forces, etc. The deflection is then, typically, measured by a laser that reflects from the top of the surface of the cantilever into a photodiode array during the scanning procedure. One of the main applications of AFM is also to study and image biological molecules and structures, such as DNA, proteins, membranes, cells, etc.[50]

1.2.1 Nanobiotechnology

The synergy between nanotechnology and biotechnology has created a new area of technology development and application - nanobiotechnology. Although this is a very recent area, nanobiotechnology can be considered a field that concerns the utilization of biological systems, such as cells, cellular components, nucleic acids, and proteins, to fabricate functional nanostructures comprised of organic and inorganic materials. But, it also concerns the development and application of instruments, originally designed to generate and manipulate nanostructured materials (e.g. AFM), to study fundamental biological processes and structures. Within this perspective, medicine and molecular diagnostics are two of the main areas to benefit from nanobiotechnology, where the unique properties of nanomaterials and nanostructures can give rise to new techniques and methods with enhanced capabilities and efficiency, towards a better healthcare system.[51,52] In particular, the use of nanotechnology (materials, devices or systems) for molecular diagnostics purposes has defined a new field, known as nanodiagnostics. This burgeoning field of interest has been

generating new and improved techniques to meet the demands of clinical diagnostics for increased sensitivity and specificity at lower costs.[53]

Several different approaches have been considered for the development of nanodiagnostics techniques and methods: nanoscale visualization (e.g. scanning probe microscopy), nanofluidics, nanoarrays, microcantilevers, nanophotonics, microbalances, nanoelectrodes, nanopores, nanowires/nanotubes, nanoparticles, etc.[53-57]

Among these new approaches, nanoparticles (NPs) are one of the most common approaches for developing biosensing markers, due to their simplicity, physicochemical malleability and high surface areas.[58] These can measure between 1 to 100 nm in diameter and be composed of one or more inorganic compounds, such as noble metals, heavy metals, iron, etc. Most of them exhibit size-related properties that differ significantly from those observed on microparticles or bulk materials. Thus, depending on their size and composition we can observe peculiar properties, such as quantum confinement in semiconductor nanocrystals, surface plasmon resonance in some metal NPs and superparamagnetism in magnetic materials.[59]

1.2.2 Quantum dots

Semiconductor nanocrystals, commonly known as Quantum dots (QDs), have found a place in modern biological analysis mainly due to their significant fluorescent optical properties, presenting higher quantum yields and photostability than conventional organic dyes.[60] In addition, their narrow emission spectra can also be easily tuned and simultaneous excitation of multiple fluorescence colors is possible with a single wavelength within the UV spectrum. Larger QDs emit a red fluorescent light while smaller QDs emit a blue fluorescent light, being this coloration directly related to the energy levels of the QDs. These nanocrystals can be made of several semiconductor materials, such as cadmium, selenium, lead, and other heavy metals, following simple chemical synthesis protocols. Unfortunately, their composition also yields QDs a high *in vivo* toxicity, especially after suffering oxidative and/or photolytic degradation of their core coatings, which releases heavy metal toxic ions into the surrounding medium. Nevertheless, recent incorporations of a stable polymer coating have been made to try circumventing this issue, but toxicity studies with these NPs still remain inconclusive.[61]

1.2.3 Noble metal nanoparticles

The physico-chemical properties (e.g. optical, catalytic, electrochemical activity, etc.) of noble metal NPs have also been of interest in many biological applications, such as in medicine and molecular diagnostics. In particular, gold NPs (AuNPs) are among the most extensively studied nanomaterials and have led to the development of innumerous techniques and methods for molecular diagnostics, imaging, drug delivery and therapeutics.[62-65]

One of the most explored properties of AuNPs is their surface plasmon resonance (SPR) – a collective oscillation of conduction electrons on the NPs surface, that can be generated through the interaction of electromagnetic waves with the NPs surface electrons (Figure 1.2 – A). This SPR presents them with exceptionally high absorption coefficients and scattering properties that allow for higher sensitivity in optical detection methods than conventional organic dyes.[66]

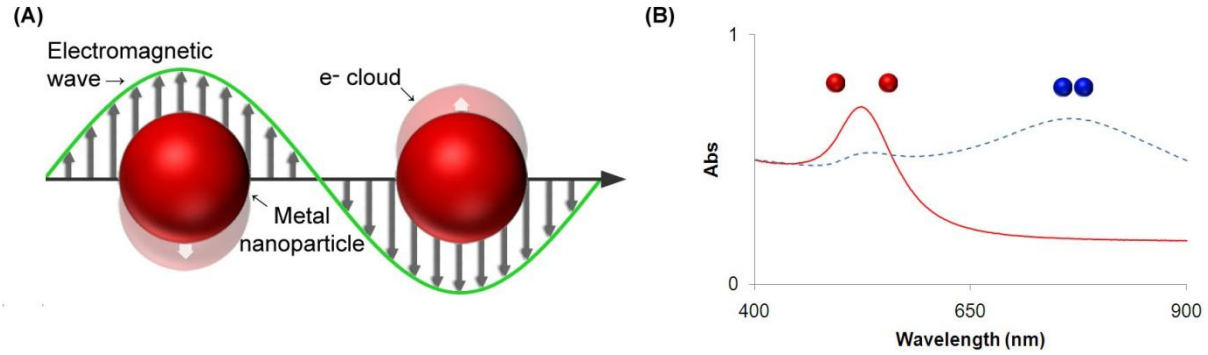

Figure 1.2 – SPR of metal NPs. (A) The interaction of the electromagnetic waves with the metal NPs surface electrons generates a surface plasmon resonance. **(B)** The inter-particle distance of AuNPs affects their SPR band peak suffering a red-shift when inter-particle distance decreases.

Typically, colloidal solutions of spherical AuNPs are red due to their SPR absorption band centered at *ca*. 520 nm. This band is weakly dependant on the size of the particle and the refractive index of the surrounding media, but strongly changes with shape and inter-particle distance.[67] In the latter case, the aggregation of AuNPs leads to a pronounced color transition from red to blue due to plasmon coupling between NPs (Figure 1.2 - B).[68]

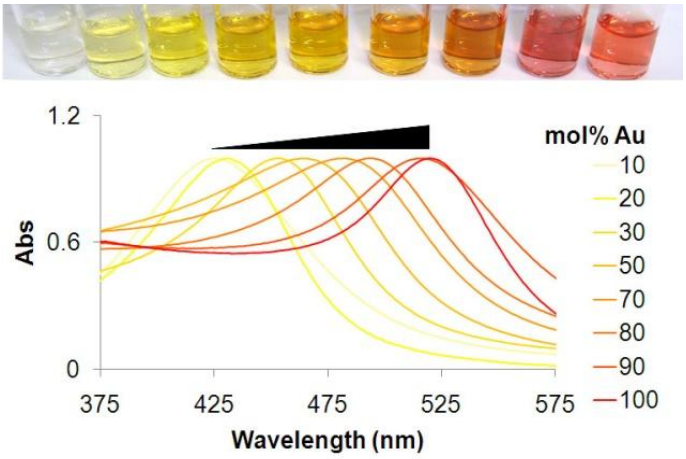

Figure 1.3 – Nanoparticle composition effect in SPR. The metal composition of gold-silver alloy NPs affects their SPR band peak and concomitant color, red-shifting with increasing ratio of gold.

In addition, nanoparticle composition in an alloy or core-shell conformation can also affect the SPR band (e.g. gold-silver NPs – see Figure 1.3)[69] or can further enhance functionality of NPs (e.g. AuNPs with magnetic core).[70]

The SPR properties of dispersed spherical metal NPs can be quantitatively predicted by Mie theory, which represents an analytical solution of Maxwell's equations for the scattering of electromagnetic radiation by spherical particles composed of an absorbing or non-absorbing material.[71] Based on this, some approaches have been made to calculate the absorption and scattering efficiencies and extinction coefficient of AuNPs with different sizes and shapes.[66]

1.2.3.1 AuNPs synthesis

The successful utilization of AuNPs in biological assays relies on the availability of synthetic methods capable of generating NPs with the desired characteristics, namely high solubility in water and adequate morphology, size dispersion and surface functionalities. Numerous synthetic strategies for the preparation of AuNPs have been reported.[72-74] Most of these strategies are based on a chemical or electrochemical reduction of a gold$^{(III)}$ precursor compound in the presence of a capping agent (i.e. a compound that binds to the nanoparticle surface blocking its growth beyond the nanometer range and stabilizing the colloid in a particular solvent). Experimental conditions of the synthesis, namely reducing agents, reaction time, temperature and capping agents, normally dictate the outcome of AuNPs' size and shape. The use of capping agents with strong affinity for gold (e.g. thiol capping agents) usually leads to a higher level of monodispersed AuNPs.[75] However, the choice of the capping agent for AuNPs synthesis should also be carefully made accordingly to the final intended functionalization and application. For example, AuNPs with strong binding capping agents can hamper further biological functionalization of the NPs and AuNPs only soluble in organic solvents cannot interact with most biological targets present in aqueous media. Due to these reasons, one of the most commonly used method for the synthesis of spherical AuNPs is the citrate reduction method of Turkevich *et al*.[76] This simple method produces fairly stable and reasonable monodispersed AuNPs in water with high-yield that can be easily functionalized with biological markers that are modified with functional groups presenting a higher binding affinity than citrate capping (e.g. thiol and amino groups). The size of the AuNPs can be easily controlled by varying the concentration of citrate in solution, with higher AuNPs being formed in the presence of lower citrate concentrations.[77] Additionally, alloy gold-silver NPs (AuAgNPs) can also be easily synthesized via a citrate co-reduction reaction with the two metals.[78]

To achieve a greater monodispersion, AuNPs can be synthesized in organic solvents but this requires an additional step of extraction of the NPs into water so that they can be further used in biological applications.[75,79]

1.2.3.2 AuNPs functionalization

The unique optical properties and high surface areas of AuNPs make them ideal candidates for developing biomarker platforms. Due to the high affinity binding of thiol to gold surfaces, citrate-capped AuNPs can be easily functionalized with biological molecules harboring a thiol moiety, such as thiol-modified ssDNA oligonucleotides. The chemical immobilization of such thiol-modified oligonucleotides on AuNPs, also known as Au-nanoprobes, has led to the development of novel detection technologies for clinical application.[62] In 1996, Mirkin and co-workers have successfully conjugated thiol-modified ssDNA oligonucleotides with AuNPs for the first time following a "salt aging" approach (herein designated as classic method).[80] In this procedure, the concentration of NaCl is gradually increased to neutralize non-specific adsorption, which can hamper thiol linkage to the AuNPs' surface. In order to assess NP functionalization, Mirkin's group also developed a fluorescent-based method to determine the surface coverage of thiol-modified oligonucleotides adsorbed on the AuNPs' surface (i.e. Au-nanoprobe density).[81] The method relies on AuNP functionalization with fluorescent modified thiol-oligonucleotides, which can be displaced by a strong reducing agent (e.g. mercaptoethanol) and quantified through fluorescence spectroscopy. Others have used a ssDNA intercalating dye instead of a fluorescence-labeled oligonucleotide and measured directly the Au-nanoprobe density.[82] In both cases, removal of the thiol-oligonucleotides from the AuNPs' surface is crucial, as fluorescence signal may be distorted, quenched or enhanced, due to fluorescence resonance energy transfer (FRET) to the AuNP or near-field coupling between the fluorescent dye and AuNPs, respectively.[83, 84]

The gradual increase in electrolyte concentration (up to ~0.7 M NaCl) over the course of oligonucleotide deposition significantly increases probe density on the surface.[81,85] The use of a spacer (e.g. poly(dT), PEG) between the recognition sequence and the alkanethiol moiety also leads to an increase in Au-nanoprobe density. The non-specific binding affinity of deoxynucleosides (dA, dT, dC and dG) to the AuNPs' surface can also affect the Au-nanoprobe density during functionalization, with dT oligonucleotide based sequences leading to denser Au-nanoprobes than dA, dC or dG based sequences.[86] The use of ultrasounds during the "salt aging" procedure can further increase Au-nanoprobe density, while reducing the salt aging procedure from 2 days to just a few hours with increased reproducibility in Au-nanoprobe functionalization.[85] The addition of surfactant molecules (e.g. SDS, Tween-20) prior to salt aging also allows a faster "salt aging" and improves reproducibility, as surfactant molecules decrease the tendency of NPs to aggregate and coalesce, particularly at high salt concentrations, while reducing non-specific binding. A high temperature (~55 °C) during the "salt aging" procedure yields Au-nanoprobes with densities similar to those obtained with ultrasounds. More elaborated approaches have also been designed to control the number and position of oligonucleotides in AuNP surface, such as by making use of DNA nanostructures,[87] or through a solid phase anisotropic synthesis-like method.[88]

More recently, other noble metal NPs were also functionalized with thiol-modified DNA oligonucleotides to be used as nanoprobes, namely silver NPs and Ag/Au core-shell NPs.[89,90] However, DNA-functionalized AgNPs are considerably less stable than Au-nanoprobes, mostly due to a lower efficiency of thiol adsorption to the AgNPs' surface.[89]

1.2.3.3 AuNPs/Au-nanoprobes stability

The stability of citrate-capped AuNPs to increasing temperature and salt concentrations is significantly enhanced by derivatization of their surfaces with thiol-modified oligonucleotides.[80] Au-nanoprobes can easily withstand moderate salt concentrations (0.1 M NaCl) and temperatures in which citrate-capped AuNPs immediately aggregate. Nevertheless, in some cases, the Au-nanoprobes can still also irreversibly aggregate at higher salt concentrations (e.g. 2 M NaCl).[91] A higher surface coverage of the AuNPs with thiol-modified oligonucleotides provides higher stability against salt-induced aggregation, which is further enhanced by functionalization with longer thiol-modified oligonucleotides.[86] The salt valence is also relevant to Au-nanoprobe salt-induced aggregation, as shown by Stakenborg *et al*.,[92] as bivalent salts (e.g. $MgCl_2$) induce aggregation of 30 nm Au-nanoprobes at lower ionic strengths than monovalent salts (e.g. NaCl). Moreover, the referred 30 nm Au-nanoprobes were thermally stable only up to 55ºC; at higher temperatures (75-95ºC) these Au-nanoprobes aggregated within 15 minutes. Still, Au-nanoprobe stability is ultimately dictated by their intrinsic properties, such as length and density.

A common theory for describing the stability of colloidal systems, such as Au-nanoprobes, is the Derjaguin–Landau–Verwey–Overbeek (DLVO) theory.[93] The standard DLVO theory suggests that the stability of a colloidal system is determined by the sum of attractive van der Waals forces and repulsive electrical double-layer forces that exist between particles as they approach each other due to Brownian motion. The balance between the attraction potential energy (ΦA) plot and the repulsion potential energy (ΦR) plot yields a total potential energy (ΦT) plot that allows predicting the overall stability of the NPs. In the case of two spherical NPs with equal radius, the attraction potential energy can be calculated by the Hamaker integral approximation (Eq. 1), where A is the Hamaker constant (e.g. for gold NPs, A = 2.5×10^{-9}J [94]), R_s is the nanoparticle radius and d is the distance between the centers of two particles.[95]

$$\Phi_A = -\frac{A}{3}\left[\frac{R_S^2}{d^2 + 4.R_S.d} + \frac{R_S^2}{d^2 + 4.R_S.d + 4.R_S^2} + \frac{1}{2}.\ln\frac{d^2 + 4.R_S.d}{d^2 + 4.R_S.d + 4.R_S^2}\right] \qquad (Eq.1)$$

The repulsion potential energy can be calculated according to the Derjaguin approximation (Eq. 2), where R_S is the NPs radius, k_B is the Boltzmann constant, T is the absolute

temperature, n_∞ is the total ion concentration in the bulk solution, Υ is the reduced surface potential and κ is a function of the ionic composition (i.e. inverse Debye length).

$$\Phi_R = \left(\frac{64.\pi.R_S.k_B.T.n_\infty.\Upsilon^2}{\kappa^2}\right).exp^{(-\kappa.d)} \quad (Eq.2)$$

According to these equations, the attraction potential energy increases in magnitude without limit as the particles approach each other. Simultaneously, the repulsive potential energy rises exponentially when particles get closer, reaching a finite value when they are in contact. The NPs may also undergo a form of irreversible aggregation, designated as coagulation, or a reversible aggregation, designated as flocculation. These two types of aggregation can be predicted by the DLVO theory, and are usually associated to a primary (in the case of coagulation) or secondary (in the case of flocculation) minimum in the total potential energy curve.[96] When the NPs are close to each other, the attractive van der Waals forces predominate and a deep minimum (i.e. primary minimum) is observed in the total potential energy curve, which is associated with the coagulation of NPs. However, an energy barrier located a little farther away from the nanoparticles' surface must first be overcome to reach this minimum, as the electric repulsion potential dominates the van der Waals attraction potential. Usually, if the barrier is greater than ~10 $k_B.T$, the collisions of two NPs produced by Brownian motion will not overcome the barrier and coagulation will not occur. Nevertheless, the NPs can still flocculate if a secondary minimum is present further away from the surface, i.e. before the energy barrier is reached.

The presence of an electrolyte in the colloidal solution influences the Debye length as predicted by the following equation:

$$\kappa^{-1} = \sqrt{\frac{\varepsilon.\varepsilon_0.k_B.T}{2.N_A.e^2.I}} \quad (Eq.3)$$

where ε is the dielectric constant, ε_0 is the permittivity of free space, N_A is the Avogadro number, e is the elementary charge and I is the ionic strength of the electrolyte. Therefore, an increase in electrolyte concentration decreases the double-layer thickness mostly due to charge screening. Moreover, it may give rise to a secondary-minimum in the total potential energy curve (i.e. aids flocculation) and decreases the energy barrier due to a decrease in the repulsive potential energy, which may lead to coagulation (see Figure 1.4).

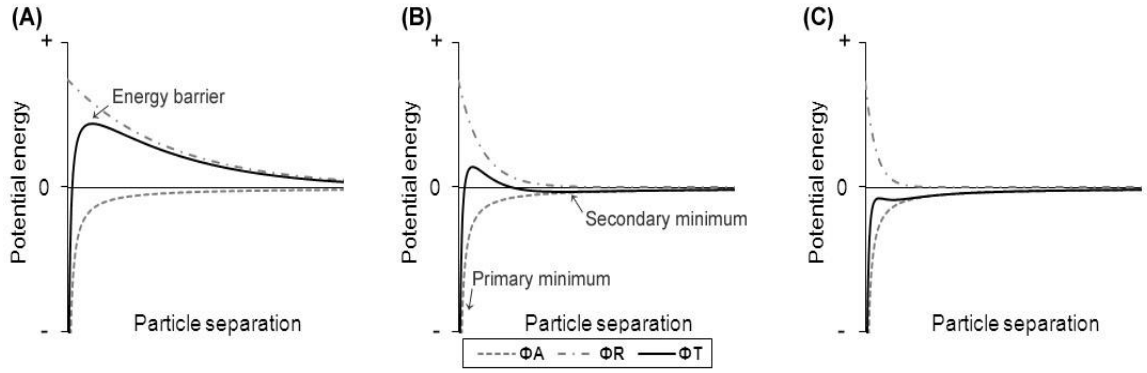

Figure 1.4 – Schematic diagrams of the variation of the repulsive (ΦR), attractive (ΦA) and total (ΦT) potential energy with nanoparticle separation according to DLVO theory and increasing ionic strength – from (A) to (C).[96]

Besides the electrolyte concentration, the repulsive potential also depends on the valence of electrolyte counter-ions. A well known generalization that agrees with the DLVO theory and considers this valence effect of added electrolyte in the stability of NPs is the Schulze-Hardy rule.[96] According to this rule, the Critical Coagulation Concentration (CCC) value of electrolyte required to coagulate the NPs can be related by a ratio of 1:0.0156:0.0014, for ions of valence 1, 2, and 3, respectively.

Although the DLVO theory can generally predict the stability of most colloidal systems, it should be noted that it is based on several assumptions and simplifications, and that it does not reflect the reality of all factors involved in the stability of the colloid. Apart from the van der Waals and the electrical double-layer forces, other interactions between charged NPs can influence their stability, such as hydration forces, hydrophobic forces, steric hindrance, among others.

1.2.4 Gold nanoparticle based molecular detection

Along with the optical properties of AuNPs, other physico-chemical properties (e.g. electrochemical activity) have been explored to develop highly sensitive methods for nucleic acid detection, some of which have already been successfully applied to biological samples. A list of these methods can be found in Appendix I, sorted by technological approach (i.e. colorimetrical, spectroscopy, electrochemical, etc.), detection limit and type of target (RNA, ssDNA, dsDNA, etc). Among these detection methods based on AuNPs, colorimetric approaches have been the most explored and, due to their simplicity and portability, are one the most promising for future diagnostic methods at point-of-care. Some of these methods are based on the color change generated by the plasmon coupling between AuNPs upon aggregation, while other methods rely on AuNPs just as a colorful reporter (i.e. making use of their superb scattering and/or absorbance properties).[80,82,97-99]

1.2.4.1 Methods using Non-functionalized AuNPs

In the case of the method developed by Li *et al*., the differential propensity of ssDNA and dsDNA adsorption to AuNPs is explored.[97] Due to the electrostatic interaction between the free bases of ssDNA and the negatively charged surface of AuNPs with a citrate capping, ssDNA confers an increased stability to the AuNPs upon increasing ionic strength. Based on this observation, Li and co-workers combined AuNPs with citrate capping with a PCR procedure, using ssDNA probes complementary to the amplicon. This way, when PCR amplification is successful, the ssDNA probes will have a complementary target to hybridize and form a dsDNA that will not adsorb to the surface of AuNPs. Hence, the AuNPs will aggregate upon an increasing ionic strength, changing color from red to blue. On the other hand, when PCR amplification fails, ssDNA probes will remain available to adsorb to surface of AuNPs and prevent aggregation upon addition of an electrolyte (Figure 1.5). Although this is a very simple and elegant approach, it requires a fine tuning of the PCR protocol in order for all primers (also in ssDNA form) to be consumed, such as to avoid a false negative. Moreover, a false negative can also arise from an amplification reaction that is not carried out due to other factors other than the lack of a complementarity target DNA in solution (e.g. inactive polymerase, lack of dNTPs, etc). A careful primer and probe design should also be taken into consideration to avoid hairpin or primer dimer formation that may lead to a false positive result.

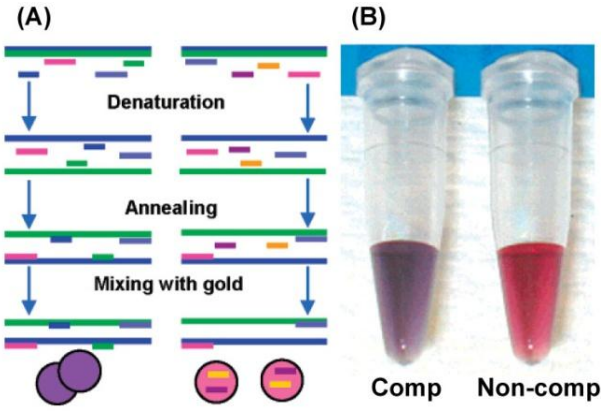

Figure 1.5 – Detection of PCR-amplified targets by bare AuNPs. (A) Schematic of the method and **(B)** colorimetric results for complementary and non-complementary targets.[97]

1.2.4.2 Methods using functionalized AuNPs

1.2.4.2.1 Cross-linking method

AuNPs functionalized with thiol-modified oligonucleotides (Au-nanoprobes) have been used in detection approaches, increasing the specificity of the methods when compared to those using non-functionalized NPs that rely on non-specific interactions between ssDNA and AuNPs. In fact, functionalization of AuNPs with thiol-modified oligonucleotides led to the first application of AuNPs in nucleic acid detection.[80] In their approach, Mirkin and co-workers

functionalized AuNPs with oligonucleotides modified with a thiol group at their 3'- and 5'-ends, whose sequences were contiguous and complementary to a target in a tail-to-tail (or head-to-tail) conformation, and were used to identify the target DNA sequence. When hybridization occurs between the sequences of the Au-nanoprobes and the target DNA, the Au-nanoprobes are drawn together and form a cross-linked network, leading to the aggregation of the AuNPs (Figure 1.6).

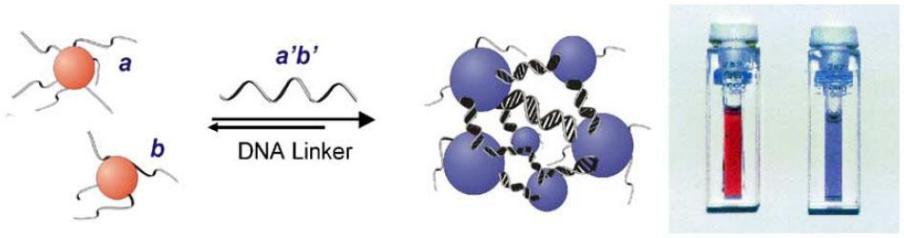

Figure 1.6 – Cross-linking method. Schematic of the method and a colorimetric result of Au-nanoprobes in absence (red solution) or presence (blue solution) of a complementary DNA target.[100]

This cross-linking aggregation promotes a change of color of the solution from red to blue, which can be observed by the naked eye in solution or spotted on reverse-phase silica plate, or can be followed by visible spectroscopy. This method allows detection of single base mismatches by controlling the denaturation temperature of the cross-linked nanostructures, as they present a sharp melting transition.[101]

1.2.4.2.2 Non-cross-linking method

Since the development of the Au-nanoprobes by Mirkin and co-workers, other methods for nucleic acid detection have been described using just one Au-nanoprobe, instead of the two required for cross-linking.

Sato's non-cross-linking approach

One of these methods has been developed by Sato and co-workers, which described a differential aggregation of the Au-nanoprobe in presence of complementary, mismatched or non-complementary targets, induced by an increasing ionic strength of the solution.[82] This non-cross-linking method was firstly developed with synthetic oligonucleotides with sequences of the same length as the Au-nanoprobe. So, when the complementary target sequences fully hybridize with the Au-nanoprobe, heteroduplexes with a blunt-end are formed and the Au-nanoprobe becomes less stable to an increasing ionic strength and aggregates, changing color from red to blue. In the presence of non-complementary targets or a target with a mismatch at the end of the Au-nanoprobe, these blunt-end heteroduplexes are not formed and the Au-nanoprobe remains dispersed and red, at the same ionic strength that led complementary/Au-nanoprobe complexes to aggregate. Unfortunately, this approach

has a limitation of application in real biological samples, since real biological targets are usually longer than the sequence of the Au-nanoprobe, and hence do not confer a blunt-end heteroduplex hybridization that is essential for the application of this method. To circumvent this limitation, Sato and co-workers used a PCR amplification followed by a single base primer extension approach to test biological samples and detect SNP at room temperature (Figure 1.7).[102]

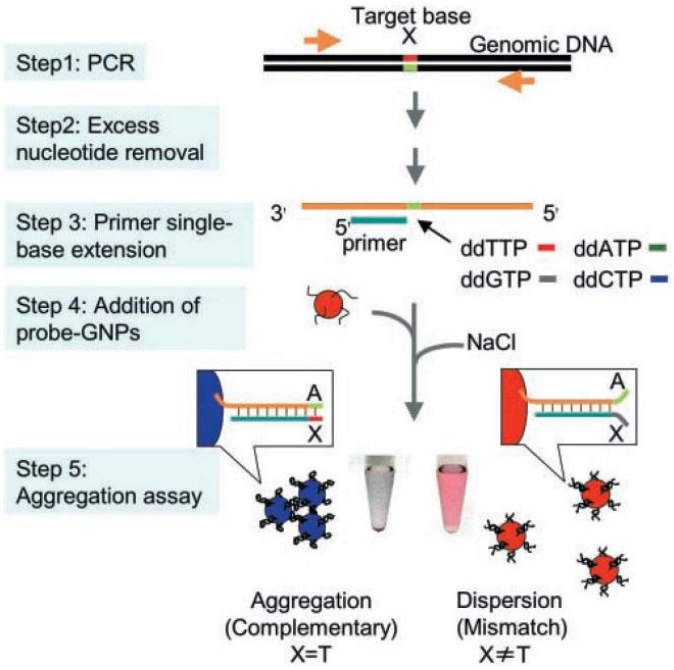

Figure 1.7 – Sato's non-cross-linking method for SNP detection. Au-nanoprobe hybridizes with the primer from single-base extension, after the PCR and washing steps. The resulting blunt end heteroduplexes provided by fully complementary targets leads to Au-nanoprobe aggregation upon increasing ionic-strength, while the Au-nanoprobes hybridized to mismatched targets remain dispersed.[102]

Our non-cross-linking approach

Following a simpler approach for nucleic acid detection in biological samples, our group has developed a non-cross-linking method that can be used to detect specific DNA and/or RNA with a longer sequence than the Au-nanoprobe sequence.[91,103,104] In this approach, the detection is achieved by color comparison upon salt addition, between solutions containing the Au-nanoprobe and either a complementary or a non-complementary target sequence. While the presence of a complementary target prevents aggregation upon salt addition and the solution remains red, the non-complementary targets do not prevent Au-nanoprobe aggregation, resulting in a visible change of color from red to blue (Figure 1.8).

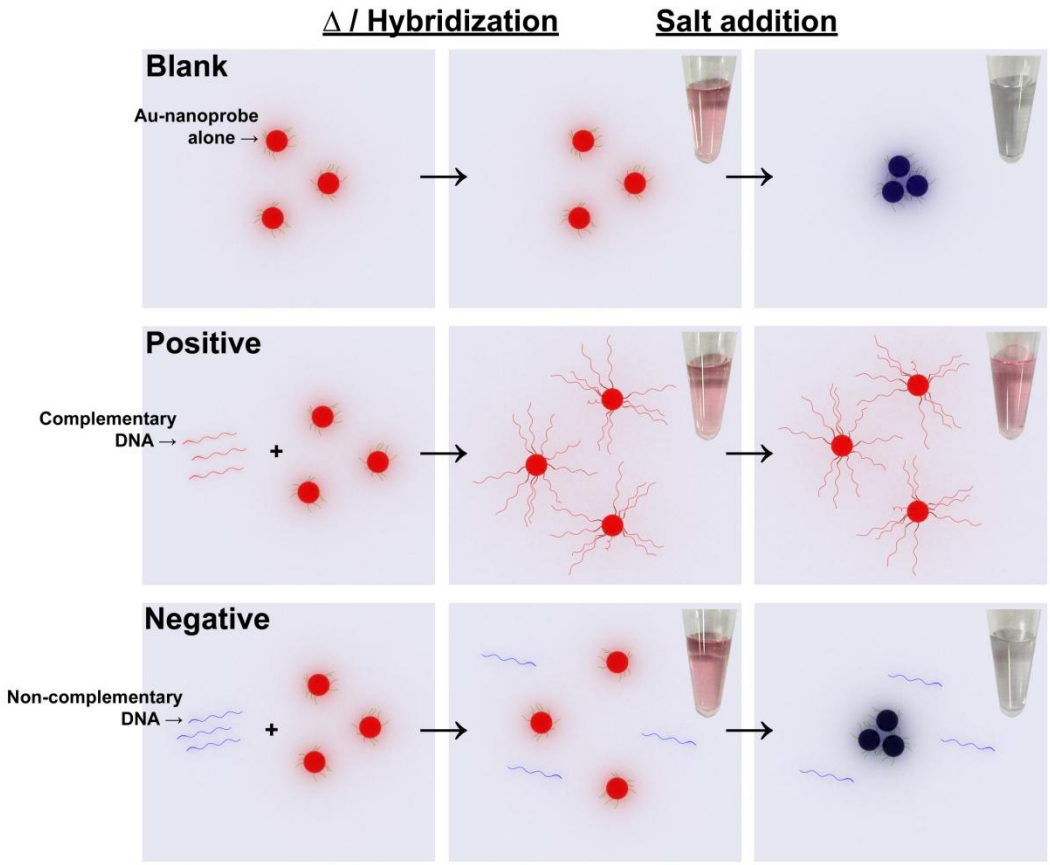

Figure 1.8 – Non-cross-linking method. Au-nanoprobe alone ("Blank") or in presence of a complementary ("Positive") or non-complementary ("Negative") target are submitted to a denaturation/hybridization step, to allow target hybridization, and then the ionic strength of solution is increased to reveal the colorimetric result.

1.2.4.2.3 Other methods

Apart from the methods based on a color variation, other methods have been developed using the AuNPs of the Au-nanoprobes as a reporter. One example is the method for detecting nucleic acid sequences through the hybridization with Au-nanoprobes in a chromatographic stripe (also known as dipstick), as described by Glynou *et al*.[98] In this approach, similarly to current pregnancy tests, biotinylated PCR products are hybridized to a specific oligo(dA)-tailed probe and loaded on the chromatographic stripe. As the buffer migrates through the stripe, the biotinylated PCR products are immobilized by streptavidin spotted in a specific location of the stripe. Finally, to detect the presence of the DNA target in the streptavidin spot, poly-dT Au-nanoprobes are used to hybridize with the poly-dA probe (Figure 1.9). Other variants of this technique have also been described by Kalogianni and co-workers to fit a specific application (e.g. SNP detection and multiplex analysis).[105,106,107] However, although the detection procedure on this method is simple and easily portable, just like pregnancy tests are, the method also requires a previous target DNA preparation protocol that is laborious and requires specialized technicians.

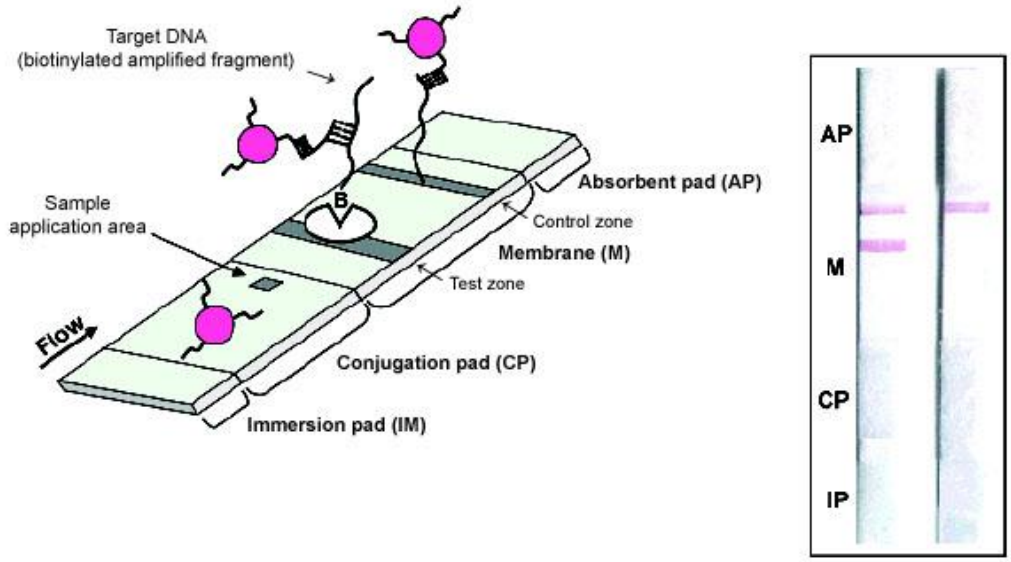

Figure 1.9 – Dip-stick method. Schematic of the method and an example of a positive (two bands) and a negative (one band) strip-test result.[98]

Using a high-throughput approach, Mirkin and co-workers also used Au-nanoprobes to substitute the conventional fluorescent labeled probes usually used to report target hybridization in a microarray platform.[99] In their method, the scattered light incident on the AuNPs of Au-nanoprobes is registered by a CCD camera and used as a signal to report complementary target hybridization. Moreover, if an additional step of silver$^{(I)}$ reduction is performed over the Au-nanoprobes surface, the scattering intensity increases and, consequently, the sensibility of the method also increases, such as up to 200 fM of genomic DNA can be detected (Figure 1.10).[108] The detection of single base mismatches is also possible at controlled temperatures and increased selectivity is observed when Au-nanoprobes are used instead of standard fluorescent probes.

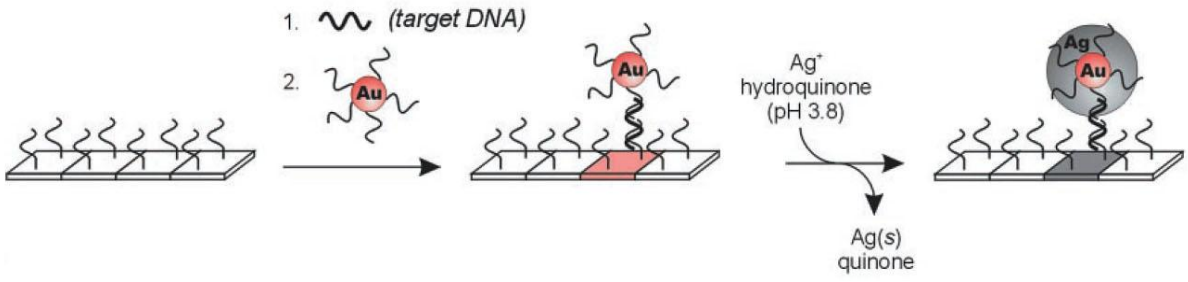

Figure 1.10 – Au-nanoprobe microarray. Schematic of microarray approach by using the Au-nanoprobe as a reporter and silver reduction to enhance signal.[99]

This method is already being commercialized by Nanosphere, Inc. (known as Verigene® system) and was one of the first nanotechnology-based diagnostic platforms to be approved by U.S. Food and Drug Administration (FDA).

The favorable optical properties of AuNPs can be further explored by different spectroscopic techniques. For instance, Au-nanoprobes can be encoded with Raman reporter molecules generating enhanced Raman signals that allow for the detection of specific nucleic acids by surface-enhanced Raman spectroscopy (SERS).[109] Additionally, the long-range plasmon coupling of AuNPs through a cross-linking hybridization approach generates an increase in SERS signal intensities by 40−200-fold (Figure 1.11).[110]

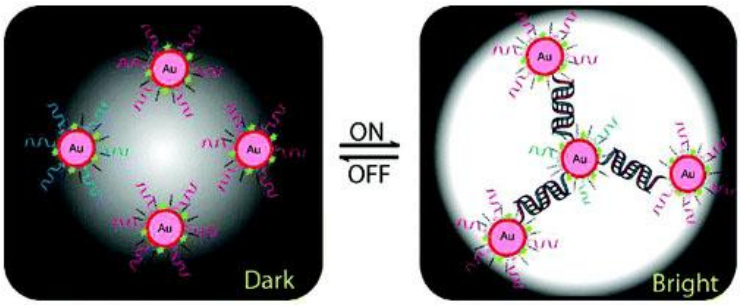

Figure 1.11 – Cross-linking nucleic acid detection by SERS. The presence of complementary targets promotes the plasmon coupling between Au-nanoprobes encoded with a Raman reporter molecule and generates an enhanced Raman signal.[110]

The electrochemical properties of Au-nanoprobes can also be used to report hybridization in a microarray platform following different electrochemical strategies (Figure 1.12).[111]

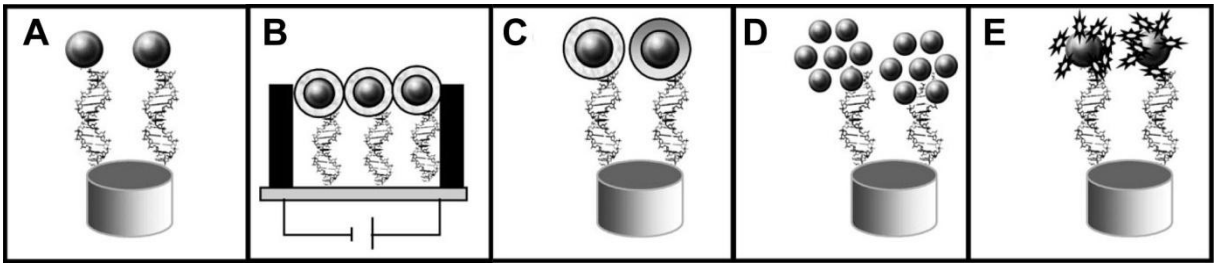

Figure 1.12 – Electrochemical DNA detection. Schematic of the different strategies used for the integration of Au-nanoprobes into DNA sensing systems: **(A)** direct detection of Au-nanoprobes anchored onto the surface of the genosensor; **(B)** conductometric detection; **(C)** enhancement with silver or gold following detection; **(D)** Au-nanoprobes as carriers of other AuNPs; **(E)** Au-nanoprobes as carriers of other electroactive labels.[111]

For instance, the hybridization of an Au-nanoprobe with a sequence anchored onto the surface of a conventional electrochemical sensor can be directly assessed by stripping or differential pulse voltammetry, or through a conductometric technique. The electrochemical

signal can be further enhanced by silver/gold reduction, or by using other AuNPs or electroactive labels attached to the Au-nanoprobe.

1.2.4.3 Other noble metal nanoparticle based molecular detection

Most nanoparticle based methods for nucleic acids detection have so far relied only on AuNPs, mainly due to their ease of functionalization with thiol-modified oligonucleotides. Nonetheless, more recently, Mirkin and coworkers have also used Ag/Au core-shell NPs functionalized with thiol-modified oligonucleotides to detect nucleic acid targets following the same cross-linking approach that was developed with Au-nanoprobes (see Section 1.2.4.2.1).[90] In their approach, the Ag/Au core-shell and pure-gold nanoprobes presented identical results, but with different optical properties (i.e. different colors). This allowed to establish a two-color-change-based method for parallel SNP analysis, providing a convenient cross-check and an assay control that offer a more accurate readout when compared to the single-color-change methods.

Apart from the Au/Ag core-shell NPs, silver NPs functionalized with thiol-modified oligonucleotides have also been used for the molecular detection of nucleic acids, following the cross-linking approach.[112]

1.3 Scope of Thesis

Most current molecular diagnostic methods for DNA and RNA characterization are still time consuming and require expensive equipment and reagents, and highly specialized laboratories and personnel. Therefore, their use in a larger number of laboratories or even at POC, and by a wider population, especially in countries with fewer resources, is still not viable. This limits the benefits from the post-genomic era that could greatly improve patient care through more efficient disease prevention and customized therapies.

Considering this issue, the main objective of this thesis was to develop a simple and inexpensive colorimetric method/kit for nucleic acid detection in biological samples, with especial focus being given to the single base mutation/SNPs detection in DNA. The method to be developed should be performed with a minimal setup protocol and independently from any expensive and specialized equipment, without compromising specificity, sensibility and reliability. Additionally, it should be affordable, quick and user-friendly to enable its use in a larger number of laboratories or at POC by unspecialized personnel. This way, the current demand for near-patient nucleic acid testing can be met.

Towards these objectives, a colorimetric method for DNA detection with a single base resolution was developed based on the non-cross-linking approach taken by our group. The

method had already been successfully applied to eukaryotic gene expression studies without retro-transcription or PCR amplification,[91] but its application to DNA and single base mutation/SNPs detection remained unexplored, and the underlying principles of this non-cross-linking method had not been clarified. Therefore, three different targets - single point mutations/SNP involved in β-thalassemia, diabetes or xenobiotic metabolism - have been selected to carry out the proof-of-concept for SNP detection and further develop the method. Additionally, studies were conducted to better understand the underlying mechanisms involved in the non-cross-linking detection, towards the optimization of the method.

1.3.1 Target selection

Genetic targets were chosen considering clinical samples availability and the commercial interests of STAB VIDA, Lda. related to targets that could potentially benefit from point-of-care diagnosis, such as those related to nutrigenomics/nutrigenetics and pharmacogenomics/pharmacogenetics. Additionally, target selection was focused on those designated by EuroGentest, a Network of Excellence for test development, harmonization, validation and standardization of services in human genetics, within which STAB VIDA, Lda. was an active partner. Considering all these aspects, β-thalassemia related mutations were the first targets to be tested for the proof-of-concept. Not only were there plenty of DNA samples but thalassemias are also a model for single gene disorders.[11] Later, to further evaluate the versatility of the method, two other targets were chosen: Diabetes and Obesity Regulated (DOR) gene, associated with diabetes and obesity;[113] and Cytochrome P450 2D6 (CYP2D6) gene, which is involved in the metabolism of xenobiotics.[114]

1.3.1.1 Beta-thalassemia

Hemoglobin is a metalloprotein responsible by oxygen-transportation in human red blood cells. It is tetramer constituted by two α- and two β-globin subunits that are covalently attached to the prosthetic oxygen-binding heme group.[115] In healthy adults, over 95% of hemoglobin is constituted by $\alpha_2\beta_2$ subunits (Hemoglobin A), between 1% and 3% is constituted by $\alpha_2\delta_2$ subunits (Hemoglobin A_2) and less than 1% is constituted by $\alpha_2\gamma_2$ subunits (Hemoglobin F, the fetal hemoglobin). The α-subunits are encoded by two α globin genes (α2 and α1) located on chromosome 16, while the γ-, δ- and β-subunits are encoded by their respective genes ($^{G}\gamma$ and $^{A}\gamma$, δ and β) located in a cluster on chromosome 11.[115] Mutations within these clusters of globin genes can lead to hemoglobinopathies, which are one of the most prevalent single-gene disorders found in humans.[116] These disorders can be the result of a reduced synthesis of one or more of the globin subunits (i.e. thalassemias) or of the synthesis of structurally abnormal hemoglobin variants, or a combination of these two cases. Among them, thalassemias make up the vast majority and can be classified according to which globin subunit synthesis is affected (e.g. in β-thalassemia, production of the β-globin

subunit is affected). The reduced synthesis of a specific globin subunit causes the formation of abnormal hemoglobin and, hence, unhealthy red blood cells are formed, causing anemia. The severity of symptoms often depends on the nature of the genotype. In the case of β-thalassemia, mutations that prevent any formation of β-subunits are classified as β^0, while mutations that allow some expression of β-subunits are classified as β^+. Clinically, β-thalassemias are usually classified as: β-thalassemia minor, which is associated with the heterozygous forms, $-/\beta^+$ or $-/\beta^0$, and also known as β-thalassemia trait; β-thalassemia intermedia, often associated with the homozygous form, β^+/β^+; β-thalassemia major, associated with the hetero- or homozygous forms, β^+/β^0 or β^0/β^0, and also known as Cooley's anemia.[117] Nevertheless, the clinical phenotype of β-thalassemia may also be modified by the coinheritance of other genetic factors at the secondary and tertiary levels mapped outside the β-globin gene cluster or by environmental factors.[118]

More than 200 different mutations in the gene encoding the hemoglobin β-chain (HBB) have been associated with β-thalassemias, some of them with high-prevalence within specific populations (for more detail, go to HbVar: Database of Human Hemoglobin Variants and Thalassemia Mutations - http://globin.cse.psu.edu/hbvar/menu.html).[119] Prevalence of β-thalassemia is higher in the Mediterranean, Middle East, Transcaucasus, Central Asia, Indian subcontinent, and Far East populations, although it is also common in populations of African heritage.[120] The most common mutations associated to β-thalassemias are point mutations in the HBB gene, except for the 619 bp deletion that accounts for 20% of the β-thalassemias in Asian Indians.[121] β^0-thalassemia alleles usually result from nonsense, frame-shift, or splicing mutations, while β^+-thalassemia alleles result from mutations in the promoter area (either the CACCC or TATA box), the polyadenylation signal, the 5' or 3' non-coding region, or by splicing abnormalities. β-thalassemia may also result from a deletion of the *locus* control region, located 5 to 25 Kb upstream from globin gene.[122]

Genetic testing for screening mutations within the HBB gene is currently available in many clinical laboratories and is used to predict the clinical phenotype in some cases, as well as in pre-symptomatic diagnosis of at-risk family members and prenatal diagnosis. Commonly occurring mutations of the HBB gene are usually detected by allele-specific priming (also known as ARMS-PCR), allele-specific oligonucleotide hybridization, restriction enzyme analysis or direct sequencing analysis, in the case of point mutations, and by Gap-PCR, in the case of deletions.[123]

1.3.1.2 DOR1

Human DOR has been reported as a nuclear co-activator that enhances the transcriptional activity of several nuclear receptors.[113] This nuclear receptor co-factor was found to be down-regulated in skeletal muscle and heart of obese mice and humans, and is located at the chromosome 20q11.22, close to *loci* linked to human obesity[124-126] and type 2

diabetes.[127-129] In fact, a G/C polymorphism in the proximal promoter of the human DOR gene, named DOR1, has been associated with obesity and type 2 diabetes in humans. This polymorphism influences the expression level of the DOR gene, in which DOR1C is the protective allele and leads to higher transcription activation. Currently, the mechanisms behind the down-regulation of the DOR gene in humans and mouse are still being investigated with the aim to identify possible targets for prevention or treatment of metabolic diseases.[130] So far, DOR is known to physically interact with the thyroid hormone receptor $TR_{\alpha 1}$ and T_3-responsive promoters, and therefore is believed to play a role in the onset and pathophysiology of obesity and type 2 diabetes in man.[113] Presently, genotyping of DOR1 is carried out by RFLP, using a *Dde*I restriction enzyme that overlaps the polymorphism. Only the DOR1C allele harbors a restriction site for this enzyme within the polymorphism *locus* and, hence, it is digested at that position (Baumgartner B, personal communication).

1.3.1.3 CYP2D6

Cytochrome P450 (CYP450) is a very large and diverse superfamily of hemoproteins, including 57 genes coding for the various CYP450 enzymes that are responsible for the metabolism of xenobiotics, including most of the pharmaceutical drugs. These genes are highly polymorphic and these differences can quantitatively or qualitatively reduce or enhance the enzymatic activity and, therefore, xenobiotic metabolism of a given individual.[131] CYP2D6 is one of the most polymorphic CYP450 genes, and is constituted by 9 exons, spanning 4.4 Kb of human chromosome 22 (22q13.1). CYP2D6 is organized in tandem with two pseudogenes - CYP2D7 and CYP2D8P. Despite constituting just a small fraction of the CYP450 enzymes present in liver, the CYP2D6 is found to be involved in the phase I metabolism of approximately 20% of the commonly prescribed drugs, including antidepressants, antihypertensive, beta-blockers, antipsychotics, and others.[132] The variability of CYP2D6 gene is considerably high between individuals and so far 122 alleles, characterized by over 130 SNPs, have been described (see http://www.cypalleles.ki.se/cyp2d6.htm for allele nomenclature). Many of these alleles lead to a significant or total loss of activity. Correlation between CYP2D6's genotype/phenotype may allow adjusting the dosage or the prescription of alternative therapies based on the genotyping of each individual,[114] which could reduce the risk of adverse reactions and/or failed treatments due to over- or sub-dosage. According to the level of metabolism, it is possible to classify the phenotype of an individual in one of four groups:[114]

- Ultrarapid metabolizer (UM) – alleles with multiple copies of the functional gene lead to a significant increase in the CYP2D6 expression, and therefore to a greater-than-normal CYP2D6 function; the treatment of individuals with this phenotype can fail due to drug sub-dosage;

- Extensive metabolizer (EM) – association of one or two totally functional alleles; these subjects have normal CYP2D6 function;

- Intermediate metabolizers (IM) – association of one allele translating to a reduced activity and one allele translating to no activity; these subjects metabolize drugs at a rate somewhere between the poor and extensive metabolizers and can be victims of over-dosage;

- Poor metabolizer (PM) – association of two alleles that translate for an inactive protein; these subjects have little or no CYP2D6 function, incurring in a risk of over-dosage.

CYP2D6 allele frequency is known to vary amongst racial/ethnic groups.[133] In European Caucasians, 71% of the CYP2D6 alleles code for a normal enzymatic activity, while 26% represent non-functional alleles. Within these non-functional alleles, the most frequent is the CYP2D6*4 allele, where over 75% of PMs Caucasians individuals carry this allele. In Asians individuals, the frequency of functional alleles represents only 50% of the CYP2D6 alleles, and 41% hold the CYP2D6*10 allele associated to a reduced enzymatic function, thus, contributing to this population slower metabolism. The frequency of functional alleles in Africans and African Americans individuals is also 50%, while 35% hold a reduced function allele, mainly CYP2D6*17.

Current genotyping methodologies of CYP2D6 are based in PCR-based assays, such as real-time PCR,[134] multiplex allele-specific PCR,[135] PCR with RFLP analysis,[136] multiplex primer extension PCR,[137] among others. High-throughput assays have also been recently developed and used, such as pyrosequencing[138] and the CYP450 GeneChip from Affymetrix, which is based on microarray technology.[139] Nonetheless, these high-throughput methods often require special laboratory facilities and equipment, and therefore allele-specific PCR and RFLP analysis are still the most widely used, despite being more laborious and low throughput.

CHAPTER 2. Materials and Methods

2.1 Materials

2.1.1 Equipment

- UV-Vis Spectrophotometer Cary 50 (Varian, USA)
- UV-Vis-NIR Spectrophotometer Cary 5000 with Peltier thermostatted accessory (Varian, USA)
- UV-Vis Spectrophotometer UV Mini-1240 (Shimadzu, Germany)
- UV-Vis Spectrophotometer Nanodrop ND-1000 (Nanodrop Technologies, USA)
- Fluorescence Spectrophotometer Cary Eclipse with Peltier thermostatted accessory (Varian, USA)
- Microplate reader Infinite M200 with Absorbance module (Tecan, Switzerland)
- Zetasizer Nano ZS system, 4 mW He-Ne laser - 633 nm (Malvern Instruments, UK)
- Real-time rotary analyzer Rotor-Gene 6000 (Corbett Research, UK)
- Thermal Cycler DNA Engine (Bio-Rad, USA)
- Thermal Cycler Tgradient (Biometra, Germany)
- Gel Doc XR+ Molecular Imager system (Bio-Rad, USA)
- Gel Logic 100 Imaging system (Kodak, USA)
- Digital SLR camera Rebel XSi (Canon, USA)
- Ultrasonic bath Elmasonic S10H (Elma, Germany)
- Wide Mini-Sub Cell GT electrophoresis cell with PowerPac Basic power supply (Bio-Rad, USA)
- E-Gel® iBase™ Power System with E-Gel® Safe Imager Invitrogen, USA)
- pH meter Basic 20 with combined glass electrode 5209 (Crison, Spain)

2.1.2 Specialized Materials

- Quartz absorption cells – 105.202-QS (Hellma, Germany)
- Quartz fluorescence cells for magnetic stirrers – 119.004F-QS (Hellma, Germany)
- Quartz fluorescence cells – 105.254-QS (Hellma, Germany)
- 384 well small volume, LoBase Polystyrene microplates, black – Cat.No.788096 (Greiner Bio-One, Germany)
- NAP-5 columns (GE Healthcare, Sweden)
- Zeta potential cells (Malvern Instruments, UK)
- E-Gel® EX pre-cast gel, 2% (Invitrogen, USA)

2.1.3 Chemical reagents

Reagent	CAS number	Distributor
Agarose	9012-36-6	Invitrogen
Ammonium chloride	12125-02-9	Merck
Ampicillin	69-53-4	Sigma-Aldrich
Bacteriological agar	9002-18-0	Difco
Betaine	107-43-7	Sigma-Aldrich
Bromophenol blue	115-39-9	Merck
Chloroform	67-66-3	Merck
DL-Dithiothreitol (DTT) solution, 1M	3483-12-3	Fluka
Ethidium bromide	1239-45-8	Sigma-Aldrich
Ficoll	26873-85-8	Sigma-Aldrich
Formamide	75-12-7	Fluka
Glycerol	56-81-5	Sigma-Aldrich
Gold(III) chloride trihydrate	16961-25-4	Sigma-Aldrich
H_2O ultra pure	7732-18-5	Fluka
Hydrochloric acid	7647-01-0	BDH
Lithium chloride	7447-41-8	Merck
Magnesium chloride	7786-30-3	Merck
Methyl sulfoxide (DMSO)	67-68-5	Sigma-Aldrich
Mineral oil	8042-47-5	Sigma-Aldrich
Nitric acid	7697-37-2	Merck
Phenol	108-95-2	Fluka
PIPES	5625-37-6	Sigma-Aldrich
Potassium chloride	7447-40-7	Merck
Proteinase K	39450-01-6	Roche
Ribonuclease A	9001-99-4	Sigma
Silver nitrate	7761-88-8	Merck
Sodium chloride	7647-14-5	Merck
Sodium citrate tribasic dihydrate	6132-04-3	Sigma-Aldrich
Sodium Dodecyl Sulfate (SDS)	151-21-3	Sigma-Aldrich
Sodium hydroxide	1310-73-2	Merck
Sodium phosphate dibasic dihydrate	10028-24-7	Merck
Sodium phosphate monobasic monohydrate	10049-21-5	Merck
Trisodium citrate	03-04-6132	Merck
Triton-X 100	9002-93-1	Sigma
Tryptone	91079-40-2	Difco

Reagent (cont.)	CAS number	Distributor
Xylene cyanol	2650-17-1	BDH
Yeast extract	8013-01-2	USB
Zinc chloride	7646-85-7	Sigma-Aldrich

2.1.4 Solutions

Phosphate buffer (10 mM)

According to the desired pH:

pH	Na_2HPO_4 (mM)	NaH_2PO_4 (mM)
6.5	3.03	6.97
7	5.77	4.23
7.5	8.15	1.85
8	9.32	0.68

Sterilize by autoclaving and store at 4ºC.

PBS

0.1M NaCl

10mM phosphate buffer of desired pH

Sterilize by autoclaving and store at 4ºC.

AGE I

0.5 M NaCl

50 mM phosphate buffer pH 7

Sterilize by autoclaving and store at 4ºC.

AGE II

2% (w/v) SDS

10 mM phosphate buffer pH 8

Sterilize by filtration (0.22 µm) and store at 4ºC. Warm up to 25ºC before use.

AGE III

1.5 M NaCl

0.01% (w/v) SDS

10 mM phosphate buffer pH 8

Sterilize by filtration (0.22 µm) and store at 4ºC. Warm up to 25ºC before use.

TB

10 mM PIPES

15 mM $CaCl_2$

250 mM KCl

55 mM $MnCl_2$

Adjust pH to 6.7 with KOH or HCl. Sterilize by filtration (0.22 µm) and store at 4ºC.

AL I

50 mM Glucose

25 mM Tris-HCl pH 8

10mM EDTA pH 8

Sterilize by autoclaving and store at 4ºC.

AL II

200 mM NaOH

1% (w/v) SDS

Prepare fresh before use (room temperature).

AL III

3M sodium acetate (adjust pH to 4.8 with glacial acetic acid)

Store at 4ºC and keep in ice during use.

TBE buffer (5x)

446 mM Tris base

445 mM boric acid

10 mM EDTA (pH8)

Store at room temperature.

LB medium (Luria-Bertani medium)

1% (w/v) tryptone

0.5% (w/v) yeast extract

171 mM NaCl

Adjust to pH 7 with NaOH. Sterilize by autoclaving and store at 4ºC.

NOTE: For solid medium, add 1.4% (w/v) of Agar.

SOB medium

2% (w/v) tryptone

0.5% (w/v) yeast extract

10 mM NaCl

2.5 mM KCl

10 mM $MgCl_2$ *

10mM $MgSO_4$*

Adjust to pH 7 with NaOH. Sterilize by autoclaving and store at 4ºC.

*NOTE: Add sterile $MgCl_2$ and $MgSO_4$ just before use.

SOC medium

Same as SOB medium plus add 20 mM glucose (sterile) after autoclaving SOB medium and cooling down to 60ºC or less.

2.1.5 Biological material

2.1.5.1 Enzymes

- Taq DNA polymerase (GE Healthcare, Sweden)
- Extensor Long PCR enzyme Mix - ThermoPrime Taq DNA polymerase + proprietary thermostable proofreading enzyme (ABGene, UK)
- *Hind*III restriction enzyme (Fermentas, Canada)
- *BamH*I restriction enzyme (Amersham Biosciences, Sweden)
- *Mva*I restriction enzyme (Fermentas, Canada)
- *Dde*I restriction enzyme (Fermentas, Canada)
- RNase A endoribonuclease (Fermentas, Canada)

2.1.5.2 DNA size markers

- GeneRuler™ DNA Ladder Mix, ready-to-use (Fermentas, Canada)

2.1.5.3 Kits

- GeneJET™ PCR Cloning Kit (Fermentas, Canada)
- GFX™ PCR DNA and Gel Band Purification Kit (GE Healthcare, Sweden)
- Quant-iT™ OliGreen® ssDNA Assay Kit (Invitrogen, USA)

2.1.5.4 E. coli strains

- *Escherichia coli* JM107

2.1.5.5 Oligonucleotides

All oligonucleotides were acquired from STAB VIDA, Lda. (Portugal)

2.1.5.5.1 Unmodified oligonucleotides

Primers

Designation	Sequence (5’ to 3’)	Tm (ºC)
bGlobF	ACTCCCAGGAGCAGGGAGGGCAGG	69
bGlobR	CAGATCCCCAAAGGACTCAAAGAACCTCTG	
bGlobLongF	AACGTGGATGAAGTTGGTGGTGAGG	68
bGlobLongR	CACTGACCTCCCACATTCCC	
Pex4-5’	CTGGTCCTCTGACTGCTC	58
Pex4-3’	CATTGAAGTCTCATGGAAGCC	
pJET1Fw	GCCTGAACACCATATCCATCC	57
pJET1Rev	GCAGCTGAGAATATTGTAGGAGATC	
CYP2D6F	GTTATCCCAGAAGGCTTTGCAGGCTTCA	66
CYP2D6R	GCCGACTGAGCCCTGGGAGGTAGGTA	
CYPex1F	GAGCCCATTTGGTAGTGAGGCAGG	62
CYPex1R	CCTCTGCCGCCCTCCAGGACC	
CYPex2F	CTGGCTTGACAAGAGGCCCTGACC	
CYPex2R	CGGAAATCTGTCTCTGTCCCCACC	
CYPex3F	CACGCGCACGTGCCCGTCCCAC	
CYPex3R	AGTTCCCGCTTTGTGCCCTTCTGC	
CYPex4F	AGGCGACCCCTTACCCGCATCTCC	
CYPex4R	CCTGCAGAGACTCCTCGGTCTCTC	
CYPex5F	AGGAGGGATTGAGACCCCGTTCTG	
CYPex5R	CCACCGTGGCAGCCACTCTCACC	
CYPex6F	CGTTCTGTCCCGAGTATGCTCTCG	
CYPex6R	CTCGGCCCCTGCACTGTTTCCCAG	
CYPex7F	GCTGACCCATTGTGGGGACGCATG	
CYPex7R	TGCTGAGCTGGGGTGAGGAGGGC	
CYPex8F	CAGTCCCCACTCTCACCCTGCATC	
CYPex8R	GAAGGGGACAGGGAGCCGGG	
CYPex9F	AGCCAGGCTCACTGACGCCCC	
CYPex9R	TGATCCCAACGAGGGCGTGAGCAG	
DOR1F	AGGAGCCGGTAGGAGGGAGTGGAG	60
DOR1Fass	AGGAGCCGGTAGGAGGGAGTGGAGATCCTC	
DOR1R	CGCCGGCGGAGACAGACAAAG	

Synthetic ssDNA targets

Designation	Sequence (5' to 3')
DOR1G_XL	GGCCGCTGCGGCGGGGCTCAGGGCACAAATTGGAACGTTCAAACAGCTGATTGTGACGTC
DOR1C_XL	GGCCGCTGCGGCGGGGCTCACGGCACAAATTGGAACGTTCAAACAGCTGATTGTGACGTC
DOR1G_20	GGCCGCTGCGGCGGGGCTCACGGCACAAATTGGAACGTTG
DOR1G_16	GGCCGCTGCGGCGGGGCTCACGGCACAAATTGGAAGGTTC
DOR1G_4	GGCCGCTGCGGCGGGGCTCACGGGACAAATTGGAACGTTC
DOR1TA	GGCCGCTGCGGCGGGGCTCATGGCACAAATTGGAACGTTC
DOR1AA	GGCCGCTGCGGCGGGGCTCAAGGCACAAATTGGAACGTTC
DOR1CA	GGCCGCTGCGGCGGGGCTCACGGCACAAATTGGAACGTTC
DOR1GA	GGCCGCTGCGGCGGGGCTCAGGGCACAAATTGGAACGTTC
CYP1846C	GGCCGCTGCGGCGGGGCTCACTGGGGGTGGGAGATGCGGG
CYP1846T	GGCCGCTGCGGCGGGGCTCATTGGGGGTGGGAGATGCGGG

2.1.5.5.2 Thiol modified (probes)

NOTE: All the following oligonucleotides are 5'-thiol-$(CH_2)_6$ modified. Resuspend in 100 µL of 1 M DTT and incubate for 1 h at room temperature. Afterwards, add 900 µL of sterile milli-Q H_2O to achieve a final concentration of 0.1M DTT. Store oligonucleotides at -20ºC.

Designation	Sequence (5' to 3')	Genbank Acc. No.
bGlob	AACCTTGATACCAAC	NG_000007
DOR1G	GAACGTTCCAATTTGTGCCG	AL109824
DOR1C	GAACGTTCCAATTTGTGCCC	
DOR1T	GAACGTTCCAATTTGTGCCT	
DOR1A	GAACGTTCCAATTTGTGCCA	
CYP1846G	CCCGCATCTCCCACCCCCAG	NG_008376
CYP1846A	CCCGCATCTCCCACCCCCAA	
CYP1846G_XL	ACGGGGAAGGCGACCCCTTACCCGCATCTCCCACCCCCAG	
CYP1846A_XL	ACGGGGAAGGCGACCCCTTACCCGCATCTCCCACCCCCAA	

Probe design:

β-thalassemia probe

The probe sequence was designed so as to harbor three of the most frequent mutations causing β-thalassemia in the Mediterranean and Portuguese populations, namely β^0IVS1, nt1 (G>A); β^+IVS1, nt2 (T>C); and β^+IVS1, nt6 (T>C).[140] A 15 nt probe oligonucleotide

sequence (bGlob probe) was derived from the β-globin gene sequence (GenBank accession no. NG_000007) so as to overlap the region harboring the previously described mutations, placing the β^0IVS1, nt1 (G>A) mismatch at the 3'-end of the thiol-modified oligonucleotide. Because of the sequence homology to the HBB pseudogene 1 (HBBP1, 77% sequence homology with HBB) a specific PCR amplification of the specific HBB target region may be needed.

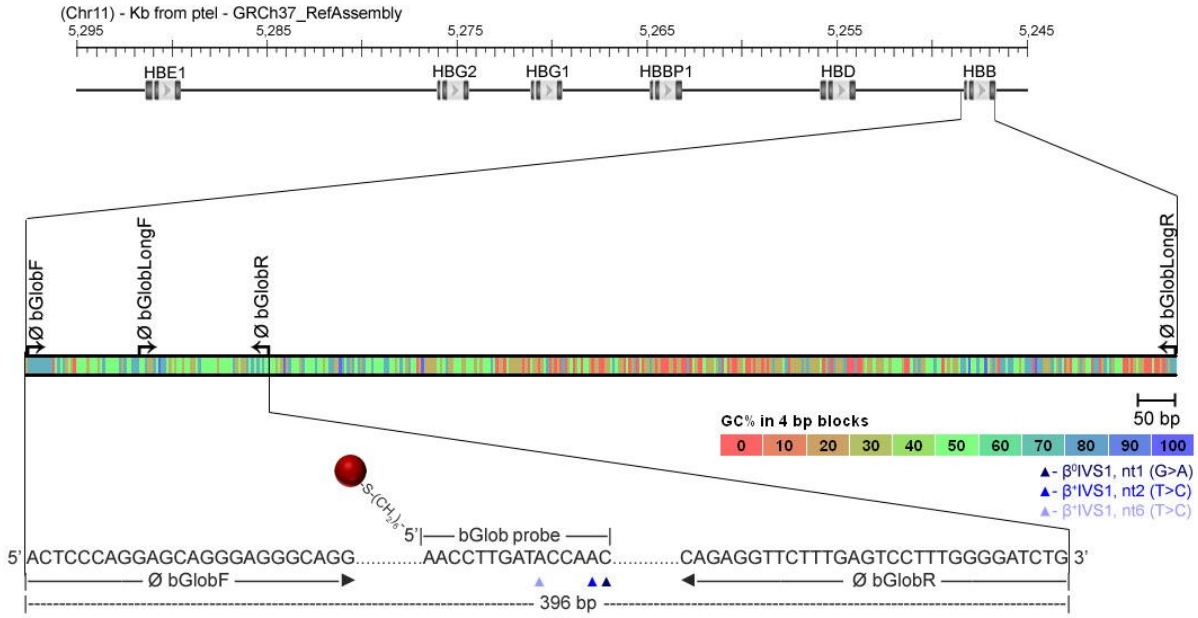

Figure 2.1 – Globin gene cluster map with corresponding location of primers and probe sequences and the position of the three most frequent mutations causing β-thalassemia in the Mediterranean and Portuguese populations. Black boxes in gene cluster represent exons.

DOR1 probes

To detect and characterize the alleles associated to DOR1 (dbSNP rs#: rs237825), two 20 nt probe oligonucleotide (DOR1C and DOR1G probes) were derived from the DOR/TP53INP2 gene sequence (GenBank accession no. AL109824). Moreover, the G/C polymorphism was designed to be located at the 3'-end of the thiol-modified oligonucleotide. The DOR1C and DOR1G probe sequence are fully complementary to the DOR1C and DOR1G alleles, respectively. Additionally, two other probes harboring an identical sequence to DOR1G/C probes but varying in the 3'-end nucleotide (A or T) were also designed to fully characterize the method (DOR1A and DOR1T probes).

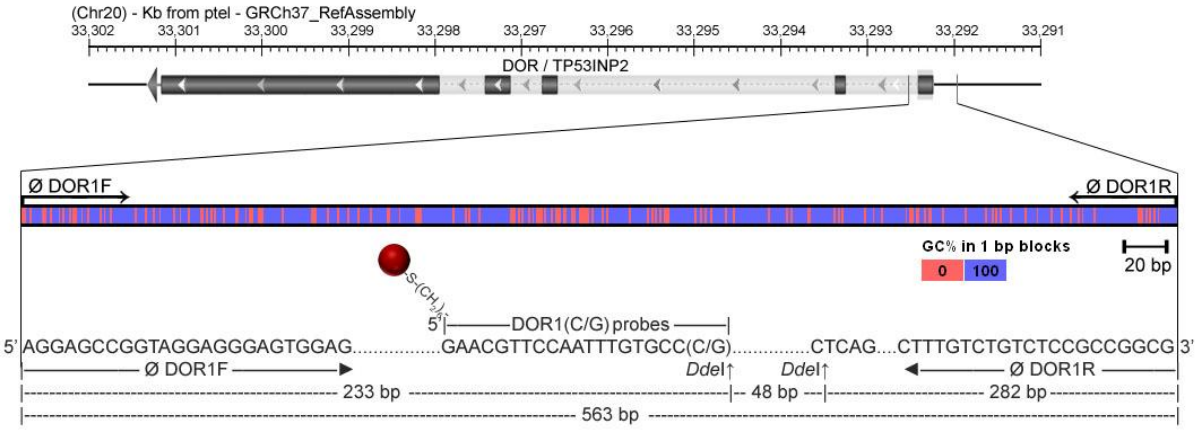

Figure 2.2 – DOR/TP53INP2 *locus* map with corresponding location of primers and probes sequences. Black boxes in gene cluster represent exons. Note: *Dde*I restriction digests the C^TCAG sequence, but not G^TCAG sequence.

CYP2D6 probes

The CYP2D6*4 allele variant leads to an inactive CYP2D6 enzyme due to a splicing defect, and is the most frequently found non-functional allele in European Caucasians. For this reason, it was the selected target to further study the single base mismatch resolution of the non-cross-linking method. Two 20 nt probes were designed to overlap the CYP2D6 gene and harbor the tag SNP associated to the non-functional CYP2D6*4 haplotype (i.e. 1846G/A SNP, dbSNP rs#:rs3892097) at their 3'-end (CYP1846G and CYP1846A probes). The sequences were derived from the CYP2D6 gene reference sequence (GeneBank ref. NG_008376). The CYP1846A probe is fully complementary to the CYP2D6*4 allele variant, while the CYP1846G probe is fully complementary to any of the other allele variants, such as CYP2D6*1 (the reference allele). Note that, unfortunately, the CYP1846G probe is also fully complementary to the CYP2D7 pseudogene which holds a 97% sequence homology with the CYP2D6 gene.[141] Therefore a specific amplification of CYP2D6 gene prior to detection may be necessary for a correct SNP analysis.

Additionally, two 40 nt probe sequences were also designed by extending the 5'-end of the previously described probe sequence with 20 nt derived from the reference sequence (CYP1846G_XL and CYP1846C_XL probes).

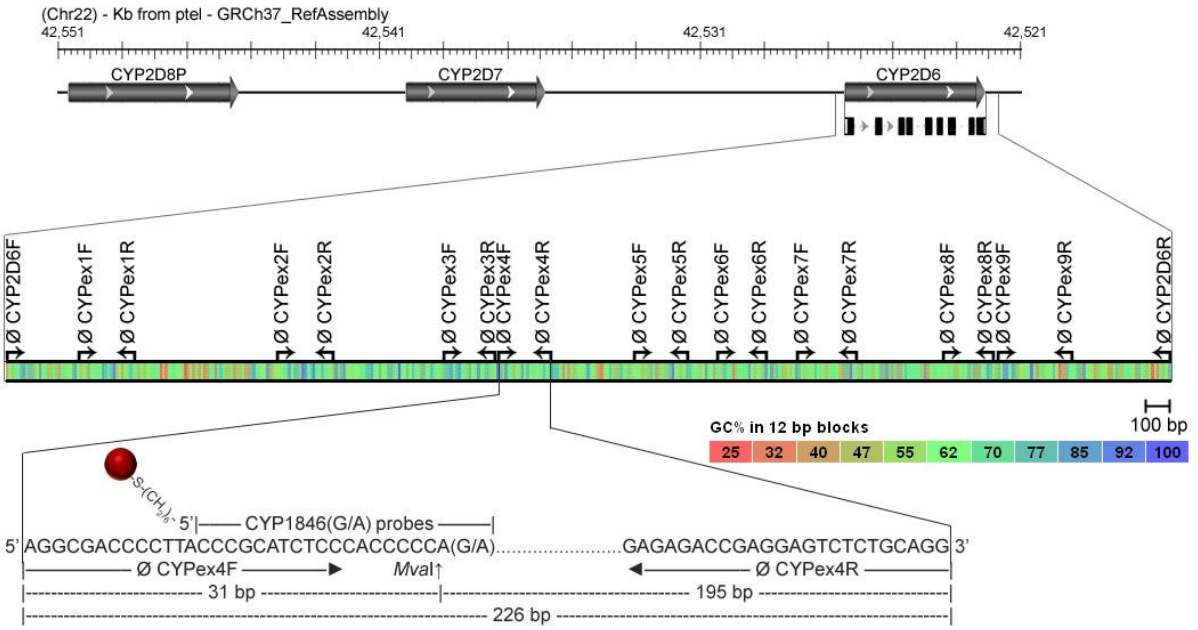

Figure 2.3 – CYP2D6 *loci* map with corresponding location of primers and probes sequences. Black boxes in gene cluster represent exons. Note: *Mva*I restriction digests the CC^WGG sequence, but not CC^WAG sequence.

2.1.5.5.3 Fluorescent modified

Designation	Sequence (5' to 3')	Modification
FAM probe	TGAGCCCCGCCGCAGCGGCC	3'-FAM

2.1.5.6 Genomic DNA

Human genomic DNA samples for:

- β-thalassemia studies were kindly provided by Prof. Leonor Osório-Almeida from Centro de Investigação em Genética Molecular Humana, Departamento de Ciências da Vida, Faculdade de Ciências e Tecnologia, Universidade Nova de Lisboa, 2829-516 Caparica, Portugal;
- CYP2D6 studies were kindly provided by Prof. Ronny DeCorte from Laboratory for Forensic Genetics and Molecular Archaeology, Centre for Human Genetics, Katholieke Universiteit Leuven, 3000 Leuven, Belgium;
- DOR1 studies were kindly provided by Dr. Bernhard Baumgartner from Institute of Veterinary Medicine, Department of Molecular Biology of Livestock, University of Göttingen, Burckhardtweg 2, 37077 Göttingen, Germany.

2.2 Methods

2.2.1 Molecular biology

2.2.1.1 Preparation of competent *E. coli* cells (adapted from Inoue *et al*.[142])

1. *E. coli* cells were inoculated on a LB agar plate and incubated at 37ºC overnight.
2. A large colony was inoculated in 125 mL SOB in a 500 mL flask, at 20ºC with vigorous shaking to OD_{600} = 0.5 (normally 24 - 36 hours).
3. The flask was placed on ice for 10 min.
4. Cells were pelleted by spinning at 1663 g for 10 min at 4ºC.
5. The cells were gently resuspended in 40 mL ice-cold TB and stored on ice for 10 min.
6. Cells were pelleted by spinning at 1663 g for 10 min at 4ºC.
7. The cells were gently resuspended in 5 mL ice-cold TB and 350 µL DMSO (DMSO was stored at -20ºC o/n before use).
8. Competent cells were aliquoted in 200 µl fractions and stored at -80ºC.

2.2.1.2 Cloning

2.2.1.2.1 Ligation

1. The amplicons of interest were submitted to electrophoresis on agarose gels (conditions varied according to the amplicon's size).
2. The amplicon's band of interest was extracted, avoiding exposure to UV light, and purified using the GFX™ PCR DNA and Gel Band Purification Kit, following manufacturer's instructions and using 50 µL of sterile milli-Q H_2O as eluent.
3. Using the GeneJET™ PCR Cloning Kit, 100 ng of the extracted DNA was inserted into a linearized blunt-end pJET1 cloning vector, following the manufacturer's Sticky-End protocol.

2.2.1.2.2 Transformation

1. Two microliters of the ligation product were added to 20 uL of *E.coli* competent cells and stored on ice for 30 minutes. A purified pUC19 plasmid was used as positive control and as negative control the ligation product was replaced by sterile milli-Q H_2O.
2. The cells were then submitted to a heat shock at 42ºC for 90 seconds and rapidly transferred to ice.
3. After 2 minutes on ice, 80 µL of SOC medium were added and the cells were incubated for 1 hour at 37ºC.
4. After incubation, 100 µL of the transformed competent cells were cultured on LB agar plates with 100 µg/mL ampicillin.
5. The plates were left at room temperature until liquid had been absorbed and then incubated at 37ºC o/n.
6. A selected transformed colony was resuspended in 25 µL of sterile milli-Q H_2O.

7. Two microliters of transformed cells were used to perform PCR using pJET1Fw and pJET1Rev primers to confirm insert ligation. The remaining cells were inoculated in 2 mL of LB medium with 100 µg/mL ampicillin and incubated at 37ºC o/n with agitation.

8. Stock solutions of the transformed cells were prepared by adding 300 µL of glycerol to 700 µL of culture, and stored at -80ºC. The remaining volume of culture was used to extract and purify the cloned plasmid, following the “Plasmid extraction and purification” protocol (step 2 onward).

2.2.1.3 Plasmid extraction and purification

1. An *E. coli* colony was inoculated in 2 mL of LB medium and 100 µg/mL ampicillin and incubated at 37ºC o/n with agitation.
2. Cells were pelleted by spinning at 16,707 g for 2 min at 4ºC in 1.5 mL eppendorfs.
3. The supernatant was discarded and the pellet was resuspended in 100 µL of ice-cold AL I solution.
4. After 5 minutes on ice, 200 µL of AL II solution was added and mixed by inversion.
5. After 5 minutes on ice, 150 µL of AL III solution was added and vigorously mixed by vortex.
6. After 5 minutes on ice, the lysate was centrifuged at 21,460 g for 5 minutes at 0ºC.
7. The supernatant was transferred to a sterile eppendorf and 2 volumes of ice-cold 100% ethanol were added.
8. The plasmid DNA was left to precipitate at -20ºC o/n (or at -80ºC for 2 hours).
9. Afterwards, the precipitate was centrifuged at 21,460 g for 15 minutes at 0ºC and the supernatant was discarded.
10. The pellet was washed with 500 µL of ice-cold 70% ethanol.
11. The pellet was left to dry at room temperature (or with the help of a speed-vac) and resuspended in 50 µL of sterile milli-Q H_2O.
12. RNase A was added to a final concentration of 25 µg/ml and incubated for 1 hour at 37ºC.
13. Two extractions with 1 volume of phenol were performed, followed by one extraction with chloroform.
14. To precipitate the plasmid DNA, the procedures from step 7 to 11 were repeated.

2.2.1.4 Enzyme mediated amplification

2.2.1.4.1 Reaction mixtures

Standard PCR

1 ×	Taq buffer
0.5 µM	Fw primer
0.5 µM	Rev primer
0.2 mM	dNTP
0.04 U/µL	Taq polymerase
200 ng	Template DNA

Long PCR

1 ×	Long PCR buffer no.2
0.5 µM	Fw primer
0.5 µM	Rev primer
0.5 mM	dNTP
0.05 U/µL	Long PCR enzyme mix
200 ng	Template DNA

Asymmetric PCR

1 ×	Taq buffer
0.01 µM	Fw primer (asymmetric)
1 µM	Rev primer
0.2 mM	dNTP
0.04 U/µL	Taq polymerase
200 ng	Template DNA

2.2.1.4.2 Reaction programs

Standard PCR

1.	5 min	94ºC	
2.	30 sec	94ºC	↰
3.	30 sec	Tm*	30x
4.	45 sec	72ºC	↲
5.	7 min	72ºC	
6.	pause	4ºC	

Long PCR

1.	2 min	94ºC	
2.	20 sec	95ºC	↰
3.	30 sec	Tm*	10x
4.	2 min	68ºC	↲
5.	20 sec	95ºC	↰
6.	30 sec	Tm*	25x (+2 sec/cycle in step 7)
7.	2 min	68ºC	↲
8.	10 min	68ºC	
9.	pause	4ºC	

Asymmetric PCR

1.	5 min	94ºC	
2.	30 sec	94ºC	↰
3.	30 sec	Tm*	40x
4.	45 sec	72ºC	↲
5.	7 min	72ºC	
6.	pause	4ºC	

2.2.1.5 Target sequence preparation

2.2.1.5.1 β-thalassemia

Genomic DNA samples from both heterozygous and homozygous individuals harboring one of three most frequent mutations causing β-thalassemia in the Mediterranean and Portuguese populations (β^0IVS1, nt1 (G>A); β^+IVS1, nt2 (T>C); β^+IVS1, nt6 (T>C)) were used as template for PCR amplification. Additionally, a 8668 bp plasmid harboring a normal HBB gene insert (i.e. plasmid p158 - see Appendix IV for plasmid sequence) was also used, either as template or as target for Au-nanoprobe hybridization. Both genomic samples and plasmid have been previously characterized by direct sequencing. As controls, samples without these mutations were used.

A 396 and 1559 bp fragment of the HBB gene, harboring the junction between intron 1 and exon 1, were PCR amplified from genomic DNA or p158 plasmid by using the bGlobF and bGlobR or bGlobLongF and bGlobLongR primers, respectively (Figure 2.1). These fragments were used as complementary or mismatched targets for the bGlob Au-nanoprobe. The plasmid p158 was also directly used as a target in Au-nanoprobe non-cross-linking assays or in a linearized form, by digesting it with *Bam*HI restriction enzyme, to be used in AFM studies.

Negative controls

Two unrelated 355 and 1565 bp amplicons were also amplified by using the Pex4-5' and Pex4-3' or the CYPex4F and CYPex7R primers, respectively; and used as non-complementary targets of the bGlob Au-nanoprobe. The shorter fragment was amplified from genomic DNA and harbored a sequence from the p53 gene, while the longer fragment was amplified from pCYP2D6*1 plasmid and harbored a sequence from the CYP2D6 gene.

2.2.1.5.2 DOR1

Fully characterized genomic DNA samples from both heterozygous and homozygous individuals for the DOR1 polymorphism were used as template for PCR amplification. In addition, two plasmids vectors pDOR1C and pDOR1G with a DOR insert, respectively harboring either the DOR1C or DOR1G alleles were used in optimization protocols. These plasmids have been characterized by direct sequencing upon reception, by using DOR1F and DOR1R primers (see Appendix IV for plasmids sequences), and were used as template reference materials for PCR amplification.

A 563 bp fragment of the DOR gene promoter, harboring the DOR1 region, was PCR amplified from either genomic or plasmid DNA by using the DOR1F and DOR1R primers, and further used as complementary/mismatched targets of DOR1C and DOR1G Au-nanoprobes (Figure 2.2). Due to the high %GC content of the DOR region (>70%), the PCR amplification of this fragment was only possible when using 6% DMSO, which is known to enhance the PCR amplification of high %GC templates.[143]

Simultaneously, the resulting amplicons were also characterized by restriction digestion using the *Dde*I restriction enzyme. The digestion of DOR1C amplicon with *Dde*I restriction enzyme yields two fragments of ~280 and ~230 bp, while the digestion of DOR1G yields two fragments of ~330 and ~230 bp (see Appendix IV, Figure A.3 - A).

A set of 40 nt oligonucleotides, named DOR1CA and DOR1GA, were also ordered to be used as complementary ssDNA targets for DOR1G and DOR1C Au-nanoprobes, respectively. The first 20 nt at 3'-end of these ssDNA targets are complementary to the Au-nanoprobes.

Alternatively, ssDNA was produced by asymmetric PCR using DOR1R and DOR1Fass primers in a ratio of 1:100. The excess of DOR1Fass primer allows to linearly amplify the ssDNA strand that is complementary to the Au-nanoprobes, after the DOR1R is consumed by the exponential amplification that yields the dsDNA. Therefore, two fragments are produced by the asymmetric PCR amplification, corresponding to the dsDNA and ssDNA amplicon. The resulting amplicons were analyzed by electrophoresis (see Appendix IV, Figure A.3 - B) and the resulting ssDNA and dsDNA fragments were extracted and purified for further analysis.

Negative controls

An unrelated 577 bp fragment harboring a fraction of CYP2D6 gene was also amplified by PCR using CYPex5F and CYPex6R primers, and 6% DMSO, to be used as a non-complementary target of both DOR1C and DOR1G Au-nanoprobes. Additionally, 40 nt oligonucleotides with an unrelated sequence were used as non-complementary synthetic targets (e.g. CYP1846C targets). Non-complementary ssDNA targets were also produced by using the CYPex5F and CYPex6R primers under the same asymmetric PCR conditions as for the complementary/mismatched targets.

2.2.1.5.3 CYP2D6

Genomic DNA samples from both CYP2D6*1/*1 and CYP2D*4/*4 homozygous individuals and CYP2D6*1/*4 heterozygous individual were available to be used as templates for PCR amplification. These samples had been previously characterized by RFLP analysis.

To generate an "unlimited" reference material of both CYP2D6*1 and *4 alleles, a 5101 bp fragment harboring the CYP2D6 gene was amplified by Long PCR using CYP2D6F and CYP2D6R primers, which specifically flank this gene,[144] and by using as template, the previously characterized genomic DNA of homozygous individuals (CYP2D6*1/*1 and CYP2D6*4/*4) (see Appendix IV, Figure A.4 - A).

The resulting ~5.1 Kb fragments were purified by excising the respective gel bands and cloned into a pJET1 vector yielding a ~8322 bp plasmids. These plasmids were then fully characterized by direct sequencing using previously described primers flanking the CYP2D6

exons, namely CYPex1F to 9F and CYPex1R to 9R,[145] and the pJET vector primers, pJET1Fw and JET1Rev (see Appendix IV for pCYP2D6*1 and pCYP2D6*4 plasmids sequences).

A 226 bp fragment of the CYP2D6 exon 4 was amplified by PCR from either genomic or plasmid DNA by using the CYPex4F and CYPex4R primers, and further used as complementary/mismatched targets of CYP1846G and CYP1846A Au-nanoprobes. These fragments were further characterized by restriction digestion using *Mva*I restriction enzyme. Within the exon 4 of CYP2D6, the CYP2D6*1 allele harbors one restriction site for this enzyme, which is not present in CYP2D6*4 allele.[146] Therefore, the digestion of CYP2D6*1 amplicon with *Mva*I restriction enzyme yields two fragments of ~31 and ~195 bp, while CYP2D6*4 amplicon remains unaltered (see Appendix IV, Figure A.4 – B).

Additionally, a set of 40 nt oligonucleotides were ordered, named CYP1864C and CYP1864T, to be used as complementary ssDNA targets for CYP1864G and CYP1864A Au-nanoprobes, respectively. The first 20 nt at 3'-end of these ssDNA targets are complementary to these Au-nanoprobes. Alternatively, ssDNA was produced by asymmetric PCR using CYPex4R and CYPex4F primers in a ratio of 1:100.

Negative controls

As non-complementary target, the previously described 396 bp fragment harboring the HBB gene sequence was used. Additionally, 40 nt oligonucleotides with an unrelated sequence were used as ssDNA synthetic targets (e.g. DOR1GA targets). Non-complementary ssDNA targets were also produced by using the bGlobF and bGlobR primers under the same asymmetric PCR conditions as for the complementary/mismatched targets

2.2.1.6 ssDNA and dsDNA extraction

The resulting product of asymmetric PCR was run in a 2% pre-cast gel on E-Gel® iBase™ Power System and isolated according to the manufacture instructions.

2.2.2 Nanotechnology

2.2.2.1 Synthesis of Nanoparticles

NOTE: All glass materials used for the synthesis of NPs were previously immersed o/n in freshly prepared *aqua regia* (1:3, HNO_3:HCl) and later vigorously washed with milli-Q H_2O (18.2 MΩ.cm at 25 °C). All metal materials used during synthesis were covered with Teflon and Milli-Q H_2O was used in all solutions.

2.2.2.1.1 AuNPs synthesis (adapted from Lee and Meisel[147])

1. In a 500 mL round bottom flask, 250 mL of 1 mM $HAuCl_4$ were brought to a boil while vigorously stirring.
2. While in reflux, 25 mL of 38.8 mM sodium citrate were quickly added and the mixture was kept refluxing for 15 minutes with continuous stirring.
3. The colloidal solution was left to cool to room temperature while keeping the continuous stirring.
4. The colloidal solution was then transferred to a 250 mL Erlenmeyer flask with a ground glass cap, covered with aluminium foil and stored in the dark at room temperature.
5. AuNPs concentration was determined by the Lambert–Beer law assuming a calculated molar absortivity for the plasmon resonance band maximum (526 nm) of 2.33×10^{8} M^{-1} cm^{-1}.
6. Morphological characterization of the AuNP was performed by Transmission Electron Microscopy (TEM) and Dynamic Light Scattering (DLS).

2.2.2.1.2 Alloy AuAgNPs synthesis (adapted from Link *et al*.[78])

1. In a 250 mL round bottom flask, 95 mL of 0.134 mM $HAuCl_4$ and 0.132mM $AgNO_3$ were brought to a boil while vigorously stirring.
2. While in reflux, 5 mL of 34 mM sodium citrate were quickly added and the mixture was kept refluxing for 15 minutes with continuous stirring.
3. The colloidal solution was left to cool to room temperature while keeping continuous stirring.
4. Afterwards the colloidal solution was decanted, after centrifuging at 233 x *g* for 20 min, to remove silver precipitate.
5. The colloidal solution was then transferred to a 100 mL Erlenmeyer flask with a ground glass cap, covered with aluminium foil and stored in the dark at room temperature.
6. AuAgNPs concentration was determined by the Lambert–Beer law assuming a calculated molar absortivity for the plasmon resonance band maximum (460 nm) of 1.19×10^{10} M^{-1} cm^{-1}.
7. Morphological characterization of the alloy AuAgNPs was performed by TEM and DLS, while the Au:Ag ratio was determined by Inductively Coupled Plasma (ICP).

2.2.2.2 Synthesis of nanoprobes

2.2.2.2.1 AuNPs functionalization - classical method (adapted from Storfhoff *et al*.[101])

1. One volume of thiol-modified oligonucleotide was extracted with two volumes of ethyl acetate.
2. The organic phase was discarded after centrifuging for 5 minutes at 21,460 g.
3. Steps 1 and 2 were repeated two more times.

4. The remaining aqueous phase was further purified through a desalting NAP-5 column, accordingly to manufacturer's instructions, using 10 mM phosphate buffer as eluent.
5. The purified thiol-modified oligonucleotide was quantified by UV/Vis spectroscopy using the extinction coefficient at 260 nm provided by the manufacturer.
6. In a polypropylene 25 mL vial with a conical skirted base, the purified thiol-modified oligonucleotide was mixed with a ~14 nM AuNPs solution in a 1:200 (AuNP:oligos) ratio.
7. After 16 h at room temperature, a certain volume of AGE I solution was slowly added to achieve a final concentration of 10 mM phosphate buffer, 0.1 M NaCl.
8. After at least 40h at room temperature, the functionalized AuNP were distributed in 1.5 mL eppendorfs and centrifuged at 21,460 g for 20 minutes.
9. The supernatant was discarded and the resulting oily pellet was washed twice with 1 mL/epp of PBS solution (pH 7) and finally redispersed in 500 µL/epp of the same solution. The resulting solutions of each eppendorf were then gathered in a polypropylene 25 mL vial with a conical skirted base.
10. The final concentration of functionalized AuNPs was determined accordingly to step 5 of the "AuNPs synthesis" protocol.
11. Aliquots of functionalized AuNPs were prepared by diluting the resulting functionalized AuNPs solution (stock solution) with PBS solution to a final concentration of 15 nM in AuNPs. Both stock and aliquot solutions were stored in the dark at 4ºC until further use.

2.2.2.2.2 AuNPs functionalization - Ultrasound method (adapted from Hurst *et al*.[85])

1. Steps 1 to 5 of the "AuNP functionalization – classical method" protocol were followed.
2. Typically, in a polypropylene 25 mL vial with a conical skirted base, the purified thiol-modified oligonucleotide was mixed with a ~14 nM AuNP solution in a 1:200 (AuNP:oligos) ratio. Other ratios have also been tested for optimization.
3. AGE II solution was then added to achieve a final concentration of 10 mM phosphate buffer, 0.01% (w/v) SDS. The solution vial was then submersed in an ultrasound bath for 10 seconds and let to rest at room temperature for 20 minutes.
4. Afterwards, the ionic strength of the solution was sequentially increased in 50 mM increments by adding a certain volume of AGE III solution up to a final concentration of 10 mM phosphate buffer, 0.3 M NaCl, 0.01% (w/v) SDS. After each increment, the vial was submersed in an ultrasound bath for 10 seconds and let to rest at room temperature for 20 minutes before the next increment. NOTE: Other final concentrations of NaCl (0.1, 0.5 and 0.7M) were also tested during optimization.
5. After an o/n period at room temperature, the functionalized AuNPs were distributed in 1.5 mL eppendorfs and centrifuged at 21,460 g for 20 minutes.

6. The supernatant was discarded and the resulting oily pellet was washed twice with 1 mL/epp of 10 mM phosphate buffer (pH 8) and once with 1 mL/epp of PBS solution (pH 8).
7. The supernatant was then finally redispersed in 500 µL/epp of the same PBS solution (pH 8). The resulting solutions of each eppendorf were then gathered in a polypropylene 25 mL vial with a conical skirted base.
8. Steps 10 and 11 of the "AuNPs functionalization – classic method" protocol were followed.

2.2.2.2.3 AuAg alloy NPs functionalization

The "AuNP functionalization – ultrasound method" protocol was followed except for the following alterations:

1. In step 2, the AuNPs solution was substituted by a ~0.1 nM alloy AuAgNPs solution and the ratio was 1:62000 (AuAgNP:oligo).
2. In step 4, the AGE III solution was added up to a final concentration of 10 mM phosphate buffer, 0.1 M NaCl, 0.01% (w/v) SDS.

2.2.2.3 Nanoprobes stability assays

1. A solution containing the Au-nanoprobe or AuAg-nanoprobe alone was prepared by heating for 10 minutes at 95ºC a certain amount (i.e. 10uL/assay of 15 nM Au-nanoprobe or 0.3 nM AuAg-nanoprobe).
2. The solution was then allowed to cool down for 30 minutes at room temperature and 10 µL/assay were mixed with different volumes of a concentrated salt solution (variable accordingly to type of salt) and using 10 mM phosphate buffer (pH variable) to fulfill a total volume of 60 µL (Au- and AuAg-nanoprobe final concentration of 2.5 nM and 0.05 nM, respectively). Other Au-nanoprobe concentrations were also tested during optimization.
3. For kinetic assays, UV–visible spectroscopic measurements were registered every 18 seconds for a total time of 30 minutes, starting 30 seconds after salt addition.
4. For all other assays, UV-visible spectroscopic measurements and digital photographs were registered 15 minutes after salt addition.

2.2.2.4 Non-cross-linking hybridization assay

1. Assay solutions containing the Au- or AuAg-nanoprobes and target DNA were prepared by mixing the appropriate DNA sample (final concentration varied) with the Au- or AuAg-nanoprobe solution (final concentration 2.5 nM or 0.05 nM, respectively), and by using 10 mM phosphate buffer (pH variable) to fulfill the final volume. A blank solution was prepared by replacing the DNA for an equivalent volume of 10 mM phosphate buffer.
2. The solutions were heated for 10 min at 95ºC and then allowed to cool down for 30 minutes at room temperature.

3. A concentrated salt solution (volume accordingly to type of salt) was added to the solutions to a final volume of 60 µL (or 30 µL).

4. UV-visible spectroscopic measurements and digital photographs were registered 15 minutes after salt addition.

2.2.2.5 Multiplex non-cross-linking hybridization assay

1. The protocol "Non-cross-linking hybridization assay" was followed, but instead of just adding just one nanoprobe, both Au- and AuAg-nanoprobes where mixed in solution.

2.2.2.6 Fluorescent assays

2.2.2.6.1 Determination of Au-nanoprobes' density (adapted from Sato *et al*.[82])

1. Thiol-modified oligonucleotides were displaced from the AuNPs' surface via addition of DTT (final concentration 100 mM) to 2.5 nM Au-nanoprobes in a total volume of 100 µL 1x TE.

2. Standard solutions were prepared by sequentially diluting (concentration range: 7.81 to 250 nM) an oligonucleotide harboring the same sequence as the Au-nanoprobes under the same conditions as Au-nanoprobes' samples.

3. After 48 h at room temperature, both standard and sample solutions were centrifuged at 21,460 g for 20 minutes and 50 µL of the supernatant were used to quantify the ssDNA in solution by using the Quant-iT™ OliGreen® ssDNA Assay kit accordingly to the manufacturer instructions.

2.2.2.6.2 Determination of Au-nanoprobes' hybridization efficiency (adapted from Demers *et al*.[81])

1. The Au-nanoprobe (final concentration 2.5 nM) was mixed with an excess of target oligonucleotide and fluorescein-modified oligonucleotide (final concentrations of 1 µM/each) in a total volume of 100 µl of 10 mM phosphate buffer (pH8). Other pH values were also tested for optimization.

2. After 10 minutes of denaturation at 95 °C, the solutions were allowed to hybridize for 30 minutes at room temperature.

3. The solutions were centrifuged at 21,460 g for 20 minutes and washed twice with 200 µL of 10 mM phosphate buffer (pH 8).

4. The precipitate was redispersed in 100 µL of 10 mM phosphate buffer (pH8).

5. Samples were denatured using sodium hydroxide (final concentration of 0.05 M) and let to rest for 2 h at room temperature.

6. Calibration curve was generated by preparing a sequential dilution of the fluorescein-modified oligonucleotide (concentration range: 0.0016 – 0.1 µM) under the same conditions as the samples.

7. Solutions were then centrifuged at 21,460 g for 20 min and 60 µL of the supernatant was taken to capture fluorescence spectra using an Ultra-Micro quartz cell.
8. To correct for loss of Au-nanoprobe during the washing process, 60 µL of 10 mM phosphate buffer (pH 8) were added to the pellet and the absorption spectra were registered using an Ultra-Micro quartz cell.

2.2.2.7 Other analysis

2.2.2.7.1 AFM analysis (sample preparation)

AFM analysis were carried out by Dr. Peter Eaton from REQUIMTE, Departamento de Química, Faculdade de Ciências, Universidade do Porto, 4169-007 Porto, Portugal, as described in Eaton *et al*.[148]

1. To prepare the AFM samples of DNA material alone (linearized plasmid and amplicons), all samples were precipitated with 1 volume of 100% (v/v) isopropanol, washed twice with 1 volume of 70% (v/v) ethanol and left to dry at room temperature to be later resuspended in a buffer suitable for deposition for AFM experiments as described by Eaton *et al*.[148]
2. To prepare the AFM samples of Au nanoprobes alone or with DNA, all the steps of the "Non-cross-linking hybridization assay" protocol, except for salt addition, were carried out.
3. The solutions were centrifuged for 25 minutes at 30,000 g and the supernatant was discarded.
4. The red oily pellet was then washed twice with 100 µL of ultra pure H2O and finally redispersed in 60 µL of the same water.

2.2.2.7.2 ICP analysis

Samples of alloy AuAgNPs were sent to Rede de Química e Tecnologia (REQUIMTE/CQFB), Caparica, Portugal, for ICP analysis. The samples were prepared by dissolving 5 mL of NPs in 5 mL of freshly prepared *aqua regia*. The original solution of *acqua regia* was used as baseline. Seven standard solutions of Au and Ag, with concentrations ranging from 1.25 to 100 mg/L, were used. Three independent measurements of each sample were registered with an Inductively Coupled Plasma-Atomic Emission Spectrophotometer equipped with a RF generator of 40.68 MHz and a type Czerny-Turner monochromator with 1.00 m (sequential).

2.2.2.7.3 TEM analysis

Samples of NPs were sent to Instituto de Ciência e Engenharia de Materiais e Superfícies (ICEMS/IST), Portugal, for TEM analysis. The samples were prepared by depositing 10 µL of the as-prepared colloidal suspensions in carbon copper grids, washing twice with 10 µL of

Milli-Q water, and air dried. TEM was performed with a HITACHI H-8100 microscope operated at 200 kV. Particle size and polydispersity were determined from the TEM pictures using the imaging software Carnoy 2.0, and by analyzing at least 100 NPs.

2.2.2.7.4 DLS analysis

The hydrodynamic diameter of the citrate capped AuNPs was determined by DLS using the Zetasizer Nano ZS system. A total volume of 500 uL of 2.5 nM AuNP was first stabilized for 15 minutes at 25ºC and then a total of 15 measurements with 13 runs each were registered. DLS analysis was performed either at Instituto de Medicina Molecular (IMM), Lisboa, Portugal or Instituto de Tecnologia Química e Biológica (ITQB), Oeiras, Portugal.

2.2.2.7.5 Zeta potential analysis

The samples of Au-nanoprobes alone and with ssDNA were prepared as in the "Non-cross-linking hybridization assay" protocol, except for replacing salt by 10 mM phosphate buffer (pH 8) and using an excess of target ssDNA (1 μM). The samples were let to stabilize for 15 minutes at 25ºC and then a total of 25 zeta potential measurements with 65 runs each were registered by using a Zetasizer Nano ZS system. Zeta potential analysis was performed either at Instituto de Medicina Molecular (IMM/UL), Lisboa, Portugal or Instituto de Tecnologia Química e Biológica (ITQB/UNL), Oeiras, Portugal.

2.2.2.7.6 Ferguson analysis

1. The samples of Au-nanoprobes alone and with ssDNA were prepared as in the "Non-cross-linking hybridization assay" protocol, except for substituting the salt with 10 mM phosphate buffer (pH 8) and using an excess of target ssDNA (1 μM).
2. The samples were then submitted to agarose gel electrophoresis with varying agarose percentages (1–3% w/v) using glycol (final concentration 2.5% v/v) as loading buffer.
3. Electrophoresis was performed for 2 hours at 4 V/cm in 0.5x TBE buffer, and the resulting electrophoretic pattern registered digitally using a white light transilluminator.
4. The positions of the bands were measured with Discovery Quantity One v.4.5.2 software using the center of the lane as reference and converted to an absolute mobility (M) velocity/field strength (cm^2/V.s) and Ferguson analysis was performed as described by Park *et al*.[149]

CHAPTER 3. Nanoprobes characterization

Characterization of the Au-nanoprobes stability against salt induced aggregation is a crucial step to develop the non-cross-linking method. In this chapter, the stability of the Au-nanoprobes to different salts, pH values and in the presence of some common reagents in molecular biology was evaluated. Moreover, the stability of AuAg-nanoprobes was also assessed to further develop a multiplex non-cross-linking method.

3.1 Introduction

The non-cross-linking method relies on the colorimetric changes of Au-nanoprobes, which is a consequence of differential stabilities in solution for increasing salt concentrations. Therefore, the characterization of Au-nanoprobe stability is a crucial step for the method's development. In the present work several studies have been carried out to evaluate the Au-nanoprobes stability in presence of different salts, at different pH values and in the presence of some common reagents used in DNA hybridization. Moreover, Au-nanoprobe stability has also been evaluated as function of functionalization protocol, i.e. the *classical* "salt-aging" protocol or by using ultrasounds.

In this chapter, as well as in subsequent chapters, all the general aspects between different nanoprobes (i.e. bGlob, DOR1 or CYP1846 probes) will be discussed as a whole, in order to simplify the evaluation and discussion of results. Nonetheless, the particular aspects of a particular nanoprobe will be highlighted when justified (e.g. when a nanoprobe behaves significantly different from other nanoprobes).

3.2 Results and Discussion

The stability of noble metal NPs, such as AuNPs, can be easily monitored by following their visible absorbance spectra, since the inter-particle distance between NPs strongly affects their SPR absorbance band due to plasmon coupling.[68] The SPR absorbance band of dispersed AuNPs shifts towards longer wavelengths when the inter-particle distance decreases. A common accepted process to determine the level of AuNPs aggregation is to follow the integral of the absorption curve in the range of 600-800 nm.[150,151] Nonetheless, this approach requires the acquisition of a full spectrum for each sample in that range of wavelengths, which could increase the time for data acquisition if multiple samples are to be analyzed (e.g. in most recent microplate readers, the spectra between 600-800 nm of 384 samples can take over 3 hours to acquire). Some authors have followed a single wavelength associated to the aggregated Au-nanoprobes to easily and quickly assess the level of aggregation[86] (e.g. a single wavelength absorbance of 384 samples takes just 1 minute to be registered by standard microplate readers). However, experimental error is associated to both approaches since the possible precipitation of Au-nanoprobes upon aggregation is not taken into consideration. Precipitation of Au-nanoprobes during data acquisition was frequently observed during the experimental procedures described in this Thesis, which can lower the absorbance of the aggregated Au-nanoprobes registered by the spectrophotometer, leading to a wrong interpretation of the observed aggregation. To overcome this problem, normalization was performed using absorbance of both single wavelengths that are characteristic of dispersed and aggregated nanoprobes - 526 nm and 600 nm for Au-nanoprobes; 460 nm and 635 nm for AuAg-nanoprobes. This normalization consists of a ratio between $Abs_{526nm\ or\ 460nm}$ and $Abs_{600nm\ or\ 635\ nm}$, where higher and lower ratio values are

associated to dispersed and aggregated nanoprobes, respectively. Moreover, because the AuNPs plasmon coupling upon aggregation does not significantly affect the absorbance at 400 nm (for Au-nanoprobes), or 340 nm (for AuAg-nanoprobes), it was used as an internal control to correct for absorbance shifts caused by phenomena that are not related to the nanoprobes SPR shift upon aggregation (e.g. precipitation, meniscus effect in the microplate reader, etc).

3.2.1 Au-nanoprobe stability

3.2.1.1 Salt effect

The stability of the Au-nanoprobes against salt-induced aggregation was first assessed for increasing concentrations of NaCl through the acquisition of spectrophotometric data at each 18 seconds for up to 30 minutes. Increasing NaCl concentrations had little or no effect on Au-nanoprobes until the CCC of electrolyte was reached. It should be noted that the CCC sometimes varied for different batches of the same probe, which may be associated to different Au-nanoprobe functionalization despite following the same experimental protocol. After the CCC was reached, the salt induced aggregation of the Au-nanoprobes which could be followed by the red-shift in the SPR band from 526 nm to 600 nm, corresponding to a color change of the solution from red to blue (Figure 3.1).

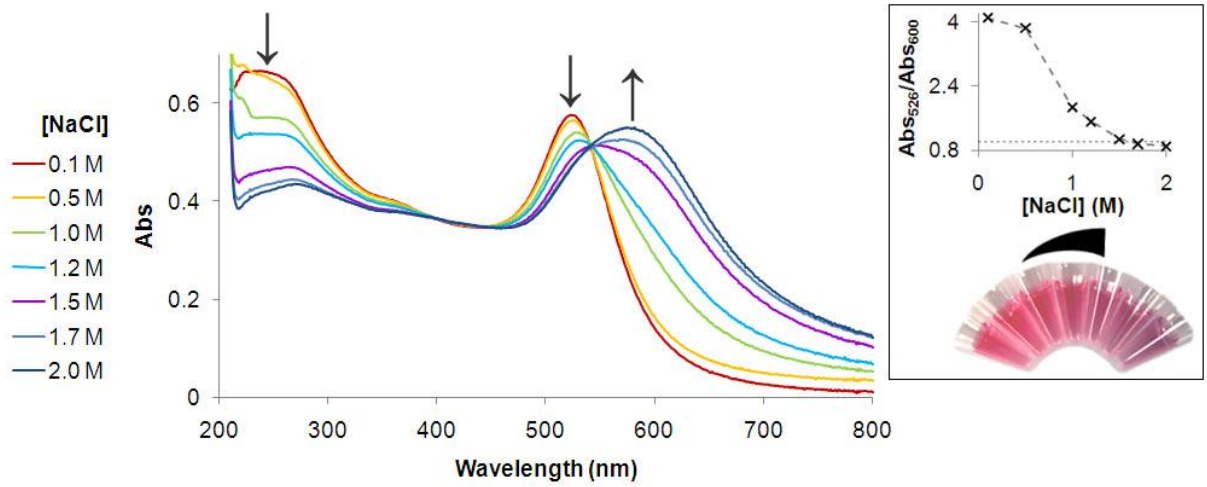

Figure 3.1 – Au-nanoprobe stability with increasing NaCl concentration. UV-visible spectra of Au-nanoprobes at different NaCl concentrations registered 15 minutes after salt addition. Arrows indicate peaks trend for increasing NaCl concentration. Inset: Ratio of Abs_{526}/Abs_{600} *vs.* NaCl concentration and the corresponding digital photos for increasing concentration of salt, from left to right.

The transition of color for increasing salt concentration can be translated by the ratio Abs_{526}/Abs_{600}, where fully aggregated Au-nanoprobes present a ratio >1 as denoted by the stabilization of the ratio value above CCC. Aggregation also causes a decrease in the absorbance of Au-nanoprobes' SPR band located in the UV region. As mentioned earlier, these spectrophotometric and colorimetric changes are a consequence of the plasmon

coupling between the AuNPs as the inter-particle distance diminishes and the Au-nanoprobes aggregate.[68]

The colorimetric changes resulting from Au-nanoprobe aggregation occur within the first 300 seconds (5 minutes) upon salt addition (Figure 3.2 - A), after which the changes to the spectra are minimal. For higher NaCl concentrations, at which the Au-nanoprobes fully aggregate, the colorimetric changes occur slightly faster (i.e. within 3 min).

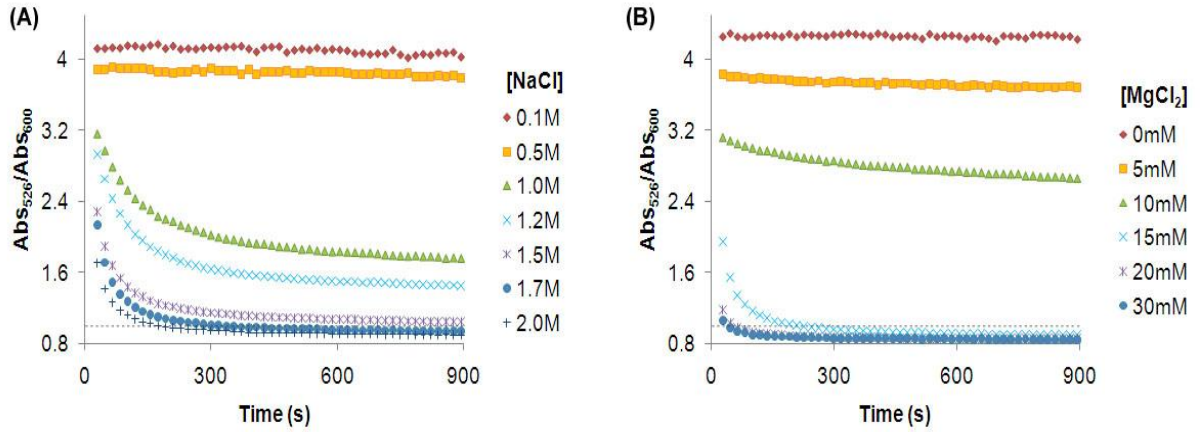

Figure 3.2 – Kinetics of Au-nanoprobe stability with increasing concentration of (A) NaCl or (B) $MgCl_2$

As previously mentioned, the CCC of electrolyte can vary with each Au-nanoprobe. In the case of NaCl, 20% of all the Au-nanoprobes synthesized within the scope of this thesis (n=35) were stable at NaCl concentrations up to 3 M. For higher concentrations, the large volumes of salt needed were incompatible with the assays' final volume. In other cases, the Au-nanoprobes aggregated between 0.5 and 3 M of NaCl, but the majority fully aggregated between 0.5 and 1.0 M NaCl (see Figure 3.3 - A). The stability of Au-nanoprobes synthesized by the classic "salt-aging" method show a significant variation in the CCC value for each batch of Au-nanoprobes (Figure 3.3 - B). This variation is greatly reduced when the Au-nanoprobes are synthesized using ultrasounds (Figure 3.3 - C).

Higher densities of thiol-modified oligonucleotides bound to the AuNPs surface have been associated with Au-nanoprobes with higher stability.[86] The observed variations in stability are, therefore, most likely associated to different Au-nanoprobe densities because the classic method is more prone to non-specific adsorptions that can lead to differences in functionalization.[85]

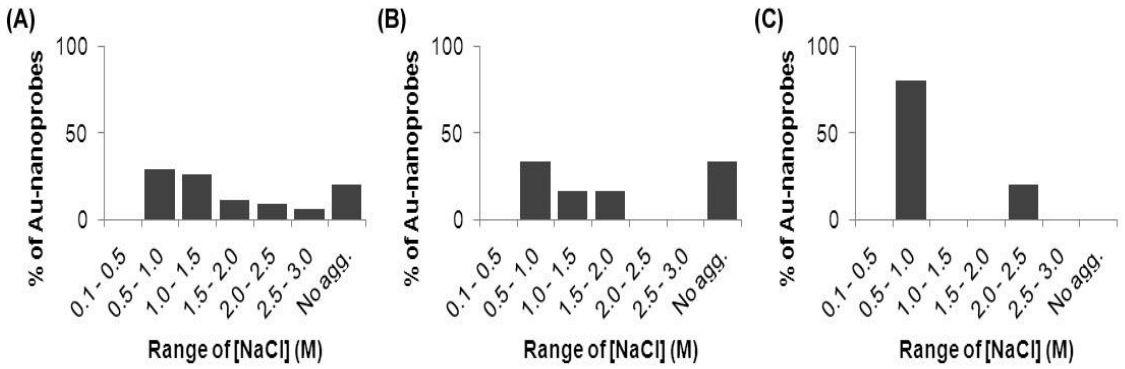

Figure 3.3 – Au-nanoprobes variability in stability with NaCl. Range of NaCl concentration that led to full aggregation of: **(A)** all Au-nanoprobes synthesized; or synthesized under the same conditions by **(B)** the classic "salt-aging" method; and **(C)** using ultrasounds. No agg. corresponds to the cases where no aggregation was observed with NaCl.

The stability of the Au-nanoprobes was also tested for increasing concentrations of other monovalent salts, namely KCl, LiCl and NH_4Cl. Aggregation patterns of the Au-nanoprobes are similar for any of these monovalent salts (Figure 3.4).

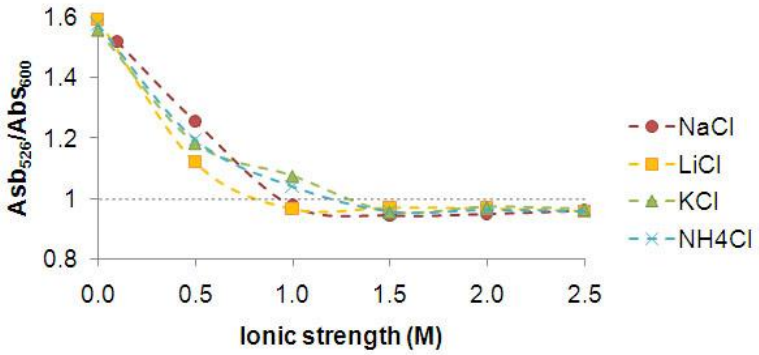

Figure 3.4 – Au-nanoprobe stability against increasing concentrations of monovalent salts

The stability of the Au-nanoprobes was also tested against increasing concentrations of divalent salts, namely $MgCl_2$, $MnCl_2$, $ZnCl_2$, $NiCl_2$ and $CaCl_2$. The use of such electrolytes allows higher ionic strengths to be attained with smaller volumes and concentrations of electrolyte solutions than those made possible by monovalent salts, thus allowing aggregation of Au-nanoprobes that was not possible with NaCl. In presence of only 10 mM of $MnCl_2$, $ZnCl_2$, $NiCl_2$ or $CaCl_2$, Au-nanoprobes immediately flocculated and solutions became opaque, while retaining their initial red color (Figure 3.5). This flocculation may be due to the existence of a secondary minimum in the DLVO profile of the Au-nanoprobes colloidal system and/or due to the coordination of the divalent metal cations (Mn^{2+}, Zn^{2+}, Ni^{2+} and Ca^{2+}) with the Au-nanoprobes' ssDNA, which can lead to the formation of a cross-linked structure.[152] In the latter, it would be expected that the Au-nanoprobes also have changed color from red to blue, which did not occur even after several days. Nonetheless, since the

flocculation generated by these salts hampered the acquisition of spectrophotometric data, their use for subsequent studies and for the development of the non-cross-linking detection method was not further considered.

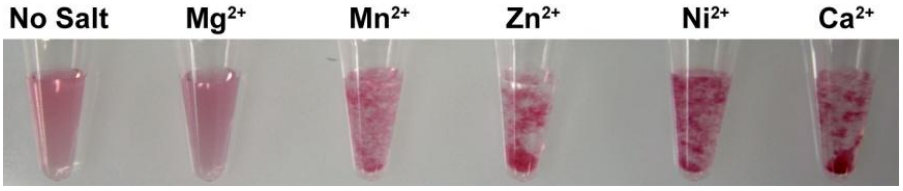

Figure 3.5 - Influence of $MgCl_2$, $MnCl_2$, $ZnCl_2$, $NiCl_2$ or $CaCl_2$ in Au-nanoprobe stability. Digital photography of Au-nanoprobes alone and in presence of 10 mM divalent salt ($MgCl_2$, $MnCl_2$, $ZnCl_2$, $NiCl_2$ and $CaCl_2$, respectively).

Interestingly, no flocculation was observed for $MgCl_2$. This can be explained by the lower effectiveness of Mg^{2+} in coordinating a DNA structure when compared to the other divalent cations.[152] As observed for the monovalent salts, $MgCl_2$ led to extensive Au-nanoprobe aggregation, and their SPR band shifted from 526 nm to 600 nm with concomitant change of color from red to blue (Figure 3.6). In this case, the color change was more intense than that observed with monovalent salts, as denoted by a slightly higher absorbance at 600 nm and, consequently, lower Abs_{526}/Abs_{600} ratio (0.91 and 0.85 for 2 M NaCl and 30 mM MgCl2, respectively).

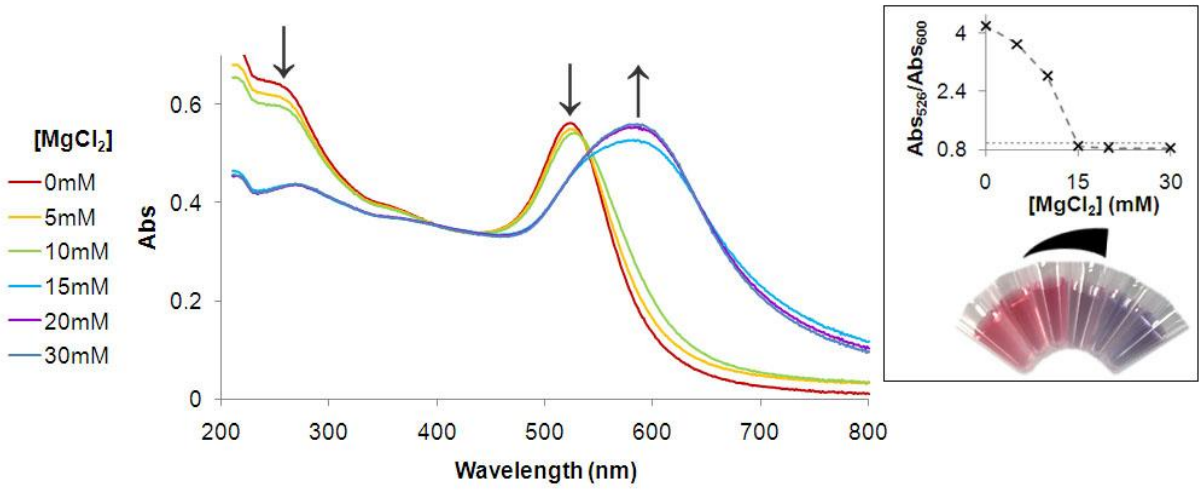

Figure 3.6 – Au-nanoprobe stability with increasing $MgCl_2$ concentration. UV-visible spectra of Au-nanoprobes at different $MgCl_2$ concentrations registered 15 minutes after salt addition. Arrows indicate peaks trend for increasing $MgCl_2$ concentration. Inset: ratio of Abs_{526}/Abs_{600} vs. $MgCl_2$ concentration and the corresponding digital photos for increasing concentration of salt, from left to right.

The majority of the Au-nanoprobes synthesized, that were tested with $MgCl_2$ (n=27), aggregated between 10 ~ 20 mM (63%) of $MgCl_2$, while other Au-nanoprobes aggregated

between 20 ~ 30 mM (26%) or 30 ~ 40 mM (11%) of $MgCl_2$. These CCC values of $MgCl_2$ are much lower than those observed for monovalent salts, even when compared in terms of their ionic strengths. Nonetheless, when comparing the CCC ratio value of monovalent and divalent salts obtained for the same Au-nanoprobes, the average of $CCC_{monovalent}$:$CCC_{divalent}$ ratio is 1:0.0158 (STD=±1:0.0066), which is in good agreement with the ratio predicted by the Schulze-Hardy rule (i.e. 1:0.0156).[96] This indicates that, as predicted by the DLVO theory, the main forces involved in the dispersion stability of the Au-nanoprobes are both attractive van der Waals forces and repulsive double-layer electrostatic forces.

3.2.1.2 pH effect

All the previous salt stability tests were performed at pH 8. However, since the charge of DNA is strongly dependent on the pH, it was hypothesized that the stability of the Au-nanoprobes could also change with pH. In fact, it has been recently demonstrated that Au-nanoprobes are stable between pH 4 and pH 12 and aggregate outside this range.[153] Because DNA hybridization occurs only between a narrow range of pH values (6.5 - 8),[154] which is an important factor for the development of the non-cross-linking method, the effect of pH in Au-nanoprobe stability in salt-induced aggregation has not been thoroughly investigated outside this range. Within this range, the effect of pH in salt-induced (increasing concentrations of NaCl or $MgCl_2$) aggregation of the Au-nanoprobes was assessed after washing and re-dispersing them in 10 mM phosphate buffer at different pH (6.5, 7, 7.5 and 8 – actual values were determined using a pH potentiometer). Results show that the Au-nanoprobes' stability in relation to salt-induced aggregation remained unaltered between pH 7.64 and pH 8.16 (Figure 3.7), and started to aggregate for lower pH values. This decrease in stability is most likely associated to the decrease of the negative charge of DNA molecules, as the solution pH approaches the isoelectric point of ssDNA (pI 4.0~4.5).

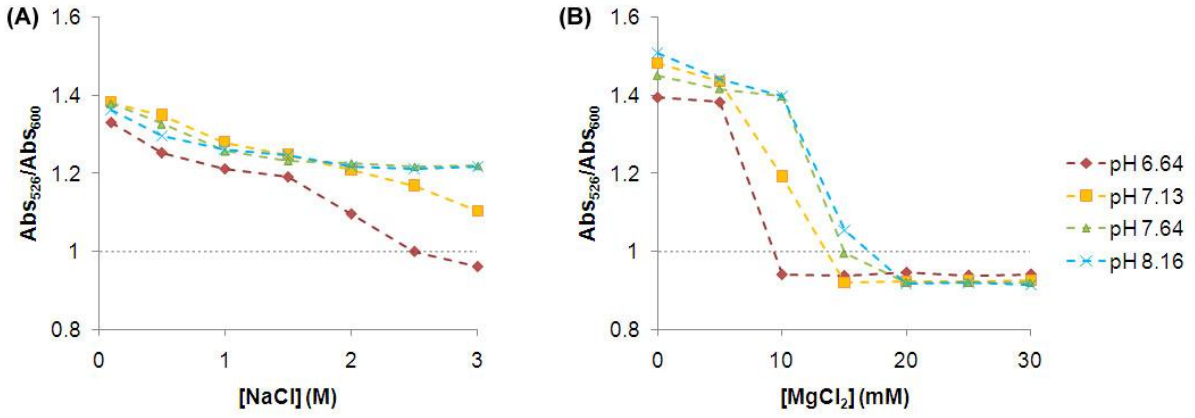

Figure 3.7 – Effect of pH in Au-nanoprobe stability against salt-induced aggregation by (A) NaCl or (B) $MgCl_2$

3.2.1.3 Au-nanoprobe concentration effect

All the previous stability tests were performed with a final concentration of 2.5 nM Au-nanoprobes, at which the associated color can be easily seen by the naked eye. Nonetheless, the salt-induced aggregation of Au-nanoprobes may be affected by their concentration in solution as this influences the probability of Au-nanoprobes' self-interaction due to Brownian motion. To test this hypothesis, a set of different Au-nanoprobe concentrations (0.5 to 5 nM) was tested at the highest NaCl concentration (2 M NaCl) and the aggregation kinetics followed by UV-visible spectrophotometry. Results show that full aggregation only begins to occur for Au-nanoprobe concentrations above 2 nM, as the SPR spectra profile no longer changes above this concentration (Figure 3.8). Moreover, the changes in the SPR spectra of Au-nanoprobes stabilized within 5 minutes upon salt addition for all Au-nanoprobes concentrations.

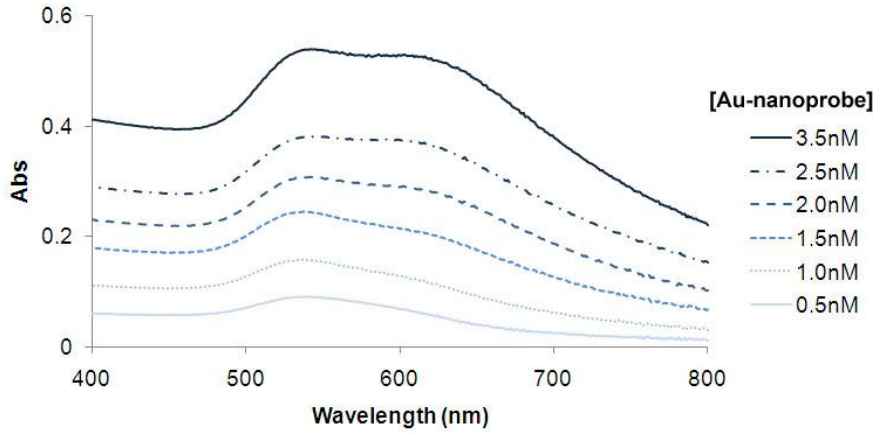

Figure 3.8 – Au-nanoprobe concentration effect in salt-induced aggregation. Spectra of Au-nanoprobe taken 15 minutes upon the addition of 2 M NaCl at different Au-nanoprobe concentrations.

These results seem to support the idea that Au-nanoprobe aggregation is hindered by lower concentrations that reduce interaction between Au-nanoprobes. Also, it indicates the existence of a minimum Au-nanoprobe concentration at which the Au-nanoprobes' SPR band completely changes at 600 nm. Considering these results, all other assays where performed using a final concentration of 2.5 nM Au-nanoprobes.

3.2.1.4 Effect of other reagents commonly used in molecular biology

The stability of the Au-nanoprobes was also tested for reagents that are commonly used in molecular biology to facilitate DNA hybridization and increase stringency (e.g. betaine, DMSO, methanol and formamide). These reagents can also be present in the biological samples to be tested, such as a PCR product of GC-rich template (e.g. DOR1 gene), and therefore it is important to anticipate their effect in Au-nanoprobe stability.

The concentrations of the tested reagents were chosen according to what is normally used in molecular biology and as far as the added volumes allowed. Assays were performed only with $MgCl_2$ in order to allow the larger volumes of other reagents. In the presence of DMSO, a polar aprotic solvent, the Au-nanoprobes stability decreased with a concentration of 0.5% DMSO (Figure 3.9 - A). This decrease in stability is most likely due to the changes in the dielectric constant of the medium surrounding the Au-nanoprobes, as DMSO has a lower dielectric constant than water. This leads to a decrease in the double-layer thickness that is responsible for the electrostatic repulsion between Au-nanoprobes (see Eq. 3 in Chapter 1, section 1.2.3.3). Moreover, the aprotic nature of DMSO should also favor the creation of dipole moments that can help facilitate the Au-nanoprobes aggregation.

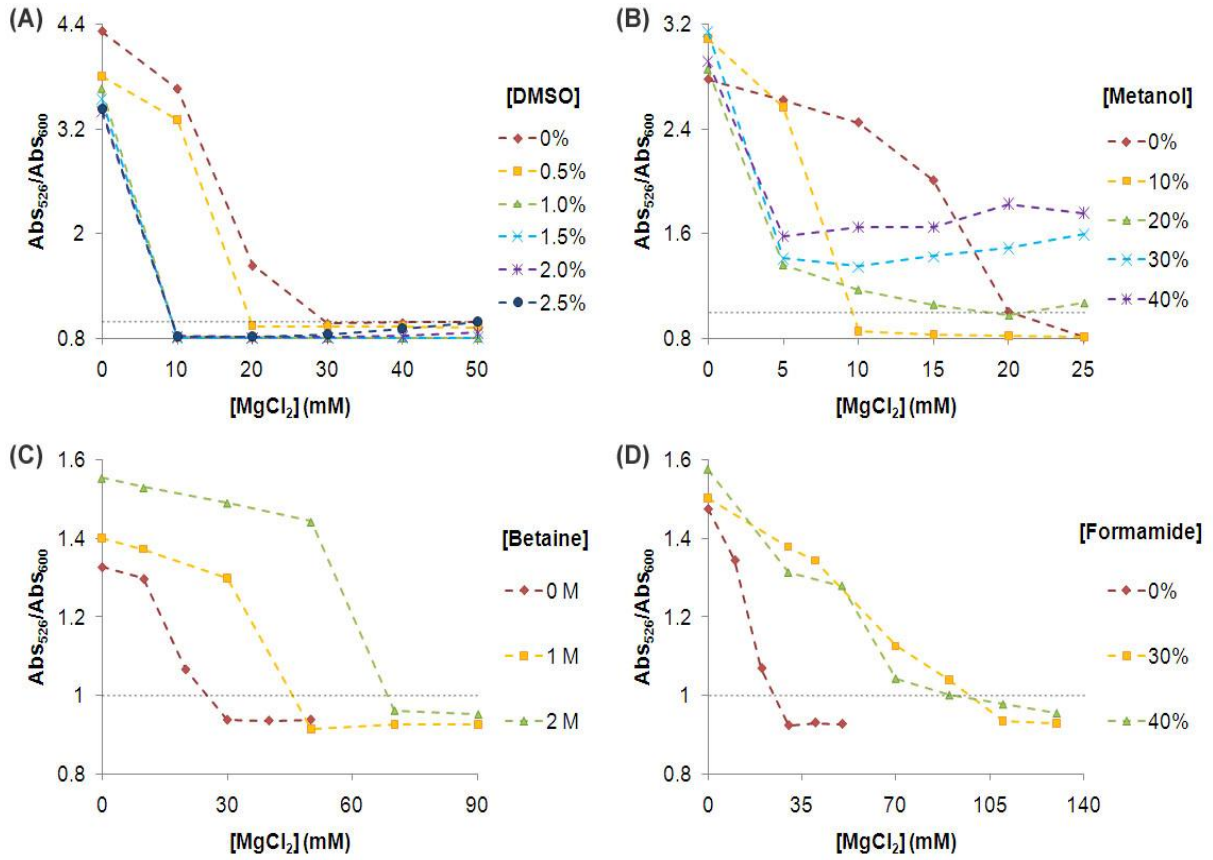

Figure 3.9 – Au-nanoprobe stability against salt-induced aggregation in presence of (A) DMSO, (B) Methanol, (C) Betaine or (D) Formamide.

The stability of the Au-nanoprobes also decreased in the presence of methanol (Figure 3.9 – B), where the CCC of $MgCl_2$ decreased by half for 10% methanol. Similarly to DMSO, methanol also has a lower dielectric constant than water, and, therefore, the increase in methanol concentration leads to a decrease in the repulsive electrostatic forces that prevent Au-nanoprobe aggregation. However, for higher concentrations of methanol, the Au-nanoprobes de-stabilization started to reverse with increasing concentrations of $MgCl_2$. This

strange effect can be due to a decrease in $MgCl_2$ solubility with increasing methanol concentrations, decreasing the effective $MgCl_2$ concentration in solution.

Contrary to what has been observed for DMSO and methanol, both betaine and formamide increased the stability of Au-nanoprobes against salt-induced aggregation. In presence of betaine, Au-nanoprobe stability increased up to 2 M betaine. In the case of formamide, Au-nanoprobe stability also increased in the presence of 30% formamide, but remained unaltered with a further increase to 40%. In both cases, the increased stability may be due to their adsorption to the AuNPs surface mediated by their amine group.

3.2.1.5 Probe density effect

To confirm the hypothesis that the variations in CCC values between Au-nanoprobes was due to different densities of thiolated oligonucleotide on the AuNP surface, a set of Au-nanoprobes was synthesized using the ultrasound protocol with increasing ratios of oligos/AuNP at different final concentrations of the electrolyte during the salt aging step. Densities of thiolated oligonucleotides were determined by fluorescence measurements after displacement of the thiol-modified oligonucleotide with DTT (Table 4.1) – see Chapter 2, section 2.2.2.6.1.

Table 3.1 – Au-nanoprobes density in pmol/cm^2 according to the ratio of oligos/AuNP and NaCl concentration during synthesis (average±STD)

		Final NaCl concentration during salt aging		
		0.1 M	**0.3 M**	**0.7 M**
Ratio of added oligos/AuNPs	**25**	Agg.[a]	Agg.[a]	-[b]
	50	5.3±1.6	8.2±1.5	-[b]
	100	11.0±1.7	24.0±1.3	-[b]
	200	11.6±1.5	25.1±3.0	-[b]
	400	-[b]	-[b]	35.5±1.9
	600	-[b]	-[b]	39.9±1.5

[a]Au-nanoprobes aggregated during synthesis; [b]conditions where not tested

Au-nanoprobes' density increased considerably with the increase of electrolyte concentration during "salt-aging" process. This can be explained by the neutralization of non-specific binding.[85] The amount of thiol-modified oligonucleotides added during the synthesis also affected the final Au-nanoprobe density, although in a lesser extent than the electrolyte variation. The stability to NaCl and $MgCl_2$ of Au-nanoprobes with different densities was then tested (Figure 3.10).

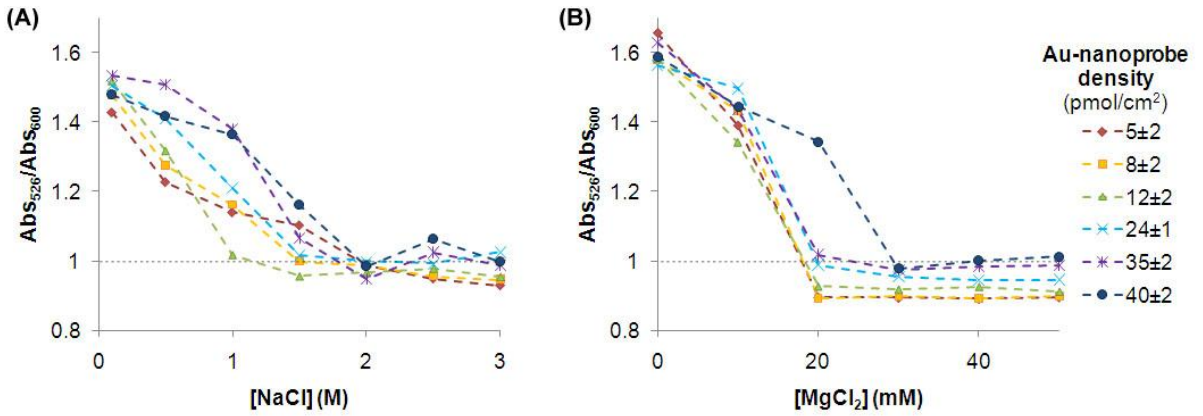

Figure 3.10 – Effect of Au-nanoprobe density in salt-induced aggregation by (A) NaCl or (B) $MgCl_2$

The Au-nanoprobes with lower oligonucleotide densities fully aggregated between 1 and 1.5 M NaCl, while Au-nanoprobes with higher densities only started to fully aggregate at 2 M NaCl (Figure 3.10 - A). On the other hand, all Au-nanoprobes aggregated with 20 mM $MgCl_2$, with exception of the Au-nanoprobe with the highest density, i.e. 40±2 pmol/cm^2 (Figure 3.10 – B). In this case, the Au-nanoprobe only fully aggregated with 30 mM $MgCl_2$. These results indicate that the Au-nanoprobe density slightly influences the stability of Au-nanoprobes, and only more intensively at higher densities. This is partially corroborated by the previous work of Mirkin and co-workers, where evidence for Au-nanoprobe stability dependence on the derivatized oligonucleotide density was demonstrated.[86]

3.2.2 AuAg-nanoprobes stability

Taking benefit from the enhanced optical properties of silver NPs and the gold availability to thiol- quasi-covalent adsorption, ~40 nm Au/Ag (0.49/0.51 ratio) alloy NPs were synthesized and functionalized with thiol-modified DNA oligonucleotides (AuAg-nanoprobes) – see Appendix III for TEM and ICP analysis of AuAgNPs. The chosen oligonucleotide sequences to functionalize these NPs were the bGlob and DOR1C probe sequences. The characterization of AuAg-nanoprobes stability is crucial to evaluate their potential application in the non-cross-linking method and the development of a multiplex approach. Therefore, the stability of such NPs and nanoprobes against increasing concentrations of NaCl, or $MgCl_2$, was assessed. Additional studies involving the synthesis and stability of AuAg-nanoprobes were the subject of the work of Jorge Dias (MSc thesis[155]), and, therefore, not addressed in the present thesis.

3.2.2.1 Salt effect

The AuAg-nanoprobes presented a higher stability against salt-induced aggregation than AuAgNPs alone. The AuAgNPs immediately aggregated with 50 mM NaCl whereas AuAg-nanoprobes remained unaltered at the same concentration. This increase in stability is due to

the derivatized oligonucleotides that, similarly to the Au-nanoprobes, provide a higher electrostatic repulsion between NPs. The stability of AuAg-nanoprobes against salt-induced aggregation was further studied in the presence of NaCl and $MgCl_2$ at pH 8. The resulting colorimetric changes were registered 15 minutes after salt addition so as to better compare results with the Au-nanoprobes.

The AuAg-nanoprobes (0.05 nM concentration) remained unaltered for NaCl concentrations of up to 0.5 M (Figure 3.11). For higher concentrations of NaCl, the SPR band peak of the AuAg-nanoprobes, originally located at 460 nm, started to decrease and a wider band started to appear between 500 and 800 nm, with a broad peak at around 635 nm. To the naked eye, a color change from yellow to grey was observed as a consequence of AuAg-nanoprobe aggregation.

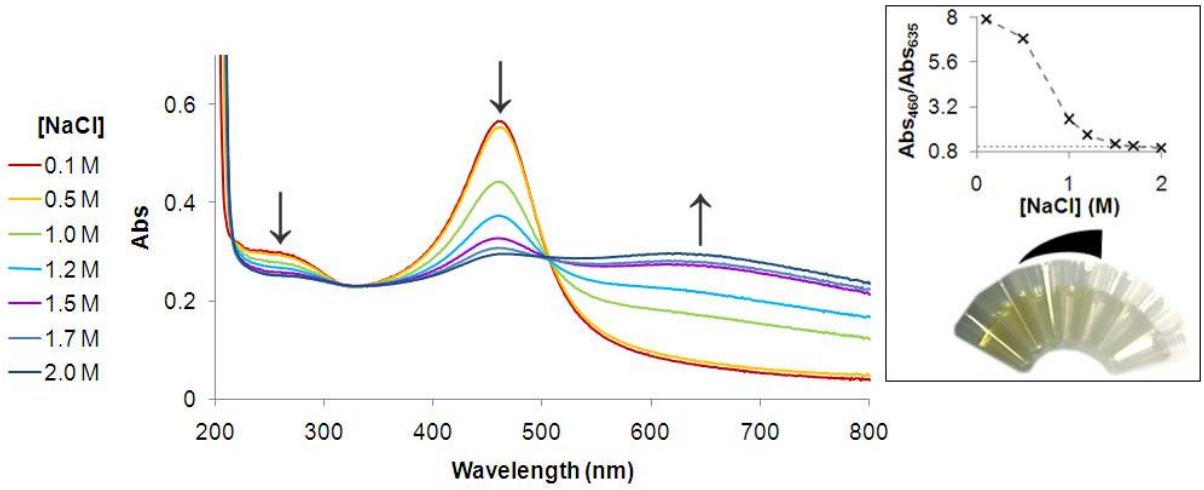

Figure 3.11 – AuAg-nanoprobe stability with increasing NaCl concentration. UV-visible spectra of 0.05 nM AuAg-nanoprobes at different NaCl concentrations registered 15 minutes after salt addition. Arrows indicate peaks trend for increasing NaCl concentration. Inset: Ratio of Abs_{460}/Abs_{635} *vs.* NaCl concentration and the corresponding digital photos for increasing concentration of salt, from left to right.

Full aggregation was attained for NaCl concentrations of 1.5 M and higher, as no further spectrophotometric changes in the SPR band were observed. The values of the Abs_{460}/Abs_{635} ratio associated to full aggregation were all below 1, similar to what is observed for the Au-nanoprobes. Apart from the visible colorimetric changes, it was also possible to observe a slight decrease in the SPR band located in the UV region of the spectrum, as a consequence of AuAg-nanoprobes salt-induced aggregation. Nonetheless, this decrease was much less pronounced than that of the Au-nanoprobes.

AuAg-nanoprobes were significantly stable up to 10 mM of $MgCl_2$ (Figure 3.12) and full aggregation was reached between 20 ~ 30 mM of $MgCl_2$. The SPR spectrum changes

induced by this divalent salt were similar to those observed for NaCl, although more pronounced with increasing salt concentration.

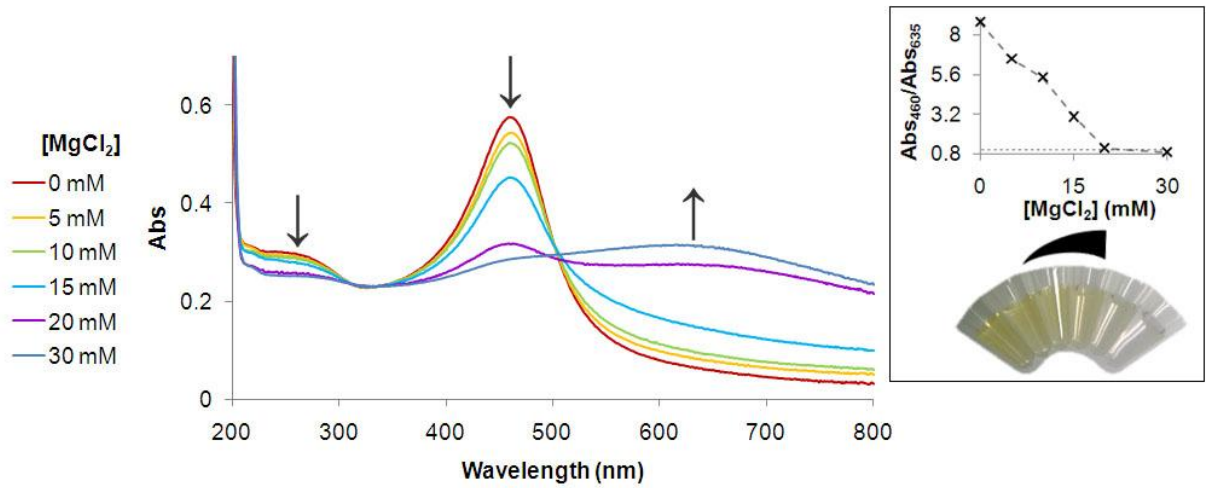

Figure 3.12 – AuAg-nanoprobe stability with increasing $MgCl_2$ concentration. UV-visible spectra of 0.05 nM AuAg-nanoprobes at different $MgCl_2$ concentrations registered 15 minutes after salt addition. Arrows indicate peaks trend for increasing $MgCl_2$ concentration. Inset: Ratio of Abs_{460}/Abs_{635} *vs.* $MgCl_2$ concentration and the corresponding digital photos for increasing concentration of salt, from left to right.

The ionic strength of NaCl needed to induce aggregation of AuAg-nanoprobes was much higher than the ionic strength of $MgCl_2$ needed for the same effect, as it was observed for the Au-nanoprobes. However, the $CCC_{monovalent}$:$CCC_{divalent}$ ratio obtained for the AuAg-nanoprobes is 1:0.0133, which is near the ratio predicted by the Schulze-Hardy rule (i.e. 1:0.0156).[96] The slight difference between the experimental ratio and the Schulze-Hardy ratio may be due to a coordination effect of Mg^{2+} cation with the functionalized AuAg-nanoprobe DNA. Nonetheless, further studies with different batches of AuAg-nanoprobes are needed to determine a more exact experimental ratio and compare it with the Schulze-Hardy ratio.

3.3 Conclusions

It was possible to induce Au-nanoprobe aggregation with increasing concentrations of salt, which can be followed by naked eye (color change from red to blue); and/or by UV-visible spectrophotometry, due to the SPR red-shift (from 526 to 600 nm). The majority of the Au-nanoprobes aggregated within 15 minutes in the presence of 1 M of any of the tested monovalent salts (i.e. NaCl, KCl, LiCl and NH_4Cl) or in the presence of 20 mM $MgCl_2$. In the presence of other divalent salts (i.e. $MnCl_2$, $ZnCl_2$, $NiCl_2$ and $CaCl_2$) the Au-nanoprobes flocculated and the solution turned opaque, impeding the assessment of the eventual colorimetric changes. Therefore, for the development of the non-cross-linking method, only

NaCl and $MgCl_2$ were considered. $MgCl_2$ showed an additional advantage due to the low concentrations needed and, hence, low volumes used to induce Au-nanoprobe aggregation. This can be extremely useful when testing diluted biological samples or when additional reagents are needed. However, $MgCl_2$ should be used carefully since it may induce some cross-linking aggregation by coordination of the nanoprobes' DNA. Results have shown that the Schulze-Hardy rule can be used to predict the CCC value of monovalent or divalent salt associated with a particular nanoprobe, provided that a salt-induced stability study is performed with at least one of the salts.

The stability of the Au-nanoprobes also decreased for pH values below 7.5 and in the presence of increasing concentrations of DMSO or methanol. Conversely, stability increased with betaine or formamide. This should be taken into account when selecting the hybridization conditions, such as reagents for DNA hybridization or when already present in the biological sample to be tested.

Full aggregation of Au-nanoprobes was also hindered by concentrations of Au-nanoprobe below 2 nM and for that reason a concentration of 2.5 nM was used herein.

Au- and AuAg-nanoprobes presented similar stabilities against salt-induced aggregation, showing that both may be used for the development of non-cross-linking based methodologies for nucleic acid detection.

The synthesis of Au-nanoprobe using ultrasounds allowed for better reproducibility between batches, when considering the variations of the CCC value associated to all Au-nanoprobes. This allows to better predict the CCC value of new batches and also synthesize the Au-nanoprobes faster than when following the classical "salt-aging" method. Hence, the ultrasound method was elected as the preferred method for the synthesis of nanoprobes.

CHAPTER 4. Using the Non-cross-linking method for SNP detection

The colorimetric properties of Au-nanoprobes have led to the development of a new class of nanobiosensors able to recognize and detect specific DNA and/or RNA sequences. A simple, easy-to-perform and inexpensive colorimetric assay for specific DNA sequence detection has been developed by our group based on the differential non-cross-linking aggregation of Au-nanoprobes. This chapter describes further developments to this non-cross-linking method towards detection of single base mutations/SNPs. Preliminary work for the development of a multiplex non-cross-linking method has also been addressed via combination of Au- and AuAg-nanoprobes.

4.1 Introduction

A simple non-cross-linking colorimetric method for specific DNA/RNA sequence detection has been being developed by our group.[91,103] The method is based on a non-cross-linking hybridization, where aggregation of the Au-nanoprobes is induced by an increasing salt concentration – the presence of complementary target prevents aggregation and the solution remains red, while non-complementary targets do not prevent Au-nanoprobe aggregation resulting in a visible change of color from red to blue. This approach has been successfully applied to detect eukaryotic gene expression from only 0.3 μg of unamplified total RNA without retro-transcription or PCR amplification[91] and in a fast and straightforward assay for *Mycobacterium tuberculosis* DNA detection in clinical samples at a final concentration of 36 ng/μL of a first-round PCR amplicon.[103]

Herein, the potential of this colorimetric method has been further explored in the detection of SNP/single-base mutations in DNA samples. As proof-of-concept, common point-mutations in the β-globin gene responsible for β-thalassemia were used. Afterwards, the method was further extended and optimized for the characterization of other SNPs targets: CYP2D6, associated to the level of xenobiotic metabolism, and DOR1, associated to obesity and Type 2 diabetes. Following optimization of SNP characterization via Au-nanoprobes, specific DNA target detection was also achieved by means of AuAg-nanoprobes. Combining these two types of nanoprobes a multiplex (dual-color) non-cross-linking method has been developed.

4.2 Results and Discussion

4.2.1 Au-nanoprobes

4.2.1.1 SNP/mutation detection: Proof-of-concept (work published in Doria G, *et al.*[156])

An Au-nanoprobe - bGlob - overlapping a region of the β-globin gene harboring three different single-point mutations causing β-thalassemia was used for the proof-of-concept of SNP/single point mutations detection via the non-cross-linking method (see Figure 2.1 in Chapter 2, section 2.1.5.5.2). To test the bGlob Au-nanoprobe, hybridization using a 396 bp fully complementary target or a 355 bp non-complementary target was performed. Three assay solutions were prepared: “Blank” – Au-nanoprobe alone; “Comp” – Au-nanoprobe in the presence of the complementary target; “Non-comp” – Au-nanoprobe in the presence of the non-complementary target. Additionally, a fourth solution (“No salt”) with the Au-nanoprobe alone without salt (substituted by 10 mM phosphate buffer) was used. The assay was performed in triplicate, photographs taken and visible spectra recorded.

After hybridization and upon salt addition, within 15 minutes, both “Blank” and “Non-comp” solutions changed color from red to blue (Figure 4.1). The color changes were corroborated by visible spectra, where an intense plasmon resonance band appears at 600–650 nm, with a concomitant decrease of the intensity of the original plasmon resonance at 526 nm.

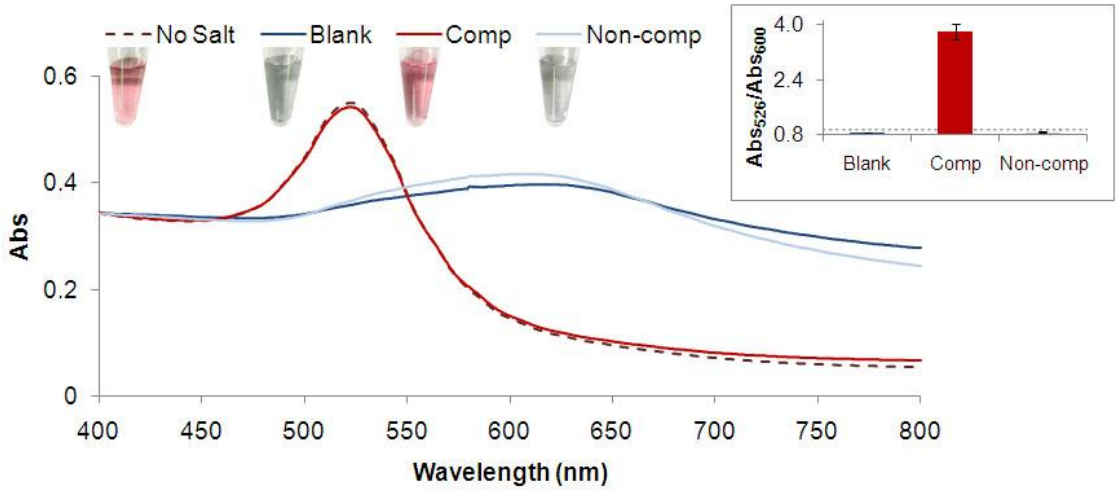

Figure 4.1 – bGlob Au-nanoprobe aggregation profiles. UV-vis spectroscopy data and photos of samples after 15 minutes incubation with [NaCl]= 2 M (except "No Salt"). Final DNA concentration of 36 ng/µL. Inset: Average Abs_{526}/Abs_{600} ratio with corresponding standard deviation of three independent assays; dashed line indicates a ratio value of 1.

In contrast, the "Comp" solution remained unaltered as confirmed by comparison with the "No salt" solution. These results were reproducible and concordant with those described earlier by the group for *M. tuberculosis* detection.[103] Similar results were obtained by using a plasmid (p158 plasmid) or a larger amplicon (1559 bp) as complementary targets. In this case, hybridization was also directly observed by AFM (see Chapter 5, section 5.2.1).[148]

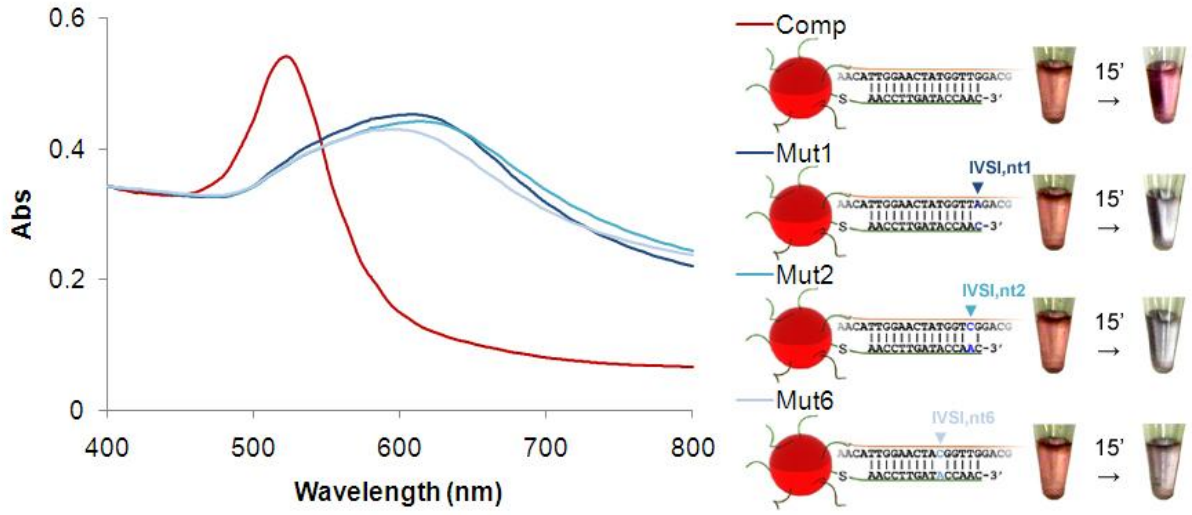

Figure 4.2 - Mutation/SNP detection. UV-Vis spectroscopy data of samples after 15 minutes incubation with [NaCl] = 2 M. Samples are Au-nanoprobe in presence of: a DNA from normal β-globin gene ("Comp"); a DNA harboring a single-point mutation IVS1, nt1 on the β-globin gene ("Mut1"); a DNA harboring a single-point mutation IVS1, nt2 on the β-globin gene ("Mut2"); and a DNA harboring a single-point mutation IVS1, nt6 on the β-globin gene ("Mut6"). The panel on the right shows the relative position of the mutation within the bGlob Au-nanoprobe sequence, marked by an inverted triangle.

Having confirmed the viability of the bGlob Au-nanoprobe to hybridize and detect a complementary target sequence, the assay was performed with three other 355 bp amplicons obtained by PCR amplification of genomic DNA samples previously screened for the presence of the β-thalassemia mutations. Figure 4.2 shows the spectrophotometric changes 15 min after increasing NaCl concentration to 2 M, in solutions containing bGlob Au-nanoprobe in presence of fully complementary target ("Comp") or in presence of targets harboring the mismatches at different positions within the region of overlap ("Mut1", "Mut2" and "Mut6").

The bGlob Au-nanoprobe clearly distinguishes between fully complementary target sequences and the presence of any of the three single-base mutations. The mismatched targets did not prevent Au-nanoprobe aggregation and the solutions changed from red to blue, as it happens with non-complementary sequences. This assay was repeated at least four times. Even though most assays exhibited a clear color distinction between complementary and mismatched samples, best reproducibility of the assay was achieved with DNA concentrations between 18 and 36 ng/µl. Below that range, the difference in color between complementary and mismatched targets was not discriminating.

As previously reported, nucleic acid sequences seem to protect AuNPs against salt induced aggregation, possibly through the electrostatic interactions between the negatively charged phosphate groups on the nucleic acid backbone.[91,103] This could explain the differences in aggregation observed for "Comp" against "Non-comp" and "Mismatched" samples. Although the presence of nucleic acid in solution may act as a "buffer" for increasing ionic strength, thus potentiating the stabilization of Au-nanoprobe in the non-aggregated form, it does not prevent aggregation at high ionic strengths when non-complementary targets are used. On the other hand, the increased stability observed for the complementary target can be explained by the fact that the full length of the Au-nanoprobe has hybridized with the complementary target DNA sequence. In the end, the resulting duplex is what actually prevents the salt induced aggregation. Destabilization of the duplex derived from the mismatch in the sequence, leads to Au-nanoprobe aggregation, and the level of such aggregation might be dependent on the position of the point mutation. In fact, this destabilization effect at room temperature was confirmed by fluorescence assays which indicate that a higher number of fully complementary targets hybridize to the Au-nanoprobe than mismatched targets, and that this difference is dependent on the mismatch position (see Chapter 5, section 5.2.2.2).

In conclusion, these results prove that the non-cross-linking method is suitable to detect SNP/single point mutations in nucleic acid sequences, such as PCR amplicons. To further analyze the versatility of the non-cross-linking SNP/mutation detection, other SNP targets were assessed.

4.2.1.2 Extending the method to other targets (DOR1 and CYP1846 SNPs)

As previously mentioned, a set of Au-nanoprobes were designed to detect SNPs within the CYP2D6 gene (i.e. CYP1846G and A probes) and the DOR1 gene (i.e. DOR1C and DOR1G probes). In each case, two Au-nanoprobes were designed to detect each possible allele, thus allowing characterization of homo- and heterozygous samples. In the case of CYP2D6, the CYP1846G and CYP1846A Au-nanoprobes are fully complementary to the CYP2D6*1 and CYP2D6*4 alleles, respectively. In the case of DOR1, the DOR1C and DOR1G Au-nanoprobes are fully complementary to the DOR1C and DOR1G alleles, respectively.

Following a similar approach to that used for the bGlob Au-nanoprobe, assays were performed with PCR amplified targets complementary, mismatched and non-complementary to each Au-nanoprobe, at a final DNA concentration of 36 ng/µL. Contrary to what it had been previously observed in the proof-of-concept upon the addition of increasing concentration of salt (NaCl or $MgCl_2$), solutions changed color from red to blue, even in presence of complementary targets. However, an assay for the CYP1846G and CYP1846C Au-nanoprobes, complementary solutions were partially stable as indicated by a faint red solution and the Abs_{526}/Abs_{600} value above 1 (Figure 4.3). The corresponding mismatched solutions were also stable, but less than solutions with the complementary targets. Taken together, these results indicate a low reproducibility that needs to be addressed in future optimizations.

The difficulty in complementary target hybridization might be due to sub-optimal hybridization conditions (i.e. high stringency), such as low salt concentration and high pH during hybridization. Additionally, the targets' %GC composition can also justify the discrimination observed for the bGlob and not for the DOR1 and CYP2D6 targets – 52%, 76% and 66%, respectively. DNA targets with high %GC contents are known to form stable secondary structures that are resistant to denaturation and, consequently, hamper probe hybridization.[157]

To try circumventing these issues, the non-cross-linking hybridization was performed in less stringent conditions (i.e. higher salt concentrations and lower pH values) and/or in the presence of reagents that facilitate DNA hybridization (i.e. DMSO, formamide, methanol and betaine). The tested salt concentrations for hybridization varied from the initial 17 mM (added with the Au-nanoprobe volume) up to 500 mM of NaCl; pH varied between 7 and 8; DMSO concentrations up to 2.5% (v/v); betaine concentrations up to 2 M; formamide concentrations up to 40% (v/v); and methanol concentrations were tested up to 10% (v/v). Other conditions of salt and reagents were prohibited either due to Au-nanoprobe destabilization/aggregation, in high concentrations (see Chapter 3, section 3.2.1.4), or to volume limitations. Additionally, the hybridization period before salt addition was extended up to 16 hours.

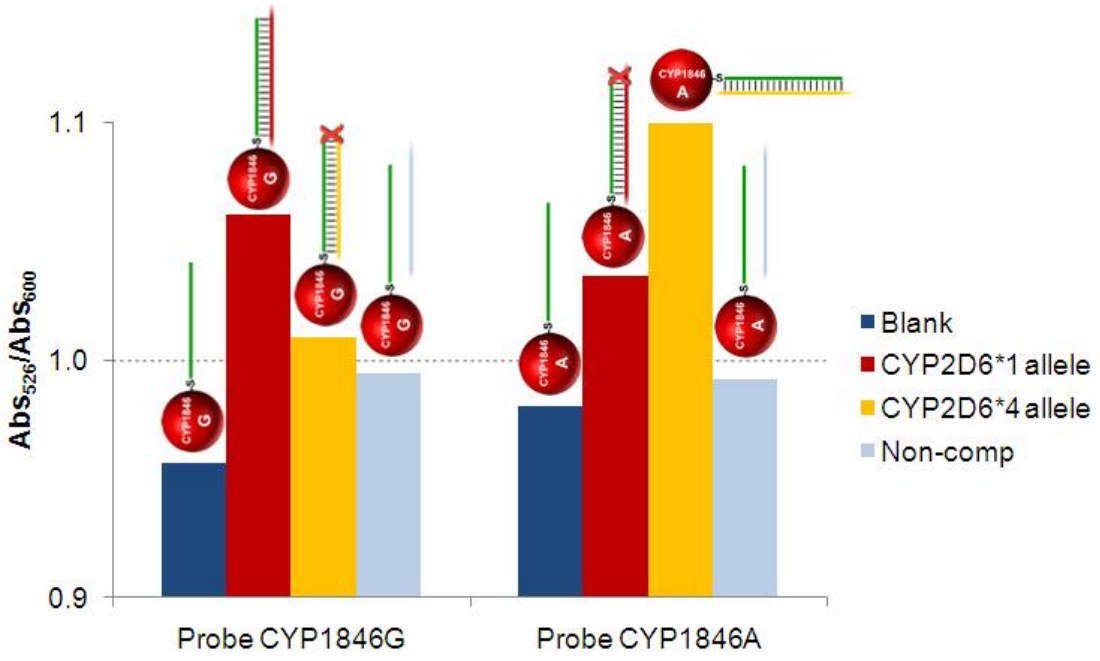

Figure 4.3 – CYP1846G/A SNP detection. The Abs_{526}/Abs_{600} ratio upon 15 minutes of NaCl adition (final concentration= 1 M) to Au-nanoprobes alone ("Blank") or in presence of a non-complementary target ("Non-comp"); or the Probe CYP1846G in the presence of its complementary target ("CYP2D6*1 allele") and mismatched target ("CYP2D6*4 allele"); or the Probe CYP1846C in the presence of its complementary target ("CYP2D6*4 allele") and mismatched target ("CYP2D6*1 allele"). Schematics represent Au-nanoprobe alone or in presence of a target, where "**X**" represents a single base mismatch at the 3'-end of Au-nanoprobe.

Unfortunately, none of the previous conditions allowed for reproducible colorimetric results with the DOR1 or CYP1846 Au-nanoprobes, as in all cases the assay solutions aggregated un-differentially upon salt addition. Moreover, the synthesis of CYP1846 Au-nanoprobes with a longer sequence (40 nt probes, CYP1846G_XL and A_XL) did not solve this hybridization issue. In some cases, the complementary, mismatched and non-complementary amplicon target samples provided stability to the Au-nanoprobes, even in very high salt concentration. It is worth mentioning that, after purification of such target samples, hybridization to Au-nanoprobes no longer stabilized them and aggregation was observed. These observations indicate the presence of contaminations that stabilize Au-nanoprobes, most likely proteins present in DNA samples that could bind non-specifically to the AuNPs surface through electrostatic interaction or cysteine residues.[158,159]

To confirm that Au-nanoprobes were actually viable to hybridize to a complementary target, the amplicon targets were substituted by synthetic ssDNA 40-mer oligonucleotides. In this case, the Au-nanoprobes retained their stability upon salt addition when in presence of a complementary target. However, it was not possible to observe a colorimetric differentiation between complementary and mismatched targets, as shown in the example of DOR1C and DOR1G Au-nanoprobes (Figure 4.4 – A). The Au-nanoprobe stability upon salt addition

decreased linearly with target concentration, showing complete aggregation at 0.025 pmol/µL (25 nM) (Figure 4.4 – B); above 0.075 pmol/µL (75 nM), the red color was retained. These results show that the method's sensitivity is probably between those for the methods described by Mirkin's and Sato's groups.[101,82] The linear trend observed for the Au-nanoprobe stability vs. target concentration has also been observed for a different target, i.e. mRNA.[160]

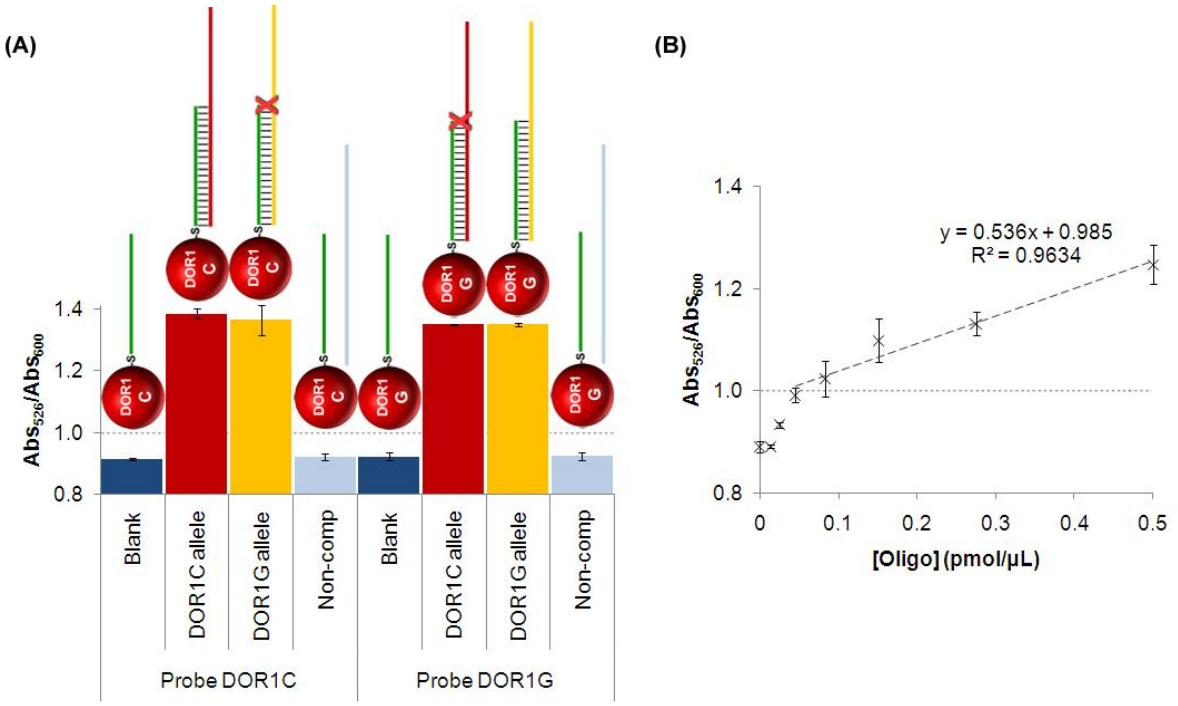

Figure 4.4 – Hybridization assay with ssDNA oligonucleotides. (A) The average Abs_{526}/Abs_{600} ratio of the Au-nanoprobes alone ("Blank") or in presence of a non-complementary target ("Non-comp"); or for the DOR1C Au-nanoprobe in the presence of its complementary target ("DOR1C allele") and mismatched target ("DOR1G allele"); or for the DOR1G Au-nanoprobe in the presence of its complementary target ("DOR1G allele") and mismatched target ("DOR1C allele"). The final ssDNA concentration is 1pmol/µL. Schematics represent Au-nanoprobe alone or in presence of a target, where "**X**" represents a single base mismatch at the 3'-end of Au-nanoprobe. **(B)** The average Abs526/Abs600 ratio of the DOR1G Au-nanoprobe in presence of complementary target. Dashed line and equation represent the linear trendline for ratio obtained with target concentrations between 0.75 and 0.5 pmol/µL. Error bars represent the standard deviation of three independent assays.

In an attempt to attain colorimetric differentiation between complementary and mismatched ssDNA oligonucleotide targets, a salt titration was performed with increasing concentrations of NaCl and $MgCl_2$. For both cases, it was not possible to discriminate between complementary and mismatched targets, while the "Blank" and "Non-comp" solutions aggregated at 1.5 M NaCl or 20 mM $MgCl_2$ (Figure 4.5).

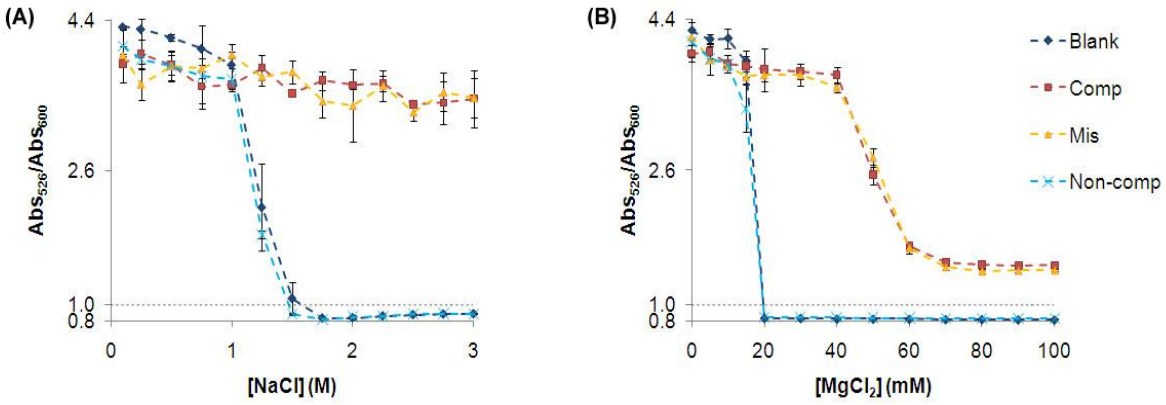

Figure 4.5 – Salt titration of Au-nanoprobe with ssDNA oligonucleotides. The average Abs_{526}/Abs_{600} ratio of the DOR1G Au-nanoprobe alone ("Blank"); in the presence of a complementary target ("Comp"); a mismatched target ("Mis"); or a non-complementary target ("Non-comp"), 15minutes after addition of **(A)** NaCl or **(B)** $MgCl_2$. Error bars represent the standard deviation of three independent assays.

It was not possible to induce aggregation for the complementary/mismatched assays even with high concentrations of NaCl. On the other hand, the complementary/mismatched solutions both started to aggregated at 40 mM $MgCl_2$ and aggregation stabilized at an Abs_{526}/Abs_{600}= 1.4 with >70 mM $MgCl_2$ (Figure 4.5 – B). In this case, the absorbance ratio did not fall below 1, mainly due to the fact that the SPR band peak of these samples did not shifted further than 560 nm. This may be related to an increased inter-particle distance upon aggregation induction.[68] If that is the case, the inter-particle distance increase might be caused by a steric hindrance provided by the ssDNA oligonucleotides hybridized to the Au-nanoprobes. This hypothesis is further supported by the measurements of the Au-nanoprobes hydrodynamics radius, which increases with the hybridization of complementary/mismatched targets (see Chapter 5, section 5.2.3.2).

Interestingly, when a second synthetic oligonucleotide, complementary to the target oligonucleotide, is added to the solution (thus generating a dsDNA synthetic target), the Au-nanoprobes are no longer stabilized by their complementary/mismatched target and aggregate upon salt addition. This suggests existence of competition between hybridization and dsDNA renaturation, which could explain why the Au-nanoprobe hybridization to the dsDNA amplicon targets was hampered, as previously observed for DOR1 and CYP2D6 targets (Figure 4.6).

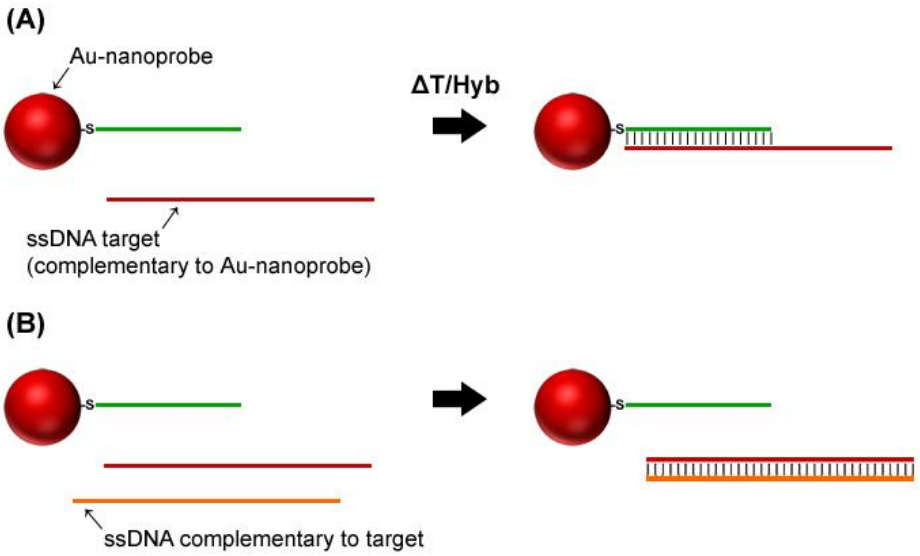

Figure 4.6 – Scheme of dsDNA target hybridization competition. (A) A complementary ssDNA target hybridizes with the Au-nanoprobe after the denaturation/hybridization (ΔT/Hyb) step, **(B)** but when a second ssDNA with a sequence complementary to the ssDNA target sequence is added to solution, the hybridization between ssDNA strands overcomes the hybridization between the target and the Au-nanoprobe, forming a dsDNA instead.

To confirm this, asymmetric PCR was used to yield both dsDNA and ssDNA amplicons. Double-stranded DNA and ssDNA were separated and purified by gel electrophoresis, and used in the non-cross-linking assay. Results clearly show that the complementary ssDNA amplicon easily hybridizes with the Au-nanoprobe, increasing protection against salt-induced aggregation, while hybridization to the dsDNA amplicon is hampered and the Au-nanoprobes aggregate (Figure 4.7). Moreover, ssDNA mismatched amplicon targets do not stabilize the Au-nanoprobe and they aggregate similarly to the Au-nanoprobes in presence of a non-complementary target.

A comparison between the results obtained for ssDNA synthetic oligonucleotides and for ssDNA produced by asymmetric PCR suggests that capability to detect SNP/mutations is influenced by the target length/complexity and, therefore, limited to more complex/longer targets. In summary, the use of asymmetric PCR overcomes the difficulties presented by GC-rich targets and allows the non-cross-linking method to the successfully detect SNP/mutations in virtually any DNA target, provided that asymmetric PCR is successful. Moreover, the use of two Au-nanoprobes, each fully complementary to each allele, should allow to fully characterize homo- and heterozygous samples (e.g. heterozygous samples stabilize both probes, while homozygous samples only stabilize one probe).

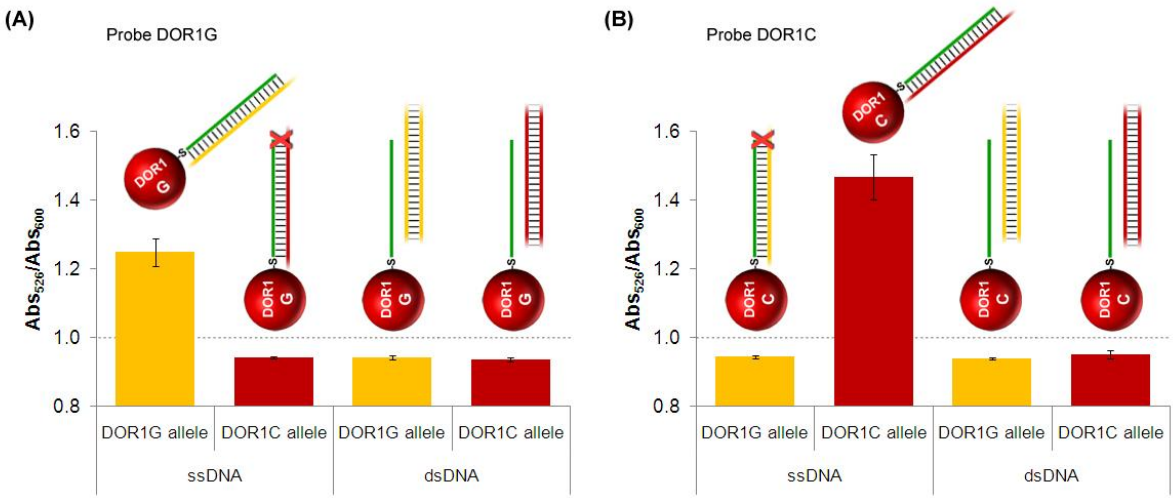

Figure 4.7 - ssDNA *vs.* dsDNA amplicon hybridization. The average Abs_{526}/Abs_{600} ratio of the **(A)** DOR1G Au-nanoprobe in presence of its ssDNA/dsDNA complementary ("DOR1G allele") and mismatched ("DOR1C allele") target; and of the **(B)** DOR1C Au-nanoprobe in presence of its ssDNA/dsDNA complementary ("DOR1C allele") and mismatched ("DOR1G allele") target. Spectra were registered 15 minutes after addition of $MgCl_2$ (final concentration= 25 mM and 45 mM $MgCl_2$ for DOR1G and DOR1C Au-nanoprobes, respectively). Final target concentration is 30 ng/µL. Schematics represent Au-nanoprobe in presence of a target, where "X" represents a single base mismatch at the 3'-end of Au-nanoprobe. Error bars represent the standard deviation of three independent assays.

4.2.2 AuAg-nanoprobes

The potential of AuAg-nanoprobes to specifically detect nucleic acids sequences based on the non-cross-linking method was tested. The stability of AuAg-nanoprobes against salt-induced aggregation was tested following hybridization to a complementary and non-complementary target (synthetic ssDNA oligonucleotides). The same procedure, as that for Au-nanoprobes, was followed and spectra taken 15 minutes upon salt addition. The SPR band of AuAg-nanoprobe alone ("Blank") and in presence of a non-complementary target ("Non-comp") shifted towards longer wavelengths, with a concomitant color change from yellow to blue (Figure 4.8). The presence of a complementary target significantly stabilized the nanoprobes and the solution retained its initial and non-aggregated yellow color. Similar results were obtained when using dsDNA amplicons as targets (396bp bGlob amplicon – see Chapter 2, section 2.2.1.5.1). Apart from the different initial SPR peak (460 nm and 526 nm for AuAg- and Au-nanoprobes, respectively) these results are in total agreement to those obtained for the Au-nanoprobes.

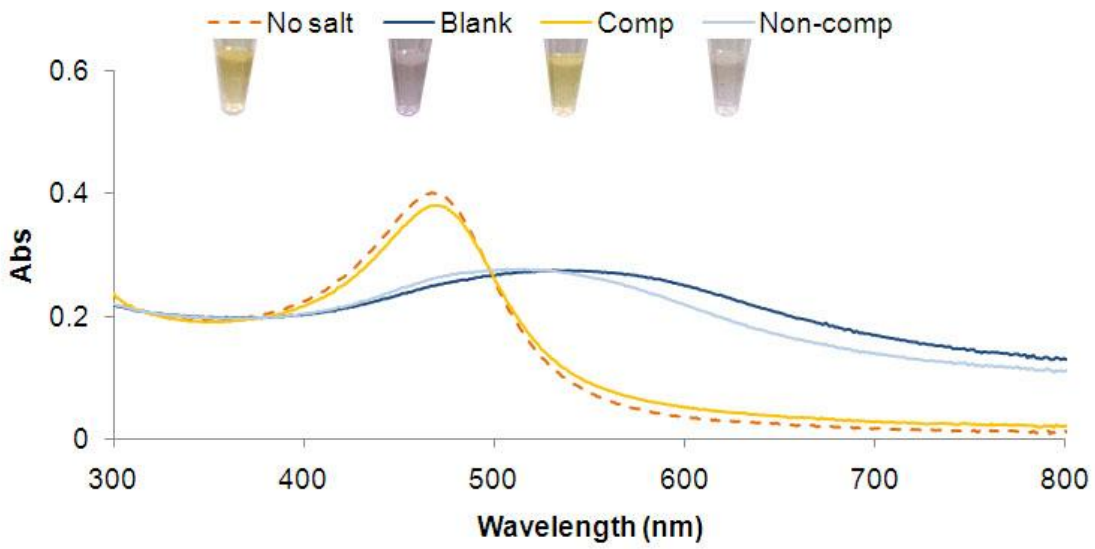

Figure 4.8 – AuAg-nanoprobe hybridization with ssDNA oligonucleotides. UV-vis spectrum of DOR1C AuAg-nanoprobe alone with no salt addition ("No salt") and 15 minutes after $MgCl_2$ addition ("Blank"); in presence of a complementary target ("Comp"); or a non-complementary target ("Non-comp"). Final concentrations of 30 mM $MgCl_2$ and 1 pmol/uL of ssDNA oligonucleotide.

4.2.3 Multiplexing: proof-of-concept

Making use of the different SPR band peak associated to the non-aggregated Au- and AuAg-nanoprobes, and based on the fact that both nanoprobes present a similar behavior upon salt addition, a multiplex approach using the non-cross-linking method was evaluated. The proof-of-concept was made by using one Au-nanoprobe (CYP1846G probe) with one AuAg-nanoprobe (DOR1C probe) at a final concentration of each nanoprobe of 2.5 and 0.05 nM, respectively. These concentrations were used to allow similar Abs_{peak} value and, thus, to facilitate the visualization of both SPR band peaks. The nanoprobes were mixed together and tested for their stability against salt-induced aggregation. A total of six assay solutions were prepared: "No salt" - nanoprobes alone with no salt addition (salt was substituted by 10mM phosphate buffer); "Blank" – nanoprobes alone; and "Au_Comp" – in presence of a complementary target to Au-nanoprobe; "AuAg_Comp" – in presence of the complementary target to AuAg-nanoprobe; "Au+AuAg_Comps" – in presence of complementary targets to each nanoprobe; "Non-comp" – in presence of a non-complementary target to either nanoprobe. All targets used were synthetic ssDNA oligonucleotides at a final concentration of 1pmol/µL. Figure 4.9 shows the UV-visible spectra and digital photographs of the nanoprobes 15 minutes after salt addition (or phosphate buffer, in the case of "No salt").

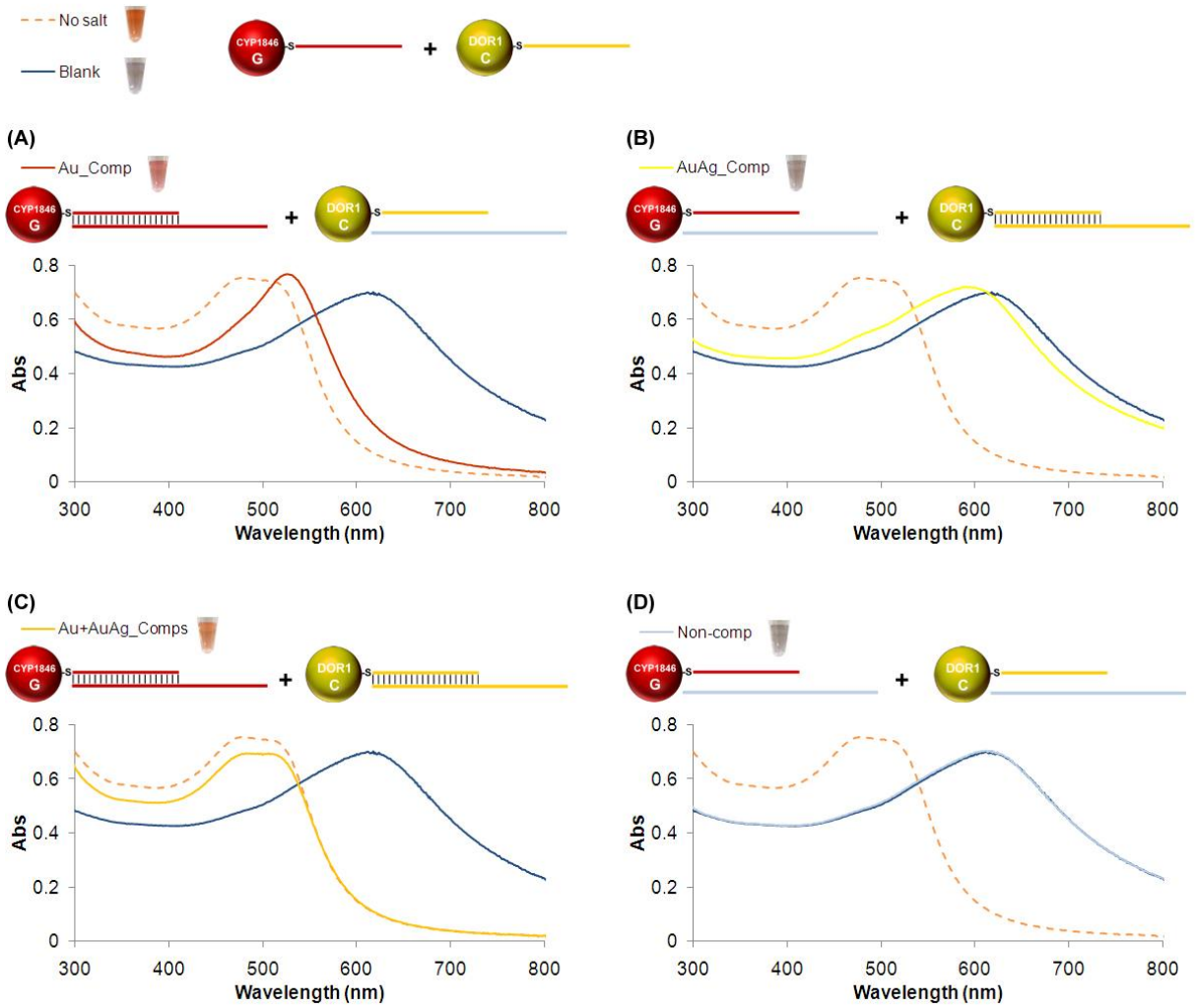

Figure 4.9 – Multiplex non-cross-linking assay. UV-visible spectra of Au-/AuAg-nanoprobes mix 15 minutes after $MgCl_2$ addition (final concentration 30 mM) and digital photographs of each solution. The nanoprobes alone – "No salt", where the salt was substituted by phosphate buffer, and "Blank" – and in presence of: **(A)** a complementary target to Au-nanoprobe – "Au_Comp"; **(B)** a complementary target to AuAg-nanoprobe – "AuAg_Comp"; **(C)** complementary targets to each nanoprobe – "Au+AuAg_Comps"; **(D)** a non-complementary target to either nanoprobe – "Non-comp". Schematics represent each nanoprobe and their complementary or non-complementary targets.

The SPR band peaks – 460 and 526 nm – of the nanoprobes alone red-shifted to a single peak – 630 nm – after salt addition, with a concomitant change in color from the original dark orange to blue ("No Salt" vs. "Blank"). In the case of the "Au_comp" solution, the SPR band with *double peaks* located at 460 and 526 nm changed to a single peak at 526 nm, and this spectrophotometric change was translated by a change from dark orange to red, indicating that only the Au-nanoprobe remained stable in the presence of its complementary target (Figure 4.9 – A). In the "AuAg_comp" solution, the SPR band peaks shifted to a single peak at longer wavelengths but in a lesser extent than "Blank" solution, changing color from dark orange to blue, indicating that both nanoprobes aggregated (Figure 4.9 – B). Nonetheless, in this case, it is still possible to observe a slight band near the 460 nm, which may indicate that

not all AuAg-nanoprobes have aggregated due to the presence of their complementary target. In presence of both complementary targets – “Au+AuAg_comp” solution – both nanoprobes remained stable and the solution retained its initial color, despite the slight decrease in the SPR absorbance intensity (Figure 4.9 – C). In the case of the “Non-comp” solution, the initial SPR band peaks red-shifted in a similar way to the “Blank” solution, with a concomitant change in color from dark orange to blue (Figure 4.9 – D).

Taken together, these results show that a multicolor/multiplex approach via the non-cross-linking method is viable, provided that further optimization permits to avoid aggregation of the AuAg-nanoprobe in presence of its complementary target. The ultimate goal of this multiplexing approach is to detect SNP/single point mutations, allowing homo- and heterozygous characterization in a single reaction.

4.3 Conclusions

It was demonstrated that the non-cross-linking method can be used for detection of SNP/single point mutations at room temperature. In the case of the bGlob Au-nanoprobe, it was possible to successfully detect three different individual β-globin gene mutations in dsDNA amplicon targets with just one Au-nanoprobe. For GC-rich sequences (e.g. DOR1 and CYP2D6 regions), the competing dsDNA renaturation hinders the target hybridization with Au-nanoprobe and hampers the detection of the respective complementary target, even in less stringent and optimal hybridization conditions. The use of less complex targets, such as ssDNA oligonucleotides or ssDNA amplicons produced by asymmetric PCR, allows overcoming this problem and enhances the reproducibility of the non-cross-linking method. Nonetheless, the discrimination of a single base mismatch is only possible with longer ssDNA targets (produced by asymmetric PCR), whereas 40-mer ssDNA oligonucleotides with a single base mismatch cannot be discriminated from fully complementary targets. The detection sensitivity of the non-cross-linking method was determined to be 73 and 75 nM for ssDNA/dsDNA amplicons and ssDNA oligonucleotide targets, respectively. This indicates that the sensitivity should be independent of target length/complexity.

The detection of specific nucleic acids sequences via the non-cross-linking method is also possible through the use of AuAg-nanoprobes. Preliminary results indicate that a multiplex assay based on the conjugation of Au- and AuAg-nanoprobes is viable to detect multiple targets in a single reaction.

CHAPTER 5. Non-cross-linking Mechanism: Proposed model and optimization

Unveiling the underlying mechanism of the non-cross-linking method may allow to better understand the single base resolution of Au-nanoprobes towards optimization. In this chapter, the use of AFM, fluorescent spectroscopy and electrophoretic mobility measurements (Ferguson analysis) allowed clarification of the nature of the forces involved in the differential colorimetric non-cross-linking aggregation and further optimize the Au-nanoprobe design to SNP/single point mutation discrimination at room temperature.

5.1 Introduction

Since the development of the first Au-nanoprobes and the cross-linking method by Mirkin and co-workers,[80] several studies have been conducted to better understand the physicochemical properties of the Au-nanoprobes/DNA target conjugates.[81,161-172] The majority of these studies focused on the mechanisms of the cross-linked Au-nanoprobe/DNA aggregates, while few have actually focused on the thermodynamics and hybridization efficiency itself between an Au-nanoprobe and complementary DNA.

To assess the hybridization efficiency between the Au-nanoprobes and DNA targets, Demers and co-workers developed a method using fluorescein-labeled ssDNA oligonucleotides as targets.[81] In their study, hybridization efficiency was shown to be linearly dependent of the Au-nanoprobe density (i.e. thiol-modified oligonucleotide coverage of the AuNPs' surface), where higher densities (up to 20 pmol/cm^2) allowed hybridization of more targets. Also, hybridization efficiency considerably increased (10-fold) with introduction of a poly(dA) or poly(dT) 20mer spacer between the propane-thiol group and the probe sequence. Introduction of such spacer leads to an enhanced binding strength between the Au-nanoprobe and the DNA target, but an increase in the length of the recognition sequence (i.e. probe sequence) actually leads to a decrease in the added strength binding provided by these spacers.[165] The steric hindrance between DNA strands is believed to be alleviated by the introduction of such spacers, which move the DNA recognition sequence further away from the AuNPs' surface. In the absence of the spacer, the DNA strands are closer to the particle surface and to each other, therefore reducing the ability of the target sequence to bind to the Au-nanoprobe. Additionally, the heteroduplexes formed on the surface of the Au-nanoprobes were shown to become progressively less stable as the fraction of hybridized DNA on the surface increases.[164] This effect on the thermodynamics of hybridization is believed to be due to electrostatic interactions between near-neighbor DNA heteroduplexes, which difficult the binding of further DNA targets. The Au-nanoprobe sequence composition has also been shown to affect the hybridization efficiency, mainly due to non-specific adsorptions occurring between the nucleotides of the thiol-modified oligonucleotide and the AuNPs surface.[169] These non-specific adsorptions are greater for oligonucleotides with higher adenine and cytosine content, and lead to a decrease in hybridization efficiency. Moreover, the position of these high affinity sequences within the derivatized thiol-modified oligonucleotide affects the extent of hybridization, where high affinity nucleotides in the center affect hybridization in less extent than when located at the end.

The specificity of the Au-nanoprobes for single base mismatches has also been studied, but always through the cross-linked approach. In this approach, the single base mismatch can be detected at a specific temperature that allows the dissociation of Au-nanoprobes/DNA

aggregates harboring the mismatch, while maintaining the complementary Au-nanoprobes/DNA aggregates unaltered.[101] This is mainly due to the extraordinarily sharp melting profiles exhibited by the heteroduplex DNA cross-linked structures formed between DNA target strands and the Au-nanoprobes. This sharp melting is attributed to a cooperative mechanism that results from the presence of multiple DNA linkers between each pair of Au-nanoprobes and a decrease in the melting temperature, as duplex DNA strands melt due to a concomitant reduction in local dielectric medium.[163,167] The sharp melting properties of the cross-linked Au-nanoprobes/DNA aggregates are affected by a number of factors, including DNA surface density, nanoparticle size and inter-particle distance.[162,163,171]

Despite all these studies, the effect of a single base mismatch in the hybridization efficiency between a non-cross-linked conjugation of Au-nanoprobe and DNA targets has never been addressed. Also, the mechanism involved in the non-cross-linking hybridization method responsible for the colorimetric differentiation between complementary, mismatched and non-complementary targets has, so far, been elusive.

Here, to better understand the mechanism of the non-cross-linking method, including its capability for single base resolution at room temperature, a combination of different techniques was used. The Au-nanoprobe capability to recognize a complementary target sequence by hybridization was directly observed by AFM.[148] Through the use of fluorescent spectroscopy, Au-nanoprobe specificity was further assessed by studying the effect of a single base mismatch in hybridization efficiency under different conditions (e.g. Au-nanoprobe length, density, etc.).[173] The Au-nanoprobe/target DNA conjugates were also characterized through a Ferguson plot analysis to infer surface charge and hydrodynamic radius differences between conjugates. Based on the attained results, a model of the non-cross-linking method mechanism is proposed, which sets up the optimal conditions for single base mismatch detection at room temperature.

5.2 Results and Discussion

5.2.1 Use of Atomic Force Microscopy to *observe* Au-nanoprobe hybridization (work published in Eaton P, Doria G, et al.[148])

AFM was used to directly observe the DNA recognition events that occur at the nanoscale involving hybridization of the target dsDNA and the Au-nanoprobes.[148] The bGlob Au-nanoprobe was used together with a plasmid harboring a fragment of the β-globin gene *locus* as target (see Chapter 2, section 2.2.1.5.1). At first, in order to evaluate hybridization of the Au-nanoprobe, the p158 plasmid was linearized by *BamH*I restriction enzyme and a fragment of ≈8668 bp was attained. At a second stage, PCR amplified 1559 bp fragment from the same plasmid was used. A 1565 bp PCR amplified fragment from the pCYP2D6*1 plasmid

was used as non-complementary target sequence. These different target molecules were manipulated so as to create a pool of targets of different lengths with the specific target region located towards one end of the molecule, thus allowing determination of relative position of the hybridization *locus* and evaluation of specificity.

AFM images of these DNA targets alone and of the Au-nanoprobe alone were first made to assess their structure (Figure 5.1). The majority of the Au-nanoprobes appeared isolated with a more or less globular morphology and height measurements (diameter) of an average of ~17 nm (Figure 5.1 - A). Although not visible in this image, a minority of the Au-nanoprobes were also observed as small aggregates (~2 to 8 Au-nanoprobes). All DNA targets could also be visualized as uniform and individual molecules with the expected length and height (Figure 5.1 - B, C and D), considering the theoretical value from crystallography of 3.2 Å per bp and the known errors associated to AFM measurements.[174]

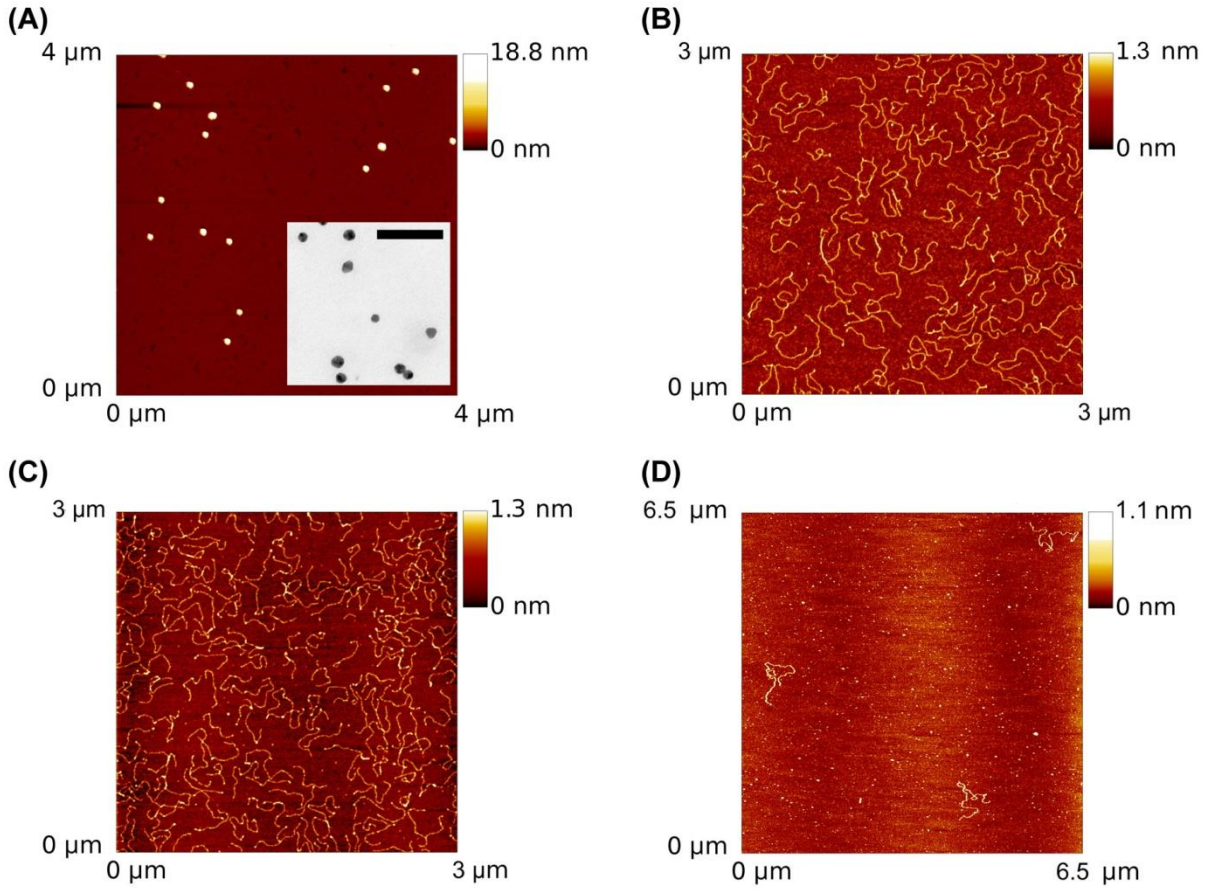

Figure 5.1 – AFM characterization of Au-nanoprobes and targets. AFM images of the **(A)** Au-nanoprobe alone - inset shows TEM of bare gold clusters, scale bar= 100 nm; and DNA alone, namely **(B)** the 1559 bp complementary amplicon, **(C)** the 1565 bp non-complementary amplicon, and **(D)** the ≈8668 bp linearized p158 plasmid.

AFM samples of Au-nanoprobes in presence of a complementary target (plasmid or amplicon) or non-complementary target were prepared by following all the steps of the non-cross-linking colorimetric assay, except for salt addition, followed by a washing step to remove the

non hybridized targets. A clear image of the Au-nanoprobes bound to the plasmid could be observed (Figure 5.2 - A). However, the plasmid DNA molecules appeared to have formed a complicated supramolecular structure that hampered a more thorough analysis. This way, it was unclear whether there is a single Au-nanoprobe bond per plasmid, as would be expected if the binding occurred by specific hybridization. Such super-structures made it impossible to ascertain where along the DNA molecule the Au-nanoprobe is bound to, and, hence, confirm specific hybridization. As mentioned earlier, the plasmid was linearized so as to localize the target sequence one third of the way along the length of the plasmid, allowing evaluation of specific binding of the Au-nanoprobe. Hybridization of Au-nanoprobes to the plasmid DNA was repeated several times and registered by AFM, but a ratio of 1:1 Au-nanoprobe/DNA target conjugates was very rarely observed. These structures may arise as a consequence of AFM sample preparation and deposition or really occur from Au-nanoprobe and target hybridization in solution.

In order to better assess the binding position of the Au-nanoprobes within the target DNA sequence and to confirm whether this binding is due to specific hybridization, a smaller DNA target (amplicon) with the Au-nanoprobe recognition site located at the end of the sequence was used. Such shorter DNA fragments reduce the potential for DNA to wrap up into complex forms, thus simplifying analysis. Indeed, the AFM image obtained with these complementary PCR fragments showed some individual Au-nanoprobe/DNA target conjugates (Figure 5.2 - B). Nevertheless, individual (non-hybridized) Au-nanoprobes and targets, and more complex structures combining more than one target, and more than one Au-nanoprobe, were also observed. In the case of the individual Au-nanoprobe/DNA target (1:1) conjugates, some of the Au-nanoprobes were located in the middle of the DNA target molecule (gray arrows), but the majority (ca. 70%) were found to be located at the end of the DNA target molecule (white arrows) as expected. In the latter, the length of the “tails” of DNA extending from the Au-nanoprobe varied from 216 to 494 nm, with a mean value of 355 nm, which was coherent with a binding due to hybridization - the theoretical length of this complementary PCR fragment (1559 bp; 3.2 Å per bp) is 499 nm and the recognition site is located at 483 nm. For the cases where a smaller “tail” was observed, the DNA could also be bonded through a specific hybridization at the end of the target, where these overhanging fragments have considerable freedom of movement and that some of them can wind back on themselves or around the Au-nanoprobe, possibly stabilized by nonspecific interactions with the AuNP surface.[175]

Further confirmation that Au-nanoprobe binding to DNA target is mediated through a hybridization mechanism was obtained through the negative control of this experiment, where a sample with a non-complementary PCR amplicon was prepared in an identical procedure as that of the complementary target. The AFM image of this non-complementary

sample only showed unbounded Au-nanoprobes (Figure 5.2 - C), as expected if binding would depend only of specific hybridization.

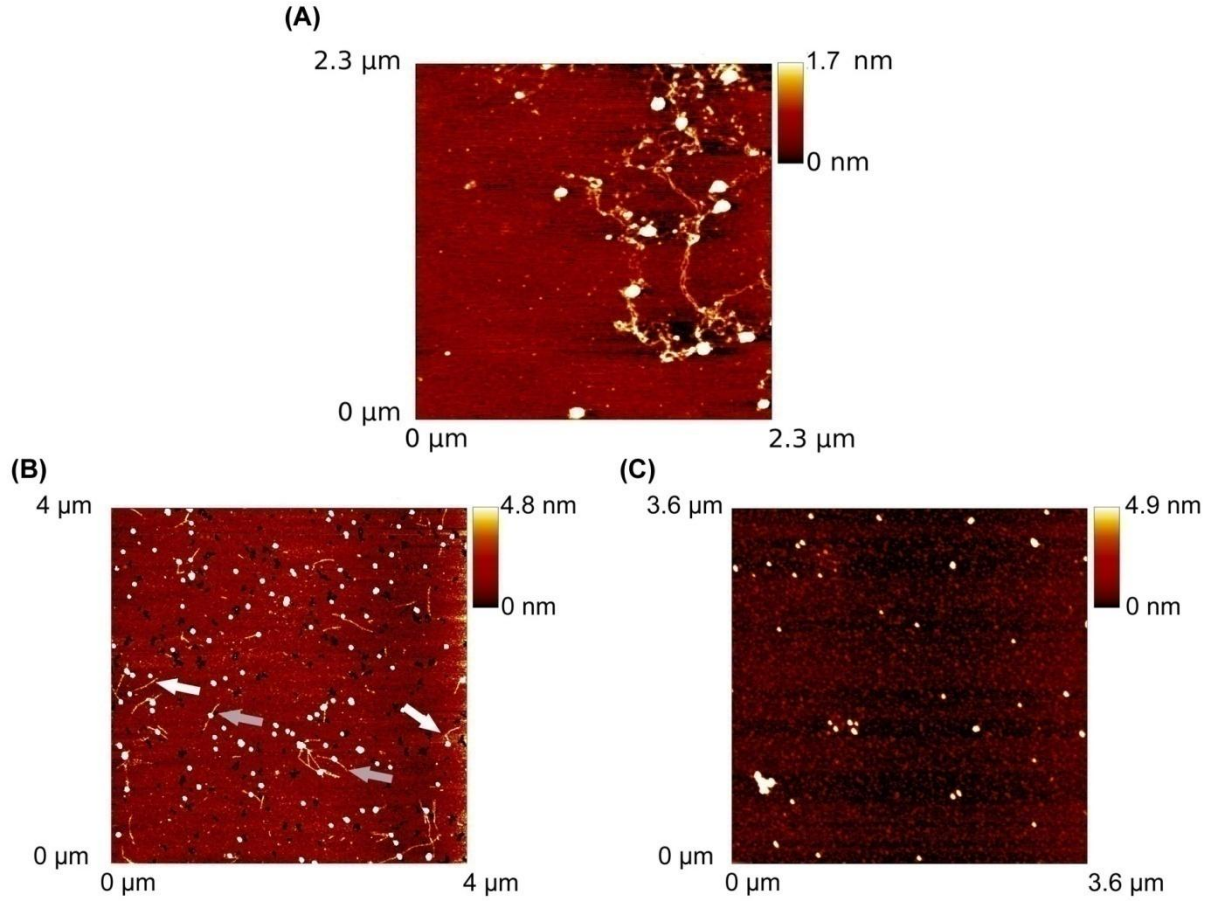

Figure 5.2 – AFM study of target hybridization. AFM image of Au-nanoprobes in presence of: **(A)** a linearized p158 plasmid; **(B)** a 1559 bp complementary amplicon; and **(C)** a 1565 bp non-complementary target. Arrows indicate 1:1 probe-target aggregates where the probe is at the end (white arrows), and in the middle (gray arrows) of the DNA molecule.

In conclusion, these results strongly support the binding by complementary hybridization as the primary interaction occurring between the Au-nanoprobes and the DNA targets. Nevertheless, 30% of the interactions apparently occurred away from the end of the PCR fragment, which is a clear signal of the occurrence of nonspecific interactions. AFM images only depict a small fraction of the whole Au-nanoprobe/DNA target population present in solution, and therefore, further studies should be carried out to give a broader image of the hybridization specificity of the Au-nanoprobes.

5.2.2 Optimizing Au-nanoprobes for specific sequence discrimination (part of this work has been published in Doria G, *et al*.[173])

To better evaluate the Au-nanoprobe specificity for sequence detection in solution, the hybridization efficiency between the Au-nanoprobe and a complementary, mismatched or non-complementary DNA target was determined through a fluorescein-labeled probe. A

similar approach to the fluorescence technique developed by Demers and co-workers[81] was used, where single stranded DNA oligonucleotides with half the sequence complementary to a fluorescent probe (FAM probe) were used as targets and the other half of their sequence was either complementary or non-complementary to the Au-nanoprobe, or produced a single base mismatch within the sequence of the Au-nanoprobe. The targets and fluorescent probe were mixed in equal amounts and in large excess to the Au-nanoprobes to avoid limiting the hybridization reaction. A blank solution was also prepared by mixing the Au-nanoprobe alone with the fluorescence probe, thus allowing evaluation of nonspecific binding between the fluorescent probe, and the Au-nanoprobe. Following the usual denaturation/hybridization protocol used in the colorimetric assay, the excess non-hybridized targets/fluorescent probes were washed out. Then, alkaline denaturation was used to free the hybridized targets/fluorescent probes, and, after centrifuge separation, the fluorescence of the supernatant was measured by fluorescent spectroscopy (Figure 5.3). The Au-nanoprobes' final concentration was also confirmed and used to correct the eventual losses of Au-nanoprobe during the washing steps. The residual contribution of fluorescein molecules in the absorption at 526 nm was neglected, since the extinction coefficient associated to the SPR absorption band of the Au-nanoprobes is several orders of magnitude higher than that of fluorescein (2.33×10^8 $cm^{-1}.M^{-1}$ and 78×10^3 $cm^{-1}.M^{-1}$, respectively). Special emphasis was given to the effect of a single base mismatch in the hybridization efficiency at room temperature.

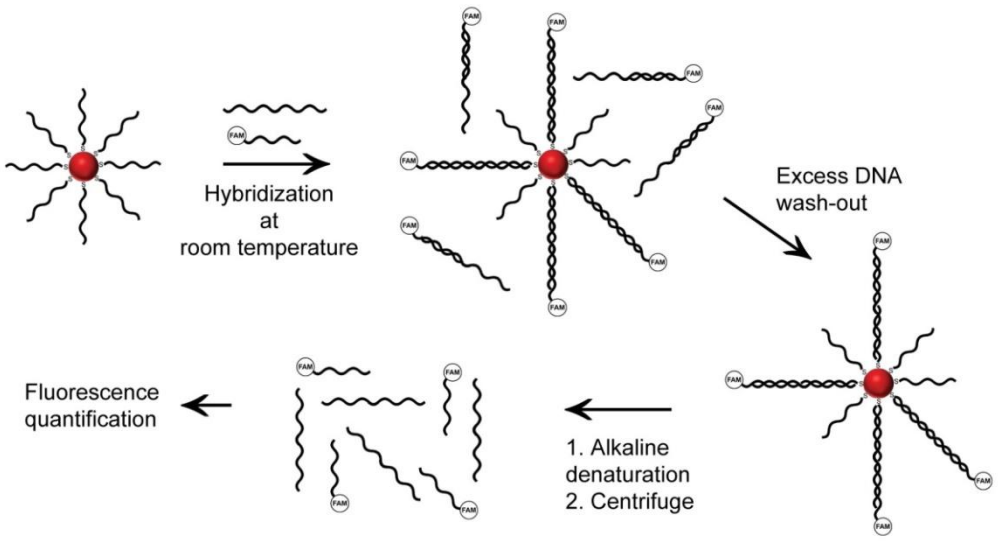

Figure 5.3 – Scheme of the fluorescence-based procedure for the determination of hybridization efficiency. The Au-nanoprobe is mixed with an excess of target and fluorescent probe and allowed to hybridize at room temperature, following the usual denaturation/hybridization protocol, to form a sandwich heteroduplex structure due to base pair complementarity. Afterwards, the excess DNA is washed-out and the bonded targets are drawn into solution by an alkaline denaturation, to be quantified by fluorescent spectroscopy.

The hybridization efficiency between the Au-nanoprobes and targets was determined under different conditions (e.g. pH, mismatch position, probe length, etc.) to evaluate the optimal conditions for Au-nanoprobe specificity and better understand what rules the non-cross-linking hybridization between target and Au-nanoprobe.

5.2.2.1 Effect of pH

The effect of pH in the hybridization efficiency of a complementary, mismatched and non-complementary target to the Au-nanoprobe was assessed, and the best pH condition for specific target hybridization determined. Four aliquots of the same Au-nanoprobe were washed and dispersed in phosphate buffer solutions with pH values ranging from 6.64 to 8.13. This interval comprises the range of pH usually used in DNA recognition techniques, such as Southern and Northern blots, DNA chip technologies, etc.[154]

Results show that the number of DNA targets bound to the Au-nanoprobe is higher for lower pH values (Figure 5.4). Nonetheless, for these pH values a significant nonspecific binding of the fluorescent probe is also observed. This nonspecific binding is most likely to happen through the exposed bases of the ssDNA fluorescent probe interacting with the AuNPs surface.[86] In the case of the non-complementary targets, a decrease in the number of bonded targets is observed most likely due to the fluorescent probe being fully hybridized to part of the non-complementary target sequence. In this case, half of the non-complementary target bases still remain exposed to bind nonspecifically to the Au-nanoprobes, but in a lesser extent. Considering these observations, the results for the complementary and mismatched target hybridization at pH 6.64 and 7.21 should be carefully considered when assessing the true hybridization efficiency and specificity.

For higher pH values the nonspecific binding decreases considerably, especially in the case of pH 8.13. At this pH, it is also possible to observe that complementary targets hybridize to the Au-nanoprobe in slightly higher number than the targets harboring a single base mismatch (G•T) at the 3'-end of the Au-nanoprobe. Hence, we can conclude that the optimal pH for specific hybridization is set to be at pH 8.

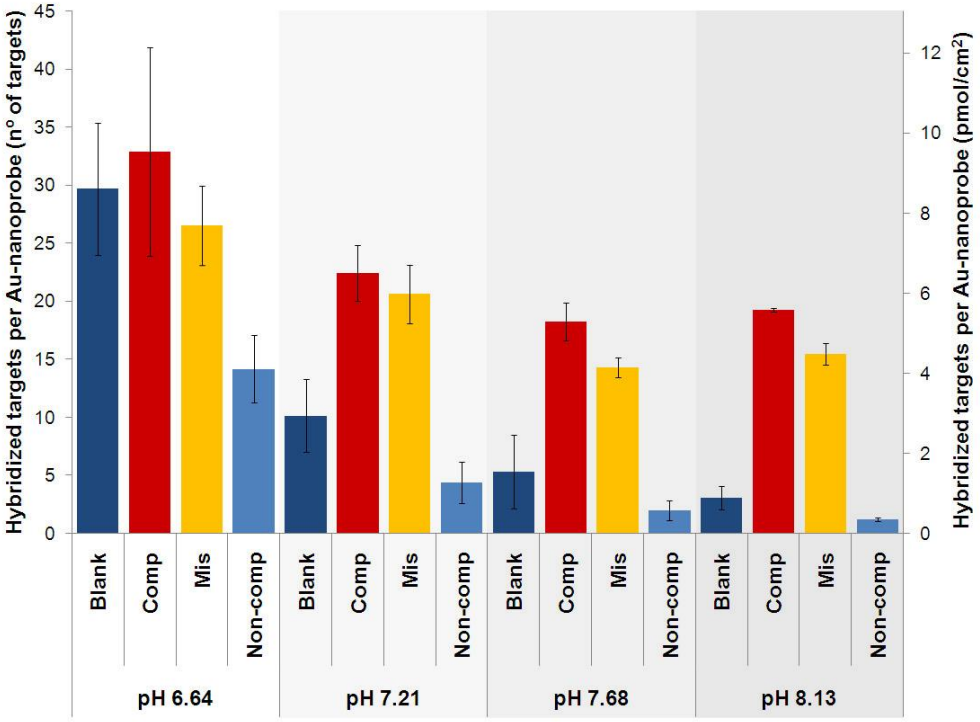

Figure 5.4 – Effect of pH in hybridization efficiency and specificity. The Au-nanoprobe (CYP1846G) in presence of a fluorescent probe (FAM) – "Blank"; and a complementary target (CYP1846C) – "Comp"; and a target (CYP1846T) harboring a single base mismatch at the 3'-end of the Au-nanoprobe – "Mis"; and a non-complementary target (DOR1C) – "Non-comp". Error bars represent standard deviation of three independent samples.

5.2.2.2 Effect of mismatch position

The effect of the position of a single base mismatch on hybridization efficiency was assessed by engendering a guanidine-guanidine (G•G) mismatch at several base positions along the sequence of the Au-nanoprobe (DOR1G) (Figure 5.5). Because the G•G mismatch is known to yield the strongest interaction among the non-Watson-Crick base paring,[176] it is most likely to allow the proper analysis of these phenomena at the molecular level. DOR1C was used as complementary target; targets DOR1GA, DOR1G_4, DOR1G16 and DOR1G_20 where used so as to generate the single base mismatch at nucleotide 1, 4, 16 and 20 of the Au-nanoprobe, respectively (considering nucleotide 1 at the 3'-end of the Au-nanoprobe oligonucleotide); and target CYP1846C as non-complementary target.

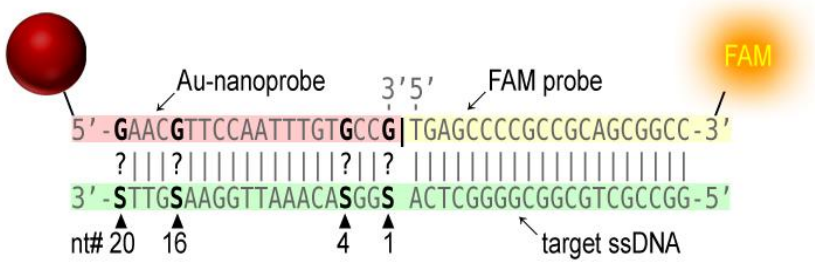

Figure 5.5 – Scheme of mismatch position along Au-nanoprobe sequence. Different ssDNA targets were used as to generate a single guanidine-guanidine mismatch or full guanidine-cytosine complementarity (S= G or C) at different positions (nt# 1 to 20) along the sequence of the Au-nanoprobe.

The best mismatch discrimination was found to be at the 3'-end of the Au-nanoprobe (i.e. nt1) – see Table 5.1. As the mismatch position approaches the 5'-end of the Au-nanoprobes' oligonucleotide sequence, discrimination between complementary and mismatched targets decreases. When the mismatch is located at the 5'-end (i.e. nt20), no discrimination is observed. This decrease of sequence specificity may be due to the decreased availability of the nucleotide bases close to the AuNP surface for base pairing interaction relative to the outer bases.[165] This way, the destabilizing effect of the mismatch in duplex stability and target hybridization efficiency is more evident when the mismatch is located at the 3'-end of the Au-nanoprobe. This effect also corroborates the previously observed results for SNP detection, in which the position of the mismatch seemed to affect Au-nanoprobe aggregation (see Chapter 4, section 4.2.1.1).[156]

In conclusion, the Au-nanoprobe presents a higher level of specificity at the 3'-end of the thiol-modified oligonucleotide, where the discrimination of a single base mismatch is best achieved.

Table 5.1 – Effect of mismatch position in hybridization efficiency

Hybridized targets per Au-nanoprobe (Average±STD)					
Single base mismatch (G•G) position*				Complementary	Non-complementary
nt1	nt4	nt16	nt20		
8.42±0.83 (2.44±0.24 pmol/cm^2)	9.69±0.87 (2.81±0.25 pmol/cm^2)	15.61±0.21 (4.53±0.06 pmol/cm^2)	20.10±0.55 (5.83±0.16 pmol/cm^2)	19.15±0.39 (5.56±0.11 pmol/cm^2)	2.98±0.70 (0.86±0.20 pmol/cm^2)

* Considering nucleotide 1 (nt1) at the 3'-end base of the Au-nanoprobe oligonucleotide

5.2.2.3 Effect of base pair complementarity

The effect of all possible base pair combinations at the 3'-end of the Au-nanoprobe was also assessed. For this purpose, a set of four different Au-nanoprobes with identical sequences, differing only at the 3'-end nucleotide (DOR1G, DOR1C, DOR1A and DOR1T, with G, C, A and T at 3'-end nucleotide, respectively) were hybridized to four different targets (DOR1CA, DOR1GA, DOR1TA and DOR1AA), each fully complementary to one of the Au-nanoprobes (Figure 5.6 – inset). The target CYP1846C was used as non-complementary target.

Data show that all complementary targets hybridized in higher numbers than targets harboring a mismatch, whereas non-complementary targets showed negligible hybridization (Figure 5.6). The hybridization of mismatched base pair variants indicates that the type of the mismatched base pair has little or no effect in hybridization efficiency. Differences in mismatch discrimination between different Au-nanoprobes are most likely due to different Au-nanoprobe densities, which have been previously reported to affect complementary target hybridization.[81]

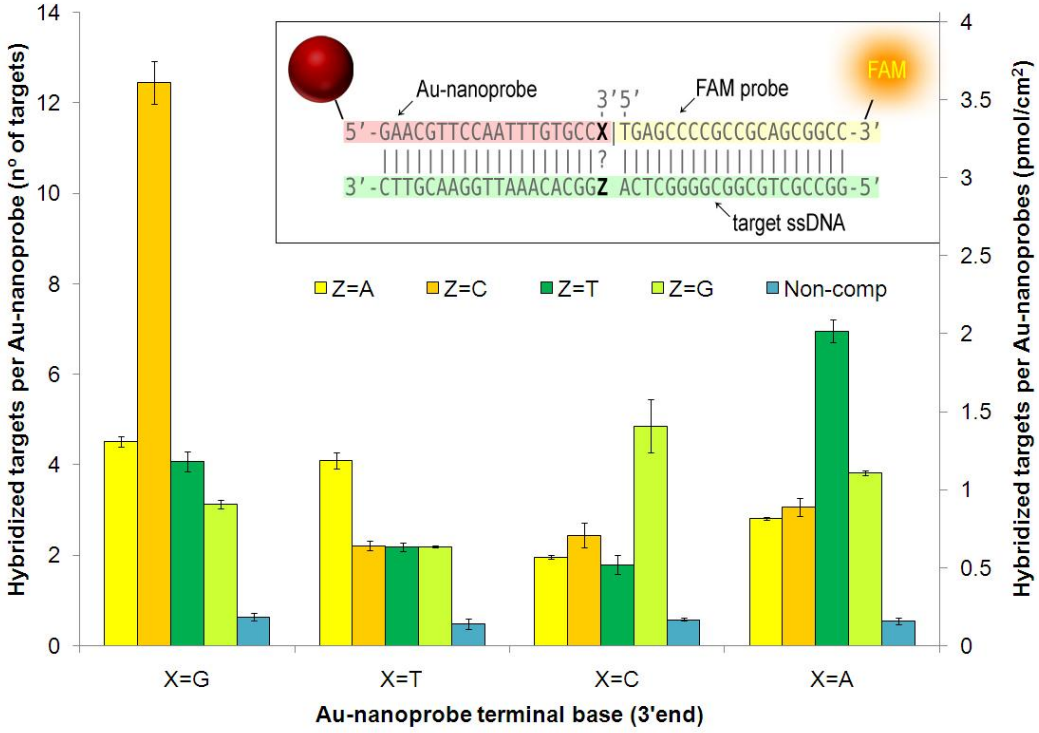

Figure 5.6 – Effect of base pairing at the 3'-end of the Au-nanoprobe on hybridization efficiency. The variable X translates for the Au-nanoprobe 3'-end base and the variable Z translates for the target base interacting with X, as shown in the inset scheme of the Au-nanoprobe and ssDNA target. Error bars represent standard deviation of three independent assays.

5.2.2.4 Effect of Au-nanoprobe density

To confirm the previous hypothesis, the effect of Au-nanoprobe density in single base mismatch discrimination (G•G) was investigated. A set of Au-nanoprobes (DOR1G) with different densities of derivatized thiol-modified oligonucleotides at the surface was used. DOR1CA was used as a complementary target, while targets DOR1GA and CYP1846C were used as mismatched and non-complementary targets, respectively.

The maximum efficiency of hybridization was observed for 83±4 oligos/AuNP, corresponding to a density of 24 pmol/cm^2 (Figure 5.7). Bellow this value, hybridization efficiency has not yet reached the maximum, as fewer oligonucleotides are present to hybridize. For densities above the maximum, more oligonucleotides are present to hybridize but increasing electrostatic repulsion and steric hindrance possibly hamper hybridization.[165] These results are in good accordance with those published by Demers and co-workers, where a linear increase in hybridization efficiency was observed up to a density of 20 pmol/cm^2 (higher densities where not evaluated).[81]

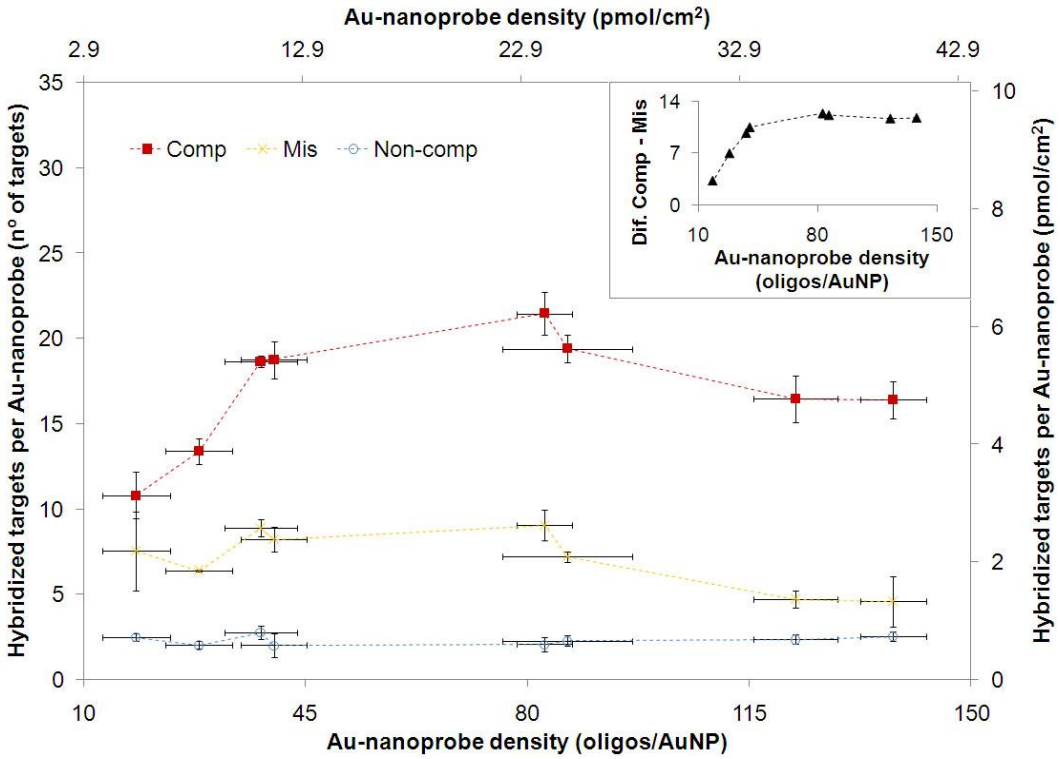

Figure 5.7 – Effect of Au-nanoprobe density in hybridization efficiency. Au-nanoprobe in presence of: a complementary target – "Comp"; a target harboring a single base mismatch G•G at the 3'-end of Au-nanoprobe – "Mis"; a non-complementary target – "Non-comp". Error bars represent standard deviation of three independent experiments and dashed lines are guides for the eye. Inset: Difference between the number of complementary and mismatched targets hybridized to the Au-nanoprobe in relation to its oligo density.

A similar effect is observed for discrimination between complementary and mismatched targets, i.e. the difference between the number of complementary targets and mismatched targets hybridized to the Au-nanoprobe (mismatch discrimination) increases gradually until reaching a plateau, beyond which the mismatch discrimination capability remains unaltered (Figure 5.7 – inset). This maximum discrimination level corresponds to an Au-nanoprobe density linked to the maximum hybridization efficiency. For lower densities, as the Au-nanoprobes' bases become more available to interact with their complementary target bases, the de-stabilizing effect of the mismatch in the duplex stability should become less pronounced.

5.2.2.5 Effect of Au-nanoprobe length

The effect of Au-nanoprobe length in hybridization efficiency and single base mismatch discrimination was also investigated by means of two Au-nanoprobes with 20 nt (CYP1846G) and 40 nt (CYP1846G_XL) sequences. The CYP1846G_XL Au-nanoprobe only differed from the CYP1846G Au-nanoprobe, in the first 20 nt starting from the 5'-end of the Au-nanoprobe. Nonetheless, the complementary (CYP1846C) and mismatched (CYP1846T) targets should only hybridize with the first 20 nt located at the 3'-end of both Au-nanoprobes (Figure 5.8).

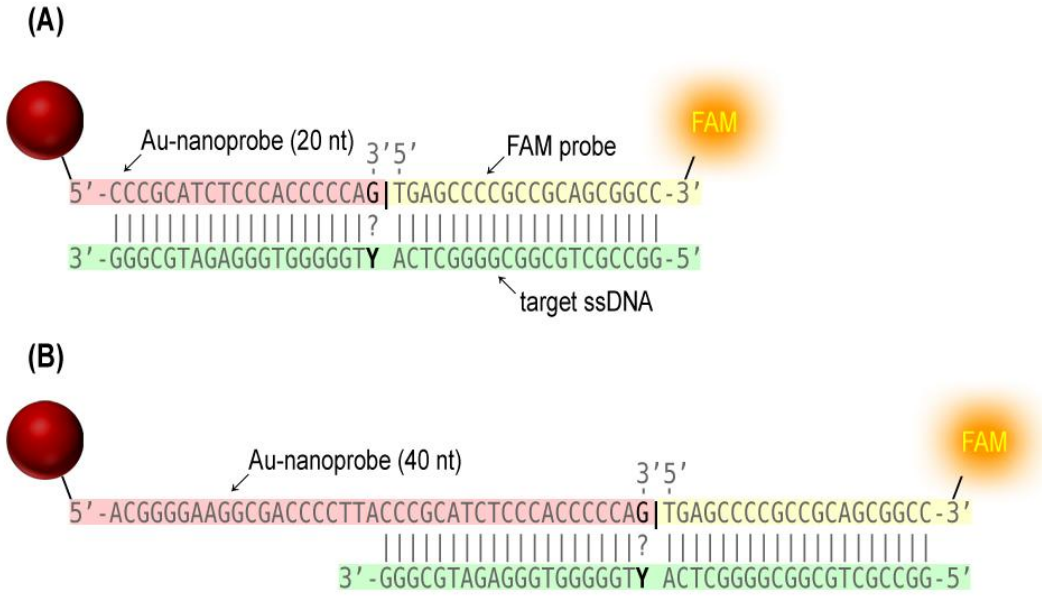

Figure 5.8 – Scheme of Au-nanoprobes with different lengths. Two Au-nanoprobes with **(A)** 20 nt or **(B)** 40 nt sequence were used to assess the effect of probe length in the hybridization efficiency with a fully complementary target or a target harboring a single base mismatch (G•T) at 3'-end of the Au-nanoprobes' sequence (Y= C or T).

The increase in the length of the Au-nanoprobe recognition sequence led to a decrease in hybridization efficiency to both complementary and mismatched targets (Table 5.2). This is

somehow consistent to what has been reported by Lytton-Jean and Mirkin, where an increase in the recognition sequence of their Au-nanoprobes led to a decrease in the enhancement of the binding strength provided by the spacer sequences used.[165] In our case, this decrease could also be due to the introduction of nucleotides with high-affinity to the AuNP surface (A and C) within the Au-nanoprobe sequence, which could difficult target hybridization.[169] Moreover, a decrease in density of the longer Au-nanoprobe could also be related to the decrease in hybridization efficiency.

The increase of the Au-nanoprobe's length also hampered discrimination between complementary and mismatched targets. This could be due to an increase in the Au-nanoprobes' bases availability to interact with their complementary target bases, which can in turn diminish the de-stabilizing effect of the mismatch within the duplex. This effect can be not only associated to an increase in the length of recognition sequence but also to the Au-nanoprobe density, as previously demonstrated. Further studies with longer sequences and different Au-nanoprobe densities should be carried out to assess the actual effect of Au-nanoprobe length in the single base mismatch discrimination at room temperature.

Table 5.2 – Effect of Au-nanoprobe length in hybridization efficiency

Hybridized targets per Au-nanoprobe (Average±STD)			
20 nt probe		40 nt probe	
Complementary	Mismatch (G•T)	Complementary	Mismatch (G•T)
15.18±0.73 (4.40±0.21 pmol/cm^2)	13.88±1.09 (4.02±0.32 pmol/cm^2)	5.42±0.32 (1.57±0.09 pmol/cm^2)	5.31±0.65 (1.54±0.19 pmol/cm^2)

5.2.2.6 Effect of target length/complexity

The effect of target length/complexity in hybridization efficiency was also partially assessed by using a longer target that generated a dangling-end at the 5'-end of the Au-nanoprobe (DOR1G). To generate a 20 nt ssDNA dangling-end at the 5'-end of the Au-nanoprobe, two 60 nt targets with a complementary sequence (DOR1C_XL) or a sequence (DOR1G_XL) harboring a single base mismatch at the 3'-end of the Au-nanoprobe, both located at the middle of the target, were used. As control, the usual 40 nt targets that generated a blunt-end at 5'-end of the Au-nanoprobe, namely DOR1CA (as complementary target) and DOR1GA (as mismatched target) were used (Figure 5.9).

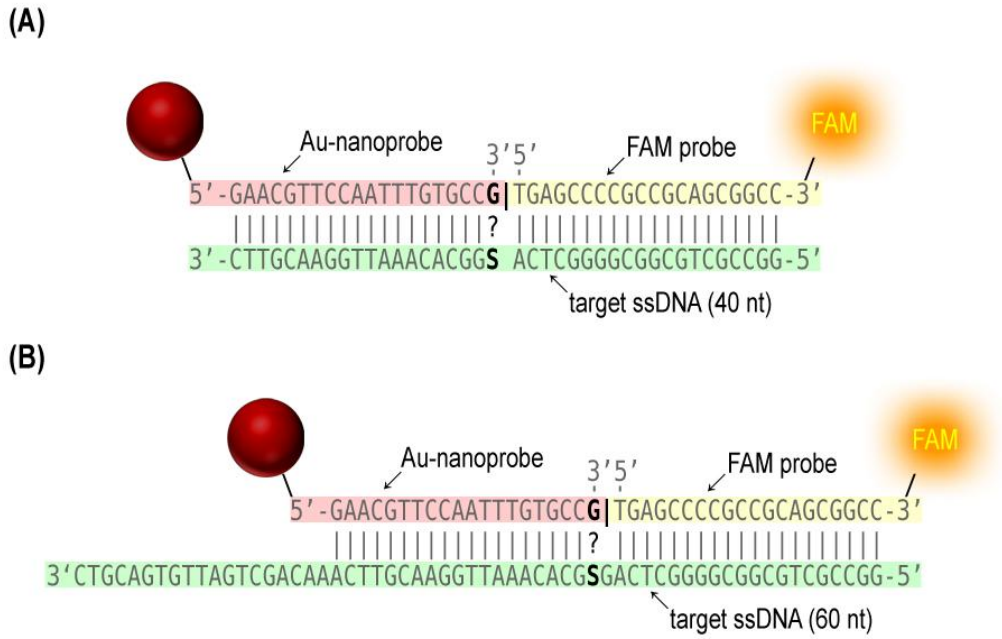

Figure 5.9 – Scheme of ssDNA targets with different lengths. A set of **(A)** 40 nt and **(B)** 60 nt ssDNA oligonucleotides, fully complementary with the Au-nanoprobe or harboring a single base mismatch (G•G) at 3'-end of the Au-nanoprobes' sequence (S= C or G) were used to assess the effect of target length/complexity in the hybridization efficiency.

The number of hybridized complementary and mismatched targets considerably decreases with longer (60 nt) targets, when compared to shorter ones (40 nt) (Table 5.3). However, discrimination between complementary and mismatched targets is still possible, despite the fact that the differential between these two targets also decreased for longer targets. Although the target's dangling-end at the 5'-end of the Au-nanoprobe is the most likely cause for the overall decrease in hybridization efficiency, the increase in target length can also generate secondary structures that may hamper hybridization to the Au-nanoprobe. Hence, further studies with longer targets, either generating a dangling-end at the 5'- or 3'-end of the Au-nanoprobe, should be carried out to confirm the real nature of the observed decrease in hybridization efficiency.

Table 5.3 – Effect of a target length in hybridization efficiency

Hybridized targets per Au-nanoprobe (Average±STD)			
40 nt targets		60 nt targets	
Complementary	Mismatch (G•G)	Complementary	Mismatch (G•G)
8.28±0.46 (2.40±0.13 pmol/cm^2)	3.47±0.62 (1.01±0.18 pmol/cm^2)	4.74±0.43 (1.37±0.12 pmol/cm^2)	2.54±0.09 (0.74±0.02 pmol/cm^2)

In summary, hybridization efficiency and SNP discrimination at room temperature is maximized with a density of 83±4 thiol-oligonucleotides (20 nt) per 13.5 nm gold nanoparticle (24 pmol/cm2) at pH 8, and when the mismatch is localized at the 3'-end of the Au-nanoprobe, i.e. away from the gold nanoparticle surface. Longer probe sequences (e.g. 40 nt) seem to decrease hybridization efficiency and hamper mismatch discrimination, while longer/more complex targets only lead to lower hybridization efficiencies, but allow mismatch discrimination.

5.2.3 Characterization of the surface charge and hydrodynamic radius using Ferguson analysis

The differential hybridization efficiency observed for fully complementary and mismatched targets considerably supports the colorimetric results obtained by the non-cross-linking method (see Chapter 4), when using longer/more complex ssDNA/dsDNA targets. Nonetheless, for shorter/less complex ssDNA oligonucleotide targets, the non-cross-linking method was unable to generate a differential colorimetric response between fully complementary and mismatched targets, despite the different hybridization efficiencies observed for these targets. Considering the negative charge associated to DNA due to the phosphate ions in its chemical backbone, it was expected that the number of targets hybridized to each Au-nanoprobe would determine a differential electrostatic repulsion between Au-nanoprobes dictating different stabilities against increasing ionic-strength and, hence, different aggregation profiles and colorimetric results between each target (i.e. fully complementary or mismatched target). On the other hand, the hybridized DNA targets may also provide the Au-nanoprobe with steric protection against aggregation, which can be less dependent on the number of targets hybridized and, therefore, explain the observed colorimetric results obtained with ssDNA oligonucleotides.

To test these hypotheses, the surface charge and the hydrodynamic radius of the Au-nanoprobe/DNA target conjugates were determined to evaluate the nature of the differential stability upon salt addition. For this study, the DOR1G Au-nanoprobe was used in conjunction with a complementary (DOR1CA), a mismatched target (DOR1GA, DOR1TA and DOR1AA) and a non-complementary (CYP1846C) target.

5.2.3.1 Surface charge of Au-nanoprobe/target conjugates

There is no satisfactory technique to determine surface charge of small particles in liquid, but a common approach relies on the measurement of zeta potential.[177] This is a function of the surface charge of the nanoparticle, the stationary layer at the interface and the nature and composition of the surrounding medium. Therefore, its value reflects the effective charge of the NPs and is closely related to the electrostatic repulsion between them, allowing

prediction of a coloidal solution's stability - i.e. the higher the zeta potential, the higher the coloidal solutions' electrostatic repulsion, thus, stability.

The first approach to measure the zeta potential of the different Au-nanoprobe/targets conjugates was made using a device based in DLS. However, this approach yielded a set of irreproducible results (data not shown). Such non-reproducibility was also recently reported by Park and Hamad-Schifferli for AuNPs smaller than 20 nm in diameter,[149] as in our case. To circumvent this issue, a Ferguson analysis procedure was proposed by Park and Hamad-Schifferli, where the surface charge and the hydrodynamic radius of AuNP/DNA conjugates can be determined through their differential migration in different agarose gel concentrations submitted to a constant electrical field (e.g. electrophoresis).

Therefore, a Ferguson analysis was introduced to assess the surface charge and the hydrodynamic radius of the Au-nanoprobe/DNA target conjugates under study. The resulting gels clearly showed a different migration pattern for the Au-nanoprobe alone and in the presence of the complementary, mismatched or non-complementary targets (see Appendix V). The Au-nanoprobe alone and in presence of a non-complementary target migrated similarly and further than the Au-nanoprobe/mismatched target conjugates, while the Au-nanoprobe/complementary target conjugates migrated less than the mismatched target conjugates. These results corroborate what had been previously observed in the fluorescence based approach (see Section 5.2.2), where complementary targets hybridized in higher number than mismatched targets, and the latter in higher number than non-complementary targets. It should be noted that the differential migration can be either due to an increase in the hydrodynamic radius of the Au-nanoprobes or due to differential electrical potentials between Au-nanoprobe/target conjugates, or a conjugation of both. To sort each factor's influence in the system, the mobility of each conjugate was plotted as function of agarose gel concentration.

The mobility vs. gel concentration plots show similar vertical offsets between conjugates samples, indicating that the electric potential at the interfacial double layer of the Au-nanoprobe does not change with hybridized targets, i.e., the superficial charge between samples is similar (Figure 5.10). This could help explain why the aggregation profiles of complementary and mismatched ssDNA oligonucleotide targets were also similar (see Figure 4.5 in Chapter 4, section 4.2.1.2). However, based on these results alone, the Au-nanoprobe alone and in presence of a non-complementary target should also present a similar aggregation profile to those of Au-nanoprobe/complementary or mismatched targets, which was not observed. This suggests the influence of another factor ruling the Au-nanoprobe conjugates' stability, such as steric hindrance.

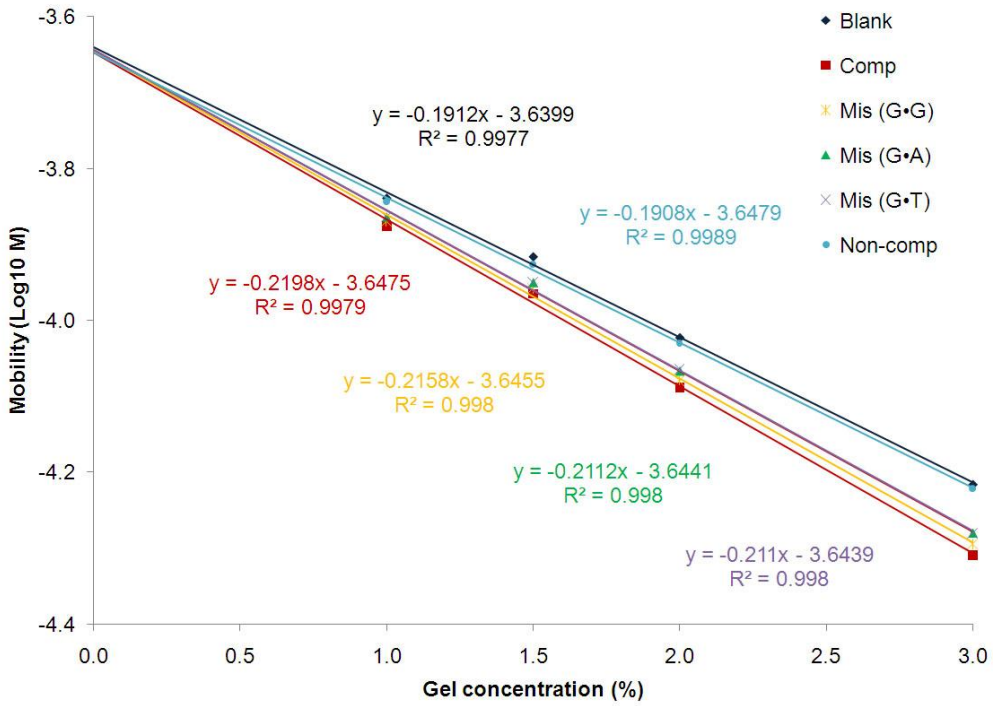

Figure 5.10 – Ferguson analysis of Au-nanoprobe/target conjugates. Electrophoretic mobility of Au-nanoprobe/target conjugates as function of agarose gel concentration. Au-nanoprobe alone – "Blank"; in presence of a complementary target – "Comp"; in presence of a target harboring a mismatch G•G at 3'-end – "Mis (G•G)"; in presence of a target harboring a mismatch G•A at 3'-end – "Mis (G•A)"; in presence of a target harboring a mismatch G•T at 3'-end – "Mis (G•T)"; in presence of a non-complementary target – "Non-comp". Linear fitting equations are presented with respective correlation coefficient.

5.2.3.2 Hydrodynamic radius of Au-nanoprobe/target conjugates

Steric hindrance can be related to different effective hydrodynamic radius of Au-nanoprobe/target conjugates, and this radius can be determined through the analysis of the slopes given by the mobility vs. gel concentration plots (Figure 5.10).[149] The Au-nanoprobe alone or in presence of a non-complementary target present slopes ca. 15% smaller than those for Au-nanoprobe hybridized to mismatched or complementary targets. The increase of the slope in these cases indicates an increase of the effective hydrodynamic diameter of the Au-nanoprobes (Table 5.4).

Table 5.4 – Effective hydrodynamic diameter of Au-nanoprobe/target conjugates

Effective hydrodynamic diameter (nm)*					
Blank	Comp	Mis(G•G)	Mis(G•A)	Mis(G•T)	Non-Comp
20.27	23.49	23.06	22.55	22.53	20.23

* determined by Ferguson analysis as described by Park and Hamad-Schifferli[149]

This increase in diameter can only be due to the presence of hybridized targets, as previously confirmed by fluorescence techniques, most probably in an extended double helix conformation with dangling unpaired bases at the 3'-end of the Au-nanoprobe.[164] These data are further corroborated by the colorimetric results obtained with $MgCl_2$ induced aggregation, where the red-shift of SPR band for Au-nanoprobe/complementary or mismatched target conjugates was smaller to that of Au-nanoprobe alone or in presence of a non-complementary target (see Figure 4.5 in Chapter 4, section 4.2.1.2). Since it is commonly accepted that the SPR band shift depends on the inter-particle distance between AuNPs,[178] these results indicate that steric hindrance of larger conjugates plays a crucial role in the colorimetric differentiation for the non-cross-linking method. The measurement of the hydrodynamic radius of the same conjugates using DLS could probably provide further evidence of such steric hindrance in solution and for different ionic strength conditions, and, therefore, should be considered for further studies.

5.3 The non-cross-linking method: proposed mechanism model

The work presented in this chapter has contributed to a better understanding of phenomena involved in Au-nanoprobe/target interactions, and helped determine the optimal conditions for single base mismatch discrimination at room temperature via the non-cross-linking method. In addition, the data generated by the different approaches allows to propose a model for the mechanism involved in the non-cross-linking differential colorimetric discrimination between complementary, mismatched and non-complementary targets. The colorimetric changes of the Au-nanoprobe solutions are a consequence of the AuNPs' SPR coupling due to Au-nanoprobe aggregation (i.e. dependent of inter-particle distance and aggregate size).[161,178] Previous reports have proposed that Au-nanoprobe stability with increasing ionic strength of the medium was due to an increase in the electrostatic repulsion between Au-nanoprobes associated with the negatively charged backbone of the hybridized nucleic acid targets.[91,103,156] However, based on the results presented in this chapter, it can be hypothesized that, in addition to that electrostatic effect, steric hindrance also plays an important role in the protective effect of hybridized targets against salt induced aggregation. This steric hindrance would then be responsible for keeping the inter-particle distance despite dipole coupling upon salt addition. Results obtained through Ferguson plot analysis indicate that the hybridization of the complementary/mismatched targets with the Au-nanoprobe leads to an increase in the hydrodynamic radius of the Au-nanoprobes, while no changes to the surface charge of the Au-nanoprobes were detected. This indicates that a strong influence of steric hindrance rather than electrostatic repulsion is responsible for the Au-nanoprobe/target differential stability in the non-cross-linking method. Moreover, this steric hindrance can be considered to be relatively independent of the number of hybridized targets to the Au-nanoprobe, which may hamper the colorimetric discrimination of a single

base mismatch by the non-cross-linking method, considering that mismatched targets also hybridize to the Au-nanoprobe (as observed for the 40 nt oligonucleotide targets). Regardless of this, colorimetrical discrimination of single base mismatches through the non-cross-linking method was still possible for longer/more complex DNA targets (see Figure 4.7 in Chapter 4, section 4.2.1.2).[156] In this case, target length and/or the relative position of the Au-nanoprobe complementary sequence within the target may lead to a decreased hybridization efficiency, as shown by fluorescent assays (see Section 5.2.2.6). When dsDNA is used as target, the hybridization kinetics involving competition of Au-nanoprobe and dsDNA renaturation may also lead to a decrease in hybridization efficiency (see Figure 4.7 in Chapter 4, section 4.2.1.2). In these situations, the hybridization efficiency may decrease down to a point when just a few complementary targets hybridize with the Au-nanoprobe, and no hybridization occurs for the mismatched target. This hypothesis is further supported by AFM results, where hybridization of a single complementary target per Au-nanoprobe was predominantly observed (see Section 5.2.1). In the case of substantially longer targets (e.g. >8000 bp), the formation of complex structures involving several Au-nanoprobes and targets is very likely to occur, which may further stabilize the Au-nanoprobes/target complexes and avoid aggregation, through steric hindrance. All these hypotheses could be further corroborated by evaluating the hybridization efficiency, surface charge and hydrodynamic radius of longer and more complex DNA/Au-nanoprobe conjugates showing differential colorimetric results. Nonetheless, the error associated with these methods may hinder the evaluation of single target per Au-nanoprobe conjugates. The use of AFM to assess hybridization between Au-nanoprobes and longer/more complex mismatched targets may also provide confirmation of the “single target *vs.* no target hybridization” hypothesis, and, therefore, should be considered in future work. It should be noted that, although the eventual observation of Au-nanoprobe/mismatched DNA target conjugates compromises the proposed hypothesis for single base mismatch discrimination, its absence will never confirm it.

The specificity of the Au-nanoprobe for single base mismatches seems to increase when the complementary fraction of the mismatched target is located in a region where stronger electrostatic interactions are most likely to occur (i.e. near the 5’-end of the Au-nanoprobe) and the mismatch is located further away from that zone (i.e. at the 3’-end of the Au-nanoprobe). These differential electrostatic regions along the Au-nanoprobe oligonucleotide sequence are only possible due to the curvature of the spherical NPs surface. The electrostatic interactions should be mostly due to near-neighbor oligonucleotides of the Au-nanoprobe and become much more pronounced with increasing Au-nanoprobe density (see Section 5.2.2.4), and should hamper hybridization of the complementary bases located near the 5’-end of the Au-nanoprobe. This effect in combination with the destabilization of the mismatch at the other end, should greatly affect the overall binding strength of the target. In

fully complementary targets, only the electrostatic destabilization near the 5'-end is present, and the overall binding strength of the target should be higher. Nevertheless, it should be noticed that electrostatic forces are not the only forces present in Au-nanoprobes/target conjugates and that other attractive/repulsive forces (e.g. hydrogen bond, steric hindrance, etc.) may intervene in target hybridization and single base mismatch discrimination.

Based on all these data and hypotheses, a mechanism is proposed for the colorimetric discrimination of a single base mismatch by the non-cross-linking method – see figure 5.11.

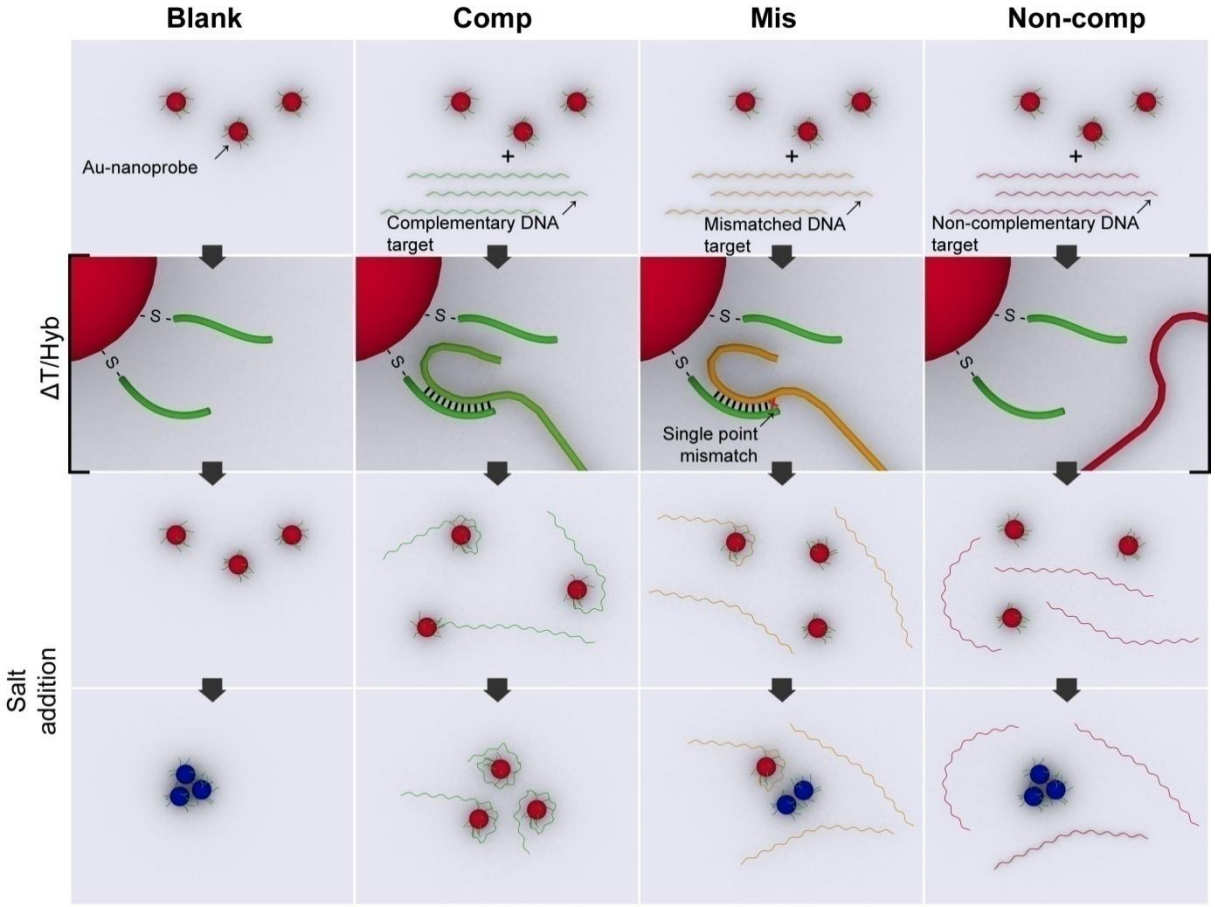

Figure 5.11 – Non-cross-linking method: proposed mechanism. The solutions containing the Au-nanoprobe alone ("Blank") or in presence of: a complementary target ("Comp"); a target harboring a single base mismatch at the 3'-end of the Au-nanoprobe sequence ("Mis"); or a non-complementary target ("Non-comp") are heated, to denaturize dsDNA/secondary structures, and then cooled to room temperature, to allow hybridization between the Au-nanoprobes and targets (ΔT/Hyb). Only complementary and mismatched targets have complementary bases to the Au-nanoprobe sequence that allows them to significantly bind to the Au-nanoprobe. Nonetheless, the greater electrostatic repulsions generated by near-neighbor oligonucleotides at the 5'-end of the Au-nanoprobe sequence decrease the hybridization efficiency and, hence, the binding strength of Au-nanoprobe/target conjugates. Ultimately, this could lead to the hybridization of a single target per Au-nanoprobe. In the case of mismatched targets, the single base mismatch at the 3'-end of the Au-nanoprobe sequence further decreases the binding strength of Au-nanoprobe/target conjugates, which could lead to no target hybridizing with the Au-nanoprobes. Upon salt addition, the increased ionic strength attenuates

the electrostatic repulsion between Au-nanoprobes' conjugates. Upon aggregation of the Au-nanoprobes, the solution changes color from red to blue (due to SPR coupling), unless steric hindrance is provided by bounded/hybridized targets. In the later case, Au-nanoprobes remain dispersed and the solution retains its initial red color.

CHAPTER 6. Commercial application for Point-of-Care (STAB VIDA)

The easy-of-use and low cost of the non-cross-linking method should allow its application at point-of-care. In this chapter, the technical issues for application at point-of-care are explored, together with the development of integrated optoelectronic/microfluidic technologies for automated sample handling and detection of colorimetric results.

6.1 STAB VIDA's global market and strategy

The main objective of this thesis was to develop a simple and cost-effective new portable method for nucleic acid detection at POC. This would meet the current demand for near-patient nucleic acid testing and STAB VIDA's commercial interests in POC molecular diagnosis. STAB VIDA (www.stabvida.com) is a Portuguese biotech company, pioneer in introducing genomics and related kits as well as products and services for the academic and clinical community. Thus far, STAB VIDA's portfolio includes kits for the detection of *Legionella* and *Dekkera/Brettanomyces*, based on PCR or a differential growing medium, respectively. More recently, STAB VIDA started to expand its market to human genotyping by providing services for human disease diagnosis (e.g. celiac disease, lactose intolerance, etc.) and parental testing. These genotyping services are currently provided through DNA collection kits that can be used by patients at POC and later sent to STAB VIDA's laboratories for further analysis. Genotyping is then performed by direct sequencing or Real-time PCR by specialized and qualified personnel. By investing in the development of a new nucleic acid detection method based on Au-nanoprobes, STAB VIDA intends to provide simple, reliable, fast and inexpensive diagnostic tests for POC, allowing cost-cutting and entering a new diagnostic industry of healthcare systems.

The non-cross-linking method developed in this thesis holds great potential and fits most of the desirable requirements for POC genetic testing, especially in areas of low economic resources. The simplicity of the method makes it user-friendly (only requiring mixing solutions and heat/cooling the samples) and the cost per assay is estimated at around €0.05/target, without the need for complex instrumentation to evaluate the final result. Nonetheless, the method, in its current format, still requires considerable optimization and scaling up before it can be applied at POC, but, in the meanwhile, can be used as a kit in standard molecular biology laboratories (including STAB VIDA's laboratories), provided that validation and certification (e.g. CE mark) are successfully achieved.

6.1.1 Medium-throughput assay kit

The non-cross-linking method can be sold as a kit with intuitive labeled reagents (e.g. "Probe", "Hybridization buffer", "Developer" (salt), "Control POS" (complementary target) and "Control NEG" (non-complementary target)) and a simplified protocol booklet[179] to be used in standard molecular biology laboratories. The protocol includes mixing the sample DNA and Control solutions with Probe and Hybridization buffer solutions, heating/cooling the mixture and adding the Developer to reveal the colorimetric result, all within 45 minutes. Afterwards, the colorimetric result can be rapidly assessed using a UV/visible spectrophotometer or microplate reader. The latter would allow for up to 384 results to be registered within seconds, which is clearly suitable for the rapid analysis of multiple samples or targets – medium-throughput.

6.1.1.1 Storage stability

Over the course of this thesis, most Au-nanoprobes proved to be stable and viable for at least 1 year when kept in a stock concentration of 15 nM at 4ºC or even at room temperature. Phosphate buffer and salt solutions are also very stable, provided that are kept sterile and in a dry environment. In the case of the salt solutions, a saturated solution should be used to avoid concentration variations that may affect the development of the colorimetric results along the time. Considering all this, the kit could be conveniently stored at room temperature, with exception for the control solutions that should be stored at 4ºC or -20ºC, with a 1 year validity (minimum). Nevertheless, a more thorough evaluation of the kit stability and viability should be performed, including for more extreme conditions (e.g. high/low temperatures, high/low humidity, etc.). The stability and viability of the Au-nanoprobe and reagents at these conditions is relevant mainly to third-world countries' laboratories, which usually lack the controlled conditions of a more advanced research/clinical laboratory.

6.1.2 Point-of-care (POC) testing

Point-of-care testing is a rapidly growing segment of the healthcare industry, with an estimate market value of around 5 Mrd. US$ (~3.5 Mrd. Euros) and a growth rate of 10.5% per year.[180] POC assays bring the resources of clinical laboratory closer to both patient and doctor. The main benefits of POC testing lies in the immediate result assessment where it is most needed (i.e. at patient's side), allowing for a decreased turnaround time and more efficient therapy management. Common sites for POC testing are patient's daily routine environments (e.g. home, work place, etc.) and clinical environments (e.g. hospital's bedside, physician's office, etc.). POC systems may also constitute an alternative for third-world countries, which lack the health care infrastructures available in more developed countries.[181]

POC assays are usually accomplished through the use of portable handheld instruments (e.g. blood glucose meter) and test kits (e.g. pregnancy test). The majority of the currently available POC assays rely on targeting proteins (e.g. antibodies and/or antigens) or hormones, or enzymatic assays that yield a direct result or via a redox/acid-base reaction. Genetic testing at point-of-care (nucleic acid POC assays) is a very attractive market, as it can be used for the molecular identification of pathogens sequences with increased specificity, test for mutations/polymorphisms associated with genetic disorders, or used in personalized therapeutics (i.e. pharmacogenetics and pharmacogenomics). A list of current POC systems for nucleic acid analysis, approved for *in vitro* diagnosis in clinical environment, can be found in Table 6.1.

Table 6.1 – Currently commercialized POC systems for nucleic acid detection

System	Integrated sample preparation	Integrated PCR	Sample maximum capacity	Assay time	Platform	Format
GeneXpert (Cepheid)	Yes	Yes	16 samples (6 targets/each)	60 min	Real-time PCR	Benchtop
Liat™ Analyzer (IQuum Inc.)	Yes	Yes	1 sample (4 targets)	60 min	Real-time PCR	Handheld
eSensor® (Osmetech)	No	No	48 samples (36 targets/each)	4h*	Microarray	Benchtop
Verigene system (Nanosphere Inc.)	No	Not required	4 samples	90 min	Microarray	Benchtop
NanoChip® NC400 (Nanogen)	No	No	2 samples (400 targets/each)	4h	Microarray	Benchtop
GeneChip® System 3000Dx (Affymetrix)	No	No	48 samples (510,000 targets/each)	n.s.	Microarray	Benchtop
R.A.P.I.D.® System (Idaho Technology Inc.)	No	Yes	32 samples (3 targets/each)	30 min*	Real-time PCR	Suitcase
Prove-it™ Lab-on-a-chip (Mobidiag)	No	Yes	5 samples	3h	Microarray	Benchtop

* does not include sample preparation and/or PCR amplification time. n.s. – not specified

Among these POC systems, only two (GeneXpert and Lyat™ Analyzer) include sample preparation - DNA extraction and PCR amplification, mainly through the use of microfluidics: which are the only fully autonomous POC genetic assays allowing a “sample in-answer out” response. These POC systems still rely on either fluorescent based real-time PCR or microarray platforms (electrical or fluorescent based), which are expensive technologies and not truly portable.

The non-cross-linking method allows for a cost-effective diagnosis, but in its current format still relies on purified DNA samples and PCR amplification, which hampers its true application at POC. Also, the colorimetric changes may sometimes be difficult to assess by the naked eye and should be quantitatively measured through the use of spectrophotometric platforms to prevent user-error and ensure a correct result interpretation. Hence, to transform the developed non-cross-linking sequence detection method in a “sample in-answer out” POC assay, these issues still need to be tackled.

6.1.2.1 Portability and colorimetric reading

The issue of portability and colorimetric reading, has been addressed via a light sensitive amorphous/nanocrystalline silicon *pi"ii"n* photovoltaic sensor to develop a simple and inexpensive system that allows to quantitatively assess the colorimetric results.[182] The different layers of this photovoltaic sensor and their thicknesses allows to tailor its spectral response band to an optimal response peak that fits the non-aggregated Au-nanoprobes SPR absorption band. Moreover, the substrate of the sensor is glass, which allows a direct application of the Au-nanoprobes sample on the back side of the sensor ensuring maximum photon capture. When a green laser light (530 nm) passes through the Au-nanoprobes sample and focuses on the photovoltaic sensor, an electrical signal will be generated accordingly to the Au-nanoprobe SPR band absorption. When the Au-nanoprobes are dispersed, the SPR band peak is located at 526 nm and most of the light from the laser is absorbed. Consequently, less light will reach the photovoltaic sensor and a decrease in the electrical signal is observed. Conversely, when the Au-nanoprobes aggregate, the SPR band peak shifts to longer wavelengths and the light from the laser is less absorbed, being able to reach the sensor with higher intensity and generate a higher electric signal (see Figure 6.1).

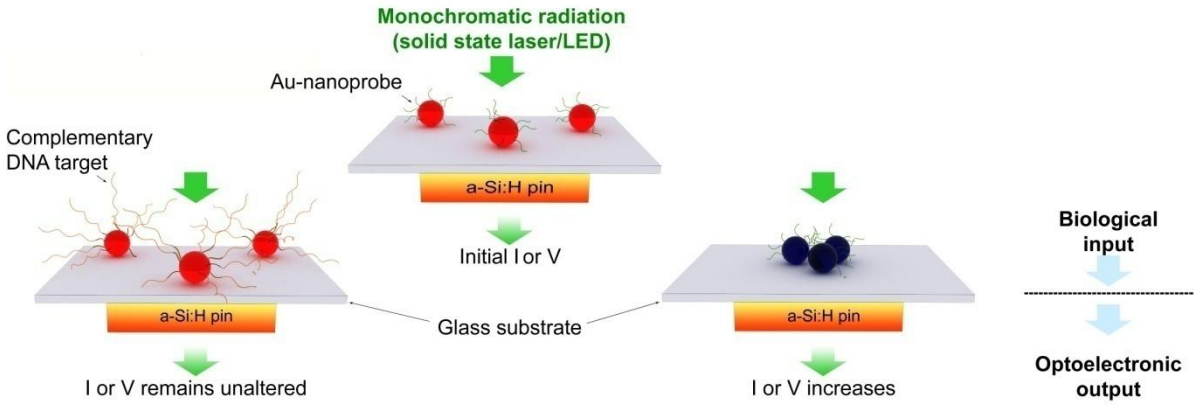

Figure 6.1 – Scheme of optoelectronic detector for Au-nanoprobe colorimetric changes[183]

Through this approach, it was possible to quantitatively assess the level of Au-nanoprobe aggregation, which has been here shown to be relevant for target quantification and SNP detection. Moreover, it was also possible to use ten times less sample volumes than what is used in colorimetric tests assessed by the naked eye.

Nevertheless, the application of the non-cross-linking method to POC is still dependent of miniaturization of the developed biosensor prototype, and requires sample preparation and PCR amplification. These issues may be solved via microfluidics for DNA extraction and PCR amplification with the photovoltaic sensor being inserted in the microchip platform.[184-186] A cost-effective portable handheld device integrating the microfluidic controls, the heating system for PCR and/or sample denaturation/hybridization and the photovoltaic sensor could be developed along with disposable microfluidic chips to mix samples and reagents, allowing

to conduct the assay in a “sample in-answer out” configuration. This way, no specialized experience would be required by the end-user, cross-contamination between samples is avoided (i.e. the chips that handle the samples are disposable), multiple targets could be assessed simultaneously (i.e. multiple Au-nanoprobes for multiple targets within amplicon can be analyzed by multiple photodetectors) and the overall costs per assay could be reduced (i.e. less reagents are needed and the most expensive low-cost components are within the portable device). Optimization and miniaturization of the photodetector is currently being pursued.[183,187,188]

6.2 Conclusions

In summary, the non-cross-linking method should be suitable to be commercialized as a kit, provided that validation and certification (e.g. CE mark) are successfully achieved. The kit can be used for medium-throughput nucleic acid target detection by specialized personnel at any standard molecular biology research/clinical laboratory, as an alternative to more expensive methodologies currently used (e.g. Real-Time PCR, RFLP, low-density DNA microarrays, etc.). In the future, integration of the non-cross-linking method in a microfluidic disposable low-cost chip could allow its application at POC by un-specialized personnel. These chips could then be processed by a portable device with a low-cost detection system, such as the light sensitive amorphous/nanocrystalline silicon *pi”ii”n* photovoltaic sensor presented in this chapter. This will allow a faster result assessment where it is most needed (i.e. at patient’s side), allowing for a decreased turnaround time and more efficient therapy management.

CHAPTER 7. General Discussions and Future Perspectives

In the post-genomic era, the demand for improved molecular diagnostic methods for use at the point-of-care allowing for the rapid, sensitive and accurate identification of pathogens and biothreat agents, early detection of cancer and genetic diseases, or for genotyping patients in personalized medicine, has steadily increased.[180] Currently available methods for the detection of specific nucleic acid sequences are still cumbersome and expensive, requiring specialized personnel and equipment. Nanobiotechnology approaches promise to offer solutions with higher sensitivity and selectivity at low costs, by exploring the peculiar physico-chemical properties of nanoscaled materials. Within these nanoscaled materials, AuNPs are one of the most promising and explored nanomaterials for molecular diagnostic applications.[62,100] Due to its simplicity, rapidness and low cost, the non-cross-linking Au-nanoprobe nucleic acid detection method presented here, holds great potential for POC diagnostic. The method has already been successfully applied to eukaryotic gene expression studies without retro-transcription or PCR amplification,[91] in a fast assay for *Mycobacterium tuberculosis* DNA detection in clinical samples,[103,104] and for SNP/mutation detection.[156]

Throughout the work presented in this thesis, several data were obtained regarding the noble metal nanoprobes' properties and their application for nucleic acid detection. From all the attained data, some constitute clear landmarks for the understanding of the non-cross-linking based detection and for the development of a commercial kit:

- The functionalization method of AuNPs based on ultrasounds allows for a faster synthesis of Au-nanoprobes with increased reproducibility between batches, when compared to the classic "salt-aging" method. This increased reproducibility grants a greater control over nanoprobe salt-induced aggregation which can be relevant to multiplexing using Au- and AuAg-nanoprobes, since it is convenient that both nanoprobes present similar stability (see Chapter 3);

- Monovalent salts and $MgCl_2$ quickly induce aggregation of nanoprobes, but $MgCl_2$ presents greater benefits for the non-cross-linking method, such as lower salt volumes needed and greater contrast in colorimetric changes. The presence of other reagents in solution (e.g. DMSO, formamide, etc.) can also further de-/stabilize the nanoprobes and, therefore, should be taken into account when performing the non-cross-linking method. Ultimately, the DLVO theory and the Schulze-Hardy rule can be used to predict the CCC value of salts to achieve nanoprobe aggregation (see Chapter 3);

- The non-cross-linking method allows to colorimetrically detect SNPs/mutations in most nucleic acids at room temperature, i.e. without the need for a controlled temperature, which is one of the main advantages over other molecular diagnostic methods. The detection can

be easily and quickly evaluated by naked eye or registered using standard spectrophotometric devices, with a sensitivity of ~70 nM target DNA (see Chapter 4);

- Both Au- and AuAg-nanoprobes can be used in the non-cross-linking method, and the simultaneous use of these nanoprobes may allow the detection of multiple targets in a single reaction, i.e. multiplexing (see Chapter 4);

- Maximum hybridization efficiency and SNP discrimination is achieved at pH8 with Au-nanoprobes holding a density of 24 pmol/cm^2 thiol-modified oligonucleotides, and when the mismatch is localized at the 3'-end of Au-nanoprobe (see Chapter 5);

- Electrostatic repulsion and steric hindrance proved to have an active role in Au-nanoprobe aggregation and, consequently, in the colorimetric changes observed for the non-cross-linking method. Between these two repulsive forces, steric hindrance proved to be the most relevant in nucleic acid and SNP/mutation detection (Chapter 5).

Through the extensive study of conditions and parameters influencing the non-cross-linking Au-nanoprobe nucleic acid detection method performance, several issues have been raised, paving the way for improvement and optimization towards use in clinical diagnostic. One of the problems that could be easily solved is the hybridization efficiency of Au-nanoprobes to dsDNA samples that affects the sensitivity and reproducibility of the method, especially for targets with a high GC-content. In some situations, this issue can be overcome by re-designing the Au-nanoprobe sequence to bind with a more accessible sequence. However, in the case of SNP/mutations this approach is not viable, and little can be done in the design of the Au-nanoprobe sequence other than varying its length (see Chapter 5, section 5.2.2.5). For 20 nt Au-nanoprobes, the density of thiol-oligonucleotide functionalized at the AuNPs surface has been shown to influence hybridization efficiency and mismatch discrimination, and, therefore, the hybridization efficiency of the 40 nt Au-nanoprobes should also be evaluated for different Au-nanoprobes density. The use of spacer d(T) sequences between the thiol- moiety and the probe sequences have also been reported to significantly improve the hybridization efficiency of Au-nanoprobes[81] and, therefore, should also be considered in future optimizations of the non-cross-linking method. Nonetheless, based on the results shown in Chapter 5, the use of longer sequences or spacers to decrease the steric congestion around the Au-nanoprobe's recognition sequence, may compromise the non-cross-linking method's capability of discriminating a mismatch at room temperature. Moreover, the longer oligonucleotides at the NP's surface may increase the stability of such Au-nanoprobes that no longer aggregate with the addition of an electrolyte in solution,

hampering their use in the non-cross-linking method. Therefore, a balance must be sought between sequence/spacer length, mismatch discrimination and Au-nanoprobe stability. Also, the use of ultrasounds to fragment long/complex targets into shorter and more accessible fragments[189] may improve hybridization efficiency with the Au-nanoprobes, and should be considered in future works.

Another approach that can increase the hybridization efficiency and mismatch discrimination without changing the Au-nanoprobe sequence length or using spacer sequences, is to use thiol-modified LNA (locked nucleic acids) or PNA (protein nucleic acids) sequences to functionalize the AuNPs. These DNA analogs molecules have been shown to possess a higher affinity and specificity to complementary DNA/RNA sequences than ssDNA oligonucleotides.[190,191] Functionalization of AuNPs with PNA has been described by Chakrabarti and co-workers, where a cysteine residue was added to either the N- or C-terminus of PNAs to provide the thiol necessary for immobilization to AuNPs.[192] These PNA-AuNPs conjugates were successfully used to colorimetrically detect a mismatch in ssDNA oligonucleotides targets by following the same non-cross-linking approach described in this thesis. Nonetheless, the application of such approach to the detection of real biological dsDNA samples has not been addressed and remains unexplored. Functionalization of AuNPs with alkanethiol-modified LNA/DNA chimeras, and their use in the detection of nucleic acid sequences following the cross-linking method, has been recently reported by McKenzie and co-workers.[193,194] These LNA-AuNPs conjugates have demonstrated to have greater sequence specificity and better binding affinity to ssDNA, or even to specifically bind to dsDNA when targeting a polypurine duplex region. Therefore, the use of such LNA-AuNPs conjugates in the non-cross-linking method could avoid the need for DNA denaturation and the problems related to rich GC-sequences. It should be pointed out that the main disadvantage of using LNA and PNA is their current high synthesis costs, which can considerably raise the costs of the proposed method.

As it frequently happens with other approaches, the direct detection of SNP/mutations in genomic DNA with Au-nanoprobes may not be possible due to highly homologous sequences present in pseudogenes, where problems with false-positive polymorphism genotyping in genes with high homology to other gene family members or pseudogenes have been reported,[195] including with the CYP2D6 and associated pseudogenes.[196] In such cases, the non-cross-linking method needs to be associated to a method that allows to specifically amplifying the sequence of interest (i.e. the target *locus*) in detriment of homologous sequences (e.g. pseudogene), since the Au-nanoprobe sequence may not be able to be designed in a non-homologous region. The use of conventional and asymmetric PCR has so far allowed flanking and specifically amplifying that sequence of interest overcoming this problem. Additionally, asymmetric PCR also improves target hybridization to the Au-nanoprobes.

Another option would be to use isothermal amplification techniques near room temperature that could circumvent the need for a thermocycler (a heated bath or a helicase could be used for DNA denaturation). A good candidate would be the helicase-dependent amplification (HDA), which is a simple method that allows the amplification of a primer-flanked region at room temperature without the need for template denaturation, and that can achieve a million-fold amplification under 1h.[197] This method could be further adapted to yield ssDNA targets for direct hybridization with Au-nanoprobes, by using different primer concentrations as in the case of asymmetric PCR. Nevertheless, HDA relies on the presence of two DNA binding proteins, namely SSB proteins and helicase accessory proteins, which may interfere with the non-cross-linking method by non-specific adsorption to the Au-nanoprobes (i.e. they may not aggregate at all with the adsorption of such proteins). Therefore, a stability test of the Au-nanoprobes against increasing concentrations of salt should be performed in the presence of such proteins to assess the viability of this method. Even so, if these proteins actually interfere with the non-cross-linking method, simple sample purification could be included.

For most applications, however, it is safe to admit that further improvements of Au-nanoprobe hybridization efficiency will allow to increase sensitivity and to directly detect SNP/mutations in genomic DNA. This would discard the need for PCR amplification, reduce false positives/negatives due to the possibility of mutation insertion by *Taq* polymerase,[198] while making the non-cross-linking a better candidate for point-of-care diagnostic.

The current sensitivity of the non-cross-linking method could be further enhanced by using bigger (e.g. 40~50 nm) AuNPs or alloy AuAgNPs, which have higher absorption coefficients and much stronger scattering properties.[66,78] By using such NPs it would be possible to explore the more sensitive properties of light scattering, which also change with AuNPs aggregation.[199] In the case of alloy AuAgNPs, it has been here demonstrated that they can be used for the detection of specific nucleic acids sequences following the non-cross-linking method. Preliminary results for the multiplexing approach have shown that the combination of Au-nanoprobes with AuAg-nanoprobes hold great potential for multiplexing, and, ultimately, for homo/heterozygous characterization in a single reaction. Still, one of the biggest challenges for this multiplexing approach is to gather two nanoprobes with similar stability against salt-induced aggregation. Nonetheless, as previously described, the functionalization of the AuNPs and AuAgNPs following the ultrasound approach has allowed to better control and reproduce the resulting nanoprobes, and this is reflected in a more constant and reproducible stability.

The application of non-cross-linking method to other type of mutations, such as deletions, insertions, gene duplications, chromosomal translocations or inversions, should also be addressed in future studies. In principle, the single nucleotide resolution of the Au-nanoprobes should allow to detect these other mutations, except, maybe, for gene duplications. In this latter case, the multiplex non-cross-linking method could be used to

relatively quantify the target gene by using a second nanoprobe as an internal control. The overall ratio between aggregated/dispersed Au-nanoprobes has been shown to linearly depend on increasing complementary target concentration (see Figure 4.4 – B in Chapter 4, section 4.2.1.2). Therefore, the presence of gene duplications could be inferred by the non-cross-linking method through the quantification of serial dilutions of the sample.

Finally, the non-cross-linking method as it is, when compared to other currently developed methods, presents both advantages and disadvantages. The main advantage is its overall cost, which is estimated to be ~€0.05 per test. Even though it looks promising when compared to other platforms, its use is more suitable for few targets in routine diagnostics and not as a high-throughput method for the analysis of a larger numbers of biomarkers. Considering this issue, the non-cross-linking method would be better suited for the assessment of few *loci* at point-of-care (medium throughput). In a laboratory setting, this method should be effective for the molecular diagnosis of pathogenic diseases, where the capability of the method to detect SNP/mutations can be used for multi-drug resistance characterization (e.g. multi-drug resistant tuberculosis[200]). Indeed, the inexpensive experimental set-up, the short developing time without the need of signal amplification or temperature control and the fact that color change can be assessed visually are of great advantage for the application of the non-cross-linking in the field, and application to other clinical relevant situations have already been shown.[104]

In summary, this thesis has successfully achieved its objectives by providing a new low-cost and fast colorimetric method to detect SNP/mutations in biological samples. The method and its application as a kit has already been protected by a pending national and international patent.[179] Therefore, the method can now be further validated and certified for commercial application as a kit and further integrated into new nano/microfluidics autonomous platforms for POC application. Based on all the information gathered within this thesis, the application of the method to other targets should now be easily achieved.

REFERENCES

[1] Venter JC, Adams MD, Myers EW, Li PW, Mural RJ, Sutton GG, Smith HO, Yandell M, Evans CA, Holt RA, Gocayne JD, Amanatides P, Ballew RM, *et al*. (2001) The sequence of the human genome. *Science*, 291:1304-1351.

[2] ENCODE Project Consortium (2004) The ENCODE (ENCyclopedia Of DNA Elements) Project. *Science*, 306:636-640

[3] The International HapMap Consortium (2005) A haplotype map of the human genome. *Nature*, 437:1299-1320.

[4] Weber JL, David D, Heil J, Fan Y, Zhao C, Marth G (2002) Human diallelic insertion/deletion polymorphisms. *Am J Hum Genet*, 71:854-862

[5] Collins FS, Brooks LD, Chakravarti A (1998) A DNA polymorphism discovery resource for research on human genetic variation. *Genome Res*, 8:1229-1231

[6] Wang Z, Moult J (2001) SNPs, protein structure, and disease. *Hum Mutation*, 17:263-270

[7] Tabor HK, Risch NJ, Myers RM (2002) Candidate-gene approaches for studying complex genetic traits: practical considerations. *Nat Rev Genet*, 3:391-397

[8] Dykes CW (1996) Genes, disease and medicine. *Br J Clin Pharmacol*, 42:683-695

[9] Bell J (2004) Predicting disease using genomics. *Nature*, 429:453-456

[10] Amberger J, Bocchini CA, Scott AF, Hamosh A (2009) McKusick's Online Mendelian Inheritance in Man (OMIM®). *Nucleic Acids Res*, 37:D793-796

[11] Weatherall DJ (2001) Phenotype-genotype relationships in monogenic disease: lessons from the thalassaemias. *Nat Rev Genet*, 2:245-255

[12] Nabholz CE, von Overbeck J (2004) Gene-environment interactions and the complexity of human genetic diseases. *J Insur Med*, 36:47-53

[13] Baptista PV (2005) Principles in genetic risk assessment. *Ther Clin Risk Manag*, 1:15-20

[14] Abramson RD, Myers TW (1993) Nucleic acid amplification technologies. *Curr Opin Biotechnol*, 4:41-47

[15] Mullis K, Faloona F, Scharf S, Saiki R, Horn G, Erlich H (1986) Specific enzymatic amplification of DNA in vitro: the polymerase chain reaction. *Cold Spring Harb Symp Quant Biol*, 1:263-273

[16] Erlich HA, Gelfand D, Sninsky JJ (1991) Recent advances in the polymerase chain reaction. *Science*, 252:1643-1651

[17] Newton CR, Graham A, Heptinstall LE, Powell SJ, Summers C, Kalsheker N, Smith JC, Markham AF (1989) Analysis of any point mutation in DNA. The amplification refractory mutation system (ARMS). *Nucleic Acids Res*, 17:2503-2516

[18] Arya M, Shergill IS, Williamson M, Gommersall L, Arya N, Patel HRH (2005) Basic principles of real-time quantitative PCR. *Expert Rev Mol Diagn*, 5:209-219

[19] Mackay J, Landt O (2007) Real-time PCR fluorescent chemistries. *Methods Mol Biol*, 353:237-261

[20] Gyllensten UB, Erlich HA (1988) Generation of single-stranded DNA by the polymerase chain reaction and its application to direct sequencing of the HLA-DQA *locus*. *Proc Natl Acad Sci USA*, 85:7652-7656

[21] SantaLucia J (1998) A unified view of polymer, dumbbell, and oligonucleotide DNA nearest-neighbor thermodynamics. *Proc Natl Acad Sci USA*, 95:1460-1465

[22] Sanchez JA, Pierce KE, Rice JE, Wangh LJ (2004) Linear-after-the-exponential (LATE)-PCR: an advanced method of asymmetric PCR and its uses in quantitative real-time analysis. *Proc Natl Acad Sci USA*, 101:1933-1938

[23] Gill P, Ghaemi A (2008) Nucleic Acid Isothermal Amplification Technologies - A Review. *Nucleos Nucleot Nucl*, 27:224-243

[24] Notomi T, Okayama H, Masubuchi H, Yonekawa T, Watanabe K, Amino N, Hase T (2000) Loop-mediated isothermal amplification of DNA. *Nucl Acids Res*, 28:e63

[25] Parida M, Sannarangaiah S, Dash PK, Rao PVL, Morita K (2008) Loop mediated isothermal amplification (LAMP): a new generation of innovative gene amplification technique; perspectives in clinical diagnosis of infectious diseases. *Rev Med Virol*, 18:407-421

[26] Enomoto Y, Yoshikawa T, Ihira M, Akimoto S, Miyake F, Usui C, Suga S, Suzuki K, Kawana T, Nishiyama Y, Asano Y (2005) Rapid diagnosis of herpes simplex virus infection by a loop-mediated isothermal amplification method. *J Clin Microbiol*, 43:951-955

[27] Kaneko H, Iida T, Aoki K, Ohno S, Suzutani T (2005) Sensitive and rapid detection of herpes simplex virus and varicella-zoster virus DNA by loopmediated isothermal amplification. *J Clin Microbiol*, 43:3290-3296

[28] Nagamine K, Watanabe K, Ohtsuka K, Hase T, Notomi T (2001) Loop-mediated isothermal amplification reaction using a nondenatured template. *Clin Chem*, 47:1742-1743

[29] Cooper DN, Schmidtke J (1984) DNA restriction fragment length polymorphisms and heterozygosity in the human genome. *Hum Genet*, 66:1-16

[30] Turner DH (1996) Thermodynamics of base pairing. *Curr Opin Struct Biol*, 6:299-304

[31] Southern EM (1975) Detection of specific sequences among DNA fragments separated by gel electrophoresis. *J Mol Biol*, 98:503-517

[32] Alwine JC, Kemp DJ, Stark GR (1977) Method for detection of specific RNAs in agarose gels by transfer to diazobenzyloxymethyl-paper and hybridization with DNA probes. *Proc Natl Acad Sci USA*, 74:5350-5354

[33] Volpi EV, Bridger JM (2008) FISH glossary: an overview of the fluorescence *in situ* hybridization technique. *Biotechniques*, 45:385-409

[34] Dufva M (2009) Introduction to microarray technology. *Methods Mol Biol*, 529:1-22

[35] Lazurkin YS, Frank-Kamenetskii MD, Trifonov EN (1970) Melting of DNA: Its study and application as a research method. *Biopolymers*, 9:1253-1306

[36] Ririe KM, Rasmussen RP, Wittwer CT (1997) Product differentiation by analysis of DNA melting curves during the polymerase chain reaction. *Anal Biochem*, 245:154-160

[37] Wittwer CT, Reed GH, Gundry CN, Vandersteen JG, Pryor RJ (2003) High-resolution genotyping by amplicon melting analysis using LCGreen. *Clin Chem*, 49:853-860

[38] Reed GH, Kent JO, Wittwer CT (2007) High-resolution DNA melting analysis for simple and efficient molecular diagnostics. *Pharmacogenomics*, 8:597-608

[39] Frueh FW, Noyer-Weidner M (2003) The use of denaturing high-performance liquid chromatography (DHPLC) for the analysis of genetic variations: impact for diagnostics and pharmacogenetics. *Clin Chem Lab Med*, 41:452-461

[40] Oberacher H (2008) On the use of different mass spectrometric techniques for characterization of sequence variability in genomic DNA. *Anal Bioanal Chem*, 391:135-149

[41] Sanger F, Nicklen S, Coulson AR (1977) Nucleotide sequence of bacteriophage *phi* X174 DNA. *Nature*, 265:687-695

[42] Shendure J, Ji H (2008) Next-generation DNA-sequencing. *Nat Biotechnol*, 26:1135-1145

[43] Feynman RP (1960) There's plenty of room at the bottom. *Engineering and Science*, 23:22-36

[44] Tseng AA, Li Z (2007) Manipulations of atoms and molecules by scanning probe microscopy. *J Nanosci Nanotechnol*, 7:2582-2595

[45] Gates BD, Xu Q, Stewart M, Ryan D, Willson CG, Whitesides GM (2005) New approaches to nanofabrication: molding, printing, and other techniques. *Chem Rev*, 105:1171-1196

[46] Lazzari M, Rodríguez-Abreu C, Rivas J, López-Quintela MA (2006) Self-assembly: a minimalist route to the fabrication of nanomaterials. *J Nanosci Nanotechnol*, 6:892-905

[47] Mulder A, Huskens J, Reinhoudt DN (2004) Multivalency in supramolecular chemistry and nanofabrication. *Org Biomol Chem*, 2:3409-3424

[48] Cui H, Feng Y, Ren W, Zeng T, Lv H, Pan Y (2009) Strategies of large scale synthesis of monodisperse nanoparticles. *Recent Pat Nanotechnol*, 3:32-41

[49] Müller DJ, Dufrêne YF (2008) Atomic force microscopy as a multifunctional molecular toolbox in nanobiotechnology. *Nat Nanotechnol*, 3:261-269

[50] Santos NC, Castanho MARB (2004) An overview of the biophysical applications of atomic force microscopy. *Biophys Chem*, 107:133-149

[51] Jain KK (2007) Applications of nanobiotechnology in clinical diagnostics. *Clin Chem*, 53:2002-2009

[52] Jain KK (2008) Nanomedicine: application of nanobiotechnology in medical practice. *Med Princ Pract*, 17:89-101

[53] Jain KK (2003) Nanodiagnostics: application of nanotechnology in molecular diagnostics. *Expert Rev Mol Diagn*, 3:153-161

[54] Jain KK (2005) Nanotechnology in clinical laboratory diagnostics. Clin Chim Acta, 358:37-54

[55] Johnson CJ, Zhukovsky N, Cass AE, Nagy JM (2008) Proteomics, nanotechnology and molecular diagnostics. *Proteomics*, 8:715-730

[56] Mirkin CA, Niemeyer CM (2004) Nanobiotechnology: Concepts, applications and perspectives. *1st ed*., Wiley-VCH, Weinheim

[57] Mirkin CA, Niemeyer CM (2007) Nanobiotechnology II: More concepts and applications. *1st ed*., Wiley-VCH, Weinheim

[58] Azzazy HM, Mansour MM (2009) In vitro diagnostic prospects of nanoparticles. *Clin Chim Acta*, 403:1-8

[59] Vollath D (2008) Nanomaterials: an introduction to synthesis, properties and applications. *1st ed*., Wiley-VCH, Weinheim

[60] Michalet X, Pinaud FF, Bentolila LA, Tsay JM, Doose S, Li JJ, Sundaresan G, Wu AM, Gambhir SS, Weiss S (2005) Quantum dots for live cells, *in vivo* imaging, and diagnostics. *Science*, 307:538-544

[61] Delehanty JB, Mattoussi H, Medintz IL (2009) Delivering quantum dots into cells: strategies, progress and remaining issues. *Anal Bioanal Chem*, 393:1091-1105

[62] Baptista P, Pereira E, Eaton P, Doria G, Miranda A, Gomes I, Quaresma P, Franco R (2008) Gold nanoparticles for the development of clinical diagnosis methods. *Anal Bioanal Chem*, 391:943-950

[63] Boisselier E, Astruc D (2009) Gold nanoparticles in nanomedicine: preparations, imaging, diagnostics, therapies and toxicity. *Chem Soc Rev*, 38:1759-1782

[64] Sperling RA, Rivera Gil P, Zhang F, Zanella M, Parak WJ (2008) Biological applications of gold nanoparticles. *Chem Soc Rev*, 37:1896-1908

[65] Huang X, Jain PK, El-Sayed IH, El-Sayed MA (2007) Gold nanoparticles: Interesting optical properties and recent applications in cancer diagnostics and therapy. *Nanomed*, 2:681-693

[66] Jain PK, Lee KS, El-Sayed IH, El-Sayed MA (2006) Calculated absorption and scattering properties of gold nanoparticles of different size, shape, and composition: applications in biological imaging and biomedicine. *J Phys Chem B*, 110:7238-7248

[67] Hu M, Chen J, Li Z, Au L, Hartland GV, Li X, Marquez M, Xia Y (2006) Gold nanostructures: engineering their plasmonics properties for biomedical applications. *Chem Soc Rev*, 35:1084-1094

[68] Jain, PK, Huang W, El-Sayed MA (2007) On the universal scaling behavior of the distance decay of plasmon coupling in metal nanoparticle pairs: A plasmon ruler equation. *Nano Lett*, 7:2080-2088

[69] Liz-Marzan LM (2006) Tailoring surface plasmons through the morphology and assembly of metal nanoparticles. *Langmuir*, 22:32-41

[70] Xu Z, Hou Y, Sun S (2007) Magnetic core/shell Fe_3O_4/Au and Fe_3O_4/Au/Ag nanoparticles with tunable plasmonic properties. *J Am Chem Soc*, 129:8698-8699

[71] Mie G (1908) Beiträge zur optik trüber medien, speziell kolloidaler metallösungen. *Ann Phys*, 330:377-445

[72] Daniel MC, Astruc D (2004) Gold nanoparticles: assembly, supramolecular chemistry, quantum-size-related properties, and applications toward biology, catalysis, and nanotechnology. *Chem Rev*, 104:293-346

[73] Green M (2005) Organometallic based strategies for metal nanocrystal synthesis. *Chem Commun*, (24):3002-3011

[74] Murphy CJ, San TK, Gole AM, Orendorff CJ, Gao JX, Gou L, Hunyadi SE, Li T (2005) Anisotropic metal nanoparticles: synthesis, assembly, and optical applications. *J Phys Chem B,* 109:13857-13870

[75] Brust M, Walker M, Bethell D, Schiffrin DJ, Whyman R (1994) Synthesis of thiol-derivatised gold nanoparticles in a two-phase liquid-liquid system. *J Chem Soc Chem Commun*, (7):801-802

[76] Turkevich J, Stevenson PC, Hillier J (1951) A study of the nucleation and growth processes in the synthesis of colloidal gold. *Discuss Faraday Soc*, 11:55-75

[77] Kimling J, Maier M, Okenve B, Kotaidis V, Ballot H, Plech A (2006) Turkevich method for gold nanoparticle synthesis revisited. *J Phys Chem B*, 110:15700-15707

[78] Link S, Wang ZL, El-Sayed MA (1999) Alloy formation of gold−silver nanoparticles and the dependence of the plasmon absorption on their composition. *J Phys Chem B*, 103:3529-3533

[79] Jana NR, Peng X (2003) Single-phase and gram-scale routes toward nearly monodisperse Au and other noble metal nanocrystals. *J Am Chem Soc*, 125:14280-14281

[80] Mirkin CA, Letsinger RL, Mucic RC, Storhoff JJ (1996) A DNA-based method for rationally assembling nanoparticles into macroscopic materials. *Nature*, 382:607-609

[81] Demers LM, Mirkin CA, Mucic RC, Reynolds RA III, Letsinger RL, Elghanian R, Viswanadham G (2000) A fluorescence-based method for determining the surface coverage and hybridization efficiency of thiol-capped oligonucleotides bound to gold thin films and nanoparticles. *Anal Chem*, 72:5535-5541

[82] Sato K, Hosokawa K, Maeda M (2003) Rapid aggregation of gold nanoparticles induced by non-cross-linking DNA hybridization. *J Am Chem Soc*, 125:8102-8103

[83] Ray PC, Fortner A, Darbha GK (2006) Gold nanoparticle based FRET assay for the detection of DNA cleavage. *J Phys Chem B*, 110:20745-20748

[84] Kühn S, Håkanson U, Rogobete L, Sandoghdar V (2006) Enhancement of single-molecule fluorescence using a gold nanoparticle as an optical nanoantenna. *Phys Rev Lett*, 97:017402

[85] Hurst SJ, Lytton-Jean AK, Mirkin CA (2006) Maximizing DNA loading on a range of gold nanoparticle sizes. *Anal Chem*, 78:8313-8318

[86] Storhoff JJ, Elghanian R, Mirkin CA, Letsinger RL (2002) Sequence-dependent stability of DNA-modified gold nanoparticles. *Langmuir*, 18:6666-6670

[87] Suzuki K, Hosokawa K, Maeda M (2009) Controlling the number and positions of oligonucleotides on gold nanoparticle surfaces. *J Am Chem Soc*, 131:7518-7519

[88] Xu X, Rosi NL, Wang Y, Huo F, Mirkin CA (2006) Asymmetric functionalization of gold nanoparticles with oligonucleotides. *J Am Chem Soc*, 128:9286-9287

[89] Steinbrück A, Csaki A, Ritter K, Leich M, Köhler JM, Fritzsche W (2008) Gold-silver and silver-silver nanoparticle constructs based on DNA hybridization of thiol- and amino-functionalized oligonucleotides. *J Biophotonics*, 1:104-113

[90] Cao YC, Jin R, Thaxton CS, Mirkin CA (2005) A two-color-change, nanoparticle-based method for DNA detection. *Talanta*, 67:449-455

[91] Baptista P, Doria G, Henriques D, Pereira E, Franco R (2005) Colorimetric detection of eukaryotic gene expression with DNA-derivatized gold nanoparticles. *J Biotechnol*, 119:111-117

[92] Stakenborg T, Peeters S, Reekmans G, Laureyn W, Jans H, Borghs G, Imberechts H (2008) Increasing the stability of DNA-functionalized gold nanoparticles using mercaptoalkanes. *J Nanopart Res*, 10:143-152

[93] Zhou J, Ralston J, Sedev R, Beattie DA (2009) Functionalized gold nanoparticles: Synthesis, structure and colloid stability. *J Colloid Interface Sci*, 331:251-262

[94] Kim T, Lee K, Gong MS, Joo SW (2005) Control of gold nanoparticle aggregates by manipulation of interparticle interaction. *Langmuir*, 21:9524-9528

[95] Hiemenz PC, Rajagopalan R (1997) Principles of colloid and surface chemistry. *3rd Ed*., Marcel Dekker, New York

[96] Myers D (1999) Surfaces, interfaces and colloids: principles and applications. *2nd Ed*., John Wiley & Sons, Inc., New York

[97] Li H, Rothberg LJ (2004) Label-free colorimetric detection of specific sequences in genomic DNA amplified by the polymerase chain reaction. *J Am Chem Soc*, 126:10958-10961

[98] Glynou K, Ioannou PC, Christopoulos TK, Syriopoulou V (2003) Oligonucleotide-functionalized gold nanoparticles as probes in a dry-reagent strip biosensor for DNA analysis by hybridization. *Anal Chem*, 75:4155-4160

[99] Taton TA, Mirkin CA, Letsinger RL (2000) Scanometric DNA array detection with nanoparticle probes. *Science*, 289:1757-1760

[100] Thaxton CS, Georganopoulou DG, Mirkin CA (2006) Gold nanoparticle probes for the detection of nucleic acid targets. *Clin Chim Acta*, 363:120-126

[101] Storhoff JJ, Elghanian R, Mucic RC, Mirkin CA, Letsinger RL (1998) One-pot colorimetric differentiation of polynucleotides with single base imperfections using gold nanoparticle probes. *J Am Chem Soc*, 120:1959-1964

[102] Sato K, Hosokawa K, Maeda M (2005) Non-cross-linking gold nanoparticle aggregation as a detection method for single-base substitutions. *Nucleic Acids Res*, 33:e4

[103] Baptista PV, Koziol-Montewka M, Paluch-Oles J, Doria G, Franco R (2006) Gold-nanoparticle-probe-based assay for rapid and direct detection of *Mycobacterium tuberculosis* DNA in clinical samples. *Clin Chem*, 52:1433-1434

[104] Costa P, Amaro A, Botelho A, Inácio J, Baptista PV (2009) Gold nanoprobes assay for identification of mycobacteria from the *Mycobacterium tuberculosis* complex. C*lin Microbiol Infect*, in press

[105] Litos IK, Ioannou PC, Christopoulos TK, Traeger-Synodinos J, Kanavakis E (2007) Genotyping of single-nucleotide polymorphisms by primer extension reaction in a dry-reagent dipstick format. *Anal Chem*, 79:395-402

[106] Litos IK, Ioannou PC, Christopoulos TK, Traeger-Synodinos J, Kanavakis E (2009) Multianalyte, dipstick-type, nanoparticle-based DNA biosensor for visual genotyping of single-nucleotide polymorphisms. *Biosens Bioelectron*, 24:3135-3139

[107] Kalogianni DP, Bravou V, Christopoulos TK, Ioannou PC, Zoumbos NC (2007) Dry-reagent disposable dipstick test for visual screening of seven leukemia-related chromosomal translocations*. Nucleic Acids Res*, 35:e23

[108] Storhoff JJ, Marla SS, Bao YP, Hagenow S, Mehta H, Lucas AD, Garimella V, Patno T, Buckingham W, Cork W, Muller UR (2004) Gold nanoparticle-based detection of genomic

DNA targets on microarrays using a novel optical detection system. *Biosens Bioelectron*, 19:875-883

[109] Cao YC, Jin R, Mirkin CA (2002) Nanoparticles with Raman spectroscopic fingerprints for DNA and RNA detection. *Science*, 297:1536-1540

[110] Qian X, Zhou X, Nie S (2008) Surface-enhanced Raman nanoparticle beacons based on bioconjugated gold nanocrystals and long range plasmonic coupling. *J Am Chem Soc*, 130:14934-14935

[111] Castañeda MT, Alegret S, Merkoçi A (2007) Electrochemical sensing of DNA using gold nanoparticles. *Electroanalysis*, 19:743-753

[112] Lee J-S, Lytton-Jean AKR, Hurst SJ, Mirkin CA (2007) Silver Nanoparticle−oligonucleotide conjugates based on DNA with triple cyclic disulfide moieties. *Nano Lett*, 7:2112-2115

[113] Baumgartner BG, Orpinell M, Duran J, Ribas V, Burghardt HE, Bach D, Villar AV, Paz JC, González M, Camps M, Oriola J, Rivera F, Palacín M, Zorzano A (2007) Identification of a novel modulator of thyroid hormone receptor-mediated action. *PLoS One*, 2:e1183

[114] Ingelman-Sundberg M (2005) Genetic polymorphisms of Cytochrome P450 2D6 (CYP2D6): clinical consequences, evolutionary aspects and functional diversity. *Pharmacogenomics J*, 5:6-13

[115] Sarnaik SA (2005) Thalassemia and related hemoglobinopathies. *Indian J Pediatr*, 72:319-324

[116] Flint J, Harding RM, Boyce AJ, Clegg JB (1993) The population genetics of the haemoglobinopathies. *Baillieres Clin Haematol*, 6:215-262

[117] Loukopoulos D (1991) Thalassemia: genotypes and phenotypes. *Ann Hematol*, 62:145-150

[118] Thein SL (2004) Genetic insights into the clinical diversity of beta thalassaemia. *Br J Haematol*, 124:264-274

[119] Patrinos GP, Giardine B, Riemer C, Miller W, Chui DHK, Anagnou NP, Wajcman H, Hardison RC (2004) Improvements in the HbVar database of human hemoglobin variants and thalassemia mutations for population and sequence variation studies. *Nucleic Acids Res*, 32:D537-541

[120] Flint J, Harding RM, Boyce AJ, Clegg JB (1998) The population genetics of the haemoglobinopathies. *Baillieres Clin Haematol*, 11:1-51

[121] Thein SL, Hesketh C, Wallace RB, Weatherall DJ (1988) The molecular basis of thalassaemia major and thalassaemia intermedia in Asian Indians: application to prenatal diagnosis. *Br J Haematol*, 70:225-231

[122] Ho PJ (1999) The regulation of beta globin gene expression and beta thalassemia. *Pathology*, 31:315-324

[123] Clark BE, Thein SL (2004) Molecular diagnosis of haemoglobin disorders. *Clin Lab Haem*, 26:159-176

[124] Dong C, Wang S, Li WD, Li D, Zhao H, Price RA (2003) Interacting genetic *loci* on chromosomes 20 and 10 influence extreme human obesity. *Am J Hum Genet*, 72:115-124.

[125] Lee JH, Reed DR, Li WD, Xu W, Joo EJ, Kilker RL, Nanthakumar E, North M, Sakul H, Bell C, Price RA (1999) Genome scan for human obesity and linkage to markers in 20q13. *Am J Hum Genet*, 64:196-209

[126] Lembertas AV, Perusse L, Chagnon YC, Fisler JS, Warden CH, Purcell-Huynh DA, Dionne FT, Gagnon J, Nadeau A, Lusis AJ, Bouchard C (1997) Identification of an obesity quantitative trait *locus* on mouse chromosome 2 and evidence of linkage to body fat and insulin on the human homologous region 20q. *J Clin Invest*, 100:1240-1247

[127] Ghosh S, Watanabe RM, Hauser ER, Valle T, Magnuson VL, Erdos MR, Langefeld CD, Balow J Jr, Ally DS, Kohtamaki K, Chines P, Birznieks G, Kaleta HS, Musick A, Te C, Tannenbaum J, Eldridge W, Shapiro S, Martin C, Witt A, So A, Chang J, Shurtleff B, Porter R, Kudelko K, Unni A, Segal L, Sharaf R, Blaschak-Harvan J, Eriksson J, Tenkula T, Vidgren G, Ehnholm C, Tuomilehto-Wolf E, Hagopian W, Buchanan TA, Tuomilehto J, Bergman RN, Collins FS, Boehnke M (1999) Type 2 diabetes: evidence for linkage on chromosome 20 in 716 Finnish affected sib pairs. *Proc Natl Acad Sci USA*, 96:2198-2203

[128] Iwasaki N, Cox NJ, Wang YQ, Schwarz PE, Bell GI, Honda M, Imura M, Ogata M, Saito M, Kamatani N, Iwamoto Y (2003) Mapping genes influencing type 2 diabetes risk and BMI in Japanese subjects. *Diabetes*, 52:209-213

[129] Vionnet N, Hani EH, Dupont S, Gallina S, Francke S, Dotte S, De Matos F, Durand E, Leprêtre F, Lecoeur C, Gallina P, Zekiri L, Dina C, Froguel P (2000) Genome-wide search for type 2 diabetes-susceptibility genes in French whites: evidence for a novel susceptibility *locus* for early-onset diabetes on chromosome 3q27-qter and independent replication of a type 2-diabetes *locus* on chromosome 1q21-q24. *Am J Hum Genet*, 67:1470-1480

[130] Armada-Bras J, Barysch SV, Renne U, Brenig B, Baumgartner A, Baumgartner BG (2007) A novel nuclear cofactor in metabolic disease. in *Hot Topic Abstracts, Int J Obesity*, 31:1484-1490

[131] Wilkinson GR (2005) Drug metabolism and variability among patients in drug response. *N Engl J Med*, 352:2211-2221

[132] Bertz RJ, Granneman GR (1997) Use of *in vitro* and *in vivo* data to estimate the likelihood of metabolic pharmacokinetic interactions. *Clin Pharmacokinet*, 32:210-258

[133] Bradford LD (2002) CYP2D6 allele frequency in European Caucasians, Asians, Africans and their descendants. *Pharmacogenomics*, 3:229-243

[134] Stamer UM, Bayerer B, Wolf S, Hoeft A, Stüber F (2002) Rapid and reliable method for Cytochrome P450 2D6 genotyping. *Clin Chem*, 48:1412-1417

[135] Stüven T, Griese EU, Kroemer HK, Eichelbaum M, Zanger UM (1996) Rapid detection of CYP2D6 null alleles by long distance- and multiplex-polymerase chain reaction. *Pharmacogenetics*, 6:417-421

[136] Sachse C, Brockmöller J, Bauer S, Roots I (1997) Cytochrome P450 2D6 variants in a Caucasian population: allele frequencies and phenotypic consequences. *Am J Hum Genet*, 60:284-295

[137] Sistonen J, Fuselli S, Levo A, Sajantila A (2005) CYP2D6 genotyping by a multiplex primer extension reaction. *Clin Chem*, 51:1291-1295

[138] Zackrisson AL, Lindblom B (2003) Identification of CYP2D6 alleles by single nucleotide polymorphism analysis using pyrosequencing. *Eur J Clin Pharmacol*, 59:521-526

[139] Chou WH, Yan FX, Robbins-Weilert DK, Ryder TB, Liu WW, Perbost C, Fairchild M, Leon J, Koch WH, Wedlund PJ (2003) Comparison of two CYP2D6 genotyping methods and assessment of genotype-phenotype relationships. *Clin Chem*, 49:542-551

[140] Faustino P, Osório-Almeida L, Barbot J, Espirito-Santo D, Gonçalves J, Romão L, Martins MC, Marques MM, Lavinha J (1992) Novel promoter and splice junction defects add to the genetic, clinical or geographic heterogeneity of beta-thalassaemia in Portuguese population. *Hum Genet*, 89:573-576

[141] Kimura S, Umeno M, Skoda RC, Meyer UA, Gonzalez FJ (1989) The human debrisoquine 4-hydroxylase (CYP2D) *locus*: sequence and identification of the polymorphic CYP2D6 gene, a related gene, and a pseudogene. *Am J Hum Genet*, 45:889-904

[142] Inoue H, Nojima H, Okayama H (1990) High efficiency transformation of *Escherichia coli* with plasmids. *Gene*, 96:23-28

[143] Sun Y, Hegamyer G, Colburn NH (1993) PCR-direct sequencing of GC-rich region by inclusion of 10% DMSO: application to mouse c-jun. *Biotechniques*, 15:372-374

[144] Johansson I, Lundqvist E, Dahl ML, Ingelman-Sundberg M (1996) PCR-based genotyping for duplicated and deleted CYP2D6 genes. *Pharmacogenetics*, 6:351-355

[145] McElroy S, Sachse C, Brockmoller J, Richmond J, Lira M, Friedman D, Roots I, Silber BM, Milos PM (2000) CYP2D6 genotyping as an alternative to phenotyping for determination of metabolic status in a clinical trial setting. *AAPS PharmSci*, 2:E33

[146] Topić E, Stefanović M, Nikolić V, Zoricić I, Ivanisević AM, Zuntar I (1998) Detection of CYP2D6*3 and 2D6*4 allelic variants by PCR-restriction fragment length polymorphism. *Clin Chem Lab Med*, 36:655-658

[147] Lee PC, Meisel D (1982) Adsorption and surface-enhanced Raman of dyes on silver and gold sols. *J Phys Chem*, 86:3391-3395.

[148] Eaton P, Doria G, Pereira E, Baptista PV, Franco R (2007) Imaging gold nanoparticles for DNA sequence recognition in biomedical applications. *IEEE Trans Nanobioscience*, 6:282-288

[149] Park S, Hamad-Schifferli K (2008) Evaluation of hydrodynamic size and zeta-potential of surface modified Au nanoparticle-DNA conjugates via Ferguson analysis. *J Phys Chem C*, 112:7611-7616

[150] Zhang F, Dressen DG, Skoda MW, Jacobs RM, Zorn S, Martin RA, Martin CM, Clark GF, Schreiber F (2008) Gold nanoparticles decorated with oligo(ethylene glycol) thiols: kinetics of colloid aggregation driven by depletion forces. *Eur Biophys J*, 37:551-561

[151] Weisbecker CS, Merritt MV, Whitesides GM (1996) Molecular selfassembly of aliphatic thiols on gold colloids. *Langmuir*, 12:3763-3772

[152] Duguid JG, Bloomfield VA (1995) Aggregation of melted DNA by divalent metal ion-mediated cross-linking. *Biophys J*, 69:2642-2648

[153] Sun L, Zhang Z, Wang S, Zhang J, Li H, Ren L, Weng J, Zhang Q (2009) Effect of pH on the interaction of gold nanoparticles with DNA and application in the detection of Human p53 gene mutation. *Nanoscale Res Lett*, 4:216-220

[154] Sambrook J, Russell DW (2001) Molecular cloning: a laboratory manual. *3rd vol., 3rd Ed.*, Cold Spring Harbor Laboratory Press, New York

[155] Dias J (2009) Noble metal nanoparticles – Au and Ag – for biodetection. *Master's thesis in Biotechnology*, Faculdade de Ciências e Tecnologia, Universidade Nova de Lisboa, Portugal

[156] Doria G, Franco R, Baptista P (2007) Nanodiagnostics: fast colorimetric method for single nucleotide polymorphism/mutation detection. *IET Nanobiotechnol*, 1:53-57

[157] Ratushna VG, Weller JW, Gibas CJ (2005) Secondary structure in the target as a confounding factor in synthetic oligomer microarray design. *BMC Genomics*, 6:31

[158] Aubin-Tam ME, Hamad-Schifferli K (2005) Gold nanoparticle-cytochrome *c* complexes: the effect of nanoparticle ligand charge on protein structure. *Langmuir*, 21:12080-12084

[159] Gomes I, Santos NC, Oliveira LMA, Quintas A, Eaton P, Pereira E, Franco R (2008) Probing surface properties of Cytochrome *c* at Au bionanoconjugates. *J Phys Chem C*, 112:16340-16347

[160] Conde J, de la Fuente JM, Baptista PV (2010) RNA quantification using gold nanoprobes - application to cancer diagnostics. *J Nanobiotechnology*, in press

[161] Storhoff JJ, Lazarides AA, Mucic RC, Mirkin CA, Letsinger RL, Schatz GC (2000) What controls the optical properties of DNA-linked gold nanoparticle assemblies? *J Am Chem Soc*, 122:4640-4650

[162] Park SY, Stroud D (2003) Theory of melting and the optical properties of gold/DNA nanocomposites. *Phys Rev B*, 67:212202

[163] Jin RC, Wu GS, Li Z, Mirkin CA, Schatz GC (2003) What controls the melting properties of DNA-linked gold nanoparticle assemblies? *J Am Chem Soc*, 125:1643-1654

[164] Xu J, Craig SL (2005) Thermodynamics of DNA hybridization on gold nanoparticles. *J Am Chem Soc*, 127:13227-13231

[165] Lytton-Jean AKR, Mirkin CA (2005) A thermodynamic investigation into the binding properties of DNA functionalized gold nanoparticle probes and molecular fluorophore probes. *J Am Chem Soc*, 127:12754-12755

[166] Park SY, Lee JS, Georganopoulou D, Mirkin CA, Schatz GC (2006) Structures of DNA-linked nanoparticle aggregates. *J Phys Chem B*, 110:12673-12681

[167] Park SY, Gibbs-Davis JM, Nguyen ST, Schatz GC (2007) Sharp melting in DNA-linked nanostructure systems: thermodynamic models of DNA-linked polymers. *J Phys Chem B*, 111:8785-8791

[168] Gibbs-Davis JM, Schatz GC, Nguyen ST (2007) Sharp melting transitions in DNA hybrids without aggregate dissolution: proof of neighboring-duplex cooperativity. *J Am Chem Soc*, 129:15535-15540

[169] Brown KA, Park S, Hamad-Schifferli K (2008) Nucleotide-surface interactions in DNA-modified Au-nanoparticle conjugates: sequence effects on reactivity and hybridization. *J Phys Chem C*, 112:7517-7521

[170] Hurst SJ, Hill HD, Mirkin CA (2008) "Three-dimensional hybridization" with polyvalent DNA-gold nanoparticle conjugates. *J Am Chem Soc*, 130:12192-12200

[171] Hill HD, Hurst SJ, Mirkin CA (2009) Curvature-induced base pair "slipping" effects in DNA-nanoparticle hybridization. *Nano Lett*, 9:317-321

[172] Chen C, Wang W, Ge J, Zhao XS (2009) Kinetics and thermodynamics of DNA hybridization on gold nanoparticles. *Nucleic Acids Res*, 37:3756-3765

[173] Doria G, Baumgartner BG, Franco R, Baptista PV (2010) Optimizing Au-nanoprobes for specific sequence discrimination. *Colloids Surf B*, in press

[174] Sanchez-Sevilla A, Thimonier J, Marilley M, Rocca-Serra J, Barbet J (2002) Accuracy of AFM measurements of the contour length of DNA fragments adsorbed on mica in air and in aqueous buffer. *Ultramicroscopy*, 92:151-158

[175] Sandström P, Boncheva M, Åkerman B (2003) Nonspecific and thiol-specific binding of DNA to gold nanoparticles. *Langmuir*, 19:7537-7543

[176] Kabeláč M, Hobza P (2007) Hydration and stability of nucleic acid bases and base pairs. *Phys Chem Chem Phys*, 9:903-917

[177] Xu R (2008) Progress in nanoparticles characterization: sizing and zeta potential measurement. *Particuology*, 6:112-115

[178] Su K-H, Wei Q-H, Zhang X, Mock JJ, Smith DR, Schultz S (2003) Interparticle coupling effects on plasmon resonances of nanogold particles. *Nano Lett*, 3:1087-1090

[179] Tavares J, Baptista P, Doria G, Flores A (2007) Método colorimétrico e estojo de detecção de sequências específicas de ácidos nucleicos através de nanopartículas metálicas funcionalizadas com oligonucleótidos modificados / Colorimetric method and kit for the detection of specific nucleic acid sequences using metal nanoparticles functionalized with modified oligonucleotides. *Patent pending* PT103730 & PCT/IB2008/051708

[180] Ehrentreich-Förster E, Andresen D (2009) Market potential of point-of-care testing. *LaboratoriumsMedizin*, 33:153-157

[181] Yager P, Domingo GJ, Gerdes J (2008) Point-of-care diagnostics for global health. *Annu Rev Biomed Eng*, 10:107-144

[182] Martins R, Baptista P, Raniero L, Doria G, Silva L, Franco R, Fortunato E (2007) Amorphous/nanocrystalline silicon biosensor for the specific identification of unamplified nucleic acid sequences using gold nanoparticle probes. *Appl Phys Lett*, 90:023903

[183] Martins R, Baptista P, Silva L, Raniero L, Doria G, Franco R, Fortunato E (2008) Identification of unamplified genomic DNA sequences using gold nanoparticle probes and a novel thin film photodetector. *J Non-Cryst Solids*, 354:2580-2584

[184] Dutta P, Morse J (2008) A review of nanofluidic patents. *Recent Pat Nanotechnol*, 2:150-159

[185] Zhang C, Xu J, Ma W, Zheng W (2006) PCR microfluidic devices for DNA amplification. *Biotechnol Adv*, 24:243-284

[186] Linder V (2007) Microfluidics at the crossroad with point-of-care diagnostics. *Analyst*, 132:1186-1192

[187] Silva LB, Baptista P, Raniero L, Doria G, Martins R, Fortunato E (2008) Characterization of optoelectronic platform using an amorphous/nanocrystalline silicon biosensor for the specific identification of nucleic acid sequences based on gold nanoparticle probes. *Sens Actuators B*, 132:508-511

[188] Bernacka-Wojcik I, Senadeera R, Wojcik PJ, Silva LB, Doria G, Baptista P, Aguas H, Fortunato E, Martins R (2010) Inkjet printed and “doctor blade” TiO_2 photodetectors for DNA biosensors. *Biosens Bioelectron*, 25:1229-1234

[189] Larguinho M, Santos HM, Doria G, Scholz H, Baptista PV, Capelo JL (2010) Development of a fast and efficient ultrasonic-based strategy for DNA fragmentation. *Talanta*, in press

[190] Vester B, Wengel J (2004) LNA (locked nucleic acid): high-affinity targeting of complementary RNA and DNA. *Biochemistry*, 43:13233-13241

[191] Pellestor F, Paulasova P (2004) The peptide nucleic acids, efficient tools for molecular diagnosis. *Int J Mol Med*, 13:521-525

[192] Chakrabarti R, Klibanov AM (2003) Nanocrystals modified with peptide nucleic acids (PNAs) for selective self-assembly and DNA detection. *J Am Chem Soc*, 125:12531-12540

[193] McKenzie F, Faulds K, Graham D (2007) Sequence-specific DNA detection using high-affinity LNA-functionalized gold nanoparticles. *Small*, 3:1866-1868

[194] McKenzie F, Faulds K, Graham D (2008) LNA functionalized gold nanoparticles as probes for double stranded DNA through triplex formation. *Chem Commun*, (20):2367-2369

[195] Marsh S, Kwok P, McLeod HL (2002) SNP databases and pharmacogenetics: great start, but a long way to go. *Hum Mutat*, 20:174-179

[196] Zanger UM, Raimundo S, Eichelbaum M (2004) Cytochrome P450 2D6: overview and update on pharmacology, genetics, biochemistry. *Naunyn Schmiedebergs Arch Pharmacol*, 369:23-37

[197] Vincent M, Xu Y, Kong H (2004) Helicase-dependent isothermal DNA amplification. *EMBO Rep*, 5:795-800

[198] Keohavong P, Thilly WG (1989) Fidelity of DNA polymerases in DNA amplification. *Proc Natl Acad Sci USA*, 86:9253-9257

[199] Storhoff JJ, Lucas AD, Garimella V, Bao YP, Müller UR (2004) Homogeneous detection of unamplified genomic DNA sequences based on colorimetric scatter of gold nanoparticle probes. *Nat Biotechnol*, 22:883-887

[200] Barnard M, Albert H, Coetzee G, O'Brien R, Bosman ME (2008) Rapid molecular screening for multidrug-resistant tuberculosis in a high-volume public health laboratory in South Africa. *Am J Respir Crit Care Med*, 177:787-792

[201] Niazov T, Pavlov V, Xiao Y, Gill R, Willner I (2004) DNAzyme-functionalized Au nanoparticles for the amplified detection of DNA or telomerase activity. *Nano Lett*, 4:1683-1687

[202] Kalogianni DP, Koraki T, Christopoulos TK, Ioannou PC (2006) Nanoparticle-based DNA biosensor for visual detection of genetically modified organisms. *Biosens Bioelectron*, 21:1069-1076

[203] Li H, Rothberg LJ (2004) DNA sequence detection using selective fluorescence quenching of tagged oligonucleotide probes by gold nanoparticles. *Anal Chem*, 76:5414-5417

[204] Li H, Rothberg L (2004) Colorimetric detection of DNA sequences based on electrostatic interactions with unmodified gold nanoparticles. *Proc Natl Acad Sci USA*, 101:14036-14039

[205] Liang RQ, Li W, Li Y, Tan CY, Li JX, Jin YX, Ruan KC (2005) An oligonucleotide microarray for microRNA expression analysis based on labeling RNA with quantum dot and nanogold probe. *Nucleic Acids Res*, 33:e17

[206] Elghanian R, Storhoff JJ, Mucic RC, Letsinger RL, Mirkin CA (1997) Selective colorimetric detection of polynucleotides based on the distance-dependent optical properties of gold nanoparticles. *Science*, 277:1078-1081

[207] Reynolds RA, Mirkin CA, Letsinger RL (2000) Homogeneous, nanoparticle-based quantitative colorimetric detection of oligonucleotides. *J Am Chem Soc*, 122:3795-3796

[208] Charrier A, Candoni N, Liachenko N, Thibaudau F (2007) 2D aggregation and selective desorption of nanoparticle probes: a new method to probe DNA mismatches and damages. *Biosens Bioelectron*, 22:1881-1886

[209] Charrier A, Candoni N, Thibaudau F (2006) DNA detection method based on the two-dimensional aggregation and selective desorption of nanoparticle probes. *J Phys Chem B*, 110:12896-12900

[210] Murphy D, O'Brien P, Redmond G (2004) Sub-picomole colorimetric single nucleotide polymorphism discrimination using oligonucleotide-nanoparticle conjugates. *Analyst*, 129:970-974

[211] Beissenhirtz MK, Elnathan R, Weizmann Y, Willner I (2007) The aggregation of Au nanoparticles by an autonomous DNA machine detects viruses. *Small*, 3:375-379

[212] Sato K, Onoguchi M, Sato Y, Hosokawa K, Maeda M (2006) Non-cross-linking gold nanoparticle aggregation for sensitive detection of single-nucleotide polymorphisms: optimization of the particle diameter. *Anal Biochem*, 350:162-164

[213] Huber M, Wei TF, Müller UR, Lefebvre PA, Marla SS, Bao YP (2004) Gold nanoparticle probe-based gene expression analysis with unamplified total human RNA. *Nucleic Acids Res*, 32:e137

[214] Bao YP, Huber M, Wei TF, Marla SS, Storhoff JJ, Müller UR (2005) SNP identification in unamplified human genomic DNA with gold nanoparticle probes. *Nucleic Acids Res*, 33:e15

[215] Yang J, Yang T, Feng Y, Jiao K (2007) A DNA electrochemical sensor based on nanogold-modified poly-2,6-pyridinedicarboxylic acid film and detection of PAT gene fragment. *Anal Biochem*, 365:24-30

[216] Wang H, Zhang C, Li Y, Qi H (2006) Electrogenerated chemiluminescence detection for deoxyribonucleic acid hybridization based on gold nanoparticles carrying multiple probes. *Anal Chim Acta*, 575:205-211

[217] Shiddiky MJ, Shim YB (2007) Trace analysis of DNA: preconcentration, separation, and electrochemical detection in microchip electrophoresis using Au nanoparticles. *Anal Chem*, 79:3724-3733

[218] Nogues C, Cohen SR, Daube S, Apter N, Naaman R (2006) Sequence dependence of charge transport properties of DNA. *J Phys Chem B*, 110:8910-8913

[219] Ozsoz M, Erdem A, Kerman K, Ozkan D, Tugrul B, Topcuoglu N, Ekren H, Taylan M (2003) Electrochemical genosensor based on colloidal gold nanoparticles for the detection of Factor V Leiden mutation using disposable pencil graphite electrodes. *Anal Chem*, 75:2181-2187

[220] Wang J, Xu D, Kawde AN, Polsky R (2001) Metal nanoparticle-based electrochemical stripping potentiometric detection of DNA hybridization. *Anal Chem*, 73:5576-5581

[221] Wang J, Polsky R, Xu D (2001) Silver-enhanced colloidal gold electrochemical stripping detection of DNA hybridization. *Langmuir*, 17:5739-5741

[222] Aha CS, Yuna YJ, Parka HJ, Junga SK, Kima W-J, Haa DH, Yun WS (2006) Electric detection of DNA hybridization by nanoparticle nanoswitch. *Curr Appl Phys*, 6:e157-e160

[223] Zhang J, Song S, Zhang L, Wang L, Wu H, Pan D, Fan C (2006) Sequence-specific detection of femtomolar DNA via a chronocoulometric DNA sensor (CDS): effects of nanoparticle-mediated amplification and nanoscale control of DNA assembly at electrodes. *J Am Chem Soc*, 128:8575-8580

[224] Castañeda MT, Merkoçi A, Pumera M, Alegret S (2007) Electrochemical genosensors for biomedical applications based on gold nanoparticles. *Biosens Bioelectron*, 22:1961-1967

[225] Bui MP, Baek TJ, Seong GH (2007) Gold nanoparticle aggregation-based highly sensitive DNA detection using atomic force microscopy. *Anal Bioanal Chem*, 388:1185-1190

[226] He L, Musick MD, Nicewarner SR, Salinas FG, Benkovic SJ, Natan MJ, Keating CD (2000) Colloidal Au-enhanced surface plasmon resonance for ultrasensitive detection of DNA hybridization. *J Am Chem Soc*, 122:9071-9077

[227] Li Y, Wark AW, Lee HJ, Corn RM (2006) Single-nucleotide polymorphism genotyping by nanoparticle-enhanced surface plasmon resonance imaging measurements of surface ligation reactions. *Anal Chem*, 78:3158-3164

[228] Yao X, Li X, Toledo F, Zurita-Lopez C, Gutova M, Momand J, Zhou F (2006) Sub-attomole oligonucleotide and p53 cDNA determinations via a high-resolution surface

plasmon resonance combined with oligonucleotide-capped gold nanoparticle signal amplification. *Anal Biochem*, 354:220-228

[229] Sato Y, Sato K, Hosokawa K, Maeda M (2006) Surface plasmon resonance imaging on a microchip for detection of DNA-modified gold nanoparticles deposited onto the surface in a non-cross-linking configuration. *Anal Biochem*, 355:125-131

[230] Wu ZS, Jiang JH, Fu L, Shen GL, Yu RQ (2006) Optical detection of DNA hybridization based on fluorescence quenching of tagged oligonucleotide probes by gold nanoparticles. *Anal Biochem*, 353:22-29

[231] Cerruti MG, Sauthier M, Leonard D, Liu D, Duscher G, Feldheim DL, Franzen S (2006) Gold and silica-coated gold nanoparticles as thermographic labels for DNA detection. *Anal Chem*, 78:3282-3288

APPENDICES

Appendix I – AuNPs based methods for nucleic acids detection

Category	Detection technique	Detection limit	Target(s)	Application to biological samples	Refs
Catalyser	Chemiluminescence	0.1nM	ssDNA	n/a	[201]
Colorimetric	Naked-eye (Dry-reagent dipstick)	2fmol; 0.16nM	dsDNA, cDNA, SNP	Prostate specific antigen; hepatitis C virus; GMO (35S promoter and nopaline synthase (NOS) terminator); mannose-binding lectin gene (MBL2)	[98,105-107,202]
Colorimetric	Naked-eye (Electrostatic interactions with unmodified AuNPs)	<100fmol - 10nM	ssDNA, dsDNA, SNP	SNPs associated with a fatal arrhythmia known as long QT syndrome (KCNE1 gene)	[97,203, 204]
Colorimetric	Naked-eye or CCD camera (sandwich hybridization)	0.4fmol	miRNA	miRNA from leaf and root of rice (*OryzasativaL.ssp.indica*) seedlings	[205]
Colorimetric	Naked-eye or optical monitoring system (cross-linking aggregation)	50pM - 10nM; 33fM (using scattered light)	ssDNA, dsDNA, SNP	methicillin-resistant *Staphylococcus aureus mecA* gene	[101,199, 206-210]
Colorimetric	UV-vis spectroscopy (aggregation induced by polymerase/nicking machine)	1pM	ssDNA	M13 phage	[211]
Colorimetric	Naked-eye or UV-vis spectroscopy (non-cross-linking aggregation)	1nM – 100nM	ssDNA, dsDNA, RNA, SNP	K-ras oncogene; cytochrome p450 CYP2D6*4 haplotype; beta-thalassemia mutations; *M. tuberculosis*; FSY1 gene expression (*S. bayanus*)	[91,102, 103,156, 212]

Category (cont.)	Detection technique	Detection limit	Target(s)	Application to biological samples	Refs
Spectroscopy	Light scattering imaging (sandwich hybridization)	50fM – 20fM	ssDNA, dsDNA, RNA, SNP	High-, medium-, low- and non-expressed genes in human brain tissue; methicillin-resistant *Staphylococcus aureus mecA* gene; Coagulation genes associated with thrombotic (factor V, factor II and MTHFR)	[99,108, 213,214]
Electrochemical	Electrochemical impedance spectroscopy	0.24nM	ssDNA, SNP	n/a	[215]
Electrochemical	Electrogenerated chemiluminescence	5pM	ssDNA	n/a	[216]
Electrochemical	Microchip gel electrophoresis with microelectrode detector	5.7amol	dsDNA	n/a	[217]
Electrochemical	Conducting atomic force microscopy (AFM)	-	ssDNA	n/a	[218]
Electrochemical	Differential pulse voltammetry	0.78fmol	ssDNA, dsDNA, SNP	Factor V Leiden mutation (MTHFR gene)	[219]
Electrochemical	Potentiometric stripping analysis	32pM - 1.5nM	ssDNA, SNP	n/a	[220,221]
Electrochemical	Conductivity across two electrodes	10pM	ssDNA	n/a	[222]
Electrochemical	Cyclic voltammetry and chronocoulometry	10fM	ssDNA	n/a	[223]
Electrochemical	Magnetically induced direct electrochemical detection	660nM	ssDNA, SNP	n/a	[224]
Microscopy	Atomic force microscopy	2.5pM	ssDNA	n/a	[225]

Category (cont.)	Detection technique	Detection limit	Target(s)	Application to biological samples	Refs
Spectroscopy	Hyper-Rayleigh scattering (Electrostatic interactions with unmodified AuNPs)	10nM	ssDNA	n/a	[83]
Spectroscopy	Surface-enhanced Raman scattering	20fM	DNA, RNA, SNP	n/a	[109]
Spectroscopy	Microarray SPR imaging (sandwich hybridization)	1.38 fM – 10pM	ssDNA, dsDNA, cDNA, SNP	familiar breast and ovarian cancer (BRCA1 gene); p53 gene expression	[226-228]
Spectroscopy	Surface plasmon resonance (SPR) imaging (non-cross-linking aggregation)	32nM	ssDNA	n/a	[229]
Spectroscopy	Fluorescence spectroscopy (quenching by AuNPs)	2nM	ssDNA	n/a	[230]
Spectroscopy	Infrared thermography	10pM – 100pM	ssDNA	n/a	[231]

Appendix II – AuNPs characterization

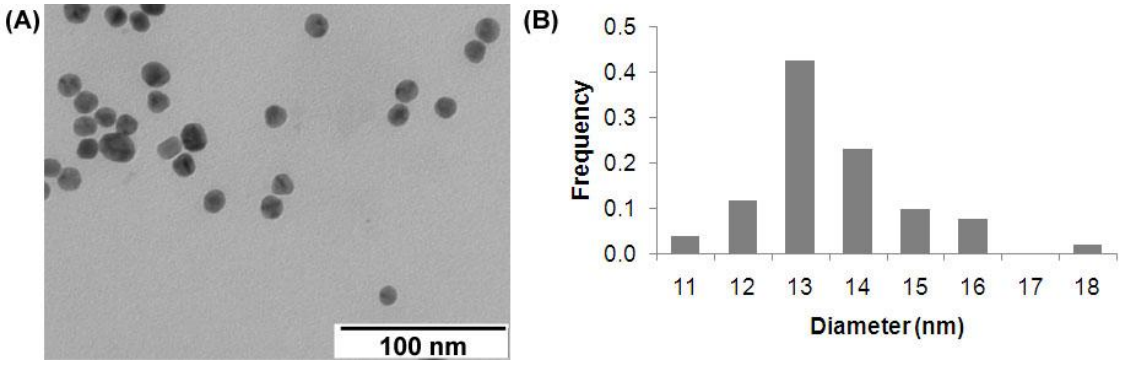

Figure A.1 – Gold nanoparticles. (A) TEM image and **(B)** size histogram corresponding to the measurements of 52 NPs. AuNPs size (nm): 13.5±1.3 (Average±STD)

Appendix III – AuAgNPs characterization

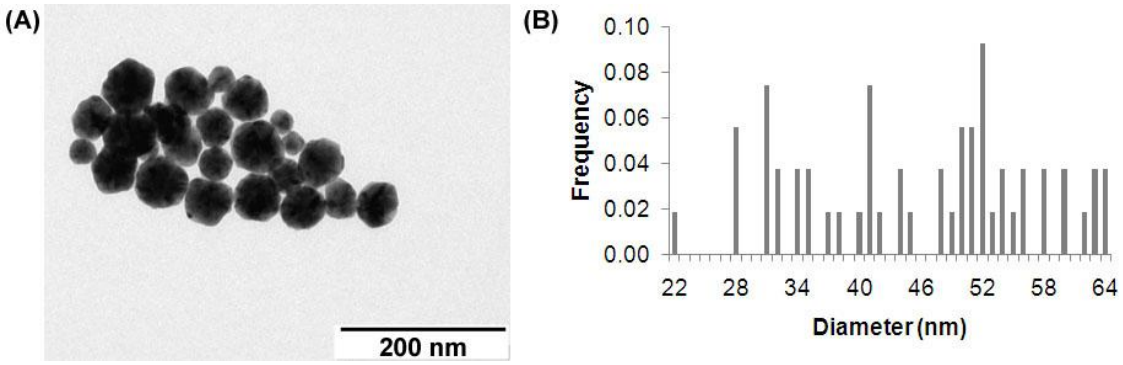

Figure A.2 – Gold-silver alloy nanoparticles. (A) TEM image and **(B)** size histogram corresponding to the measurements of 54 NPs with an average Au:Ag ratio of 0.49:0.51, as determined by ICP – element concentration: Ag= 0.0046 g/L and Au= 0.0082 g/L. AuAgNPs size (nm): 45.8±11.2 (Average±STD).

Appendix IV – Reference Materials (maps and sequences)

HBB material

Plasmid p158

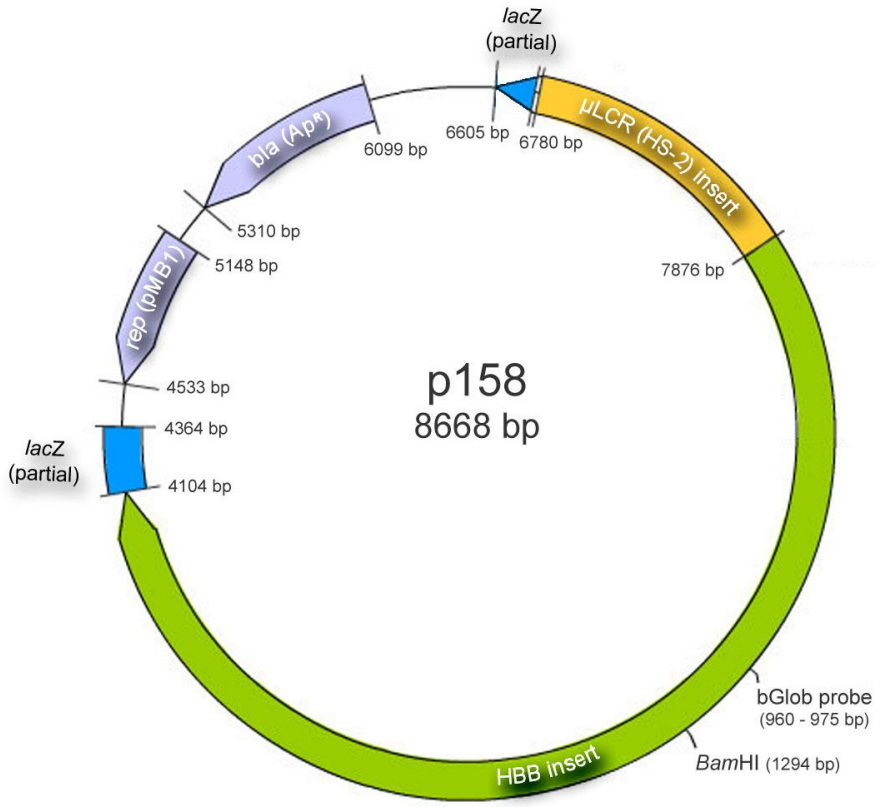


```
   1 GTTAACCTCC TATTTGACAC CACTGATTAC CCCATTGATA GTCACACTTT
  51 GGGTTGTAAG TGACTTTTTA TTTATTTGTA TTTTTGACTG CATTAAGAGG
 101 TCTCTAGTTT TTTATCTCTT GTTTCCCAAA ACCTAATAAG TAACTAATGC
 151 ACAGAGCACA TTGATTTGTA TTTATTCTAT TTTTAGACAT AATTTATTAG
 201 CATGCATGAG CAAATTAAGA AAAACAACAA CAAATGAATG CATATATATG
 251 TATATGTATG TGTGTATATA TACACACATA TATATATATA TTTTTTCTTT
 301 TCTTACCAGA AGGTTTTAAT CCAAATAAGG AGAAGATATG CTTAGAACCG
 351 AGGTAGAGTT TTCATCCATT CTGTCCTGTA AGTATTTTGC ATATTCTGGA
 401 GACGCAGGAA GAGATCCATC TACATATCCC AAAGCTGAAT TATGGTAGAC
 451 AAAACTCTTC CACTTTTAGT GCATCAACTT CTTATTTGTG TAATAAGAAA
 501 ATTGGGAAAA CGATCTTCAA TATGCTTACC AAGCTGTGAT TCCAAATATT
 551 ACGTAAATAC ACTTGCAAAG GAGGATGTTT TTAGTAGCAA TTTGTACTGA
 601 TGGTATGGGG CCAAGAGATA TATCTTAGAG GGAGGGCTGA GGGTTTGAAG
 651 TCCAACTCCT AAGCCAGTGC CAGAAGAGCC AAGGACAGGT ACGGCTGTCA
 701 TCACTTAGAC CTCACCCTGT GGAGCCACAC CCTAGGGTTG GCCAATCTAC
 751 TCCCAGGAGC AGGGAGGGCA GGAGCCAGGG CTGGGCATAA AAGTCAGGGC
 801 AGAGCCATCT ATTGCTTACA TTTGCTTCTG ACACAACTGT GTTCACTAGC
 851 AACCTCAAAC AGACACCATG GTGCATCTGA CTCCTGAGGA GAAGTCTGCC
 901 GTTACTGCCC TGTGGGGCAA GGTGAACGTG GATGAAGTTG GTGGTGAGGC
 951 CCTGGGCAGG TTGGTATCAA GGTTACAAGA CAGGTTTAAG GAGACCAATA
```

1001 GAAACTGGGC ATGTGGAGAC AGAGAAGACT CTTGGGTTTC TGATAGGCAC
1051 TGACTCTCTC TGCCTATTGG TCTATTTTCC CACCCTTAGG CTGCTGGTGG
1101 TCTACCCTTG GACCCAGAGG TTCTTTGAGT CCTTTGGGGA TCTGTCCACT
1151 CCTGATGCTG TTATGGGCAA CCCTAAGGTG AAGGCTCATG GCAAGAAAGT
1201 GCTCGGTGCC TTTAGTGATG GCCTGGCTCA CCTGGACAAC CTCAAGGGCA
1251 CCTTTGCCAC ACTGAGTGAG CTGCACTGTG ACAAGCTGCA CGTGGATCCT
1301 GAGAACTTCA GGGTGAGTCT ATGGGACGCT TGATGTTTTC TTTCCCCTTC
1351 TTTTCTATGG TTAAGTTCAT GTCATAGGAA GGGGATAAGT AACAGGGTAC
1401 AGTTTAGAAT GGGAAACAGA CGAATGATTG CATCAGTGTG GAAGTCTCAG
1451 GATCGTTTTA GTTTCTTTTA TTTGCTGTTC ATAACAATTG TTTTCTTTTG
1501 TTTAATTCTT GCTTTCTTTT TTTTTCTTCT CCGCAATTTT TACTATTATA
1551 CTTAATGCCT TAACATTGTG TATAACAAAA GGAAATATCT CTGAGATACA
1601 TTAAGTAACT TAAAAAAAAA CTTTACACAG TCTGCCTAGT ACATTACTAT
1651 TTGGAATATA TGTGTGCTTA TTTGCATATT CATAATCTCC CTACTTTATT
1701 TTCTTTTATT TTTAATTGAT ACATAATCAT TATACATATT TATGGGTTAA
1751 AGTGTAATGT TTTAATATGT GTACACATAT TGACCAAATC AGGGTAATTT
1801 TGCATTTGTA ATTTTAAAAA ATGCTTTCTT CTTTTAATAT ACTTTTTTGT
1851 TTATCTTATT TCTAATACTT TCCCTAATCT CTTTCTTTCA GGGCAATAAT
1901 GATACAATGT ATCATGCCTC TTTGCACCAT TCTAAAGAAT AACAGTGATA
1951 ATTTCTGGGT TAAGGCAATA GCAATATCTC TGCATATAAA TATTTCTGCA
2001 TATAAATTGT AACTGATGTA AGAGGTTTCA TATTGCTAAT AGCAGCTACA
2051 ATCCAGCTAC CATTCTGCTT TTATTTTATG GTTGGGATAA GGCTGGATTA
2101 TTCTGAGTCC AAGCTAGGCC CTTTTGCTAA TCATGTTCAT ACCTCTTATC
2151 TTCCTCCCAC AGCTCCTGGG CAACGTGCTG GTCTGTGTGC TGGCCCATCA
2201 CTTTGGCAAA GAATTCACCC CACCAGTGCA GGCTGCCTAT CAGAAAGTGG
2251 TGGCTGGTGT GGCTAATGCC CTGGCCCACA AGTATCACTA AGCTCGCTTT
2301 CTTGCTGTCC AATTTCTATT AAAGGTTCCT TTGTTCCCTA AGTCCAACTA
2351 CTAAACTGGG GGATATTATG AAGGGCCTTG AGCATCTGGA TTCTGCCTAA
2401 TAAAAAACAT TTATTTTCAT TGCAATGATG TATTTAAATT ATTTCTGAAT
2451 ATTTTACTAA AAAGGGAATG TGGGAGGTCA GTGCATTTAA AACATAAAGA
2501 AATGAAGAGC TAGTTCAAAC CTTGGGAAAA TACACTATAT CTTAAACTCC
2551 ATGAAAGAAG GTGAGGCTGC AAACAGCTAA TGCACATTGG CAACAGCCCC
2601 TGATGCATAT GCCTTATTCA TCCCTCAGAA AAGGATTCAA GTAGAGGCTT
2651 GATTTGGAGG TTAAAGTTTT GCTATGCTGT ATTTTACATT ACTTATTGTT
2701 TTAGCTGTCC TCATGAATGT CTTTTCACTA CCCATTTGCT TATCCTGCAT
2751 CTCTCAGCCT TGACTCCACT CAGTTCTCTT GCTTAGAGAT ACCACCTTTC
2801 CCCTGAAGTG TTCCTTCCAT GTTTTACGGC GAGATGGTTT CTCCTCGCCT
2851 GGCCACTCAG CCTTAGTTGT CTCTGTTGTC TTATAGAGGT CTACTTGAAG
2901 AAGGAAAAAC AGGGGTCATG GTTTGACTGT CCTGTGAGCC CTTCTTCCCT
2951 GCCTCCCCCA CTCACAGTGA CCCGGAATCT GCAGTGCTAG TCTCCCGGAA
3001 CTATCACTCT TTCACAGTCT GCTTTGGAAG GACTGGGCTT AGTATGAAAA
3051 GTTAGGACTG AGAAGAATTT GAAAGGCGGC TTTTTGTAGC TTGATATTCA
3101 CTACTGTCTT ATTACCCTGT CATAGGCCCA CCCCAAATGG AAGTCCCATT
3151 CTTCCTCAGG ATGTTTAAGA TTAGCATTCA GGAAGAGATC AGAGGTCTGC

3201 TGGCTCCCTT ATCATGTCCC TTATGGTGCT TCTGGCTCTG CAGTTATTAG
3251 CATAGTGTTA CCATCAACCA CCTTAACTTC ATTTTTCTTA TTCAATACCT
3301 AGGTAGGTAG ATGCTAGATT CTGGAAATAA AATATGAGTC TCAAGTGGTC
3351 CTTGTCCTCT CTCCCAGTCA AATTCTGAAT CTAGTTGGCA AGATTCTGAA
3401 ATCAAGGCAT ATAATCAGTA ATAAGTGATG ATAGAAGGGT ATATAGAAGA
3451 ATTTTATTAT ATGAGAGGGT GAAACCCTCA AAATGAAATG AAATCAGACC
3501 CTTGTCTTAC ACCATAAACA AAAATAAATT TGAATGGGTT AAAGAATTAA
3551 ACTAAGACCT AAAACCATAA AAATTTTTAA AGAAATCAAA AGAAGAAAAT
3601 TCTAATATTC ACGTTGCAGC CGTTTTTGAA TTTGATATGA GAAGCAAAGG
3651 CAACAAAAGG AAAAATAAAG AAGTGAGGCT ACATCAAACT AAAAAATTTC
3701 CACACAAAAA AGAAAACAAT GAACAAATGA AAGGTGAACC ATGAAATGGC
3751 ATATTTGCAA ACCAAATATT TCTTAAATAT TTTGGTTAAT ATCCAAAATA
3801 TATAAGAAAC ACAGATGATT CAATAACAAA CAAAAAATTA AAAATAGGAA
3851 AATAAAAAAA TTAAAAAGAA GAAAATCCTG CCATTTATGC GAGAATTGAT
3901 GAACCTGGAG GATGTAAAAC TAAGAAAAAT AAGCCTGACA CAAAAAGACA
3951 AATACTACAC AACCTTGCTC ATATGTGAAA CATAAAAAAG TCACTCTCAT
4001 GGAAACAGAC AGTAGAGGTA TGGTTTCCAG GGGTTGGGGG TGGGAGAATC
4051 AGGAAACTAT TACTCAAAGG GTATAAAATT TCAGTTATGT GGGATGAATA
4101 AATTCTAGAG TCGACCTGCA GGCATGCAAG CTTGGCGTAA TCATGGTCAT
4151 AGCTGTTTCC TGTGTGAAAT TGTTATCCGC TCACAATTCC ACACAACATA
4201 CGAGCCGGAA GCATAAAGTG TAAAGCCTGG GGTGCCTAAT GAGTGAGCTA
4251 ACTCACATTA ATTGCGTTGC GCTCACTGCC CGCTTTCCAG TCGGGAAACC
4301 TGTCGTGCCA GCTGCATTAA TGAATCGGCC AACGCGCGGG GAGAGGCGGT
4351 TTGCGTATTG GGCGCTCTTC CGCTTCCTCG CTCACTGACT CGCTGCGCTC
4401 GGTCGTTCGG CTGCGGCGAG CGGTATCAGC TCACTCAAAG GCGGTAATAC
4451 GGTTATCCAC AGAATCAGGG GATAACGCAG GAAAGAACAT GTGAGCAAAA
4501 GGCCAGCAAA AGGCCAGGAA CCGTAAAAAG GCCGCGTTGC TGGCGTTTTT
4551 CCATAGGCTC CGCCCCCCTG ACGAGCATCA CAAAAATCGA CGCTCAAGTC
4601 AGAGGTGGCG AAACCCGACA GGACTATAAA GATACCAGGC GTTTCCCCCT
4651 GGAAGCTCCC TCGTGCGCTC TCCTGTTCCG ACCCTGCCGC TTACCGGATA
4701 CCTGTCCGCC TTTCTCCCTT CGGGAAGCGT GGCGCTTTCT CATAGCTCAC
4751 GCTGTAGGTA TCTCAGTTCG GTGTAGGTCG TTCGCTCCAA GCTGGGCTGT
4801 GTGCACGAAC CCCCCGTTCA GCCCGACCGC TGCGCCTTAT CCGGTAACTA
4851 TCGTCTTGAG TCCAACCCGG TAAGACACGA CTTATCGCCA CTGGCAGCAG
4901 CCACTGGTAA CAGGATTAGC AGAGCGAGGT ATGTAGGCGG TGCTACAGAG
4951 TTCTTGAAGT GGTGGCCTAA CTACGGCTAC ACTAGAAGGA CAGTATTTGG
5001 TATCTGCGCT CTGCTGAAGC CAGTTACCTT CGGAAAAAGA GTTGGTAGCT
5051 CTTGATCCGG CAAACAAACC ACCGCTGGTA GCGGTGGTTT TTTTGTTTGC
5101 AAGCAGCAGA TTACGCGCAG AAAAAAAGGA TCTCAAGAAG ATCCTTTGAT
5151 CTTTTCTACG GGGTCTGACG CTCAGTGGAA CGAAAACTCA CGTTAAGGGA
5201 TTTTGGTCAT GAGATTATCA AAAAGGATCT TCACCTAGAT CCTTTTAAAT
5251 TAAAAATGAA GTTTTAAATC AATCTAAAGT ATATATGAGT AAACTTGGTC
5301 TGACAGTTAC CAATGCTTAA TCAGTGAGGC ACCTATCTCA GCGATCTGTC
5351 TATTTCGTTC ATCCATAGTT GCCTGACTCC CCGTCGTGTA GATAACTACG

5401 ATACGGGAGG GCTTACCATC TGGCCCCAGT GCTGCAATGA TACCGCGAGA
5451 CCCACGCTCA CCGGCTCCAG ATTTATCAGC AATAAACCAG CCAGCCGGAA
5501 GGGCCGAGCG CAGAAGTGGT CCTGCAACTT TATCCGCCTC CATCCAGTCT
5551 ATTAATTGTT GCCGGGAAGC TAGAGTAAGT AGTTCGCCAG TTAATAGTTT
5601 GCGCAACGTT GTTGCCATTG CTACAGGCAT CGTGGTGTCA CGCTCGTCGT
5651 TTGGTATGGC TTCATTCAGC TCCGGTTCCC AACGATCAAG GCGAGTTACA
5701 TGATCCCCCA TGTTGTGCAA AAAAGCGGTT AGCTCCTTCG GTCCTCCGAT
5751 CGTTGTCAGA AGTAAGTTGG CCGCAGTGTT ATCACTCATG GTTATGGCAG
5801 CACTGCATAA TTCTCTTACT GTCATGCCAT CCGTAAGATG CTTTTCTGTG
5851 ACTGGTGAGT ACTCAACCAA GTCATTCTGA GAATAGTGTA TGCGGCGACC
5901 GAGTTGCTCT TGCCCGGCGT CAATACGGGA TAATACCGCG CCACATAGCA
5951 GAACTTTAAA AGTGCTCATC ATTGGAAAAC GTTCTTCGGG GCGAAAACTC
6001 TCAAGGATCT TACCGCTGTT GAGATCCAGT TCGATGTAAC CCACTCGTGC
6051 ACCCAACTGA TCTTCAGCAT CTTTTACTTT CACCAGCGTT TCTGGGTGAG
6101 CAAAAACAGG AAGGCAAAAT GCCGCAAAAA AGGGAATAAG GGCGACACGG
6151 AAATGTTGAA TACTCATACT CTTCCTTTTT CAATATTATT GAAGCATTTA
6201 TCAGGGTTAT TGTCTCATGA GCGGATACAT ATTTGAATGT ATTTAGAAAA
6251 ATAAACAAAT AGGGGTTCCG CGCACATTTC CCCGAAAAGT GCCACCTGAC
6301 GTCTAAGAAA CCATTATTAT CATGACATTA ACCTATAAAA ATAGGCGTAT
6351 CACGAGGCCC TTTCGTCTCG CGCGTTTCGG TGATGACGGT GAAAACCTCT
6401 GACACATGCA GCTCCCGGAG ACGGTCACAG CTTGTCTGTA AGCGGATGCC
6451 GGGAGCAGAC AAGCCCGTCA GGGCGCGTCA GCGGGTGTTG GCGGGTGTCG
6501 GGGCTGGCTT AACTATGCGG CATCAGAGCA GATTGTACTG AGAGTGCACC
6551 ATATGCGGTG TGAAATACCG CACAGATGCG TAAGGAGAAA ATACCGCATC
6601 AGGCGCCATT CGCCATTCAG GCTGCGCAAC TGTTGGGAAG GGCGATCGGT
6651 GCGGGCCTCT TCGCTATTAC GCCAGCTGGC GAAAGGGGGA TGTGCTGCAA
6701 GGCGATTAAG TTGGGTAACG CCAGGGTTTT CCCAGTCACG ACGTTGTAAA
6751 ACGACGGCCA GTGAATTCGA GCTCGGTACG GTACCAGTGG GGCCTCTAAG
6801 ACTAAGTCAC TCTGTCTCAC TGTGTCTTAG CCAGTTCCTT ACAGCTTGCC
6851 CTGATGGGAG ATAGAGAATG GGTATCCTCC AACAAAAAAA TAAATTTTCA
6901 TTTCTCAAGG TCCAACTTAT GTTTTCTTAA TTTTTAAAAA AATCTTGACC
6951 ATTCTCCACT CTCTAAAATA ATCCACAGTG AGAGAAACAT TCTTTTCCCC
7001 CATCCCATAA ATACCTCTAT TAAATATGGA AAATCTGGGC ATGGTGTCTC
7051 ACACCTGTAA TCCCAGCACT TTGGGAGGCT GAGGTGGGTG GACTGCTTGG
7101 AGCTCAGGAG TTCAAGACCA TCTTGGACAA CATGGTGATA CCCTGCCTCT
7151 ACAAAAAGTA CAAAAATTAG CCTGGCATGG TGGTGTGCAC CTGTAATCCC
7201 AGCTATTAGG GTGGCTGAGG CAGGAGAATT GCTTGAACCC GGGAGGCGGA
7251 GGTTGCAGTG AGCTGAGATC GTGCCACTGC ACTCCAGCCT GGGGGACAGA
7301 GCACATTATA ATTAACTGTT ATTTTTTACT TGGACTCTTG TGGGGAATAA
7351 GATACATGTT TTATTCTTAT TTATGATTCA AGCACTGAAA ATAGTGTTTA
7401 GCATCCAGCA GGTGCTTCAA AACCATTTGC TGAATGATTA CTATACTTTT
7451 TACAAGCTCA GCTCCCTCTA TCCCTTCCAG CATCCTCATC TCTGATTAAA
7501 TAAGCTTCAG TTTTTCCTTA GTTCCTGTTA CATTTCTGTG TGTCTCCATT
7551 AGTGACCTCC CATAGTCCAA GCATGAGCAG TTCTGGCCAG GCCCCTGTCG

7601 GGGTCAGTGC CCCACCCCCG CCTTCTGGTT CTGTGTAACC TTCTAAGCAA
7651 ACCTTCTGGC TCAAGCACAG CAATGCTGAG TCATGATGAG TCATGCTGAG
7701 GCTTAGGGTG TGTGCCCAGA TGTTCTCAGC CTAGAGTGAT GACTCCTATC
7751 TGGGTCCCCA GCAGGATGCT TACAGGGCAG ATGGCAAAAA AAAGGAGAAG
7801 CTGACCACCT GACTAAAACT CCACCTCAAA CGGCATCATA AAGAAAATGG
7851 ATGCCTGAGA CAGAATGTGA CATATTCTAG AATATATTAT TTCCTGAATA
7901 TATATATATA TATACACATA TACGTATATA TATATATATA TATATATTTG
7951 TTGTTATCAA TTGCCATAGA ATGATTAGTT ATTGTGAATC AAATATTTAT
8001 CTTGCAGGTG GCCTCTATAC CTAGAAGCGG CAGAATCAGG CTTTATTAAT
8051 ACATGTGTAT AGATTTTTAG GATCTATACA CATGTATTAA TATGAAACAA
8101 GGATATGGAA GAGGAAGGCA TGAAAACAGG AAAAGAAAAC AAACCTTGTT
8151 TGCCATTTTA AGGCACCCCT GGACAGCTAG GTGGCAAAAG GCCTGTGCTG
8201 TTAGAGGACA CATGCTCACA TACGGGGTCA GATCTGACTT GGGGTGCTAC
8251 TGGGAAGCTC TCATCTTAAG GATACATCTC AGGCCAGTCT TGGTGCATTA
8301 GGAAGATGTA GGCAACTCTG ATCCTGAGAG GAAAGAAACA TTCCTCCAGG
8351 AGAGCTAAAA GGGTTCACCT GTGTGGGTAA CTGTGAAGGA CTACAAGAGG
8401 ATGAAAAACA ATGACAGACA GACATAATGC TTGTGGGAGA AAAAACAGGA
8451 GGTCAAGGGG ATAGAGAAGG CTTCCAGAAG AATGGCTTTG AAGCTGGCTT
8501 CTGTAGGAGT TCACAGTGGC AAAGATGTTT CAGAAATGTG ACATGACTTA
8551 AGGAACTATA CAAAAAGGAA CAAATTTAAG GAGAGGCAGA TAAATTAGTT
8601 CAACAGACAT GCAAGGAATT TTCAGATGAA TGTTATGTCT CCACTGAGCT
8651 TCTTGAGGTT AGCAGCTG

DOR1 material

DOR1 amplicons

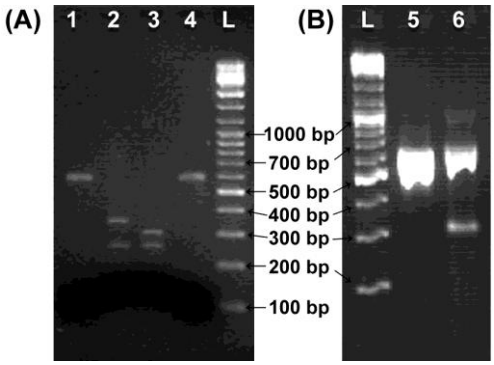

Figure A.3 – Electrophoresis analysis of DOR1 amplicons (A) digested by *Dde*I restriction enzyme or (B) produced by asymmetric PCR. Conditions: **(A)** 1.5% agarose, 80V for 1 h in 1x TBE; **(B)** 2% agarose, 80V for 1h30min in 1x TBE. Lanes: "1"- DOR1G amplicon; "2"- digested DOR1G amplicon; "3"- digested DOR1C amplicon; "4"- DOR1C amplicon; "L"- GeneRuler™ DNA Ladder Mix; "5"- DOR1C amplified by conventional PCR; "6"- DOR1C amplified by asymmetric PCR.

Plasmid pDOR1G

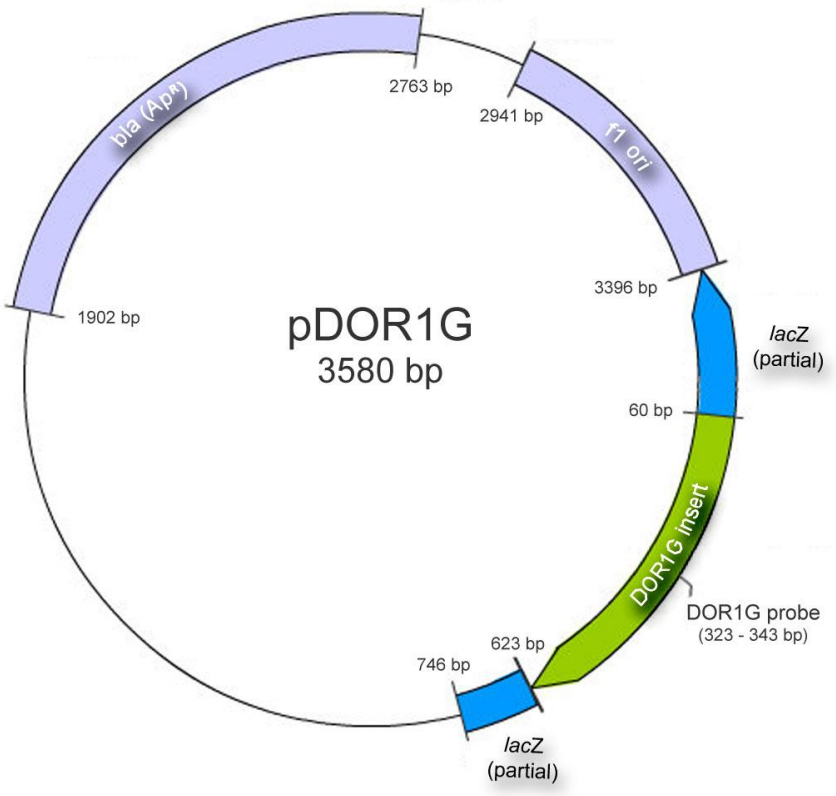


```
  1 GGGCGAATTG GGCCCGACGT CGCATGCTCC CGGCCGCCAT GGCGGCCGCG
 51 GGAATTCGAT TCGCCGGCGG AGACAGACAA AGGCCCGGGC GCGGGGGGCG
101 CAGGGCGTGT CCGTGGCAGG GGAGCCCCCA GGCCCACCCG GGTCGGGACT
151 CACCTGGGGG CGGGAGGGGG GCGGCACGGC GTTGAGGTAG TTGTGCGGCG
201 GGGCGTCCCA GGGTCGCCGG CCGCTCACAG GCCGGGCCGC ATCGCCGGGA
```

```
 251 CTCGCGGGGG AGGCGGCGGG GCCGCGGTCG CTCCGGGCTG CTGAGCTCGC
 301 CCGCGGGGCT TTGAGTCTGT GCGGCCGCTG CGGCGGGGCT CACGGCACAA
 351 ATTGGAACGT TCAAACAGCT GATTGTGACG TCACAAAGGG GCCCGCCCGC
 401 CTCGCGTCAC CGGCTGGCGG GGCGGCGGCC AATCCCGGGC TGCGGATCCC
 451 CCCCTGCCCC TCCCCTCCCC TCCCCTCCCG GTTTGCGGGC CGGGCGCTCG
 501 GGCCGGGAAA CGTTCTCGGA ACCGGGAGGG TGAGTGTTCG GGGAGGCAGC
 551 TGCGGGGAGC TGGGAGCCCT GCGCCGCGGC GAGCTCTCCG CGAGGAGGAT
 601 CTCCACTCCC TCCTACCGGC TCCTAATCAC TAGTGAATTC GCGGCCGCCT
 651 GCAGGTCGAC CATATGGGAG AGCTCCCAAC GCGTTGGATG CATAGCTTGA
 701 GTATTCTATA GTGTCACCTA AATAGCTTGG CGTAATCATG GTCATAGCTG
 751 TTTCCTGTGT GAAATTGTTA TCCGCTCACA ATTCCACACA ACATACGAGC
 801 CGGAAGCATA AAGTGTAAAG CCTGGGGTGC CTAATGAGTG AGCTAACTCA
 851 CATTAATTGC GTTGCGCTCA CTGCCCGCTT TCCAGTCGGG AAACCTGTCG
 901 TGCCAGCTGC ATTAATGAAT CGGCCAACGC GCGGGGAGAG GCGGTTTGCG
 951 TATTGGGCGC TCTTCCGCTT CCTCGCTCAC TGACTCGCTG CGCTCGGTCG
1001 TTCGGCTGCG GCGAGCGGTA TCAGCTCACT CAAAGGCGGT AATACGGTTA
1051 TCCACAGAAT CAGGGGATAA CGCAGGAAAG AACATGTGAG CAAAAGGCCA
1101 GCAAAAGGCC AGGAACCGTA AAAAGGCCGC GTTGCTGGCG TTTTTCCATA
1151 GGCTCCGCCC CCCTGACGAG CATCACAAAA ATCGACGCTC AAGTCAGAGG
1201 TGGCGAAACC CGACAGGACT ATAAAGATAC CAGGCGTTTC CCCCTGGAAG
1251 CTCCCTCGTG CGCTCTCCTG TTCCGACCCT GCCGCTTACC GGATACCTGT
1301 CCGCCTTTCT CCCTTCGGGA AGCGTGGCGC TTTCTCATAG CTCACGCTGT
1351 AGGTATCTCA GTTCGGTGTA GGTCGTTCGC TCCAAGCTGG GCTGTGTGCA
1401 CGAACCCCCC GTTCAGCCCG ACCGCTGCGC CTTATCCGGT AACTATCGTC
1451 TTGAGTCCAA CCCGGTAAGA CACGACTTAT CGCCACTGGC AGCAGCCACT
1501 GGTAACAGGA TTAGCAGAGC GAGGTATGTA GGCGGTGCTA CAGAGTTCTT
1551 GAAGTGGTGG CCTAACTACG GCTACACTAG AAGAACAGTA TTTGGTATCT
1601 GCGCTCTGCT GAAGCCAGTT ACCTTCGGAA AAAGAGTTGG TAGCTCTTGA
1651 TCCGGCAAAC AAACCACCGC TGGTAGCGGT GGTTTTTTTG TTTGCAAGCA
1701 GCAGATTACG CGCAGAAAAA AAGGATCTCA AGAAGATCCT TTGATCTTTT
1751 CTACGGGGTC TGACGCTCAG TGGAACGAAA ACTCACGTTA AGGGATTTTG
1801 GTCATGAGAT TATCAAAAAG GATCTTCACC TAGATCCTTT TAAATTAAAA
1851 ATGAAGTTTT AAATCAATCT AAAGTATATA TGAGTAAACT TGGTCTGACA
1901 GTTACCAATG CTTAATCAGT GAGGCACCTA TCTCAGCGAT CTGTCTATTT
1951 CGTTCATCCA TAGTTGCCTG ACTCCCCGTC GTGTAGATAA CTACGATACG
2001 GGAGGGCTTA CCATCTGGCC CCAGTGCTGC AATGATACCG CGAGACCCAC
2051 GCTCACCGGC TCCAGATTTA TCAGCAATAA ACCAGCCAGC CGGAAGGGCC
2101 GAGCGCAGAA GTGGTCCTGC AACTTTATCC GCCTCCATCC AGTCTATTAA
2151 TTGTTGCCGG GAAGCTAGAG TAAGTAGTTC GCCAGTTAAT AGTTTGCGCA
2201 ACGTTGTTGC CATTGCTACA GGCATCGTGG TGTCACGCTC GTCGTTTGGT
2251 ATGGCTTCAT TCAGCTCCGG TTCCCAACGA TCAAGGCGAG TTACATGATC
2301 CCCCATGTTG TGCAAAAAAG CGGTTAGCTC CTTCGGTCCT CCGATCGTTG
2351 TCAGAAGTAA GTTGGCCGCA GTGTTATCAC TCATGGTTAT GGCAGCACTG
2401 CATAATTCTC TTACTGTCAT GCCATCCGTA AGATGCTTTT CTGTGACTGG
```

2451 TGAGTACTCA ACCAAGTCAT TCTGAGAATA GTGTATGCGG CGACCGAGTT
2501 GCTCTTGCCC GGCGTCAATA CGGGATAATA CCGCGCCACA TAGCAGAACT
2551 TTAAAAGTGC TCATCATTGG AAAACGTTCT TCGGGGCGAA AACTCTCAAG
2601 GATCTTACCG CTGTTGAGAT CCAGTTCGAT GTAACCCACT CGTGCACCCA
2651 ACTGATCTTC AGCATCTTTT ACTTTCACCA GCGTTTCTGG GTGAGCAAAA
2701 ACAGGAAGGC AAAATGCCGC AAAAAAGGGA ATAAGGGCGA CACGGAAATG
2751 TTGAATACTC ATACTCTTCC TTTTTCAATA TTATTGAAGC ATTTATCAGG
2801 GTTATTGTCT CATGAGCGGA TACATATTTG AATGTATTTA GAAAAATAAA
2851 CAAATAGGGG TTCCGCGCAC ATTTCCCCGA AAAGTGCCAC CTGATGCGGT
2901 GTGAAATACC GCACAGATGC GTAAGGAGAA AATACCGCAT CAGGAAATTG
2951 TAAGCGTTAA TATTTTGTTA AAATTCGCGT TAAATTTTTG TTAAATCAGC
3001 TCATTTTTTA ACCAATAGGC CGAAATCGGC AAAATCCCTT ATAAATCAAA
3051 AGAATAGACC GAGATAGGGT TGAGTGTTGT TCCAGTTTGG AACAAGAGTC
3101 CACTATTAAA GAACGTGGAC TCCAACGTCA AAGGGCGAAA AACCGTCTAT
3151 CAGGGCGATG GCCCACTACG TGAACCATCA CCCTAATCAA GTTTTTTGGG
3201 GTCGAGGTGC CGTAAAGCAC TAAATCGGAA CCCTAAAGGG AGCCCCCGAT
3251 TTAGAGCTTG ACGGGGAAAG CCGGCGAACG TGGCGAGAAA GGAAGGGAAG
3301 AAAGCGAAAG GAGCGGGCGC TAGGGCGCTG GCAAGTGTAG CGGTCACGCT
3351 GCGCGTAACC ACCACACCCG CCGCGCTTAA TGCGCCGCTA CAGGGCGCGT
3401 CCATTCGCCA TTCAGGCTGC GCAACTGTTG GGAAGGGCGA TCGGTGCGGG
3451 CCTCTTCGCT ATTACGCCAG CTGGCGAAAG GGGGATGTGC TGCAAGGCGA
3501 TTAAGTTGGG TAACGCCAGG GTTTTCCCAG TCACGACGTT GTAAAACGAC
3551 GGCCAGTGAA TTGTAATACG ACTCACTATA

Plasmid pDOR1C

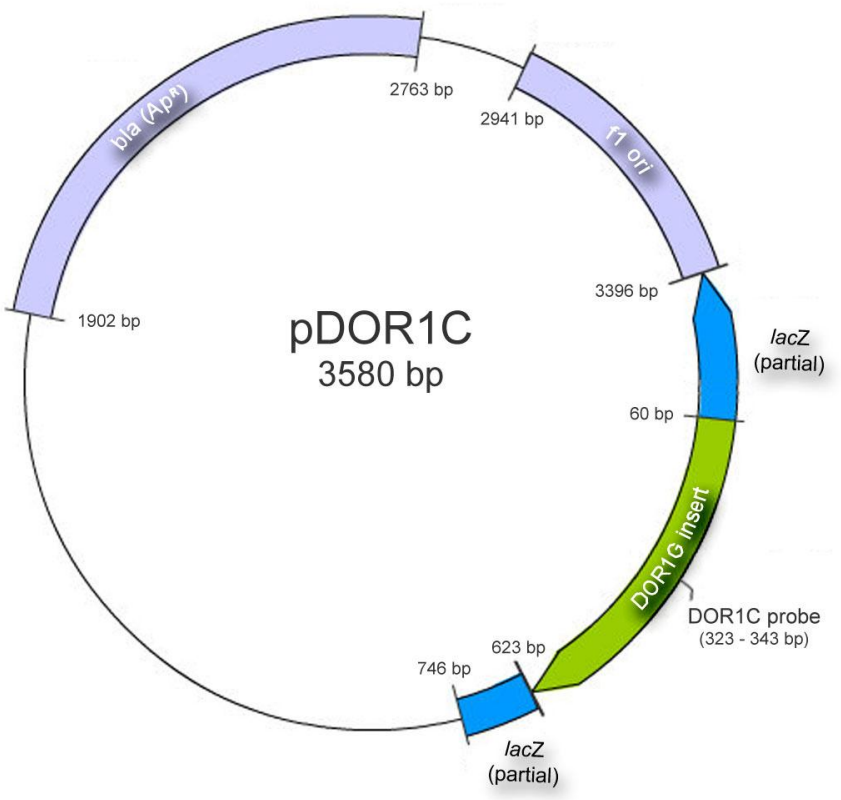


```
   1 GGGCGAATTG GGCCCGACGT CGCATGCTCC CGGCCGCCAT GGCGGCCGCG
  51 GGAATTCGAT TCGCCGGCGG AGACAGACAA AGGCCCGGGC GCGGGGGGCG
 101 CAGGGCGTGT CCGTGGCAGG GGAGCCCCCA GGCCCACCCG GGTCGGGACT
 151 CACCTGGGGG CGGGAGGGGG GCGGCACGGC GTTGAGGTAG TTGTGCGGCG
 201 GGGCGTCCCA GGGTCGCCGG CCGCTCACAG GCCGGGCCGC ATCGCCGGGA
 251 CTCGCGGGGG AGGCGGCGGG GCCGCGGTCG CTCCGGGCTG CTGAGCTCGC
 301 CCGCGGGGCT TTGAGTCTGT GCGGCCGCTG CGGCGGGGCT CAGGGCACAA
 351 ATTGGAACGT TCAAACAGCT GATTGTGACG TCACAAAGGG GCCCGCCCGC
 401 CTCGCGTCAC CGGCTGGCGG GGCGGCGGCC AATCCCGGGC TGCGGATCCC
 451 CCCCTGCCCC TCCCCTCCCC TCCCCTCCCG GTTTGCGGGC CGGGCGCTCG
 501 GGCCGGGAAA CGTTCTCGGA ACCGGGAGGG TGAGTGTTCG GGGAGGCAGC
 551 TGCGGGGAGC TGGGAGCCCT GCGCCGCGGC GAGCTCTCCG CGAGGAGGAT
 601 CTCCACTCCC TCCTACCGGC TCCTAATCAC TAGTGAATTC GCGGCCGCCT
 651 GCAGGTCGAC CATATGGGAG AGCTCCCAAC GCGTTGGATG CATAGCTTGA
 701 GTATTCTATA GTGTCACCTA AATAGCTTGG CGTAATCATG GTCATAGCTG
 751 TTTCCTGTGT GAAATTGTTA TCCGCTCACA ATTCCACACA ACATACGAGC
 801 CGGAAGCATA AAGTGTAAAG CCTGGGGTGC CTAATGAGTG AGCTAACTCA
 851 CATTAATTGC GTTGCGCTCA CTGCCCGCTT TCCAGTCGGG AAACCTGTCG
 901 TGCCAGCTGC ATTAATGAAT CGGCCAACGC GCGGGGAGAG GCGGTTTGCG
 951 TATTGGGCGC TCTTCCGCTT CCTCGCTCAC TGACTCGCTG CGCTCGGTCG
1001 TTCGGCTGCG GCGAGCGGTA TCAGCTCACT CAAAGGCGGT AATACGGTTA
1051 TCCACAGAAT CAGGGGATAA CGCAGGAAAG AACATGTGAG CAAAAGGCCA
1101 GCAAAAGGCC AGGAACCGTA AAAAGGCCGC GTTGCTGGCG TTTTTCCATA
1151 GGCTCCGCCC CCCTGACGAG CATCACAAAA ATCGACGCTC AAGTCAGAGG
```

1201 TGGCGAAACC CGACAGGACT ATAAAGATAC CAGGCGTTTC CCCCTGGAAG
1251 CTCCCTCGTG CGCTCTCCTG TTCCGACCCT GCCGCTTACC GGATACCTGT
1301 CCGCCTTTCT CCCTTCGGGA AGCGTGGCGC TTTCTCATAG CTCACGCTGT
1351 AGGTATCTCA GTTCGGTGTA GGTCGTTCGC TCCAAGCTGG GCTGTGTGCA
1401 CGAACCCCCC GTTCAGCCCG ACCGCTGCGC CTTATCCGGT AACTATCGTC
1451 TTGAGTCCAA CCCGGTAAGA CACGACTTAT CGCCACTGGC AGCAGCCACT
1501 GGTAACAGGA TTAGCAGAGC GAGGTATGTA GGCGGTGCTA CAGAGTTCTT
1551 GAAGTGGTGG CCTAACTACG GCTACACTAG AAGAACAGTA TTTGGTATCT
1601 GCGCTCTGCT GAAGCCAGTT ACCTTCGGAA AAAGAGTTGG TAGCTCTTGA
1651 TCCGGCAAAC AAACCACCGC TGGTAGCGGT GGTTTTTTTG TTTGCAAGCA
1701 GCAGATTACG CGCAGAAAAA AAGGATCTCA AGAAGATCCT TTGATCTTTT
1751 CTACGGGGTC TGACGCTCAG TGGAACGAAA ACTCACGTTA AGGGATTTTG
1801 GTCATGAGAT TATCAAAAAG GATCTTCACC TAGATCCTTT TAAATTAAAA
1851 ATGAAGTTTT AAATCAATCT AAAGTATATA TGAGTAAACT TGGTCTGACA
1901 GTTACCAATG CTTAATCAGT GAGGCACCTA TCTCAGCGAT CTGTCTATTT
1951 CGTTCATCCA TAGTTGCCTG ACTCCCCGTC GTGTAGATAA CTACGATACG
2001 GGAGGGCTTA CCATCTGGCC CCAGTGCTGC AATGATACCG CGAGACCCAC
2051 GCTCACCGGC TCCAGATTTA TCAGCAATAA ACCAGCCAGC CGGAAGGGCC
2101 GAGCGCAGAA GTGGTCCTGC AACTTTATCC GCCTCCATCC AGTCTATTAA
2151 TTGTTGCCGG GAAGCTAGAG TAAGTAGTTC GCCAGTTAAT AGTTTGCGCA
2201 ACGTTGTTGC CATTGCTACA GGCATCGTGG TGTCACGCTC GTCGTTTGGT
2251 ATGGCTTCAT TCAGCTCCGG TTCCCAACGA TCAAGGCGAG TTACATGATC
2301 CCCCATGTTG TGCAAAAAAG CGGTTAGCTC CTTCGGTCCT CCGATCGTTG
2351 TCAGAAGTAA GTTGGCCGCA GTGTTATCAC TCATGGTTAT GGCAGCACTG
2401 CATAATTCTC TTACTGTCAT GCCATCCGTA AGATGCTTTT CTGTGACTGG
2451 TGAGTACTCA ACCAAGTCAT TCTGAGAATA GTGTATGCGG CGACCGAGTT
2501 GCTCTTGCCC GGCGTCAATA CGGGATAATA CCGCGCCACA TAGCAGAACT
2551 TTAAAAGTGC TCATCATTGG AAAACGTTCT TCGGGGCGAA AACTCTCAAG
2601 GATCTTACCG CTGTTGAGAT CCAGTTCGAT GTAACCCACT CGTGCACCCA
2651 ACTGATCTTC AGCATCTTTT ACTTTCACCA GCGTTTCTGG GTGAGCAAAA
2701 ACAGGAAGGC AAAATGCCGC AAAAAAGGGA ATAAGGGCGA CACGGAAATG
2751 TTGAATACTC ATACTCTTCC TTTTTCAATA TTATTGAAGC ATTTATCAGG
2801 GTTATTGTCT CATGAGCGGA TACATATTTG AATGTATTTA GAAAAATAAA
2851 CAAATAGGGG TTCCGCGCAC ATTTCCCCGA AAAGTGCCAC CTGATGCGGT
2901 GTGAAATACC GCACAGATGC GTAAGGAGAA AATACCGCAT CAGGAAATTG
2951 TAAGCGTTAA TATTTTGTTA AAATTCGCGT TAAATTTTTG TTAAATCAGC
3001 TCATTTTTTA ACCAATAGGC CGAAATCGGC AAAATCCCTT ATAAATCAAA
3051 AGAATAGACC GAGATAGGGT TGAGTGTTGT TCCAGTTTGG AACAAGAGTC
3101 CACTATTAAA GAACGTGGAC TCCAACGTCA AAGGGCGAAA AACCGTCTAT
3151 CAGGGCGATG GCCCACTACG TGAACCATCA CCCTAATCAA GTTTTTTGGG
3201 GTCGAGGTGC CGTAAAGCAC TAAATCGGAA CCCTAAAGGG AGCCCCCGAT
3251 TTAGAGCTTG ACGGGGAAAG CCGGCGAACG TGGCGAGAAA GGAAGGGAAG
3301 AAAGCGAAAG GAGCGGGCGC TAGGGCGCTG GCAAGTGTAG CGGTCACGCT
3351 GCGCGTAACC ACCACACCCG CCGCGCTTAA TGCGCCGCTA CAGGGCGCGT

```
3401 CCATTCGCCA TTCAGGCTGC GCAACTGTTG GGAAGGGCGA TCGGTGCGGG
3451 CCTCTTCGCT ATTACGCCAG CTGGCGAAAG GGGGATGTGC TGCAAGGCGA
3501 TTAAGTTGGG TAACGCCAGG GTTTTCCCAG TCACGACGTT GTAAAACGAC
3551 GGCCAGTGAA TTGTAATACG ACTCACTATA
```

CYP2D6 material

CYP2D6 amplicons

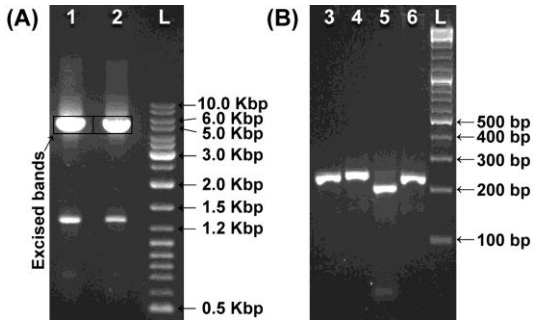

Figure A.4 – Electrophoresis analysis of CYP2D6 amplicons (A) produced by Long PCR or (B) by PCR and digested with *Mva*I restriction enzyme. Conditions: **(A)** 1% agarose, 80V for 1 h in 1x TBE; **(B)** 2% agarose, 60V for 1h30 in 1x TBE. Lanes: "1"- CYP2D6*1/*1 Long PCR amplicon; "2"- CYP2D6*4/*4 Long PCR amplicon; "3"- CYP2D6*4 amplicon; "4"- CYP2D6*4 amplicon digested by *Mva*I; "5"- CYP2D6*1 amplicon digested by *Mva*I; "6"- CYP2D6*1 amplicon; "L"- GeneRuler™ DNA Ladder Mix.

Plasmid pCYP2D6*1

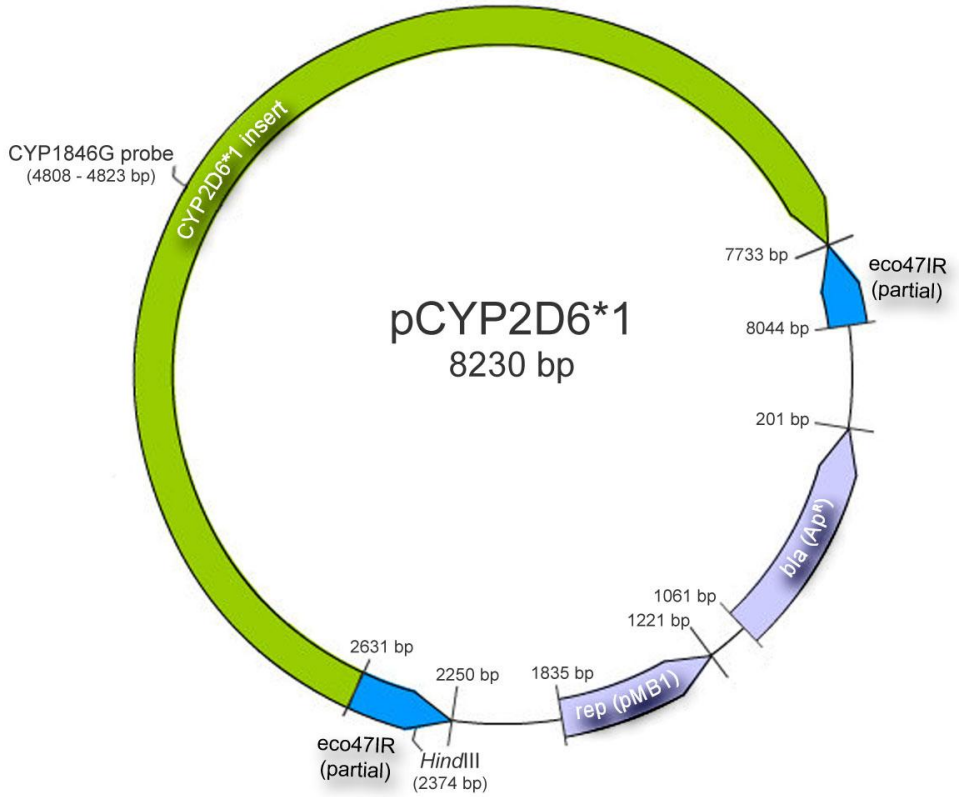


```
  1 GACGAAAGGG CCTCGTGATA CGCCTATTTT TATAGGTTAA TGTCATGATA
 51 ATAATGGTTT CTTAGACGTC AGGTGGCACT TTTCGGGGAA ATGTGCGCGG
101 AACCCCTATT TGTTTATTTT TCTAAATACA TTCAAATATG TATCCGCTCA
151 TGAGACAATA ACCCTGATAA ATGCTTCAAT AATATTGAAA AAGGAAGAGT
```

```
 201 ATGAGTATTC AACATTTCCG TGTCGCCCTT ATTCCCTTTT TTGCGGCATT
 251 TTGCCTTCCT GTTTTTGCTC ACCCAGAAAC GCTGGTGAAA GTAAAAGATG
 301 CTGAAGATCA GTTGGGTGCA CGAGTGGGTT ACATCGAACT GGATCTCAAC
 351 AGCGGTAAGA TCCTTGAGAG TTTTCGCCCC GAAGAACGTT TTCCAATGAT
 401 GAGCACTTTT AAAGTTCTGC TATGTGGCGC GGTATTATCC CGTATTGACG
 451 CCGGGCAAGA GCAACTCGGT CGCCGCATAC ACTATTCTCA GAATGACTTG
 501 GTTGAGTACT CACCAGTCAC AGAAAAGCAT CTTACGGATG GCATGACAGT
 551 AAGAGAATTA TGCAGTGCTG CCATAACCAT GAGTGATAAC ACTGCGGCCA
 601 ACTTACTTCT GACAACGATC GGAGGACCGA AGGAGCTAAC CGCTTTTTTG
 651 CACAACATGG GGGATCATGT AACTCGCCTT GATCGTTGGG AACCGGAGCT
 701 GAATGAAGCC ATACCAAACG ACGAGCGTGA CACCACGATG CCTGTAGCAA
 751 TGGCAACAAC GTTGCGCAAA CTATTAACTG GCGAACTACT TACTCTAGCT
 801 TCCCGGCAAC AATTAATAGA CTGGATGGAG GCGGATAAAG TTGCAGGACC
 851 ACTTCTGCGC TCGGCCCTTC CGGCTGGCTG GTTTATTGCT GATAAATCTG
 901 GAGCCGGTGA GCGTGGGTCT CGCGGTATCA TTGCAGCACT GGGGCCAGAT
 951 GGTAAGCCCT CCCGTATCGT AGTTATCTAC ACGACGGGGA GTCAGGCAAC
1001 TATGGATGAA CGAAATAGAC AGATCGCTGA GATAGGTGCC TCACTGATTA
1051 AGCATTGGTA ACTGTCAGAC CAAGTTTACT CATATATACT TTAGATTGAT
1101 TTAAAACTTC ATTTTTAATT TAAAAGGATC TAGGTGAAGA TCCTTTTTGA
1151 TAATCTCATG ACCAAAATCC CTTAACGTGA GTTTTCGTTC CACTGAGCGT
1201 CAGACCCCGT AGAAAAGATC AAAGGATCTT CTTGAGATCC TTTTTTTCTG
1251 CGCGTAATCT GCTGCTTGCA AACAAAAAAA CCACCGCTAC CAGCGGTGGT
1301 TTGTTTGCCG GATCAAGAGC TACCAACTCT TTTTCCGAAG GTAACTGGCT
1351 TCAGCAGAGC GCAGATACCA AATACTGTCC TTCTAGTGTA GCCGTAGTTA
1401 GGCCACCACT TCAAGAACTC TGTAGCACCG CCTACATACC TCGCTCTGCT
1451 AATCCTGTTA CCAGTGGCTG CTGCCAGTGG CGATAAGTCG TGTCTTACCG
1501 GGTTGGACTC AAGACGATAG TTACCGGATA AGGCGCAGCG GTCGGGCTGA
1551 ACGGGGGGTT CGTGCACACA GCCCAGCTTG GAGCGAACGA CCTACACCGA
1601 ACTGAGATAC CTACAGCGTG AGCTATGAGA AAGCGCCACG CTTCCCGAAG
1651 GGAGAAAGGC GGACAGGTAT CCGGTAAGCG GCAGGGTCGG AACAGGAGAG
1701 CGCACGAGGG AGCTTCCAGG GGGAAACGCC TGGTATCTTT ATAGTCCTGT
1751 CGGGTTTCGC CACCTCTGAC TTGAGCGTCG ATTTTTGTGA TGCTCGTCAG
1801 GGGGGCGGAG CCTATGGAAA AACGCCAGCA ACGCGGCCTT TTTACGGTTC
1851 CTGGCCTTTT GCTGGCCTTT TGCTCACATG TTCTTTCCTG CGTTATCCCC
1901 TGATTCTGTG GATAACCGTA TTACCGCCTT TGAGTGAGCT GATACCGCTC
1951 GCCGCAGCCG AACGACCGAG CGCAGCGAGT CAGTGAGCGA GGAAGCGGAA
2001 GAGCGCCCAA TACGCAAACC GCCTCTCCCC GCGCGTTGGC CGATTCATTA
2051 ATGCAGCTGG CACGACAGGT TTCCCGACTG GAAAGCGCTG CAGGGGCCCG
2101 GGATCCAATT GGCAGTGAGC GCAACGCAAT TAATGTGAGT TAGCTCACTC
2151 ATTAGGCACC CCAGGCTTTA CACTTTATGC TTCCGGCTCG TATAATGTGT
2201 GGAATTGTGA GCGGATAACA ATTTCACACA GGAGGTTTAA ACTTTAAACA
2251 TGTCAAAAGA GACGTCTTTT GTTAAGAATG CTGAGGAACT TGCAAAGCAA
2301 AAAATGGATG CTATTAACCC TGAACTTTCT TCAAAATTTA AATTTTTAAT
2351 AAAATTCCTG TCTCAGTTTC CTGAAGCTTG CTCTAAACCT CGTTCAAAAA
```

2401 AAATGCAGAA TAAAGTTGGT CAAGAGGAAC ATATTGAATA TTTAGCTCGT
2451 AGTTTTCATG AGAGTCGATT GCCAAGAAAA CCCACGCCAC CTACAACGGT
2501 TCCTGATGAG GTGGTTAGCA TAGTTCTTAA TATAAGTTTT AATATACAGC
2551 CTGAAAATCT TGAGAGAATA AAAGAAGAAC ATCGATTTTC CATGGCAGCT
2601 GAGAATATTG TAGGAGATCT TCTAGAAAGA TTATCCCAGA AGGCTTTGCA
2651 GGCTTCAGGA GCTTGGAGTG GGGAGAGGGG GTGACTTCTC CGACCAGGCC
2701 CCTCCACCGG CCTACCCTGG GTAAGGGCCT GGAGCAGGAA GCAGGGGCAA
2751 GAACCTCTGG AGCAGCCCAT ACCCGCCCTG GCCTGACTCT GCCACTGGCA
2801 GCACAGTCAA CACAGCAGGT TCACTCACAG CAGAGGGCAA AGGCCATCAT
2851 CAGCTCCCTT TATAAGGGAA GGGTCACGCG CTCGGTGTGC TGAGAGTGTC
2901 CTGCCTGGTC CTCTGTGCCT GGTGGGGTGG GGGTGCCAGG TGTGTCCAGA
2951 GGAGCCCATT TGGTAGTGAG GCAGGTATGG GGCTAGCAGC ACTGGTGCCC
3001 CTGGCCGTGA TAGTGGCCAT CTTCCTGCTC CTGGTGGACC TGATGCACCG
3051 GCGCCAACGC TGGGCTGCAC GCTACCCACC AGGCCCCCTG CCACCGCCCG
3101 GGCTGGGCAA CCTGCTGCAT GTGGACTTCC AGAACACACC ATACTGCTTC
3151 GACCAGGTGA GGGAGGAGGT CCTGGAGGGC GGCAGAGGTG CTGAGGCTCC
3201 CCTACCAGAA GCAAACATGG ATGGTGGGTG AAACCACAGG CTGGACCAGA
3251 AGCCAGGCTG AGAAGGGGAA GCAGGTTTGG GGGACGTCCT GGAGAAGGGC
3301 ATTTATACAT GGCATGAAGG ACTGGATTTT CCAAAGGCCA AGGAAGAGTA
3351 GGGCAAGGGC CTGGAGGTGG AGCTGGACTT GGCAGTGGGC ATGCAAGCCC
3401 ATTGGGCAAC ATATGTTATG GAGTACAAAG TCCCTTCTGC TGACACCAGA
3451 AGGAAAGGCC TTGGGAATGG AAGATGAGTT AGTCCTGAGT GCCGTTTAAA
3501 TCACGAAATC GAGGATGAAG GGGGTGCAGT GACCCGGTTC AAACCTTTTG
3551 CACTGTGGGT CCTCGGGCCT CACTGCTCAC CGGCATGGAC CATCATCTGG
3601 GAATGGGATG CTAACTGGGG CCTCTCGGCA ATTTTGGTGA CTCTTGCAAG
3651 GTCATACCTG GGTGACGCAT CCAAACTGAG TTCCTCCATC ACAGAAGGTG
3701 TGACCCCCAC CCCCGCCCCA CGATCAGGAG GCTGGGTCTC CTCCTTCCAC
3751 CTGCTCACTC CTGGTAGCCC CGGGGGTCGT CCAAGGTTCA AATAGGACTA
3801 GGACCAGTAG TCTGGGGTGA TCCTGGCTTG ACAAGAGGCC CTGACCCTCC
3851 CTCTGCAGTT GCGGCGCCGC TTCGGGGACG TGTTCAGCCT GCAGCTGGCC
3901 TGGACGCCGG TGGTCGTGCT CAATGGGCTG GCGGCCGTGC GCGAGGCGCT
3951 GGTGACCCAC GGCGAGGACA CCGCCGACCG CCCGCCTGTG CCCATCACCC
4001 AGATCCTGGG TTTCGGGCCG CGTTCCCAAG GCAAGCAGCG GTGGGGACAG
4051 AGACAGATTT CCGTGGGACC CGGGTGGGTG ATGACCGTAG TCCGAGCTGG
4101 GCAGAGAGGG CGCGGGGTCG TGGACATGAA ACAGGCCAGC GAGTGGGGAC
4151 AGCGGGCCAA GAAACCACCT GCACTAGGGA GGTGKGAGCA TGGGGACGAG
4201 GGCGGGGCTT GTGACGAGTG GGCGGGGCCA CTGCCGAGAC CTGGCAGGAG
4251 CCCAATGGGT GAGGCTGGCG CATTTCCCAG CTGGAATCCG GTGTCGAAGT
4301 GGGGGGCGGG GACCGCACCT GTGCTGTAAG CTCAGTGTGG GTGGCGCGGG
4351 GCCCGCGGGG TCTTCCCTGA GTGCAAAGGC GGTCAGGGTG GGCAGAGACG
4401 AGGTGGGGCA AAGCCCTGCC CCAGCCAAGG GAGCAAGGTG GATGCACAAA
4451 GAGTGGGCCC TGTGACCAGC TGGACAGAGC CAGGGACTGC GGGAGACCAG
4501 GGGGAGCATA GGGTTGGAGT GGGTGGTGGA TGGTGGGGCT AATGCCTTCA
4551 TGGCCACGCG CACGTGCCCG TCCCACCCCC AGGGGTGTTC CTGGCGCGCT

4601 ATGGGCCCGC GTGGCGCGAG CAGAGGCGCT TCTCCGTGTC CACCTTGCGC
4651 AACTTGGGCC TGGGCAAGAA GTCGCTGGAG CAGTGGGTGA CCGAGGAGGC
4701 CGCCTGCCTT TGTGCCGCCT TCGCCAACCA CTCCGGTGGG TGATGGGCAG
4751 AAGGGCACAA AGCGGGAACT GGGAAGGCGG GGGACGGGGA AGGCGACCCC
4801 TTACCCGCAT CTCCCACCCC CAGGACGCCC CTTTCGCCCC AACGGTCTCT
4851 TGGACAAAGC CGTGAGCAAC GTGATCGCCT CCCTCACCTG CGGGCGCCGC
4901 TTCGAGTACG ACGACCCTCG CTTCCTCAGG CTGCTGGACC TAGCTCAGGA
4951 GGGACTGAAG GAGGAGTCGG GCTTTCTGCG CGAGGTGCGG AGCGAGAGAC
5001 CGAGGAGTCT CCGCAGGGCG AGCTCCCGAG AGGTGCCGGG GCTGGACTGG
5051 GGCCTCGGAA GAGCAGGATT TGCATAGATG GGTTTGGGAA AGGACATTCC
5101 AGGAGACCCC ACTGTAAGAA GGGCCTGGAG GAGGAGGGGA CATCTCAGAC
5151 ATGGTCGTGG GAGAGGTGTG CCCGGGTCAG GGGGCACCAG GAGAGGCCAA
5201 GGACTCTGTA CCTCCTATCC ACGTCAGAGA TTTCGATTTT AGGTTTCTCC
5251 TCTGGGCAAG GAGAGAGGGT GGAGGCTGGC ACTTGGGGAG GGACTTGGTG
5301 AGGTCAGGGG TAAGGACAGG CAGGCCCTGG GTCTACCTGG AGATGGCTGG
5351 GGCCTGAGAC TTGTCCAGGT GAACGCAGAG CACAGGAGGG ATTGAGACCC
5401 CGTTCTGTCT GGTGTAGGTG CTGAATGCTG TCCCCGTCCT CCTGCATATC
5451 CCAACGCTGG CTGGCAAGGT CCTACGCTTC CAAAAGGCTT TCCTGACCCA
5501 GCTGGATGAG CTGCTAACTG AGCACAGGAT GACCTGGGAC CCAGCCCAGC
5551 CCCCCCGAGA CCTGACTGAG GCCTTCCTGG CAGAGATGGA GAAGGTGAGA
5601 GTGGCTGCCA CGGTGGGGGG CAAGGGTGGT GGGTTGAGCG TCCCAGGAGG
5651 AATGAGGGGA GGCTGGGCAA AAGGTTGGAC CAGTGCATCA CCCGGCGAGC
5701 CGCATCTGGG CTGACAGGTG CAGAATTGGA GGTCATTTGG GGGCTACCCC
5751 GTTCTGTCCC GAGTATGCTC TCGGCCCTGC TCAGGCCAAG GGGAACCCTG
5801 AGAGCAGCTT CAATGATGAG AACCTGCGCA TAGTGGTGGC TGACCTGTTC
5851 TCTGCCGGGA TGGTGACCAC CTCGACCACG CTGGCCTGGG GCCTCCTGCT
5901 CATGACCCTA CATCCGGATG TGCAGCGTGA GCCCATCTGG GAAACAGTGC
5951 AGGGGCCGAG GGAGGAAGGG TACAGGCGGG GGCCCATGAA CTTTGCTGGG
6001 ACACCCGGGG CTCCAAGCAC AGGCTTGACG AGGATCCTGT AAGCCTGACC
6051 TCCTCCAACA TAGGAGGCAA GAAGGAGTGT CAGGGCCGGA CCCCCTGGGT
6101 GCTGACCCAT TGTGGGGACG CATGTCTGTC CAGGCCGTGT CCAACAGGAG
6151 ATCAACGACG TGATAGGGCA GGTGCGGCGA CCAGAGATGG GTGACCAGGC
6201 TCACATGCCC TACACCACTG CCGTGATTCA TGAGGTGCAG CGCTTTGGGG
6251 ACATCGTCCC CCTGGGTGTG ACCCATATGA CATCCCGTGA CATCGAAGTA
6301 CAGGGCTTCC GCATCCCTAA GGTAGGCCTG GCGCCCTCCT CACCCCAGCT
6351 CAGCACCAGC ACCTGGTGAT AGCCCCAGCA TGGCTACTGC CAGGTGGGCC
6401 CACTCTAGGA ACCCTGGCCA CCTAGTCCTC AATGCCGCCA CACTGACTGT
6451 CCCCACTTGG GTGGGGGGTC CAGAGTATAG GCAGGGCTGG CCTGTCCATC
6501 CAGAGCCCCT GTCTAGTGGG GAGACAAACC AGGACCTGCC AGAATGTTGG
6551 AGGACCCAAC GCCTGCAGGG AGAGGGGGCA GTGTGGGTGC CTCTGAGAGG
6601 TGTGACTGCG CCCTGCTGTG GGGTCGGAGG GGGTACTGTG GAGCTTCTCG
6651 GGCGCAGGAC TAGTTGACAG AGTCCAGCTG TGTGCCAGGC AGTGTGTGTC
6701 CCCCGTGTGT TTGGTGGCAG GGGTCCCAGC ATCCTAGAGT CCAGTCCCCA
6751 CTCTCACCCT GCATCTCCTG CCCAGGGAAC GACACTCATC ACCAACCTGT

6801 CATCGGTGCT GAAGGATGAG GCCGTCTGGG AGAAGCCCTT CCGCTTCCAC
6851 CCCGAACACT TCCTGGATGC CCAGGGCCAC TTTGTGAAGC CGGAGGCCTT
6901 CCTGCCTTTC TCAGCAGGTG CCTGTGGGGA GCCCGGCTCC CTGTCCCCCT
6951 CCGTGGAGTC TTGCAGGGGT ATCACCCAGG AGCCAGGCTC ACTGACGCCC
7001 CTCCCCTCCC CACAGGCCGC CGTGCATGCC TCGGGGAGCC CCTGGCCCGC
7051 ATGGAGCTCT TCCTCTTCTT CACCTCCCTG CTGCAGCACT TCAGCTTCTC
7101 GGTGCCCACT GGACAGCCCC GGCCCAGCCA CCATGGTGTC TTTGCTTTCC
7151 TGGTGAGCCC ATCCCCCTAT GAGCTTTGTG CTGTGCCCCG CTAGAATGGG
7201 GTACCTAGTC CCCAGCCTGC TCCCTAGCCA GAGGCTCTAA TGTACAATAA
7251 AGCAATGTGG TAGTTCCAAC TCGGGTCCCC TGCTCACGCC CTCGTTGGGA
7301 TCATCCTCCT CAGGGCAACC CCACCCCTGC CTCATTCCTG CTTACCCCAC
7351 CGCCTGGCCG CATTTGAGAC AGGGGTACGT TGAGGCTGAG CAGATGTCAG
7401 TTACCCTTGC CCATAATCCC ATGTCCCCCA CTGACCCAAC TCTGACTGCC
7451 CAGATTGGTG ACAAGGACTA CATTGTCCTG GCATGTGGGG AAGGGGCCAG
7501 AATGGGCTGA CTAGAGGTGT CAGTCAGCCC TGGATGTGGT GGAGAGGGCA
7551 GGACTCAGCC TGGAGGCCCA TATTTCAGGC CTAACTCAGC CCACCCCACA
7601 TCAGGGACAG CAGTCCTGCC AGCACCATCA CAACAGTCAC CTCCCTTCAT
7651 ATATGACACC CCAAAACGGA AGACAAATCA TGGCGTCAGG GAGCTATATG
7701 CCAGGGCTAC CTACCTCCCA GGGCTCAGTC GGCATCTTGC TGAAAAACTC
7751 GAGCCATCCG GATGGATATG GTGTTCAGGC ACAAGTGTTA AAGCAGTTGA
7801 TTTTATTCAC TATGATGAAA AAAACAATGA ATGGAACCTG CTCCAAGTTA
7851 AAAATAGAGA TAATACCGAA AACTCATCGA GTAGTAAGAT TAGAGATAAT
7901 ACAACAATAA AAAAATGGTT TAGAACTTAC TCACAGCGTG ATGCTACTAA
7951 TTGGGACAAT TTTCCAGATG AAGTATCATC TAAGAATTTA AATGAAGAAG
8001 ACTTCAGAGC TTTTGTTAAA AATTATTTGG CAAAAATAAT ATAATTCGAA
8051 TTCACGTGTC GACGAGCTCG CGGCCGCATG CTAGCTTAAG CCAGCCCCGA
8101 CACCCGCCAA CACCCGCTGA CGCGCCCTGA CGGGCTTGTC TGCTCCCGGC
8151 ATCCGCTTAC AGACAAGCTG TGACCGTCTC CGGGAGCTGC ATGTGTCAGA
8201 GGTTTTCACC GTCATCACCG AAACGCGCGA

Plasmid pCYP2D6*4

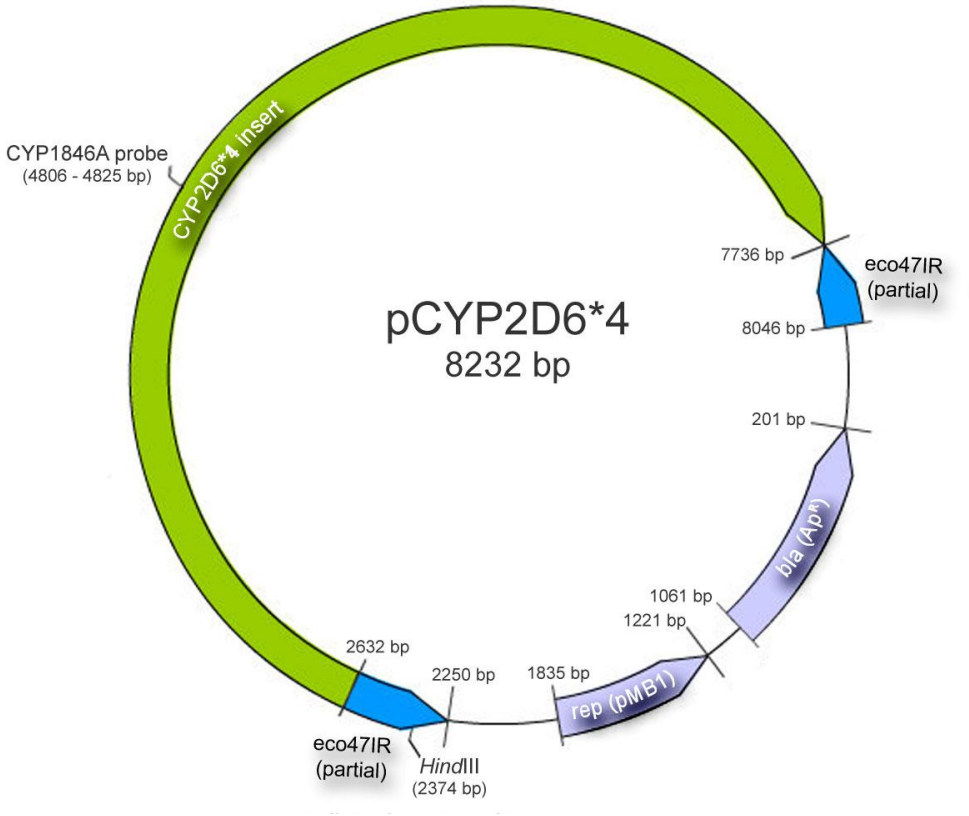


```
   1 GACGAAAGGG CCTCGTGATA CGCCTATTTT TATAGGTTAA TGTCATGATA
  51 ATAATGGTTT CTTAGACGTC AGGTGGCACT TTTCGGGGAA ATGTGCGCGG
 101 AACCCCTATT TGTTTATTTT TCTAAATACA TTCAAATATG TATCCGCTCA
 151 TGAGACAATA ACCCTGATAA ATGCTTCAAT AATATTGAAA AAGGAAGAGT
 201 ATGAGTATTC AACATTTCCG TGTCGCCCTT ATTCCCTTTT TTGCGGCATT
 251 TTGCCTTCCT GTTTTTGCTC ACCCAGAAAC GCTGGTGAAA GTAAAAGATG
 301 CTGAAGATCA GTTGGGTGCA CGAGTGGGTT ACATCGAACT GGATCTCAAC
 351 AGCGGTAAGA TCCTTGAGAG TTTTCGCCCC GAAGAACGTT TTCCAATGAT
 401 GAGCACTTTT AAAGTTCTGC TATGTGGCGC GGTATTATCC CGTATTGACG
 451 CCGGGCAAGA GCAACTCGGT CGCCGCATAC ACTATTCTCA GAATGACTTG
 501 GTTGAGTACT CACCAGTCAC AGAAAAGCAT CTTACGGATG GCATGACAGT
 551 AAGAGAATTA TGCAGTGCTG CCATAACCAT GAGTGATAAC ACTGCGGCCA
 601 ACTTACTTCT GACAACGATC GGAGGACCGA AGGAGCTAAC CGCTTTTTTG
 651 CACAACATGG GGGATCATGT AACTCGCCTT GATCGTTGGG AACCGGAGCT
 701 GAATGAAGCC ATACCAAACG ACGAGCGTGA CACCACGATG CCTGTAGCAA
 751 TGGCAACAAC GTTGCGCAAA CTATTAACTG GCGAACTACT TACTCTAGCT
 801 TCCCGGCAAC AATTAATAGA CTGGATGGAG GCGGATAAAG TTGCAGGACC
 851 ACTTCTGCGC TCGGCCCTTC CGGCTGGCTG GTTTATTGCT GATAAATCTG
 901 GAGCCGGTGA GCGTGGGTCT CGCGGTATCA TTGCAGCACT GGGGCCAGAT
 951 GGTAAGCCCT CCCGTATCGT AGTTATCTAC ACGACGGGGA GTCAGGCAAC
1001 TATGGATGAA CGAAATAGAC AGATCGCTGA GATAGGTGCC TCACTGATTA
1051 AGCATTGGTA ACTGTCAGAC CAAGTTTACT CATATATACT TTAGATTGAT
1101 TTAAAACTTC ATTTTTAATT TAAAAGGATC TAGGTGAAGA TCCTTTTTGA
```

1151 TAATCTCATG ACCAAAATCC CTTAACGTGA GTTTTCGTTC CACTGAGCGT
1201 CAGACCCCGT AGAAAAGATC AAAGGATCTT CTTGAGATCC TTTTTTTCTG
1251 CGCGTAATCT GCTGCTTGCA AACAAAAAAA CCACCGCTAC CAGCGGTGGT
1301 TTGTTTGCCG GATCAAGAGC TACCAACTCT TTTTCCGAAG GTAACTGGCT
1351 TCAGCAGAGC GCAGATACCA AATACTGTCC TTCTAGTGTA GCCGTAGTTA
1401 GGCCACCACT TCAAGAACTC TGTAGCACCG CCTACATACC TCGCTCTGCT
1451 AATCCTGTTA CCAGTGGCTG CTGCCAGTGG CGATAAGTCG TGTCTTACCG
1501 GGTTGGACTC AAGACGATAG TTACCGGATA AGGCGCAGCG GTCGGGCTGA
1551 ACGGGGGGTT CGTGCACACA GCCCAGCTTG GAGCGAACGA CCTACACCGA
1601 ACTGAGATAC CTACAGCGTG AGCTATGAGA AAGCGCCACG CTTCCCGAAG
1651 GGAGAAAGGC GGACAGGTAT CCGGTAAGCG GCAGGGTCGG AACAGGAGAG
1701 CGCACGAGGG AGCTTCCAGG GGGAAACGCC TGGTATCTTT ATAGTCCTGT
1751 CGGGTTTCGC CACCTCTGAC TTGAGCGTCG ATTTTTGTGA TGCTCGTCAG
1801 GGGGGCGGAG CCTATGGAAA AACGCCAGCA ACGCGGCCTT TTTACGGTTC
1851 CTGGCCTTTT GCTGGCCTTT TGCTCACATG TTCTTTCCTG CGTTATCCCC
1901 TGATTCTGTG GATAACCGTA TTACCGCCTT TGAGTGAGCT GATACCGCTC
1951 GCCGCAGCCG AACGACCGAG CGCAGCGAGT CAGTGAGCGA GGAAGCGGAA
2001 GAGCGCCCAA TACGCAAACC GCCTCTCCCC GCGCGTTGGC CGATTCATTA
2051 ATGCAGCTGG CACGACAGGT TTCCCGACTG GAAAGCGCTG CAGGGGCCCG
2101 GGATCCAATT GGCAGTGAGC GCAACGCAAT TAATGTGAGT TAGCTCACTC
2151 ATTAGGCACC CCAGGCTTTA CACTTTATGC TTCCGGCTCG TATAATGTGT
2201 GGAATTGTGA GCGGATAACA ATTTCACACA GGAGGTTTAA ACTTTAAACA
2251 TGTCAAAAGA GACGTCTTTT GTTAAGAATG CTGAGGAACT TGCAAAGCAA
2301 AAAATGGATG CTATTAACCC TGAACTTTCT TCAAAATTTA AATTTTTAAT
2351 AAAATTCCTG TCTCAGTTTC CTGAAGCTTG CTCTAAACCT CGTTCAAAAA
2401 AAATGCAGAA TAAAGTTGGT CAAGAGGAAC ATATTGAATA TTTAGCTCGT
2451 AGTTTTCATG AGAGTCGATT GCCAAGAAAA CCCACGCCAC CTACAACGGT
2501 TCCTGATGAG GTGGTTAGCA TAGTTCTTAA TATAAGTTTT AATATACAGC
2551 CTGAAAATCT TGAGAGAATA AAAGAAGAAC ATCGATTTTC CATGGCAGCT
2601 GAGAATATTG TAGGAGATCT TCTAGAAAGA TGTTATCCCA GAAGGCTTTG
2651 CAGGCTTCAG GAGCTTGGAG TGGGGAGAGG GGGTGACTTC TCCGACCAGG
2701 CCCCTCCACC GGCCTACCCT GGGTAAGGGC CTGGAGCAGG AAGCAGGGGC
2751 AAGAACCTCT GGAGCAGCCC ATACCCGCCC TGGCCTGACT CTGCCACTGG
2801 CAGCACAGTC AACACAGCAG GTTCGCTCAC AGCAGAGGGC AAAGGCCATC
2851 ATCAGCTCCC TTTATAAGGG AAGGGTCACG CGCTCGGTGT GCTGAGAGTG
2901 TCCTGCCTGG TCCTCTGTGC CTGGTGGGGT GGGGGTGCCA GGTGTGTCCA
2951 GAGGAGCCCA TTTGGTAGTG AGGCAGGTAT GGGGCTAGAA GCACTGGTGC
3001 CCCTGGCCGT GATAGTGGCC ATCTTCCTGC TCCTGGTGGA CCTGATGCAC
3051 CGGCGCCAAC GCTGGGCTGC ACGCTACTCA CCAGGCCCCC TGCCACTGCC
3101 CGGGCTGGGC AACCTGCTGC ATGTGGACTT CCAGAACACA CCATACTGCT
3151 TCGACCAGGT GAGGGAGGAG GTCCTGGAGG GCGGCAGAGG TGCTGAGGCT
3201 CCCCTACCAG AAGCAAACAT GGATGGTGGG TGAAACCACA GGCTGGACCA
3251 GAAGCCAGGC TGAGAAGGGG AAGCAGGTTT GGGGGACTTC CTGGAGAAGG
3301 GCATTTATAC ATGGCATGAA GGACTGGATT TTCCAAAGGC CAAGGAAGAG

3351 TAGGGCAAGG GCCTGGAGGT GGAGCTGGAC TTGGCAGTGG GCATGCAAGC
3401 CCATTGGGCA ACATATGTTA TGGAGTACAA AGTCCCTTCT GCTGACACCA
3451 GAAGGAAGGC CTTGGGAATG GAAGATGAGT TAGTCCTGAG TGCCGTTTAA
3501 ATCACGAAAT CGAGGATGAA GGGGGTGCAG TGACCCGGTT CAAACCTTTT
3551 GCACTGTGGG TCCTCGGGCC TCACTGCTCA CCGGCATGGA CCATCATCTG
3601 GGAATGGGAT GCTAACTGGG GCCTCTCGGC AATTTTGGTG ACTCTTGCAA
3651 GGTCATACCT GGGTGACGCA TCCAAACTGA GTTCCTCCAT CACAGAAGGT
3701 GTGACTCCCA CCCCCGCCCC AGGATCAGGA GGCTGGGTCT CCTCCTTCCA
3751 CCTGCTCACT CCTGGTAGCC CCGGGGGGTC GTCCAAGGTT CAAATAGGAC
3801 TAGGACCTGT AGTCTGGGGG GATCCTGGCT TGACAAGAGG CCCTGACCCT
3851 CCCTCTGCAG TTGCGGCGCC GCTTCGGGGA CGTGTTCAGC CTGCAGCTGG
3901 CCTGGACGCC GGTGGTCGTG CTCAATGGGC TGGCGGCCGT GCGCGAGGCG
3951 ATGGTGACCC GCGGCGAGGA CACGGCCGAC CGCCCGCCTG TGCCCATCAC
4001 CCAGATCCTG GGTTTCGGGC CGCGTTCCCA AGGCAAGCAG CGGTGGGGAC
4051 AGAGACAGAT TTCCGTGGGA CCCGGGTGGG TGATGACCGT AGTCCGAGCT
4101 GGGCAGAGAG GGCGCGGGGT CGTGGACATG AAACAGGCCA GCGAGTGGGG
4151 ACAGCGGGCC AAGAAACCAC CTGCACTAGG GAGGTGTGAG CATGGGGACG
4201 AGGGCGGGGC TTGTGACGAG TGGGCGGGGC CACTGCCGAG ACCTGGCAGG
4251 AGCCCAATGG GTGAGGCTGG CGCATTTCCC AGCTGGAATC CGGTGTCGAA
4301 GTGGGGGGCG GGGACCGCAC CTGTGCTGTA AGCTCAGTGT GGGTGGCGCG
4351 GGGCCCGCGG GGTCTTCCCT GAGTGCAAAG GCGGTCAGGG TGGGCAGAGA
4401 CGAGGTGGGG CAAAGCCCTG CCCCAGCCAA GGGAGCAAGG TGGATGCACA
4451 AAGAGTGGGC CCTGTGACCA GCTGGACAGA GCCAGGGACT GCGGGAGACC
4501 AGGGGGAGCA TAGGGTTGGA GTGGGTGGTG GATGGTGGGG CTAATGCCTT
4551 CATGGCCACG CGCACGTGCC CGTCCCACCC CCAGGGGTGT TCCTGGCGCG
4601 CTATGGGCCC GCGTGGCGCG AGCAGAGGCG CTTCTCCGTC TCCACCTTGC
4651 GCAACTTGGG CCTGGGCAAG AAGTCGCTGG AGCAGTGGGT GACCGAGGAG
4701 GCCGCCTGCC TTTGTGCCGC CTTCGCCAAC CACTCCGGTG GGTGATGGGC
4751 AGAAGGGCAC AAAGCGGGAA CTGGGAAGGC GGGGGACGGG GAAGGCGACC
4801 CCTTACCCGC ATCTCCCACC CCCAAGACGC CCCTTTCGCC CCAACGGTCT
4851 CTTGGACAAA GCCGTGAGCA ACGTGATCGC CTCCCTCACC TGCGGGCGCC
4901 GCTTCGAGTA CGACGACCCT CGCTTCCTCA GGCTGCTGGA CCTAGCTCAG
4951 GAGGGACTGA AGGAGGAGTC GGGCTTTCTG CGCGAGGTGC GGGGCGAGAG
5001 ACCGAGGAGT CTCTGCAGGG CGAGCTCCCG AGAGGTGCCG GGGCTGGACT
5051 GGGGCCTCGG AAGAGCAGGA TTTGCGTAGA TGGGTTTGGG AAAGGACATT
5101 CCAGGAGACC CCACTGTAAG AAGGGCCTGG AGGAGGAGGG GACATCTCAG
5151 ACATGGTCGT GGGAGAGGTG TGCCCGGGTC AGGGGGCACC AGGAGAGGCC
5201 AAGGACTCTG TACCTCCTAT CCACGTCAGA GATTTCGATT TTAGGTTTCT
5251 CCTCTGGGCA AGGAGAGAGG GTGGAGGCTG GCACTTGGGG AGGGACTTGG
5301 TGAGGTCAGT GGTAAGGACA GGCAGGCCCT GGGTCTACCT GGAGATGGCT
5351 GGGGCCTGAG ACTTGTCCAG GTGAACGCAG AGCACAGGAG GGATTGAGAC
5401 CCCGTTCTGT CTGGTGTAGG TGCTGAATGC TGTCCCCGTC CTCCTGCATA
5451 TCCCAGCGCT GGCTGGCAAG GTCCTACGCT TCCAAAAGGC TTTCCTGACC
5501 CAGCTGGATG AGCTGCTAAC TGAGCACAGG ATGACCTGGG ACCCAGCCCA

5551 GCCCCCCCGA GACCTGACTG AGGCCTTCCT GGCAGAGATG GAGAAGGTGA
5601 GAGTGGCTGC CACGGTGGGG GGCAAGGGTG GTGGGTTGAG CGTCCCAGGA
5651 GGAATGAGGG GAGGCTGGGC AAAAGGTTGG ACCAGTGCAT CACCCGGCGA
5701 GCCGCATCTG GGCTGACAGG TGCAGAATTG GAGGTCATTT GGGGGCTACC
5751 CCGTTCTGTC CCGAGTATGC TCTCGGCCCT GCTCAGGCCA AGGGGAACCC
5801 TGAGAGCAGC TTCAATGATG AGAACCTGCG CATAGTGGTG GCTGACCTGT
5851 TCTCTGCCGG GATGGTGACC ACCTCGACCA CGCTGGCCTG GGGCCTCCTG
5901 CTCATGATCC TACATCCGGA TGTGCAGCGT GAGCCCATCT GGGAAACAGT
5951 GCAGGGGCCG AGGGAGGAAG GGTACAGGCG GGGGCCCATG AACTTTGCTG
6001 GGACACCCGG GGCTCCAAGC ACAGGCTTGA CCAGGATCCT GTAAGCCTGA
6051 CCTCCTCCAA CATAGGAGGC AAGAAGGAGT GTCAGGGCCG GACCCCCTGG
6101 GTGCTGACCC ATTGTGGGGA CGCATGTCTG TCCAGGCCGT GTCCAACAGG
6151 AGATCGACGA CGTGATAGGG CAGGTGCGGC GACCAGAGAT GGGTGACCAG
6201 GCTCACATGC CCTACACCAC TGCCGTGATT CATGAGGTGC AGCGCTTTGG
6251 GGACATCGTC CCCCTGGGTG TGACCCATAT GACATCCCGT GACATCGAAG
6301 TACAGGGCTC CCGCATCCCT AAGGTAGGCC TGGCGCCCTC CTCACCCCAG
6351 CTCAGCACCA GCCCCTGGTG ATAGCCCCAG CATGGCTACT GCCAGGTGGG
6401 CCCACTCTAG GAAACCTGGC CACCTAGTCC TCAATGCCAC CACACTGACT
6451 GTCCCCACTT GGGTGGGGGG TCCAGAGTAT AGGCAGGGCT GGCCTGTCCA
6501 TCCAGAGCCC CCGTCTAGTG GGGAGACAAA CCAGGACCTG CCAGAATGTT
6551 GGAGGACCCA GCGCCTGCAG GGAGAGGGGG CAGTGTGGGT GCCTCTGAGA
6601 GGTGTGACTG CGCCCTGCTG TAGGGTCGGA GAGAGTACTG TGGAGCTTCT
6651 CGGGCGCAGG ACTAGTTGAC AGAGTCCAGC TGTGTGCCAG GCAGTGTGTG
6701 TCCCCCGTGT GTTTGGTGGC AGGGGTCCCA GCATCCTAGA GTCCAGTCCC
6751 CACTCTCACC CTGCATCTCC TGCCCAGGGA ACGACACTCA TCACCAACCT
6801 GTCATCGGTG CTGAAGGATG AGGCCGTCTG GGAGAAGCCC TTCCGCTTCC
6851 ACCCCGAACA CTTCCTGGAT GCCCAGGGCC ACTTTGTGAA GCCGGAGGCC
6901 TTCCTGCCTT TCTCAGCAGG TGCCTGTGGG GAGCCCGGCT CCCTGTCCCC
6951 TTCCGTGGAG TCTTGCAGGG GTATCACCCA GGAGCCAGGC TCACTGACGC
7001 CCCTCCCCTC CCCACAGGCC GCCGTGCATG CCTCGGGGAG CCCCTGGCCC
7051 GCATGGAGCT CTTCCTCTTC TTCACCTCCC TGCTGCAGCA CTTCAGCTTC
7101 TCGGTGCCCA CTGGACAGCC CCGGCCCAGC CACCATGGTG TCTTTGCTTT
7151 CCTGGTGACC CCATCCCCCT ATGAGCTTTG TGCTGTGCCC CGCTAGAATG
7201 GGGTACCTAG TCCCCAGCCT GCTCCCTAGC CAGAGGCTCT AATGTACAAT
7251 AAAGCAATGA GGTAGTTCCA ACTCGGGTCC CCTGCTCACG CCCTCGTTGG
7301 GATCATCCTC CTCAGGGCAA CCCCACCCCT GCCTCATTCC TGCTTACCCC
7351 ACCGCCTGGC CGCATTTGAG ACAGGGGTAT GTTGAGGCTG AGCAGATGTC
7401 AGTTACCCTT GCCCATAATC CCATGTCCCC CACTGACCCA ACTCTGACTG
7451 CCCAGATTGG TGACAAGGAC TACATTGTCC TGGCATGTGG GGAAGGGGCC
7501 AGAATGGGCT GACTAGAGGT GTCAGTCAGC CCTGGATGTG GTGGAGAGGG
7551 CAGGACTCAG CCTGGAGGCC CATATTTCAG GCCTAACCCA GCCCACCCCA
7601 CATCAGGGAC AGCAGTCCTG CCAGCACCAT CACAACAGTC ACCTCCCTTC
7651 ATATATGACA CCCCAAAACG GAAGACAAAT CATGGCGTCA GGGAGCTATA
7701 GGCCAGGGCT ACCTACCTCC CAGGGCTCAG TCGGCATCTT GCTGAAAAAC

7751 TCGAGCCATC CGGATGGATA TGGTGTTCAG GCACAAGTGT TAAAGCAGTT
7801 GATTTTATTC ACTATGATGA AAAAAACAAT GAATGGAACC TGCTCCAAGT
7851 TAAAAATAGA GATAATACCG AAAACTCATC GAGTAGTAAG ATTAGAGATA
7901 ATACAACAAT AAAAAAATGG TTTAGAACTT ACTCACAGCG TGATGCTACT
7951 AATTGGGACA ATTTTCCAGA TGAAGTATCA TCTAAGAATT TAAATGAAGA
8001 AGACTTCAGA GCTTTTGTTA AAAATTATTT GGCAAAAATA ATATAATTCG
8051 AATTCACGTG TCGACGAGCT CGCGGCCGCA TGCTAGCTTA AGCCAGCCCC
8101 GACACCCGCC AACACCCGCT GACGCGCCCT GACGGGCTTG TCTGCTCCCG
8151 GCATCCGCTT ACAGACAAGC TGTGACCGTC TCCGGGAGCT GCATGTGTCA
8201 GAGGTTTTCA CCGTCATCAC CGAAACGCGC GA

Appendix V – Ferguson Analysis Gels

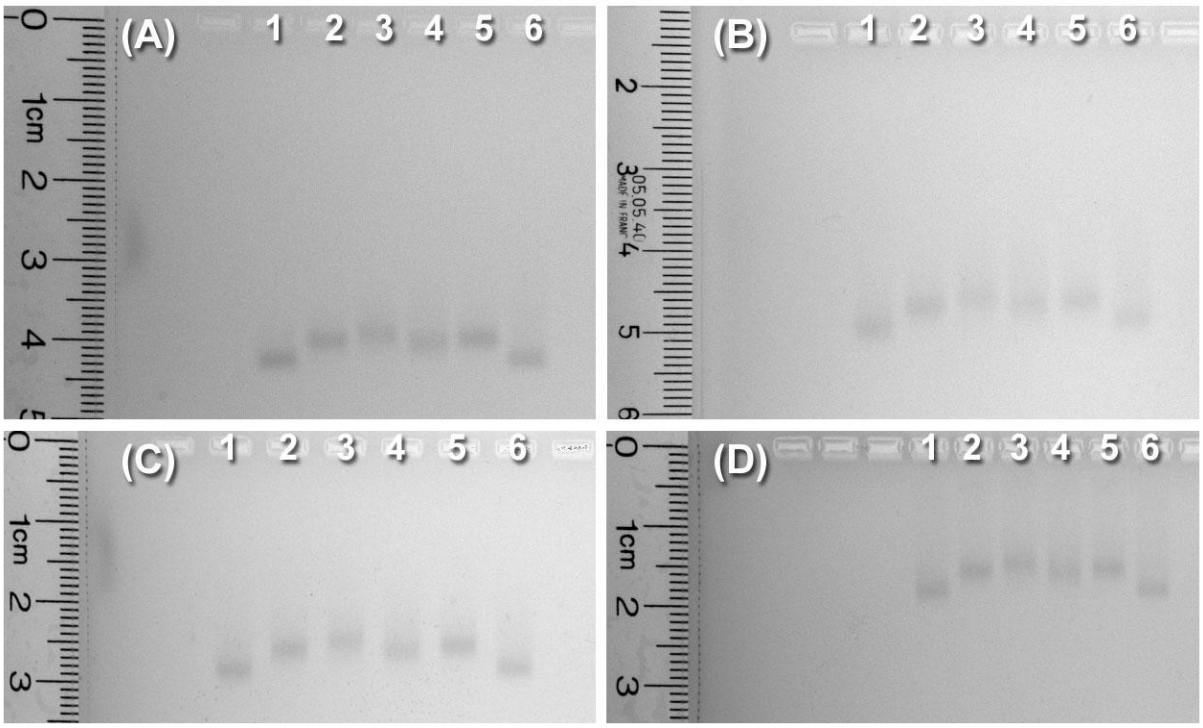

Figure A.5 – Electrophoresis analysis of Au-nanoprobe conjugates in different agarose gel concentrations: (A) 1%, **(B)** 1.5%, **(C)** 2% and **(D)** 3% (w/v) agarose. Conditions: 2 hours at 4 V/cm in 0.5x TBE buffer. Lanes: "1"- Au-nanoprobe alone and in presence of: "2"- a target harboring a single base mismatch at the 3'-end of the Au-nanoprobe (G•G); "3"- a complementary target; "4"- a target harboring a single base mismatch (G•T); or "5"- (G•A) at the 3'-end of the Au-nanoprobe; or "6"- a non-complementary target.